The Role of Ataxin-2 in Metabolism and Disease

Dissertation
zur Erlangung des Doktorgrades
der Naturwissenschaften
vorgelegt beim Fachbereich Biowissenschaften
der Johann-Wolfgang-Goethe-Universität
in Frankfurt am Main

von
Nesli Ece Şen
aus Yalova, Türkei
Frankfurt, 2020
(D30)

Vom Fachbereich Biowissenschaften (15) der Johann-Wolfgang-Goethe-Universität als Dissertation angenommen.

Dekan:	Prof. Dr. Sven Klimpel
Gutachter:	Prof. Dr. Jörg Soppa
	Prof. Dr. Georg Auburger

Datum der Disputation:

“Hayatta en hakiki mûrşit ilimdir.”

“The supreme guide in life is science.”

Mustafa Kemal Atatürk

1924

ACKNOWLEDGEMENTS

First of all, I would like to state my sincere gratitude to all the thesis committee members for devoting time into evaluating and improving this thesis with their valuable insights, especially to my *Gutachters* Prof. Jörg Soppa and Prof. Georg Auburger.

It is not easy leaving your family behind to embark upon your own adventures at a young age, yet it is equally as hard saying goodbye to my surrogate family now, much later in life. I am eternally thankful to the twist of fate leading me to meet Prof. Georg Auburger and Dr. Suzana Gispert-Sanchez. As Prof. Auburger thoroughly fulfills the definition of *Doktorvater* with his guidance, endless support and care for students, Suzana has been an irreplacable mentor and inspiration in all terms. I cannot possibly thank them enough for everything they have done, and all that I have learnt from them. I will always cherish the scientific and philosophical understanding I gained here, and will proudly carry their legacy with me.

My gratitude to Aleksandar is ineffable. With his precision and exceptional technical skills, he has outgrown his “student” title soon enough. Next to the invaluable experimental help, his emotional support and unconditional belief in me have brought confidence back to my life, and me back to the benchside where I belong. His influence on our work and my personality has been life-altering, which I hope will persist in many years to come.

Jana, Gabi and Aneesha are the embodiment of “through thick and thin”. They have always been there to help, to talk, to have office coffee-time, to take a walk, to celebrate, to calm me down, to motivate, to share many good memories as well as the hard times, and overall to make life so much better. Their friendship will be deeply missed.

I am thankful to Melanie and Julia for their excellent work with animals, and help through many times of devastating paper submissions. I feel privileged to have shared a lab with Leona, Marina R., Stella, Zeynep Ece, Sylvia and Luis Enrique throughout these years. I owe loads of thanks to many former members of the Auburger Lab, namely Birgitt, Marina J., Nadine, Jorge, Michael, Isabel and Ewa for their contributions; as well as to Frau Carolina, Frau Milagro, Dr. Gelhardt, Dr. Empting, Frau Janton, Herr Allerberger and Herr Titok for their constant support to our laboratory. Likewise, I deeply appreciate the kind help provided by Prof. Donat Kögel and his team members Benedikt, Hildegard, Janina, Nina, Abigail, Lisa and Katharina.

I had the pleasure of working with many brilliant collaborators, at the top of which comes Dr. David Meierhofer and Beata with their outstanding scientific cooperation and friendship over many years, during which they kindly hosted me in their lab. Dr. Kay Seidel ran to rescue many times when we needed his expertise, and instructed me through one of the hardest protocols I had to perform. Thanks to him, we met Prof. Stephan Baader who made a remarkable contribution to our work in the most efficient way possible. I am also thankful to Dr. Ulrich Pilatus and Woon-Hyung for their long-term devotion and help. I would like to extend my thanks to Prof. Aaron Gitler, whose pioneering work has brought me into this field in the first place. Both him and his team members, Lindsay and Steven,

have been very friendly and collaborative in many projects; it has been a true pleasure working with them. Doubtless, I am sincerely grateful to my former supervisor Prof. A. Nazlı Başak, thanks to whom I got to work on this amazing topic and learnt my way around academia. Also, I would like to acknowledge Prof. Jernej Ule, Ricardo, GenXPro team, Dr. Florian Freudenberg and Dilhan for their time and valuable contributions. A big thank you goes to Annett, for her tireless help in animal work and kindness.

I cordially thank all the patients and family members, especially Suna and İnan Kıraç, for their cooperativity and alturistic contributions to science. This work was rendered possible with the generous financial support from Deutsche Forschungsgemeinschaft, Universitätsklinikum Frankfurt and Max Planck Institute for Bain Reseach. It has been an honour to enroll in International Max Planck Research School for Neural Circuits, and I am thankful to all MPIBR members, mainly to Irina, Maren and Arjan for their patience and all the help. I would especially like to thank Prof. Erin Schuman for being the role-model she is, and for everything I have learnt in her lab, which would have been impossible elsewhere. I am grateful to all the lab members, particularly to Susu and Bea for valuable teachings. I also respectfully acknowledge Prof. Thomas Deller, Prof. Jochen Röper and Prof. Helmuth Steinmetz for their long standing ties with our lab and especially supporting this work.

I am lucky beyond measures to have met all the amazing people through IMPRS; Claudia, Julio, Fabio, Diane, Irina, Mantian, Tamas and Anne-Sophie, all the amazing people of the Niederrad Campus; Elif, Tamara, Galip, Müjgan and Strahinja, and all the amazing people who have been there as long as I can remember; Derya, Duygu, Doğuş and Hamid. They have been great friends, true confidants and firm support I can always rely on. I would like to pay special thanks to Hamid for all the happy memories, selfless deeds and making me a more interesting person, and to Elif for her exhaustless technical help as great as her friendship.

A healthy life style does not come easy to PhD students. I am deeply grateful to Olga and Dominik for their help in keeping active. Our training sessions, albeit full of sweat and tears, have brightened my mood and many of the dark days. Their companionship made me love the pain; as where is no pain, can be no gain.

Last but not least, I am the proud last generation of a pedigree full of love, support and intellect. Over the time course of this thesis, all of us overcame intolerable difficulties by standing strong together. I thank to my mother, step-father, grandparents, aunts, uncles and cousins for continuous emotional support, interesting philosophical talks, occasional heated discussions, and all together for making me who I am today.

I dedicate this work to my mother, to whom I owe every bit of my physical and personal self, and to my beloved Batty. Writing these words on what was going to be his 8th birthday, I reminisce his beautiful eyes, tender voice and all the magic he brought into my life unknowingly. Half of my heart will lie forever next to him…

This thesis is based on the following publications:

Sen NE, Gispert S, Auburger G. **PINK1 and Ataxin-2 as modifiers of growth.** *Oncotarget*. 2017 May 16;8(20):32382-32383. doi: 10.18632/oncotarget.16636. [#]

Sen NE*, Canet-Pons J*, Halbach MV*, Arsovic A, Pilatus U, Chae WH, Kaya ZE, Seidel K, Rollmann E, Mittelbronn M, Meierhofer D, De Zeeuw CI, Bosman L, Gispert S, Auburger G. **Generation of an *Atxn2*-CAG100 knock-in mouse reveals N-acetylaspartate production deficit due to early *Nat8l* dysregulation.** *Neurobiol Dis.* 2019 Dec;132:104559. doi: 10.1016/j.nbd.2019.104559. [##]

Sen NE, Arsovic A, Meierhofer D, Brodesser S, Oberschmidt C, Canet-Pons J, Kaya ZE, Halbach MV, Gispert S, Sandhoff K, Auburger G. **In Human and Mouse Spino-Cerebellar Tissue, Ataxin-2 Expansion Affects Ceramide-Sphingomyelin Metabolism.** *Int J Mol Sci.* 2019 Nov 21;20(23). doi: 10.3390/ijms20235854. [#]

TABLE OF CONTENTS

1. Zusammenfassung 1

2. Summary 9

3. Introduction 15

3.1. SCA2 distribution, symptoms and neuropathology 16

3.2. Genetics of SCA2, *ATXN2* locus and disease modifiers 19

3.3. *ATXN2* involvement in other neurodegenerative diseases 21

3.4. Ataxin-2 function, basis of pathology and mouse models 22

4. Aim 28

5. Results and Discussion 29

5.1. ATXN2 involvement in regulation of growth 29

5.2. An authentic mouse model of SCA2: first molecular findings 31

5.3. Spinocerebellar lipid profiles of SCA2 in mice and men 37

6. Conclusion 42

7. List of Figures 44

8. List of Abbreviations 45

9. References 47

10. Appendix 57

I. Publication #1 57

II. Publication #2 61

III. Publication #3 81

IV. Written Declarations 111

V. Complete List of Publications of the Candidate 113

VI. *Curriculum vitae* 115

1. ZUSAMMENFASSUNG

Spinocerebelläre Ataxie Typ 2 (SCA2) ist eine autosomal-dominant vererbte neurodegenerative Bewegungsstörung, die durch eine hohe Anzahl an CAG-Wiederholungen im *ATXN2*-Gen über 33 Einheiten hinaus verursacht wird. Gesunde Personen haben 22-23 Wiederholungen. Erste Symptome von SCA2 sind unkoordinierte Bewegungen, ataktischer Gang und Verlangsamung der sakkadischen Augenbewegungen parallel zu einer früh ausgeprägten Atrophie von Spinocerebellum und Hirnstamm. Die am stärksten von der ATXN2-Expansion betroffenen Zellen sind die Purkinjezellen des Kleinhirns und Motoneurone des Rückenmarks. Später manifestieren die Patienten distale Amyotrophie, Atem- und Schluckprobleme, Depressionen und kognitiven Verfall, verursacht durch die weit verbreitete Degeneration des gesamten Gehirns. Der auffällige Verlust an Gehirnmasse aufgrund einer schweren Myelinfettatrophie geht mit einer Verringerung der peripheren Fettspeicher einher. Nach dem verheerenden Fortschreiten der Krankheit, deren Schweregrad und Dauer von der Anzahl der CAG-Wiederholungen, dem individuellen genetischen Hintergrund und Umweltfaktoren abhängt, erliegen die Patienten SCA2 hauptsächlich aufgrund eines Atemversagens im Endstadium. Höhere CAG-Wiederholungszahlen führen zu einer früheren Manifestation der Krankheit und einem schnelleren Fortschreiten. Neben SCA2 erhöhen mittlere und kurze pathogene CAG-Expansionen im *ATXN2*-Gen (26-39 Wiederholungen) das Risiko für das Auftreten anderer neurodegenerativer Erkrankungen. In verschiedenen Kohorten auf der ganzen Welt treten Erkrankungen wie Amyotrophe Lateralsklerose (ALS), fronto-temporale lobäre Demenz (FTLD), Parkinson (PD) mit Tauopathien, sowie weitere wichtige Syndrome wie progressive supranukleäre Lähmung (PSP) auf.

Ataxin-2 (ATXN2) ist ein ubiquitär exprimiertes zytosolisches Protein. Am bekanntesten ist es für seine Beteiligung an neurodegenerativen Erkrankungen, die durch die erweiterte Polyglutamin (polyQ)-Domäne verursacht werden, welche einem genomischen (CAG)n-Trakt entspricht. Diese N-terminale polyQ-Domäne hat keine bekannte Funktion, außer die Aggregationsneigung von mutiertem ATXN2 zu erhöhen und die Interaktion mit anderen polyQ-haltigen Proteinen zu erleichtern, was zu deren Sequestrierung führt. Die fortschreitende Akkumulation von ATXN2 und auch die seiner Interaktionspartner in zytosolischen Ansammlungen liegt dem molekularen Pathomechanismus zugrunde. Neben der polyQ-Domäne enthält ATXN2 auch eine Like-Sm-Domäne (Lsm), eine Lsm-assoziierte Domäne (LsmAD), mehrere Prolin-reiche Domänen (PRD) und ein mit Poly(A)-Bindungsprotein (PABP) wechselwirkendes Motiv (PAM2).

ATXN2 bindet über seine Lsm/LsmAD-Domänen direkt an eine große Anzahl von Transkripten und reguliert deren Qualität und Translationsrate. Auf ähnliche Weise verändert ATXN2 durch seine direkte Interaktion mit PABP über das PAM2-Motiv indirekt das Schicksal einer noch größeren Anzahl von Transkripten und der globalen Translation. Mehrere, über das Protein verstreute, PRDs helfen ATXN2 bei der Interaktion mit Rezeptoren für Wachstumsfaktoren und anderen Endozytosefaktoren, wodurch die Nährstoffaufnahme und die nachgeschaltete Signalübertragung moduliert werden.

ATXN2 ist ein Stressreaktionsfaktor. Daher spielt seine Beteiligung an der Nährstoffaufnahme eine entscheidende Rolle für die Fähigkeit der Zelle, herausfordernde Bedingungen zu überstehen. Bei Nährstoffmangel, oxidativem Stress, Proteotoxizität, Hitzestress oder Ca2+-Ungleichgewicht relokalisiert ATXN2 zusammen mit PABP, mehreren eukaryotischen Translationsinitiationsfaktoren und vielen anderen RNA-bindenden Proteinen (RBP) mit deren Zieltranskripten und der kleinen ribosomalen Untereinheit in zytosolische Ribonukleoproteinpartikel, die als Stressgranulate (SGs) bekannt sind. Diese modulieren gemeinsam die Stabilität der eingeschlossenen Transkripte und begünstigen die Reifung und Translation von IRES-abhängigen Stressantwortproteinen, entsprechend dem spezifischen Bedarf. Viele RBPs interagieren entweder direkt oder RNA-abhängig in den SGs, und aufgrund der großen Anzahl von ALS-verursachenden Mutationen, die in ihnen identifiziert wurden (wie TDP-43, FUS, TIA-1, hnRNPA2 / B1), entwickelten sich SGs zu einem bedeutenden Thema in der Neuropathologie. Akute SGs dienen dazu, die Translation und das Wachstum zu stoppen und Energie nur zum Überleben zu verwenden, bis der Stress verschwindet. Eine chronische SG-Assemblierung aktiviert jedoch schließlich Apoptose, was zum Zelltod führt. Während die polyQ-Expansionen in ATXN2 die SG-Stabilität verbessern, ihre Dissoziationsrate nach Stress verringern und zu aberranten posttranslationalen Modifikationen anderer SG-Komponenten wie TDP-43 führen, verzögert der vollständige Verlust von ATXN2 die SG-Bildung und führt zu leicht auflösbaren Aggregaten.

Die meisten Stressoren, die eine SG-Bildung induzieren, gehen mit einem Energiedefizit einher. Daher ist es logisch, dass die letztendliche Aufgabe von SGs darin besteht, weiteres Wachstum zu stoppen, wenn es sich die Zelle nicht leisten kann, zu wachsen. In Hefen wurde der diesem Wachstumsstopp zugrundeliegende molekulare Mechanismus als Sequestrierung des wichtigsten Komplexes für Wachstumsregulation Target-of-Rapamycin Complex 1 (TORC1) in SGs in ATXN2-abhängiger Weise erklärt. Die Repressorwirkung von ATXN2 auf TORC1 bei Säugetieren (mTORC1) und die globale Proteintranslation wurde bereits in früheren Studien beschrieben. Der vollständige Verlust der ATXN2-Funktion in der Knock-out-Maus (*Atxn2*-KO) führte zu einer mTORC1-

Hyperaktivität und einer transkriptionellen Hochregulation mehrerer ribosomaler Untereinheiten, was auf einen erhöhten Bedarf dieser Proteine hinweist. Übereinstimmend mit den vermehrten Wachstumssignalen führte der vollständige Verlust von ATXN2 bei Mäusen zu Fettleibigkeit mit Insulinresistenz und Diabetes, was in einem scharfen Kontrast zum atrophischen Zustand von SCA2-Patienten steht. Darüber hinaus zeigten globale Proteom- und Metabolom-Studien an Lebergeweben von *Atxn2*-KO-Mäusen eine starke Herunterregulierung des Abbauweges der verzweigt-kettigen Aminosäuren (BCAA). Dies weist auf eine Akkumulation von BCAAs im Blut und im peripheren Gewebe hin, welches derzeit der am stärksten korrelierte Biomarker von Diabetes ist. Darüber hinaus zeigte ATXN2-Null-Hefe unter verschiedenen Stressbedingungen eine Vielzahl relevanter Dysregulationen von Stoffwechselwegen wie Glykolyse, Tricarbonsäure (TCA)-Zyklus und oxidativer Phosphorylierung. Eine andere Studie an Hefen belegte die Bedeutung von ATXN2 im Umgang mit Überakkumulationsstress durch mitochondriale Vorläufer-Eiweißen (mPOS). Dieser wird durch das Versagen des Proteinimports durch Mitochondrienmembranen und die Peptidakkumulation im Zytosol verursacht. Interessanterweise reagiert auf Stress nicht nur die subzelluläre Lokalisation von ATXN2, sondern auch auf dessen Transkriptionsregulation. Es wurde gezeigt, dass ein längerer Nährstoffmangel ATXN2-Transkripte und ATXN2-Proteinspiegel in verschiedenen Zelltypen induziert, was seine Notwendigkeit während Stresssituationen weiter untermauert. Zusammengenommen zeigen diese Ergebnisse, dass die ursprüngliche ATXN2-Funktion aufgrund ihrer Relokalisierungsdynamik eine enorme Bedeutung für die Steuerung des Stoffwechselgleichgewichts unter normalen Bedingungen und unter Stressbedingungen hat.

Während es relativ gradlinig ist, Modelle mit Funktionsverlusten zu untersuchen, um die normale Aufgabe des Proteins zu verstehen, war die Untersuchung derselben Aspekte in Krankheitsmodellen eine Herausforderung. Die durch Proteinaggregation bedingte Pathologie ist ein komplexes Zusammenspiel aus toxischem Funktionsgewinn aufgrund der fortschreitenden Sequestrierung von Interaktionspartnern und deren aberranten Modifikation, und einem teilweisen Funktionsverlust aufgrund der Sequestrierung des Proteins selbst in den Aggregaten und folgendem Mangel an normaler intrazellulärer Aktivität. Um die expansionsbedingten Effekte von ATXN2 zu untersuchen, wurden mehrere transgene Mausmodelle mit einer gezielten Expression des mutierten Proteins nur in Kleinhirn-Purkinje-Neuronen erzeugt. Diese Mäuse entwickelten in kurzer Zeit auffällige zytosolische Aggregate aufgrund der unkontrollierten Überexpression des mutierten Konstrukts, was zu motorischen Ausfallerscheinungen führte. Abgesehen von der Fehlfunktion des Kleinhirns zeigten diese Mausmodelle jedoch keine der anderen SCA2-assoziierten Merkmale, wie z. B. die Beteiligung anderer Hirnregionen, Zelltypen und

peripherem Gewebe. Somit wurde das erste Knock-In (KIN) Modell mit 42 CAG-Wiederholungen generiert, welche am entsprechenden genomischen Ort eingefügt wurden, der die endogene Expression des mutierten Proteins antreibt. Leider zeigten *Atxn2*-CAG42-KIN-Mäuse nur in sehr späten Stadien bei normalen Lebensdauer milde Krankheitszeichen mit minimalem Phänotyp peripherer Atrophie, was sie für die Untersuchung der Krankheitspathologie in seinem gesamten Spektrum nicht praktikabel machte.

Jahrzehnte nach seiner Identifizierung als verursachendes Protein für SCA2 wird die normale Funktion, Verteilung und dynamische Regulation von ATXN2 nun etwas klarer. Der genaue Einfluss der polyQ-Expansion blieb jedoch weitgehend ungelöst, abgesehen von der Verursachung von zytosolischen Aggregaten in Purkinjezellen. Insbesondere die energetische Bedeutung durch die Mutation wäre angesichts der ausgeprägten Stoffwechselergebnisse und des Größen-Phänotyps, der bei Organismen mit ATXN2-Mangel beobachtet wird, von besonderer Bedeutung. Daher haben wir uns vorgenommen, einige entscheidende Fragen in dieser Hinsicht zu beantworten: **(i) Welche Veränderungen treten im Körper während der Erkrankung auf? (ii) Wie tragen andere Zelltypen oder Regionen des Zentralnervensystems zur Krankheitspathologie bei?** und **(iii) Wie verändert sich der Hirnstoffwechsel während der Erkrankung?**

Welche Veränderungen treten im Körper während der Erkrankung auf? Es ist bekannt, dass ATXN2 in einer Vielzahl von Geweben exprimiert wird, von denen einige für das metabolische Gleichgewicht sehr wichtig sind, wie z. B. Leber und Muskel. Hinzu kommt, dass SCA2-Patienten eine starke Gewichtsreduktion und eine periphere Atrophie aufweisen. Es ist daher plausibel, dass die Expansionspathologie sowohl den Körper als auch das Gehirn betrifft. Obwohl Verlaufsstudien in sehr großen Kohorten durchgeführt wurden, die eine Korrelation von Beginn und Fortschreiten der Krankheit mit der Expansionsgröße zeigten, fehlte ein zuverlässiger molekularer Biomarker zur Messung des Pathologiezustands bei einem Individuum, möglichst gewinnbar durch eine nicht-invasive Methode. Um dies zu erreichen, führten wir eine Hochdurchsatz-RNA-Sequenzierungsanalyse durch, bei der die Blutproben von SCA2-Patienten mit alters- und geschlechtsentsprechenden gesunden Familienmitgliedern verglichen wurden. Das wichtigste Ergebnis dieser Studie war die ATXN2-abhängige Expressionsregulation von PTEN-induzierter-Kinase-1 (PINK1), einem autosomal rezessiven vererbten Parkinson-Gen. Erhöhte *PINK1*-Transkripte im Patientenblut im Vergleich zu verringerten Spiegeln in *Atxn2*-KO-Mausgeweben zeigten die Abhängigkeit der PINK1-Aktivität von ATXN2, welche im Hinblick auf das bei SCA2-Patienten beobachtete Parkinson-Verhalten sehr relevant ist, sowie von *ATXN2*-Expansionen, die ein Risiko für Parkinson-Syndrome darstellen. Darüber hinaus wurde dank der auf Stress reagierenden PINK1-Aktivität, insbesondere bei der

Beseitigung geschädigter Mitochondrien durch Mitophagie, erstmals der Zusammenhang zwischen ATXN2 bei Säugetieren und mitochondrialer Dysfunktion als weit verbreiteter Aspekt von Neurodegeneration hergestellt.

Neben seiner Beteiligung an PD ist PINK1 aufgrund seiner Verbindung zur Signalkaskade für Wachstumsfaktor-Rezeptoren über Phosphatase-And-Tensin-Homolog (PTEN) und Proteinkinase B (PKB/Akt) auch ein wichtiger Faktor bei Krebs. Es wurde gezeigt, dass hohe PINK1-Spiegel den bekannten Warburg-Effekt bei Krebs auslösen, weshalb seine Modulation als therapeutischer Ansatz vorgeschlagen wurde. Interessanterweise wurde auch bei Krebs eine erhöhte ATXN2-Expression beobachtet, was die Empfindlichkeit gegenüber Chemotherapie erhöhte. Da ATXN2 auch mit den Wachstumsfaktorrezeptoren und schließlich mit mTORC1 assoziiert ist, eröffnet eine Dysregulation der PINK1-Spiegel in Patienten- und Mausproben im Zusammenhang mit Neurodegeneration, Fettleibigkeit oder Krebs einen bisher unentdeckten Weg und verbindet ATXN2 mit den Kraftwerken der Zelle: Mitochondrien. Diese Ergebnisse müssen zukünftig in größeren Kohorten getestet werden, um den vorgeschlagenen Zusammenhang zu festigen. Angesichts der Bedeutung von PINK1 bei der Parkinson-Krankheit, die durch die Degeneration dopaminerger Neuronen im Mittelhirn verursacht wird, und der Parkinson-Symptome bei SCA2-Patienten, die sich aus einer ähnlichen Pathologie ergeben, ist die Erstellung eines authentischen SCA2-Modells mit einer starken neurologischen Signatur und einer weit verbreiteten Pathologie dringend erforderlich, um interessante zusätzliche Untersuchungen der zerebellären Phänomene durchzuführen. Darüber hinaus bietet dieses Modell eine einzigartige Gelegenheit, den Beitrag anderer Zelltypen im Gehirn und metabolische Veränderungen während des gesamten Krankheitsverlaufs zu untersuchen.

Wie tragen andere Zelltypen oder Regionen des Zentralnervensystems zur Krankheitspathologie bei? Wie verändert sich der Hirnstoffwechsel im Zuge der Erkrankung? Aufgrund der dringenden Notwendigkeit eines guten Systems zur Untersuchung der Krankheit als Ganzes haben wir das erste authentische Mausmodell für SCA2 generiert, nämlich die *Atxn2*-CAG100-KIN-Maus bei der 100 CAG-Einheiten an den entsprechenden Ort eingefügt wurden. Detaillierte Analysen auf genetischer, phänotypischer, verhaltensbezogener und histologischer Ebene bestätigen alle die derzeit verfügbaren Patientendaten und bekräftigten somit die Gültigkeit dieses Modells. Die Interpretation dieser Befunde teilte den Krankheitsprozess in drei Kategorien ein: Prä-manifeste Phase mit kleinen zytosolischen ATXN2-Q100-Ansammlungen im Alter von 3 Monaten, manifeste Phase mit größeren Ansammlungen im Alter von etwa 6 Monaten, und Endphase mit massiven Aggregaten, die auch andere Proteine binden, mit 14 Monaten. Zu diesem Zeitpunkt erforderten schwere motorische Dysfunktionen und übermäßiger

Gewichtsverlust die Tötung der *Atxn2*-CAG100-KIN-Tiere, um Leiden zu vermeiden, und definierten die Lebensspanne dieses Modells auf etwa die Hälfte einer Wildtyp-Maus.

Das Screening von Kleinhirnmetaboliten im Endstadium ergab ein ausgeprägtes Energiedefizit, das durch die Verringerung von Glutamat und N-Acetylaspartat (NAA) angezeigt wird, welche normalerweise die beiden am häufigsten vorkommenden Metabolite im Gehirn sind. Insbesondere die Reduktion von NAA, einem Marker für neuronale Gesundheit, war aufgrund seiner Rolle bei der Energiespeicherung im ZNS und der Myelinisierung bemerkenswert. Da Untersuchungen mit Bildgebung des Gehirns und *post mortem* Histologien bei SCA2-Patienten eine starke Demyelinisierung zeigten, untersuchten wir die molekularen Mechanismen, die der Produktion und Verwendung von NAA zugrunde liegen. Expressionsanalysen der wichtigen Signalwegkomponenten auf Transkript- und Proteinebene im *Atxn2*-CAG100-KIN-Kleinhirn während der gesamten Erkrankung ergaben, dass N-Acetyltransferase-8-Like (NAT8L), das NAA-produzierende Enzym in Neuronen, der am frühesten und am stärksten betroffene unter allen getesteten Faktoren ist. Niedrigere Spiegel seines Transkripts und Proteins im prä-manifesten Stadium deuteten auf ein sehr frühes Defizit in der NAA-Produktion hin, worauf später in der symptomatischen Phase die Verringerung des Aspartoacetylase (ASPA) Spiegels, des NAA-Abbauenzyms in Oligodendrozyten, folgte. Zusammengenommen zeigten die Daten, dass die Hauptursache für das Myelinisierungsproblem das Defizit in der neuronalen NAA-Produktion durch NAT8L ist. Neben Neuronen wird NAT8L auch in Adipozyten exprimiert. Unter Berücksichtigung der Beteiligung von ATXN2 am Fettsäurestoffwechsel testeten wir die *Nat8l*-Expression in Fettgewebe- und Blutproben von *Atxn2*-CAG100-KIN-Mäusen, sowie Blutproben von SCA2-Patienten. Alle Proben zeigten eine konsistente Herunterregulierung. Darüber hinaus zeigten *Atxn2*-CAG100-KIN-Fibroblasten unter adipogener Differenzierung ein *Nat8l*-Induktionsdefizit im Vergleich zu WT-Zellen, was den direkten Einfluss von ATXN2-Q100 auf das *Nat8l*-Transkriptniveau weiter bestärkt. Daher haben wir nicht nur das erste authentische Mausmodell für SCA2 mit allen Krankheitszeichen generiert, sondern auch ein frühes und schleichendes Energiedefizit im gesamten Körper festgestellt, was eine die Nervenbahnen betreffende und periphere Atrophie auslöst, die in späteren Krankheitsstadien beobachtet wird.

Nachdem wir den frühen NAA-Produktionsdefekt in *Atxn2*-CAG100-KIN-Mäusen festgestellt hatten, der möglicherweise auf ein breiteres Acetyl-CoA-Defizit zurückzuführen sein könnte, untersuchten wir die Lipidprofile des Kleinhirns von SCA2-Patienten und des spinocerebellären Gewebes der *Atxn2*-CAG100-KIN Mäuse. Das Hochdurchsatz-Metabolom-Screening verschiedener Lipide in Mausgeweben zeigte eine gute Übereinstimmung mit den selten autopsierten SCA2-Patientenproben hinsichtlich einer

signifikanten Reduktion von Ceramiden und langkettigen Sphingomyelinen (C24-26), welches beide Plasmamembranlipide sind. Im Gegensatz dazu waren kurzkettige Sphingomyeline (C18-22), die hauptsächlich in Neuronen vorkommen, signifikant erhöht. C24-26-Sphingomyeline kommen hochkonzentriert in Oligodendrozyten vor, die die mehrschichtige Myelinhülle um Axone bilden, und daher repräsentativ für diesen Zelltyp sind. Zusätzlich zu verringerten langkettigen Sphingomyelinen waren auch Cholesterin und Sulfatide als zusätzliche Lipide der Myelinscheide im SCA2-Kleinhirn signifikant reduziert, was insgesamt auf eine schwere Myelinatrophie hinweist. Da alle hier analysierten Metabolite dynamisch verarbeitet und ineinander umgewandelt werden, haben wir die mit diesen komplizierten molekularen Pfaden verbundenen Enzyme untersucht, um die Kausalkette in *Atxn2*-CAG100-KIN-Geweben besser zu verstehen. Ceramide bestehen aus einem Sphingosin-Grundgerüst und einer Fettsäurekette und sind die einfachsten Einheiten, die zu Sphingomyelinen oder Galactosylceramiden weiterverarbeitet werden können, um strukturell in die wachsende Plasmamembran eingebaut zu werden. Auf ähnliche Weise können Sphingomyeline bei Bedarf zu Ceramid zurück metabolisiert werden, und Ceramid kann zum Recycling in verschiedenen subzellulären Kompartimenten weiter abgebaut werden. Bei der Analyse aller Enzym-Isoformen stellten wir eine kollektive Reduktion aller Enzyme, die an der an der Fettsäureverlängerung beteiligt sind, fest, was zu einem *de novo* Ceramid-Produktionsdefizit sowohl in Neuronen als auch in Oligodendrozyten führte. Reduzierte Spiegel des lysosomalen Sphingomyelin-Abbauenzyms erklärten auch die geringe Ceramid-Häufigkeit im Vergleich zur Akkumulation langkettiger Sphingomyeline. Obwohl ausführlichere biochemische Analysen dazu beitragen können, die Details weiter aufzuklären, haben wir mit dieser neuen Studie erstmals das Gesamtlipidprofil in SCA2-Nervengewebe dokumentiert und als zentrale Faktoren der ATXN2-Pathologie in verschiedenen Zelltypen Fettsäure-Elongase-Isoformen identifiziert, die unter der Kontrolle von mTORC1 stehen.

All diese Befunden zusammengenommen, beeinflusst die ATXN2-Pathologie mit Sicherheit eine Vielzahl von Stoffwechselwegen, sowohl im Nerven als auch im peripheren Gewebe. Anstatt dass das mutierte Protein selektiv auf eine geringe Anzahl von Enzymen abzielt, die an verschiedenen Signalwegen beteiligt sind, scheint es wahrscheinlicher, dass ATXN2 diesen modulatorischen Effekt ausübt, indem es mit einem Hauptregulator des Stoffwechsels interagiert oder die Homöostase einfachster energetischer Einheiten wie Acetyl- CoA stört. Ein häufiger Grund für das NAA- und Ceramid-Produktionsdefizit könnte beispielsweise auch ein Acetyl-CoA-Mangel sein, da er sowohl für Metabolite als auch für Tausende andere komplexe Lipide ein Baustein ist. Obwohl die direkte Wechselwirkung zwischen Hefe-ATXN2 und mTORC1-Orthologen in Säugetiersystemen bestätigt werden

muss, könnte ATXN2 aufgrund seiner RNA-Bindungsnatur alternativ die mTORC1-Funktion durch die Regulierung bestimmter Signalwegkomponenten modulieren, deren Zwischenprodukte direkt die Nährstoffverfügbarkeit signalisieren, wie z. B. Glykolyse oder BCAA-Abbau. Dies könnte den enormen phänotypischen Unterschied zwischen ATXN2-Verlust und Toxizität erklären und sollte in zukünftigen Studien unbedingt berücksichtigt werden.

2. SUMMARY

Spinocerebellar ataxia type 2 (SCA2) is an autosomal dominant neurodegenerative movement disorder caused by expansion of CAG repeats in the *ATXN2* gene beyond 33 units, while healthy individuals carry 22-23 repeats. First symptoms of SCA2 include uncoordinated movement, ataxic gait and slowing of the saccadic eye movements in line with the early pronounced atrophy of cerebellum, spinal cord and brainstem. Cerebellar Purkinje cells and spinal cord motor neurons are the most affected cells from ATXN2 expansions. Later on, patients manifest distal amyotrophy, problems in breathing and swallowing, depression and cognitive decline caused by widespread degeneration throughout the brain. The striking loss of mass in the brain, due to severe myelin fat atrophy, is accompanied by a similar reduction in the peripheral fat stores. After the devastating progression of disease, the severity and duration of which depends on the CAG repeat size, genetic background and environmental factors, patients succumb to SCA2 mostly because of respiratory failure at the terminal stage. Larger repeat sizes lead to an earlier manifestation of the disease and a more rapid progression. Aside from SCA2, intermediate-length and short pathogenic CAG expansions in *ATXN2* between 26-39 repeats significantly increase the risk of developing other neurodegenerative disorders, such as amyotrophic lateral sclerosis (ALS), fronto-temporal lobar dementia (FTLD) or Parkinson plus tauopathies like progressive supranuclear palsy (PSP) in various cohorts across the world.

Ataxin-2 (ATXN2) is a ubiquitously expressed cytosolic protein most famous for its involvement in neurodegenerative disease caused by the expanded poly-glutamine (polyQ) domain corresponding to a genomic (CAG)n tract. This N-terminal polyQ domain has no known function, other than increasing the aggregation propensity of mutant ATXN2 and facilitating interaction with other polyQ containing proteins, leading to their sequestration. The progressive accumulation of ATXN2 into cytosolic foci, and also that of its interaction partners over time, underlies the molecular pathomechanism. Next to polyQ domain, ATXN2 also contains a Like-Sm domain (Lsm), an Lsm-associated domain (LsmAD), multiple proline-rich domains (PRD) and a Poly(A)-Binding-Protein (PABP)-interacting motif (PAM2).

Through its Lsm/LsmAD domains, ATXN2 directly binds to a large number of transcripts, regulating their quality and translation rate. In a similar fashion, through its direct interaction with PABP via PAM2 motif, ATXN2 indirectly modifies the fate of even larger number of transcripts and global translation. Several PRDs scattered across the protein help ATXN2 associate with growth factor receptors and other endocytosis factors, modulating nutrient uptake and downstream signaling.

ATXN2 is a stress response factor. Therefore, its involvement in nutrient uptake plays a crucial part in cell's capability to overcome non-permissive conditions. Upon nutrient deprivation, oxidative stress, proteotoxicity, heat stress or Ca^{2+} imbalance, ATXN2 relocalizes into cytosolic ribonucleoprotein particles known as stress granules (SGs), together with PABP, several eukaryotic translation initiation factors, many other RNA-binding proteins (RBP) with their target transcripts and the small ribosomal subunit. Collectively, they modulate the stability of the trapped transcripts, favoring the maturation and translation of IRES-dependent stress response proteins instead, according to the specific need. Many RBPs interact either directly or in an RNA-dependent manner in the SGs, and due to the large number of ALS-causing mutations identified in them (such as TDP-43, FUS, TIA-1, hnRNPA2/B1), SGs became a hot topic in neuropathology. Acute SGs serve to halt translation and growth, and to spend energy only for survival until stress disappears. However, chronic SG assembly eventually activates apoptotis leading to cell death. While the polyQ expansions in ATXN2 enhance SG stability, reduce their dissociation rate after stress, and lead to aberrant post-translational modifications of other SG components like TDP-43, complete loss of ATXN2 delays SG formation and results in easily dissolvable foci.

Most of the stressors that induce SG formation eventually converge on energetic deficit. Therefore, it is logical that the ultimate task of SGs is to stop further growth when it cannot be afforded. In yeast, the molecular mechanism underlying this growth arrest was explained as sequestration of the master growth regulator complex, Target-of-Rapamycin Complex 1 (TORC1), into SGs in an ATXN2-dependent manner. The repressor effect of ATXN2 on mammalian TORC1 (mTORC1) and global protein translation had already been documented in earlier studies; complete loss of ATXN2 function in knock-out mouse (*Atxn2*-KO) resulted in mTORC1 hyperactivity and transcriptional upregulation of multiple ribosomal subunits indicating an increased need for these machines. In agreement with the hyperactive growth signals, and in a crisp contrast with the atrophic state of SCA2 patients, complete loss of ATXN2 in mouse led to obesity with insulin resistance and diabetes. In addition, global proteome and metabolome studies in *Atxn2*-KO mouse liver revealed a major downregulation of the branched chain amino acid (BCAA) degradation pathway, suggesting an accumulation of BCAAs in the blood and peripheral tissues, which is currently the most strongly correlated biomarker of diabetes. Moreover, ATXN2-null yeast under different stress conditions showed a plethora of relevant metabolic pathway dysregulations, such as glycolysis, tricarboxylic acid (TCA) cycle and oxidative phosphorylation. Another study in yeast revealed the importance of ATXN2 in dealing with mitochondrial precursor over-accumulation stress (mPOS), caused by the failure in protein import through mitochondrial membranes and peptide accumulation in the cytosol. Interestingly, not only the subcellular

localization of ATXN2 is responsive to stress, but also its transcriptional regulation. Prolonged nutrient deprivation was shown to induce ATXN2 transcript and protein levels in various cell types, further delineating its necessity during stress. Put together, these findings indicate a vast importance of native ATXN2 function in controlling metabolic balance under normal and stress conditions thanks to its relocalization dynamics.

While it is relatively more straightforward to study loss-of-function models to understand the normal function of the protein, investigation of the same aspects in disease models have been challenging. Protein aggregation driven pathology is a complex mixture of toxic gain-of-function due to the progressive sequestration of interaction partners and their aberrant modification, and a partial loss-of-function due to the sequestration of the seeding protein itself in the aggregates, and lack of its normal spatial activity. In order to examine the expansion related effects of ATXN2, several transgenic mouse models have been generated with a targeted expression of the mutant protein only in cerebellar Purkinje neurons. These mice developed remarkable cytosolic aggregates in a relatively short time period due to the uncontrolled over-expression of the mutant construct, causing motor deficit signs. However, aside from the cerebellar malfunction, these models represented none of the other SCA2-associated features, such as the involvement of other brain regions, cell types and the peripheral tissues. Thus, the first knock-in (KIN) model was generated with 42 CAG repeats inserted into the corresponding genomic locus driving endogenous expression of the mutant protein. Unfortunately, the *Atxn2*-CAG42-KIN mice manifested very mild disease signs only at the very late stages of the normal lifespan with almost no peripheral atrophy phenotype, rendering them inefficacious to study disease pathology as a whole spectrum.

Decades after its identification as the causative protein in SCA2, the normal function, distribution and dynamic regulation of ATXN2 is now somewhat unveiled. Yet, the exact impact of polyQ expansion, other than causing cytosolic aggregates in Purkinje cells, remained largely unsolved. Especially the energetic burden of the mutation would be of special importance, considering the pronounced metabolic outcomes and the increased size phenotype observed in ATXN2 deficient organisms. Hence, we set out to tackle several crucial questions in this regard: **(i)** ***What changes in the body nutrition during disease?*** **(ii)** ***How do other cell types or regions of the central nervous system contribute to disease pathology?*** and **(iii)** ***How does the brain metabolism change in disease?***

What changes in the body during disease? ATXN2 is known to be expressed in a wide variety of tissues some of which are very important for metabolic balance, such as liver and muscle. Adding this onto the fact that SCA2 patients manifest a severe weight reduction and overall peripheral atrophy, it is only plausible that the expansion pathology hits body as

well as the brain. Although there have been longitudinal studies correlating the disease onset and progression with expansion size in very large cohorts, a reliable molecular biomarker to measure the state of pathology in an individual with a non-invasive method has been missing. In order to address this, we conducted a high-throughput RNA sequencing analysis comparing the blood samples from SCA2 patients and age- and sex-matched healthy family members. The major finding of this study was the ATXN2-dependent expression regulation of PTEN-induced-kinase-1 (PINK1), an autosomal recessive Parkinson's disease (PD) gene. Increased *PINK1* transcript in patient blood vs. decreased levels in *Atxn2*-KO mouse tissues indicated a dependence of PINK1 activity on ATXN2, which is very relevant in light of the Parkinsonian behavior observed in SCA2 patients, as well as *ATXN2* expansions posing a risk for Parkinsonism syndromes. Moreover, thanks to the stress-responsive PINK1 activity, especially in the elimination of damaged mitochondria by mitophagy, the link between mammalian ATXN2 and mitochondrial dysfunction, as a vastly common aspect of neurodegeneration, was established for the first time.

Next to its involvement in PD, PINK1 is also an important factor in cancer due to its connection to the growth factor receptor signaling via Phosphatase-And-Tensin-Homolog (PTEN) and Protein Kinase B (PKB/Akt). High PINK1 levels was shown to trigger the well-known Warburg effect in cancer, thus its modulation was suggested as a therapeutic approach. Intriguingly, increased ATXN2 expression was also observed in cancer, enhancing sensitivity against chemotherapy. As ATXN2 is also associated with the growth factor receptors and eventually mTORC1, dysregulation of PINK1 levels in patient and mouse samples in the context of neurodegeneration, obesity or cancer opens a previously undiscovered path, and connects ATXN2 to the powerhouse of the cell: mitochondria. These findings, of course, need to be tested in larger cohorts to consolidate the suggested link. Given the importance of PINK1 in PD caused by dopaminergic neuron degeneration in the midbrain, and the Parkinsonian signs in SCA2 patients resulting from a similar pathology, generation of an authentic SCA2 model with a strong neurological signature and widespread pathology is highly necessary to study interesting extra-cerebellar phenomena as such. In addition, this model would provide a unique opportunity to dissect the contribution of other cell types in the brain, and metabolic alterations throughout the disease course.

How do other cell types or regions of the central nervous system contribute to disease pathology? How does the brain metabolism change in disease? Due to the dire need of a good system to study the disease as a whole, we generated the first authentic mouse model of SCA2, namely the *Atxn2*-CAG100-KIN mouse with the insertion of 100 CAG units to the corresponding locus. Detailed analyses at the genetic, phenotypic, behavioral,

and histologic levels all replicated the currently available patient data and confirmed the validity of this model. The interpretation of these findings divided the disease process into three categories: pre-onset phase with small cytosolic ATXN2-Q100 foci at 3 months of age, manifestation phase with larger foci at around 6 months, and the terminal phase with massive aggregates sequestering other proteins at 14 months. At this stage, severe motor dysfunction and excess weight loss required sacrificing of the *Atxn2*-CAG100-KIN animals in order to avoid suffering, defining the lifespan of this model as about half of a wildtype mouse.

Cerebellar metabolite screening at terminal stage revealed a prominent energetic deficit indicated by the reductions in glutamate and N-acetylaspartate (NAA), which are normally the two most abundant metabolites in the brain. Especially the reduction in NAA, a marker of neuronal health, was noteworthy due to its role in energy storage in the CNS and myelination. Since brain imaging and *post mortem* histology studies demonstrated a strong demyelination in SCA2 patients, we investigated the molecular mechanisms underlying NAA production and utilization further. Expression analyses of the important pathway components at the transcript and protein levels in *Atxn2*-CAG100-KIN cerebellum throughout disease revealed N-Acetyltransferase-8-Like (NAT8L), the NAA producing enzyme in neurons, to be the first and most affected among all the factors tested. Lower levels of its transcript and protein at the pre-onset stage suggested a very early deficit in NAA production, that was followed later at the symptomatic phase by the reduction in Aspartoacetylase (ASPA) levels, the NAA breakdown enzyme in oligodendrocytes. Put together, data indicated that the primary cause of the myelination problem is the deficit in neuronal NAA production by NAT8L. In addition to neurons, NAT8L is also expressed in adipocytes. With the involvement of ATXN2 in fatty acid metabolism in mind, we tested *Nat8l* expression in adipose tissue and blood samples from *Atxn2*-CAG100-KIN mice together with blood samples from SCA2 patients, all of which displayed a consistent downregulation. Moreover, *Atxn2*-CAG100-KIN fibroblasts under adipogenic differentiation regimen showed a *Nat8l* induction deficit compared to WT cells, further strengthening the direct impact of ATXN2-Q100 on *Nat8l* transcript levels. Therefore, in addition to generating the first authentic mouse model of SCA2 possessing all the disease signs, we revealed an early and insidious energetic deficit throughout the body, seeding the nervous and peripheral atrophy observed in later stages.

After establishing the early NAA production defect in *Atxn2*-CAG100-KIN mouse, which could potentially arise from a more broad acetyl-CoA deficit, we set out to examine the lipid profiles of SCA2 patient cerebellum and *Atxn2*-CAG100-KIN spino-cerebellar tissue. High-throughput metabolome screening of various lipid species in mouse tissues displayed good agreement with the rarely autopsied SCA2 patient sample regarding significant

reductions in ceramides and long fatty acid chain (C24-26) sphingomyelins, both of which are plasma membrane lipids. In contrast, short fatty acid chain (C18-22) sphingomyelins mainly found in neurons were significantly increased. C24-26 sphingomyelins are highly concentrated in, and therefore representative of, the oligodendrocytes that form the multi-layered myelin sheath around axons. In addition to decreased long chain sphingomyelins, also cholesterol and sulfatides, as accompanying lipids in the myelin sheath, were found significantly reduced in SCA2 cerebellum, collectively pointing to a severe myelin atrophy. As all the metabolites analyzed here are dynamically processed and converted into one another, we investigated the enzymes associated with these intricate molecular pathways in order to better understand the chain of causality in *Atxn2*-CAG100-KIN tissues. Ceramides consist of a sphingosine backbone and a fatty acid chain, and are the simplest units that can be further processed towards sphingomyelins or galactosylceramides to structurally incorporate into the growing plasma membrane. In a similar fashion, upon need, sphingomyelins can be metabolized back to ceramide, and ceramide can be broken down even further in distinct subcellular compartments for recycling. Upon analyzing all the enzyme isoforms, we noticed a collective reduction of all fatty acid elongation enzymes, consequently leading to *de novo* ceramide production deficit in both neurons and oligodendrocytes. Reduced levels of lysosomal sphingomyelin breakdown enzyme also explained the low ceramide abundance vs. accumulation of long chain sphingomyelins. Although more elaborate biochemical analyses could help further enlightening the details, with this initial study we documented the overall lipid profile in SCA2 nervous tissue for the first time, and identified fatty acid elongase isoforms, which are under control of mTORC1, as the most central factors affected by ATXN2 pathology in various cell types.

All these findings combined, ATXN2 pathology assuredly interferes with a plethora of metabolic pathways in both nervous and peripheral tissues. Rather than the mutant protein selectively targeting a handful of enzymes involved in various pathways, it seems more likely that ATXN2 exerts this modulatory effect by interacting with a master regulator of metabolism, or by interfering with the homeostasis of simplest energetic units, such as acetyl-CoA. For instance, a common reason underlying the NAA and ceramide production deficit could simply be acetyl-CoA deficiency, as it is a building block for both metabolites, as well as thousands of other complex lipids. Although the direct interaction between yeast ATXN2 and mTORC1 orthologs has to be validated in mammalian systems, given its RNA-binding nature, ATXN2 could alternatively modulate mTORC1 function by regulating certain pathway components, the intermediates of which directly signal nutrient availability, such as glycolysis or BCAA degradation. This could explain the vast phenotypic difference between ATXN2 loss and toxicity, and definitely should be addressed in future studies.

3. INTRODUCTION

What an interesting time to do science... Discovery of the DNA double helix in 1953, and initiation of the human genome project in 1990 have paved the way for the identification of countless genetic variations among humans. Some have been fun and interesting, such as *TAS2R38* gene variations leading to "super-tasting" of food and drinks[1], or *ALDH2* variations causing extra blushed cheeks upon alcohol consumption[2], but some discoveries have been devastating, yet crucial for the common good, such as *BRCA1* mutations in cancer[3]. Ever since the discovery of first disease-causing gene *Huntingtin* (*HTT*)[4,5] by positional cloning, countless novel mutations have been emerging every day linked to cardiovascular disorders, developmental problems, metabolic diseases, neurodegeneration and cancer. Moreover, these mutations and the associated signaling cascades inform us about the molecular mechanisms of disease, and help developing a cure for the genetic or idiopathic disorders.

Although recently developed high throughput genome sequencing technologies reveal vast numbers of variations in an unbiased manner, pioneering studies in mutation screening utilized targeted approaches by analyzing pieces of the genome and looking for linkage associations of the marker regions. Expectedly, they first revealed a rather deleterious type of genomic variation – repeat expansion mutations. While investigating the associated locus for spinobulbar muscular atrophy, a dynamic CAG trinucleotide tract on X chromosome corresponding to Androgen Receptor gene was identified as the first example of repeat expansion mutations[6], followed by CAG expansions in *Huntingtin* for Huntington's disease (HD)[5] and *Ataxin-1* (*ATXN1)* in spinocerebellar ataxia type 1 (SCA1)[7]. With a similar approach, Gispert *et al.* aimed to identify the genomic locus associated with a unique type of autosomal dominantly inherited olivoponto-cerebellar atrophy frequently seen in Cuba, that resembles the previously described phenotype of Indian patients[8]. Linkage analyses revealed the significant association of Chr. 12q.24 locus with disease segregation in the Cuban pedigrees[9]. Further investigation of this locus also revealed a CAG trinucleotide repeat expansion in patients, hence naming this newly identified gene *Ataxin-2* (*ATXN2*), responsible for the disease spinocerebellar ataxia type 2 (SCA2)[10–12].

3.1. SCA2 distribution, symptoms and neuropathology

SCA2 belongs to the autosomal dominant cerebellar ataxia (ADCA) group of disorders. Uncoordinated movement, gait ataxia and dysarthria are the major common symptoms for all ADCAs, although some subtypes show various other signs that are used in differential diagnosis[13]. To date, more than 50 types of ADCAs have been identified with distinct genes and/or mutation types responsible. Trinucleotide repeat expansions emerge as a dominating group, underlying more than 25 types of neurological disorders, 8 of which are classified as spinocerebellar ataxia (SCA1, 2, 3, 6, 7, 8, 12, 17)[14]. All ADCAs collectively have an estimated prevalence of 1-5:100.000 worldwide[15,16]. Yet, geographical variability is relatively high for certain subtypes due to founder populations or population growth rate differences. SCA2 is the second most frequent type of ADCAs corresponding to 15% of all the worldwide prevalence, following SCA3 with 21% prevalence. While SCA3 is substantially frequent in Portugal, Brazil and China, SCA2 is more frequent in Cuba, Spain, Italy, Turkey and India[13,15,17–21]. The highest frequency of SCA2 is found in Holguin, Cuba, where more than 1000 descendants of the founder ancestor reside, yielding a 500/100.000 prevalence and an incidence rate of 18 per year[22].

Mean age of disease onset (AO) in SCA2 is 3rd-4th decade of life, although the AO heavily depends on the CAG expansion size and genetic background in terms of other modifying variations. Unusual cases of disease manifestation before 10 years or after 60 years of age have been described. As all repeat expansion-associated disorders, anticipation is an observed phenomenon in SCA2, with increased repeat sizes in consecutive generations resulting in earlier disease onset and a more rapid progression[14,23]. Although the average disease duration is approximately 15 years in SCA2, some extreme cases have also been documented with more than 50 years of survival after disease onset. Various medical and pharmaceutical interventions are being utilized to alleviate the symptoms and provide a more comfortable life to the patients, but currently there is no approved cure targeting the primary cause of the disease. Patients are most often prescribed levodopa, a dopamine precursor frequently used in Parkinson's disease (PD) treatment to relieve the parkinsonism signs, such as tremor and rigidity. Likewise, magnesium supplementation is used to alleviate muscle cramps, and deep brain stimulation was shown to help with postural tremor as in PD[22]. Most recent experimental therapeutic approaches using anti-sense oligonucleotides targeting *Atxn2* transcript to lower the expression of the mutant protein will be discussed below in detail.

Numerous SCA subtypes share common pathomechanisms at the molecular and anatomical levels, although they result from different types of mutations in different genes. Neuronal malfunction in the cerebellum is the most pronounced hallmark of all SCAs, with several other central nervous system (CNS) regions showing differential spatio-temporal pathology in different disease subtypes[24] (**Figure 1**).

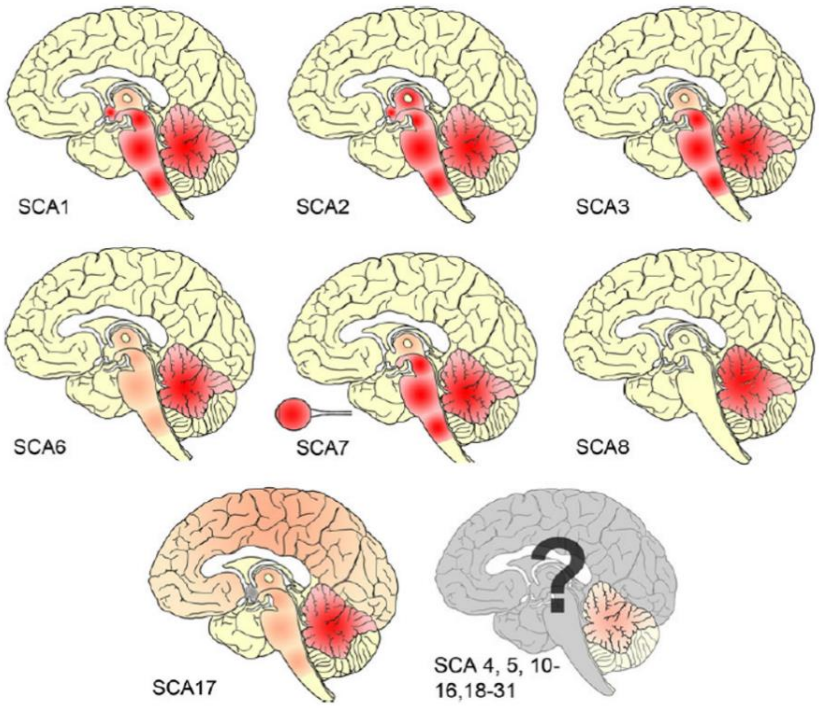

Figure 1: Graphical visualization of the pathology in different SCA types[24]. The affected CNS regions in each disease are highlighted with red color on midsagittal sections.

SCA2 initially manifests with uncoordinated limbs, ataxic gait, and dysarthria, together with tremor and postural rigidity. Early loss of eye saccade velocity is specific to SCA2, and is used for differential diagnosis[8,25]. Later symptoms in disease progression include distal amyotrophy, dysphagia, gastrointestinal and exocrine dysfunction, emotional instability, attention loss and cognitive decline[22]. These symptoms with additional neurological signs progress in time, first requiring special care for the patient, and eventually leading to decease mostly due to respiratory failure. All symptoms put together, frontotemporal cortex, cranial-cervical spinal cord, pons and especially cerebellum are considered to be the main sites of pathology in SCA2 (**Figure 2A**).

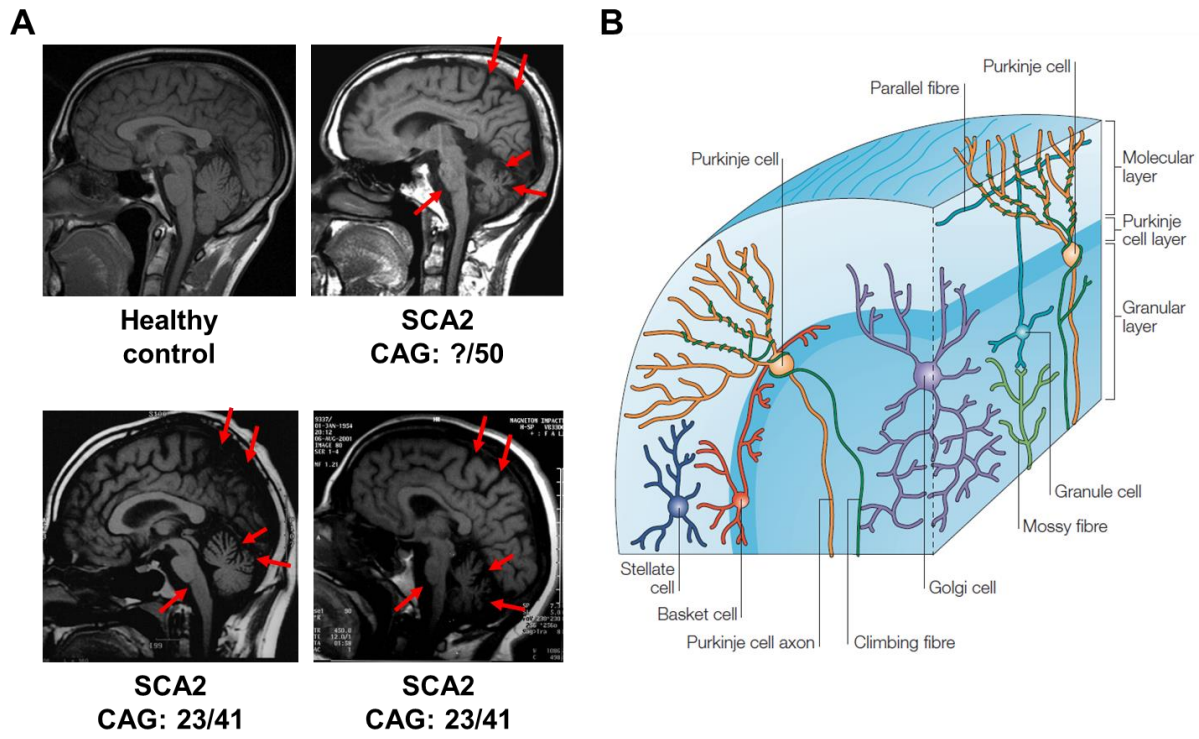

Figure 2: Widespread nervous system atrophy in SCA2. **(A)** MRI scans of a healthy individual and three SCA2 patients from independent studies showing pronounced spino-cerebellar atrophy with cortical degeneration in the midsagittal section. Red arrows point to atrophic regions. *ATXN2*-CAG expansion sizes of the patients are indicated below the images[26–28]; **(B)** Schematic representation of the cerebellar cortex structure and synaptic circuits[29].

Cerebellar cortex is composed of three layers: Molecular layer (ML), Purkinje cell layer (PL) and Granular cell layer (GL)[29] (**Figure 2B**). Purkinje cell somata are located next to each other at PL and extend their dendrites towards ML, where they receive excitatory glutamatergic input from parallel fibers as the axonal projections of granule cells, or climbing fibers as the axonal projections of inferior olivary nucleus in medulla[30]. Climbing fibers convey the information from spinal cord, vestibular system, sensory and motor cortices onto Purkinje cells, and help regulating coordination and motor timing. Inhibitory input towards Purkinje cells are mediated by the GABAergic synapses of Basket cells onto the axon initial segment and by the Stellate cells onto the dendrites[29]. Purkinje cells are the sole output of cerebellar cortex, receiving both excitatory and inhibitory input from different sources, computing the data and providing a cumulative response down to the deep cerebellar nuclei to modulate balance, coordination and movement time, therefore are a very important component of the spino-cerebellar circuitry[29–31].

Post-mortem neuropathology studies suggest that Purkinje cells in cerebellar cortex and motor neurons in spinal cord are the most and earliest affected cell groups in SCA2, followed by decreased volume of the cerebellar granular layer, degeneration of dopaminergic neurons in the midbrain substantia nigra, atrophy of the thalamus and frontotemporal lobe at later stages of the disease[23]. Among the widespread cerebellar degeneration, the remaining Purkinje and granule cells also show abnormal morphology with altered dendritic arborizations, reduced number of dendritic spines and axonopathy[22]. These selectively affected CNS regions and cell types correlate with the early and late symptoms of disease; cerebellar and midbrain degeneration explains the early incoordination, ataxic gait and parkinsonism signs, loss of motor neurons underlie distal amyotrophy, and frontotemporal degeneration with enlarged ventricles correspond to memory problems, cognitive decline and emotional instability.

3.2. Genetics of SCA2, *ATXN2* locus and disease modifiers

The molecular mechanism underlying these early and late aspects of neuropathology is the progressive aggregation of the mutant Ataxin-2 (ATXN2) protein due to the genomic CAG expansion. *ATXN2* gene has 25 exons and covers ~130 kb of nuclear DNA[32]. The CAG tract is located in the first exon, where healthy individuals most commonly have 22 repeats usually interrupted with CAA triplets in the pattern $(CAG)_8$-CAA-$(CAG)_4$-CAA-$(CAG)_8$. Both CAG and CAA triplets code for glutamine (Glu, Q) amino acid, yielding a protein with 22 glutamines in the poly-glutamine (polyQ) domain. SCA2 patients have been found to carry more than 34 repeats with or without CAA units. The interrupting CAA units were argued[33] to have minor effect on the pathogenicity of the mutant protein, since they also code for Q and do not alter the tertiary structure of the polypeptide chain. However, they are beneficial in increasing the structural stability of the genomic locus and reduce the expansion likelihood[34,35]. Some extreme cases with >200 repeats have been identified resulting in fatality before 2 years of age[36,37]. Interestingly, in addition to extra-cerebellar signs such as parkinsonism and lateral amyotrophy observed in SCA2, *ATXN2* expansions are also observed in other spinal cord or midbrain associated disorders like amyotrophic lateral sclerosis (ALS) or PD. Intermediate-length repeats between 27-33 units have been associated with increased risk for ALS[38], and countless more publications have revealed the modifying role of *ATXN2* mutations in various neurodegenerative disorders ever since. Further details regarding the modifying effect of *ATXN2* and its therapeutic implications will be discussed in the coming sections.

Aside from modifier effects in other disorders, CAG repeat length in *ATXN2* also has an impact on AO and disease severity in the context of SCA2. As in all repeat expansion associated disorders, there is an inverse correlation between the expansion size and AO; longer expansions lead to earlier manifestation of the symptoms with a fast progressing disease course[39]. Anticipation between consecutive generations contributes to the AO variation among family members as well. Genomic instability at the CAG tract has been observed more during paternal transmission in SCA2, that could move the AO of the progeny almost 30 years earlier in extreme cases[36].

Although strong correlations between repeat size and AO are established for very large alleles and among family members, a big portion of AO variability among unrelated SCA2 patients carrying the same repeat size is largely unsolved. The AO variation is especially high among individuals with rather short pathogenic alleles between 36-40 repeats. Alleles that are shorter or longer than this interval show a somewhat uniform profile in terms of AO and disease symptoms[11,40–42]. This phenomenon could be explained by the influence of genetic, epigenetic and environmental factors. Initial studies suggested that homozygosity for *ATXN2* CAG expansion had no influence on AO[12]. However, later studies revealed earlier manifestation of the disease and rapid progression in homozygous SCA2 patients[43,44]. PolyQ domain containing proteins are known to interact with each other in aggregates, and numerous CAG expansion mutations in different genes had been described in several subtypes of SCA. Therefore, with the aim of finding genetic modifiers of SCA2 onset and severity, other known ataxia genes with CAG expansions were investigated. Significantly high occurrence of long CAG alleles in *RAI1* and *CACNA1A* genes were observed in SCA2 patients, explaining 4.1% and 5.8% of previously unsolved AO variation, respectively[45,46].

In addition to genetic modifiers, epigenetic modifications have also been found to play a role in disease parameters, and expressivity of the mutation. The promoter region of *ATXN2* contains a CpG island without a TATA box[47]. Hypermethylation of this locus showed high correlation with CAG expansion, which could arise from an autonomic response to shut down the production of the mutant transcript and protein[48]. Indeed, expanded allele specific *de novo* hypermethylation was reported to delay AO and lead to a milder disease progression[49]. Conversely, hypomethylation of this locus was reported to enhance anticipation in a family without a change in CAG repeat number[48].

3.3. *ATXN2* involvement in other neurodegenerative diseases

In an effort to map the interaction network of ataxia-causing proteins, and to reveal a common underlying mechanism, a pioneering study investigated the interaction between 54 proteins involved in 23 types of ataxia via yeast-2-hybrid screening. Eighteen proteins showed either direct or indirect interaction, revealing a common molecular basis for ataxia. In this study, ATXN2 was shown to have a direct interaction with only ATXN1[50]. Further characterization of this relationship validated the physical interaction, revealing that ATXN2 contributes to SCA1 pathology via its sequestration into intranuclear protein aggregates seeded by expanded ATXN1[51]. Increase in ATXN2 transcript and protein abundance was also found to have a modifier effect on AO and disease severity in yet another CAG-associated disorder, SCA3[52]. In addition, SCA3 disease onset and progression profile are influenced by the hypermethylation of *ATXN2* promoter, showing and earlier onset up to eight years[48].

Due to a shared mutation type in polyQ domains, and similarity of the disease signs, many SCA causing proteins were suspected to play a pathogenic role in other closely related disease subtypes. With no surprise, many associations among ataxia proteins have been discovered partially describing the molecular pathomechanism; be it via direct protein interaction, abundance modulation or sequestration. An interesting work by Elden *et al.* revealed a groundbreaking role of ATXN2 in various neuronal maladies, in a way previously overlooked. TDP-43 is a nuclear RNA binding protein (RBP) regulating mRNA processing and stability. Mutations in *TARDBP* gene (encoding TDP-43) cause ALS due to increased aggregation propensity of the protein. However, TDP-43 aggregates are also observed in sporadic form of ALS without an underlying mutation. First establishing the modifier effect of ATXN2 on TDP-43-associated pathology in yeast, a large ALS cohort was genotyped for *ATXN2* CAG repeat expansions; revealing a significantly high occurrence of non-pathogenic "intermediate-length" expansions between 27-33 repeats in ALS patients[38]. Following this study, many ALS cohorts of various ethnical backgrounds have been examined, all supporting the significant association of *ATXN2* intermediate-length expansions with the clinical and molecular parameters of either familial or sporadic ALS[53–58]. In addition, these expansions were documented to co-occur more frequently in *C9orf72* GGGGCC hexanucleotide repeat expansion carriers, which is the most common genetic cause of ALS[59,60].

Following ALS, *ATXN2* expansions were also found as significant risk factors in levodopa-responsive parkinsonism syndromes, although the associated CAG tract range

was larger reaching upto 39 repeats[35,61,62]. Investigation of a hereditary spastic paraplegia cohort revealed that intermediate-length repeat expansions in *ATXN2* influenced the AO and modified disease course[63]. Moreover, CAG expansions of more than 30 repeats in *ATXN2* were also found significantly associated with disease manifestation in progressive supranuclear palsy[64].

Aside from neurodegenerative movement disorders, *ATXN2* genomic locus has also been found associated with psychiatric disease. Psychotic disturbance usually occurs at late stages in SCA2 due to increased psychological burden together with widespread degeneration of the brain. Interestingly, a case study reported prodromal manifestation of paranoid type schizophrenia in an *ATXN2* CAG expansion carrier at the age of 22, who presented first SCA2 signs almost ten years later[65]. Another study revealed the significant association of a non-synonymous single nucleotide polymorphism in *ATXN2* locus with schizophrenia by supposedly increasing the stability of the ATXN2 protein[66].

The most striking discovery regarding the modulatory impact of ATXN2 in neurodegeneration has been made rather recently. Suppression of ATXN2 levels in a strong mouse model of ALS with TDP-43 over-expression rescued the drastic neurological phenotype and remarkably extended the survival from 25 days to over a year[67]. Interfering with ATXN2 levels either via genetic knock-out or postnatal injection of tailor-made anti-sense oligonucleotides (ASOs) showed similar effects, providing the possibility to modulate disease course at pre-onset stage without genetic alterations. The same ASO approach also proved to be immensely beneficial in different mouse models of SCA2[68]. Successful utilization of ASO technology in independent disease models surely raises hopes for the first effective therapy in SCA2, and highlights the importance of ATXN2 as a valuable therapeutic target in multiple maladies.

3.4. Ataxin-2 function, basis of pathology and mouse models

ATXN2 is an evolutionarily conserved ~140 kDa cytosolic protein ubiquitously expressed throughout the body. High ATXN2 expression was found in brain, heart, skeletal muscle, placenta, pancreas and liver[10,12]. In CNS, ATXN2 is strongly expressed in Purkinje cells, spinal cord motor neurons and large neurons of the substantia nigra, moderately expressed in basal ganglia and hippocampus[69]. In contrast to some other types of SCA, nuclear inclusions have not been observed in SCA2, but cytoplasmic aggregates were found throughout the affected CNS regions[70].

Its structure and function has remained relatively unchanged from yeast to humans, although the polyQ domain came into being rather recently in the evolutionary timeline first appearing in the great apes[71] (**Figure 3**). Many of the model organisms widely used in biomedical research contain only one glutamine residue at the polyQ-corresponding site, suggesting that the main function of ATXN2 is not exerted by this domain.

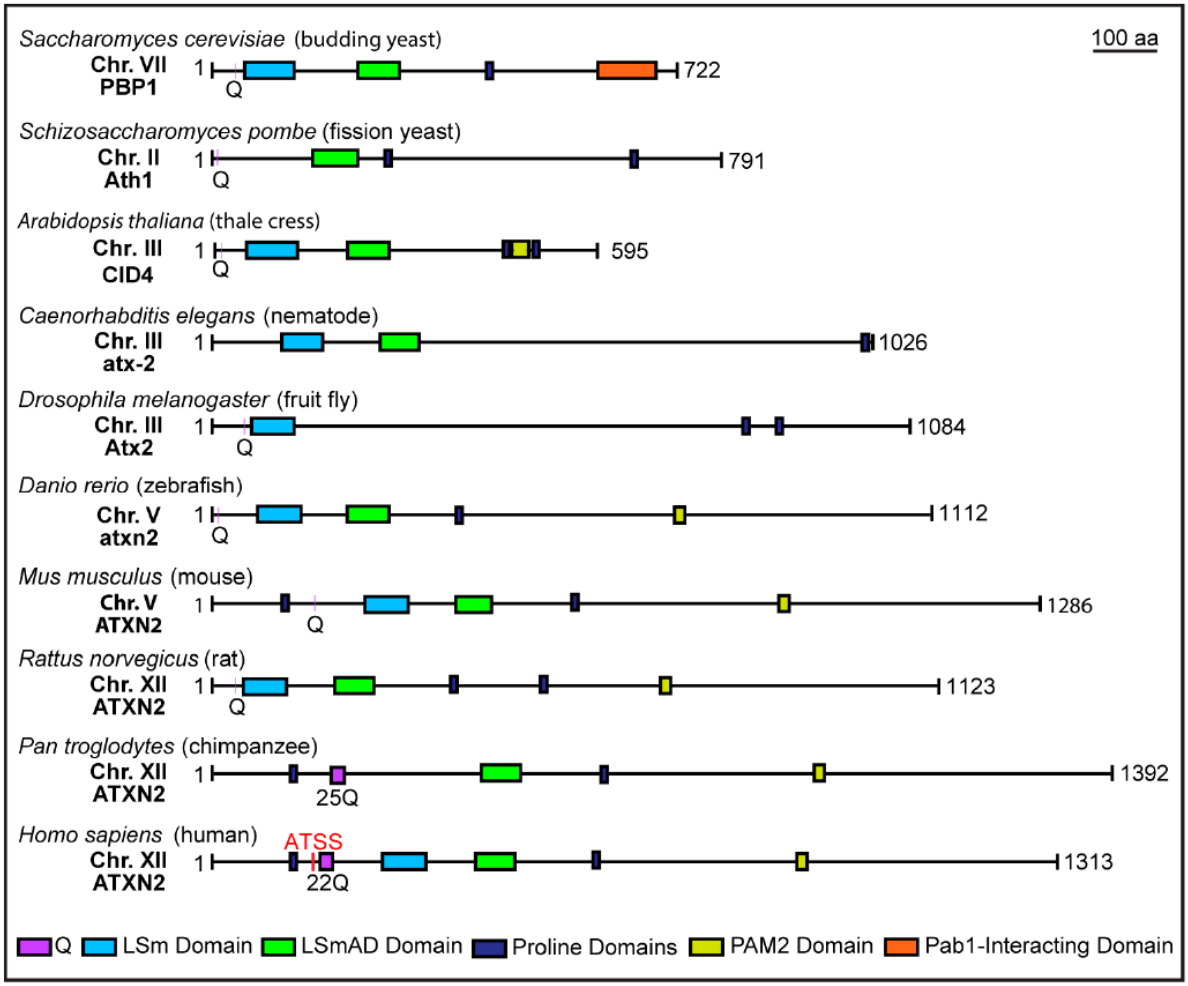

Figure 3: Protein structure of ATXN2 and its orthologs throughout evolution[71]. Diagrams indicate the genomic loci and different names of ATXN2 orthologs in respective species, number of amino acids of each protein, and domain distributions. Conserved functional domains are highlighted with matching colors across species.

Aside from the polyQ domain, ATXN2 contains N-terminal Like-Sm (Lsm) and Lsm-associated domain (LsmAD), C-terminal PABP-interacting motif (PAM2) and multiple proline-rich domains (PRD) scattered around the protein[72]. All, or a large subset, of these domains in ATXN2 are well conserved across species, implying their necessity and importance for a

proper function. Judging by its protein structure and the accumulating experimental evidence over decades, ATXN2 activity can be classified into 3 major aspects: (i) regulation of RNA stability and translation, (ii) modulation of plasma membrane dynamics for nutrient uptake and (iii) polyQ-driven pathogenesis.

Lsm family proteins are collectively involved in RNA metabolism by regulating pre-mRNA splicing, deadenylation-dependent de-capping and mRNA decay in nucleus and cytoplasm[73]. LsmAD domain contains an ER-exit signal and a Clathrin-mediated trans-Golgi signal facilitating the association of ATXN2 with the Golgi apparatus, and their deletion results in altered localization dynamics[74,75]. Direct interaction of ATXN2 with its approximately 7000 RNA targets is suggested to be maintained via Lsm/LsmAD domains[76]. Quite interestingly, this region of the *ATXN2* transcript exactly corresponding to Lsm/LsmAD domains undergoes reverse-splicing to generate a circular-RNA by the well-known splice factor Quaking (QKI) during epidermal-mesenchymal transition in cancer metastasis[77]. Furthermore, ATXN2 ortholog in *C. elegans* was shown to regulate the translational repressor activity of the QKI ortholog during germline maturation[78]. ATXN2 and QKI also share a common protein interaction, namely RNA-Binding-Fox-1-Homolog-1 (RBFOX1; also named ATXN2-binding-protein-1, A2BP1), which is another RNA-binding protein involved in alternative splicing especially during nervous system development and the evolution of human brain[79–82]. Moreover, through its interaction with microRNAs, ATXN2 ortholog in *D. melanogaster* was shown to regulate the translation dynamics of numerous mRNAs, ultimately modulating synaptic plasticity and olfactory habituation[83], shedding more light onto the importance of ATXN2 in RNA dynamics from different perspectives.

Aside from its direct interaction with RNA molecules or other modulatory factors, ATXN2 interacts with the canonical translation machinery through its direct interaction with Poly(A)-Binding-Protein (PABP) via PAM2 motif[84]. This enables the indirect interaction of ATXN2 with a plethora of transcripts and a capability to modulate global translation in a time- and environmental condition-dependent manner. Whether due to direct mRNA interaction via Lsm/LsmAD domains, or indirectly via PABP, ATXN2 associates with the poly-ribosomes contributing to the stabilization of the complex and the target mRNAs[85]. Indeed, the PABP-dependent interaction of ATXN2 ortholog in *S. cerevisiae* with Poly(A)-Nuclease is essential to finetune poly(A) tail trimming to maintain the stability of the complex[86].

The dynamic control of translation machinery and which transcripts are to be actively translated become especially important under stress conditions due to energy constraint. For this, some components of the translation machinery and many redundant transcripts via their interacting RBPs relocalize into cytosolic ribonucleoprotein particles known as stress

granules (SGs). A number of nuclear RBPs involved in RNA splicing and processing also translocate into cytosolic SGs, repressing the maturation and translation of their interacting transcripts. ATXN2 orthologs in different species also localize to PABP-positive SGs under various stress conditions (**Figure 4**), such as heat shock, glucose deprivation, oxidative stress and cytolosic Ca^{2+} imbalance[87–90]. While some studies suggest that the loss of ATXN2 delays SGs formation[67,91], others have found no difference in SG dynamics in its absence[87]. Of note, yeast ortholog of ATXN2 was found to sequester the master growth regulator TORC1 into SGs through direct interaction with the complex component Kog1 (RPTOR in mammals)[89,90,92,93]. Therefore, SGs exert the ultimate outcome of growth arrest under non-permissive conditions by repressing the global translation and sparing the readily available energy for upregulating stress response factors, such as ATXN2 itself[87,94]. However, information regarding the conservation of this TORC1 sequestration mechanism in mammals is currently lacking.

Quite importantly, the association of ATXN2 with SGs is believed to lay the ground for its polyQ-driven pathogenesis. It interacts with a number of ALS-associated proteins in SGs (**Figure 4**), such as TDP-43, FUS, Profilin-1 and TIA1[38,67,95–97], which is believed to underlie its modifier effect. For instance, expansion of the polyQ domain, even to an intermediate size, was shown to increase the cytosolic accumulation of TDP-43, and enhanced its C-terminal phosphorylation and fragmentation as markers of toxicity[98]. Post translational modifications like phosphorylation and ubiquitination occur dynamically in the SGs, and determine the assembly/disassembly of the components. By increasing the retention time of the SGs due to the aggregation propensity of the expanded polyQ domain, mutant ATXN2 leads to aberrant modifications and sequestration of its interaction partners in the SGs, which evolves into massive cytosolic aggregates later in disease progression[98]. Not only in the context of ALS, but also in a SCA2 mouse model with global expression of ATXN2-Q42 (*Atxn2*-CAG42-KIN mouse), chronic sequestration of PABP, as a widely accepted SG marker and ATXN2 interactor, was documented in cerebellum and cortex[99].

Atxn2-CAG42-KIN mouse model was generated by inserting 42 CAG repeats into the corresponding *Atxn2* genomic locus in order to study the disease dynamics throughout the lifespan. Unfortunately, the level of toxicity implemented by the ATXN2-Q42 protein over the two year lifespan of a mouse was insufficient to drive a strong neurological phenotype, even at a very old age[99]. Several other SCA2 mouse models with transgenic over-expression of the mutant protein have also been generated[70,100–104], but due to the targeted expression of the transgene only in Purkinje cells, they have only been useful in dissecting a restricted portion of the neuronal excitation deficits, and not so much of the native ATXN2 function.

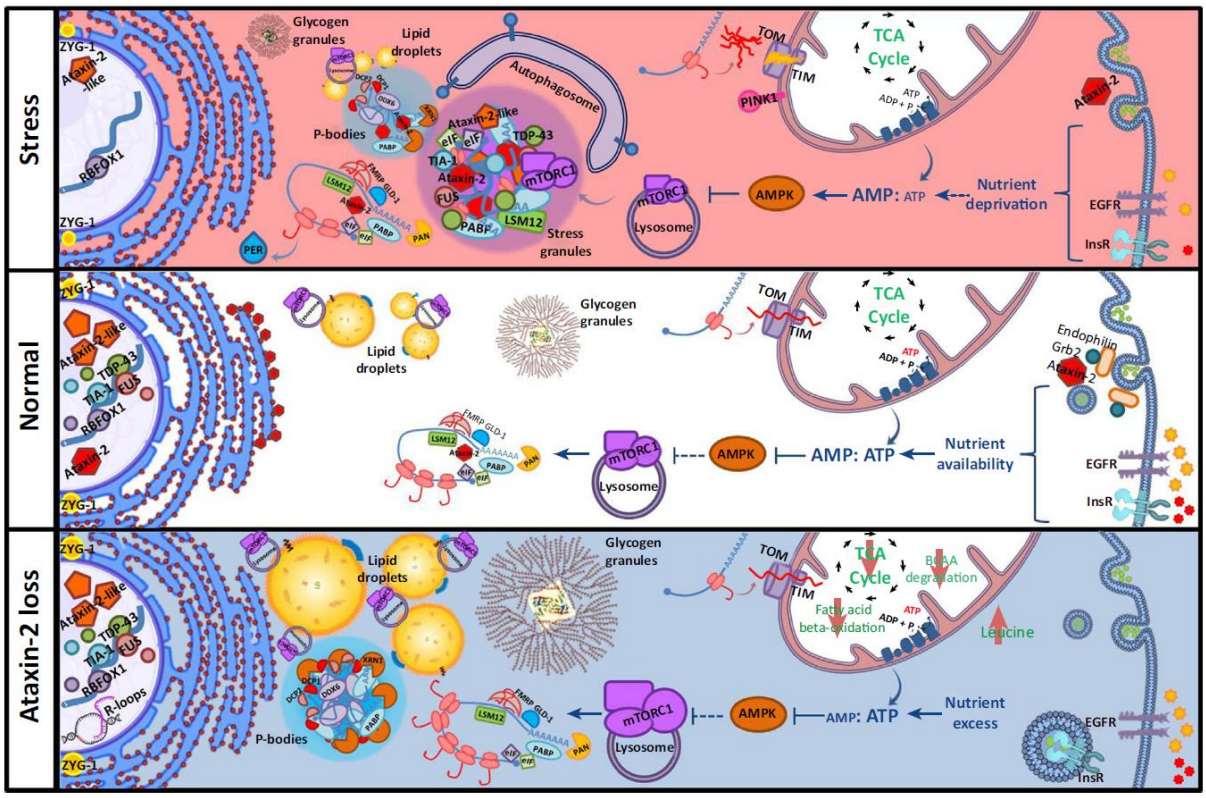

Figure 4: Schematic representation of ATXN2-associated mechanisms[72]. Subcellular localization of ATXN2 and its interactions partners under normal, stress and ATXN2-loss conditions are depicted.

Numerous studies employed yeast and mammalian cell culture systems, and demonstrated the association of ATXN2 with polysomes on the rough-ER[105], and its physical interaction with SH3-domain containing proteins, such as endophilin A1/A3[84,106] and Grb2/Src[106,107], through multiple PRD domains (**Figure 4**). Through its association with endophilins, that are involved in vesicle endocytosis machinery, ATXN2 was shown to regulate the internalization dynamics of epidermal growth factor receptor (EGFR)[106]. Aside from the disease models, *Atxn2* knock-out mouse (*Atxn2*-KO) was generated to examine the physiological function of the protein, and quite intriguingly complete loss of ATXN2 caused no neurological deficit or ataxic signs in mice, but led to an early-onset progressive weight gain, and eventually insulin resistance with diabetes[108]. Enlarged lipid droplets and glycogen granules in *Atxn2*-KO mice tissues contrasted with the atrophic nature of SCA2, and pointed out to a metabolic switch that depends on ATXN2 loss vs. toxicity. For instance, increased mTORC1 activity was observed in *Atxn2*-KO cells under mild growth factor deprivation[87], contrary to its sequestration into SGs and repression in normal cells (**Figure 4**). Global proteome analysis of *Atxn2*-KO liver revealed significant reductions in branched chain amino

acid (BCAA) and fatty acid degradation pathways[109], in agreement with the increased peripheral BCAA levels observed in obesity[110]. A similar approach studying the proteome of ATXN2-deficient yeast under different stress conditions also detected dysregulations in numerous metabolic pathways, like glycolysis, TCA cycle, oxidative phosphorylation and amino acid degradation[94]. Considering the fact that SGs form under various non-permissive conditions all converging onto energetic deficit eventually, association of the SG component ATXN2 with plasma membrane endocytic machinery and also with the downstream translation machinery neatly links these two seemingly separate cellular compartments together and conveys stress signals in a direct route.

Overall, the involvement of ATXN2 in general nutrient metabolism and stress response control has been established rather later than its function as an RNA-binding protein and a regulator of global translation. Therefore, many of the metabolic outcomes remained under-studied in ATXN2-dependent disease, although the aggregation-associated aspects have been thoroughly examined, failing to identify a certain pathway for therapeutic manipulation. Instead, ATXN2 itself was targeted with anti-sense oligonucleotides in the only promising rescue study conducted so far. Given the plethora of metabolic alterations towards excess fat accumulation, obesity and diabetes observed in *Atxn2*-KO mouse, opposed to the overall atrophic phenotype observed in disease, it is highly likely that the therapeutic benefit of diminishing ATXN2 expression in neurological disease comes from this metabolic switch. Furthermore, the most affected neuron types in the CNS from ATXN2 pathology are known to be cerebellar Purkinje cells and spinal cord motor neurons. Despite their spatial distance, both are among the largest neurons in the CNS with massive dendritic and axonal extensions, and an enourmous metabolic burden due to excessive need for protein synthesis, quality control, transport and proper degradation, all the while responding to constant synaptic stimulus. Therefore, impaired metabolic/autophagic homeostasis naturally affects these larger neurons to a greater extent. Hence, it becomes exceptionally important to dissect the metabolic dysregulations in SCA2 to get a complete overview of the disease mechanism, and not only in the brain, but throughout the body.

4. AIM

In order to unravel the metabolic burden of ATXN2 pathology in disease we addressed several central questions as follows:

Publication #1:

(i) How is the blood transcriptome, as a readout of the peripheral alterations, dysregulated in disease? Could it be used to establish molecular blood biomarkers to measure disease progression or the beneficial value of a future therapy in individuals?

(ii) How would the newly defined relationship between ATXN2 and PINK1 levels in blood functionally relate to the global control of growth vs. death decision?

Publication #2:

(iii) Generation and characterization of the first authentic SCA2 mouse model (*Atxn2*-CAG100-KIN) at the genetic, behavioral, histological and molecular levels.

(iv) How is the brain metabolism altered in *Atxn2*-CAG100-KIN mouse? Which enzymes could be responsible for the observed metabolite dysregulations, and which enzyme is altered first in the disease progress?

Publication #3:

(v) How do the lipid profiles of cerebellum and spinal cord change in *Atxn2*-CAG100-KIN mouse; what are the common aspects between two tissue types? Are these also observed in SCA2 patient material?

(vi) Which enzymes could be responsible for the observed metabolic dysregulations? In addition to single enzymes, which parts of the complex lipid metabolism network is collectively affected in *Atxn2*-CAG100-KIN spino-cerebellar tissue?

All together, does ATXN2 pathology target certain pathways, or have a more global impact due to interfering with most basic metabolites and/or signaling cascades?

5. RESULTS AND DISCUSSION

5.1. ATXN2 involvement in regulation of growth

Two faces of the ATXN2 gain-of-function vs. loss-of-function coin has been established: atrophy vs. obesity. However, the molecular mechanisms underlying either outcome, and how they are regulated by ATXN2 were yet to be defined. While *Atxn2*-KO mice were being investigated for the obesity-associated aspects, studying the ATXN2 expansion-driven peripheral atrophy has been more challenging due to the lack of a mouse model presenting such phenotype. Overcoming the necessity for an animal model, a high-throughput RNA-sequencing (RNA-seq) analysis using SCA2 patient blood samples was performed in order to understand the peripheral impact of ATXN2 pathology, and in hopes to identify biomarkers to monitor disease progression[111].

Gene Set Enrichment Analysis of the expression data revealed numerous significantly altered pathways highly associated with known ATXN2 function, such as a downregulation in generic transcription pathway, and upregulations in mRNA translation and stability regulation pathways, and ER-Golgi associated pathways. Quite interestingly, *KEGG_Parkinson's disease* and *KEGG_Huntington's disease* pathways were also found upregulated, potentially indicating mitochondrial dysfunction, which is a common aspect of various neurodegenerative disorders[112], for the first time in SCA2. In light of the *ATXN2* intermediate length expansion involvement in PD pathogenesis, the pathway components were examined in detail, revealing significantly increased transcript abundance of *PINK1* (PTEN-induced kinase-1), an autosomal recessive PD gene, in SCA2 blood.

Further investigation of *Pink1* transcript levels in *Atxn2*-KO mouse cerebellum and liver showed decreased levels in contrast to patient data. Given that *PINK1* is transcriptionally induced under stress, especially nutrient deprivation[113], the increased *PINK1* abundance in highly atrophic SCA2 patient tissue with enhanced autophagy versus decreased *Pink1* abundance in obese *Atxn2*-KO mouse tissue with excess accumulation of nutrients represents a strong correlation between PINK1 activity, therefore mitochondrial dysfunction, and ATXN2.

PINK1 is a Serine/Threonine kinase responsible for mitochondrial quality control and elimination of dysfunctional mitochondria via targeted autophagy, namely mitophagy[114]. Autosomal recessive mutations in *PINK1* causing a loss of normal protein function leads to juvenile onset PD[115] due to the accumulation of dysfunctional mitochondria and increased oxidative stress mainly affecting midbrain dopaminergic neurons[116]. Upon activation, PINK1

phosphorylates and activates the ubiquitin ligase PARKIN, another autosomal recessive PD gene, facilitating the successful elimination of dysfunctional mitochondria[114]. Aside from their involvement in PD, PINK1 and PARKIN are also investigated in the context of cancer due to their modulatory effect on metabolic control and tumor suppression[117]. Over-expression or increased activity of the major tumor suppressor protein Phosphatase-And-Tensin-Homolog (PTEN) leads to increased *PINK1* expression in various cancer types[118]. PTEN is a phosphatase suppressing the canonical growth factor signaling by counteracting the PI3K (phosphoinositide-3-kinase)-dependent phosphorylation of phosphatidylinositol-4,5-bisphosphate (PIP_2) into phosphatidylinositol-3,4,5-trisphosphate (PIP_3) at the plasma membrane. In the presence of growth factors, PIP_3 production activates Protein Kinase B (Akt/PKB), the central hub in growth factor signaling, that further activates mTORC1 and enhances anabolic activity[118]. In parallel to its function in mitochondrial clearance, PINK1 was also shown to activate Akt, leading to increased anaerobic glycolysis over mitochondrial respiration, known as the Warburg effect in cancer[119]. Therefore, modulating PINK1 level or activity has been proposed as a therapeutic approach in cancer[120,121].

Strikingly, increased *ATXN2* expression was also evident in pro-apoptotic neuroblastoma cells and tumors, and the forced over-expression of ATXN2 sensitized therapy-resistant neuroblastoma cells to apoptosis[122]. Furthermore, suppression of ATXN2 levels with anti-sense oligonucleotides (ASOs) in mouse models of ALS and SCA2 showed immense benefit regarding motor function and survival[67,68]. Considering the obesity and excess nutrient storage phenotype in *Atxn2*-KO mice due to the hyperactivation of PI3K-Akt-mTORC1 siganling axis, ATXN2-dependent modulation of either carcinogenesis or neuropathology potentially targets the same core metabolic pathway.

Although neurodegeneration and cancer seem to be two distinct ends of the disease spectrum, at the heart of both lies the same crucial molecular decision: survival vs. death. While the molecular signature of disrupted metabolic control, mitochondrial dynamics and proteostasis drives post-mitotic neurons towards apoptosis, actively proliferating cancer cells benefit from excess growth factor pathway stimulation[118]. And in both disorders, ATXN2 and PINK1 seemingly have a common influence on the regulation of growth vs. death. Both proteins are stress response factors trying to ensure survival under nonpermissive conditions, and the recent findings revealed their molecular connection showing that PINK1 levels are modulated depending on ATXN2 gain or loss of function. All in all, not only the assessment of *ATXN2* or *PINK1* levels in patient tissue could be informative regarding the trophic state, but also the careful modulation of either factor holds great promise for alleviating signs of neurodegenerative disease or cancer.

5.2. An authentic mouse model of SCA2: first molecular findings

Readily available mouse models of ATXN2 pathology, which are largely based on the over-expression of the mutant protein specifically in Purkinje neurons, have been instrumental in understanding cell-autonomous aspects of the disease only in cerebellum, such as the dysregulations in Ca^{2+} spikes and neuronal excitability[100–103,123]. However, they fell short in explaining extra-cerebellar involvement, such as that of spinal cord, or the contribution of other cell types in the central nervous system. The first knock-in (KIN) mouse with 42 CAG repeats inserted into the corresponding genomic locus in *Atxn2* (*Atxn2*-CAG42-KIN) was generated by our group, and has been helpful in dissecting several more general pathomechanisms including the sequestration of PABP by ATXN2-Q42 into insolubility[99], induction of the ubiquitin ligase complex member FBXW8 to degrade ATXN2-Q42[124], and partial loss of function profile exerted by ATXN2-Q42 in the cerebellum on the regulation of Ca^{2+} homeostasis factors[125]. However, endogenous expression of ATXN2-Q42 was not sufficient to drive a strong aggregation pathology and manifestation of severe neurological signs within the approximately two year long lifespan of a mouse[99], making it unsuitable to study the terminal phase of the disease.

Thanks to the tireless efforts of many former and current members, our lab generated the first authentic mouse model of ATXN2 pathology with 100 CAG repeats inserted into the *Atxn2* genomic locus (*Atxn2*-CAG100-KIN)[126]. The expanded *Atxn2* gene contains the intact murine promoter and exon-intron structure, and is under endogenous expression control. Longitudinal monitoring of the *Atxn2*-CAG100-KIN animals in terms of genetic stability of the expansion, survival, weight profile, motor behavior, neuropathology and *in vivo* brain imaging showed strong, if not perfect, correlation to what is observed in SCA2 patients for the same criteria. To begin with, CAG repeat sizes in actively dividing somatic cells usually show an increase over time and a mosaic pattern in patients[40]. Such an observation of genetic instability has not been reported for the previous over-expression or CAG42 knock in models of SCA2, but enlargement of the repeat size in successive generations and somatic mosaicism was observed in *Atxn2*-CAG100-KIN animals resembling the patients.

An important and devastating aspect of SCA2, like many other neurodegenerative maladies, is the shortened lifespan due to progressive atrophy and multi-system failure[23]. Heterozygous and homozygous *Atxn2*-CAG100-KIN animals were monitored regularly over months in terms of total weight that indicates the peripheral atrophy, and of motor function that indicates the progression of the disease, therefore neuronal atrophy. Severe motor deficits and weight loss observed in homozygous *Atxn2*-CAG100-KIN animals at 14 months

of age mandated sacrifice in order to avoid suffering, therefore establishing the survival rate of this model upto 14 months which corresponds to the half of normal lifespan. Even at earlier ages, homozygous *Atxn2*-CAG100-KIN animals displayed significantly higher number of deceased cases due to unknown reasons. Weight profiles were examined for male and female animals separately, revealing a very interesting difference at earlier stages of the disease: male *Atxn2*-CAG100-KIN animals continuously displayed reduced weight compared to their age- and sex-matched controls throughout lifespan, however female *Atxn2*-CAG100-KIN animals initially displayed increased weight in comparison to the WT animals upto 6 months of age, and then showed a radical shift towards weight loss, reaching a significant reduction by 9 months and progressively decreasing until the terminal stage. In addition, the number of mutant female offspring was significantly less than expected for Mendelian inheritance.

Behavioral assessments to measure motor coordination on a rotating rod showed a significant deficit in *Atxn2*-CAG100-KIN animals starting from 5-6 months of age irrespective of gender, progressively worsening until 14 months. When left free in an open field, *Atxn2*-CAG100-KIN animals initially showed increased activity around 2-3 months of age, which drastically reverted to a reduced activity phenotype by 5-6 months. The vertical movements (balancing upright for exploration or seeking food) were affected more severely from the disease progression than horizontal movements, mirroring the gait ataxia in SCA2 patients. The important hallmarks in motor phenotype, i.e. the pre-onset “hyper-activity” period around 3 months, first appearance of disease signs by 6 months and terminal phase of 14 months, substantially coincided with important time points in the weight profile of female animals. Given the fact that *Atxn2*-KO colony (i) has an increased weight phenotype, (ii) has shown reduced number of mutant female offspring, and (iii) displayed motor hyper-activity in open field tests[108], the pre-onset stage in *Atxn2*-CAG100-KIN lifespan seems to exert a loss of native ATXN2 function effect at the phenotypic level especially in females. Quite interestingly, this initial increase in body weight followed by a rapid decrease was also documented in SCA2 families, further strengthening the authenticity of this mouse model[127].

In accordance with the severely reduced body weight and motor function at the terminal stage, whole brain size also showed a significant reduction in both genders. Histological assessment of ATXN2 distribution throughout the CNS revealed its normal expression in various regions, such as cerebral cortex, ventral forebrain, hippocampus, brainstem, cerebellum and spinal cord. Aggregate formation in *Atxn2*-CAG100-KIN tissue was observed in most of the studied regions at 14 months, which was especially noteworthy in cerebellum, brainstem and spinal cord, revealing a classical olivo-ponto-cerebellar atrophy

pattern well documented in patients[72]. The involvement of spinal cord dysfunction is also crucial, since the motor neuron associated signs, such as muscle cramps and impaired conduction velocity caused by axon demyelination and loss of subcutaneous fat, appear even earlier than cerebellar ataxia in SCA2 patients[72].

In cerebellum, the aggregation dynamics of ATXN2-Q100 protein, and its potential sequestration of PABP as reported earlier for ATXN2-Q42[99] were investigated at pre-onset, symptomatic and terminal stages. Across all ages, both ATXN2 and PABP showed a diffuse distribution in WT Purkinje neurons. At the pre-onset stage of 3 months, ATXN2-Q100 partially showed a diffuse distribution, and partially localized in small cytosolic foci negative for PABP signal. At the symptomatic stage of 6 months, cytosolic foci became larger sequestrating most of the diffuse ATXN2-Q100 pool, and occasionally showed PABP positive signal indicating the commence of its sequestration. At the terminal stage of 14 months, ATXN2-Q100 aggregates were very large, had sequestrated substantial amount of the soluble protein, localized towards the initial segment of primary dendrite, and were PABP positive. Indeed, the isolation of expanded protein from cerebellum at this age for immunoblots proved to be a daunting task; only a very small fraction of ATXN2-Q100 protein could be recovered from the cytosolic fraction, which showed a strong decrease in abundance compared to WT animals. The insoluble protein fraction supposedly containing aggregates and heavy structural complexes, although treated with high detergent concentrations and reducing agents, could not solubilize the ATXN2-Q100 protein from the cerebellar aggregates at 14 months. On the other hand, expanded *Atxn2* transcript showed a subtle reduction in cerebellum at 3 months of age (down to 87%), mildly decreasing at 6 and 14 months (to 85% and 70%, respectively).

Different clones of primary murine embryonal fibroblast (MEF) cultures were prepared from WT and *Atxn2*-CAG100-KIN embryos to further characterize the expanded transcript and protein characteristics *in vitro*. In actively dividing cells, expanded *Atxn2* transcript showed a stronger decrease (to 50%) than the nervous tissue expression, and a very prominent deficit at the protein level (down to 10%). Immunocytological assessment of the normal and ATXN2-Q100 protein showed similarly diffuse cytosolic distribution under normal conditions in WT and *Atxn2*-CAG100-KIN MEFs, yet the ATXN2 signal in KIN cells was visibly weaker in line with the reduced protein expression. The stress response capacity of the ATXN2-Q100 protein was found intact: upon oxidative stress induction with sodium arsenite, both normal and ATXN2-Q100 proteins relocalized into cytosolic stress granules (SGs) together with PABP. Quantification of the global protein synthesis rate in *Atxn2*-CAG100-KIN MEFs showed no significant difference compared to WT cells, indicating that

the severe reduction in ATXN2-Q100 levels is a specific regulation of the mutant protein, but not a general translational malfunction of the KIN cells.

In sum, the expansion reduced soluble ATXN2 levels in peripheral cells and nervous tissue. While the actively dividing cells did not show cytosolic foci, post-mitotic neurons displayed a progressive aggregation process starting earlier than the first disease signs appear. Such reduced expression and diffuse distribution of other polyQ-related ataxia proteins have been reported before[128,129], where the aggregate formation was only observed upon neuronal differentiation and glutamatergic stimulation in cell culture. These reports are in excellent alignment with our findings. Moreover, the severely reduced peripheral expression of ATXN2-Q100 could also explain the initial "KO-like" phase observed in *Atxn2*-CAG100-KIN animals in terms of embryonal anomalies leading to reduction in female offspring, weight gain and short term motor hyper-activity.

Establishing the authenticity of *Atxn2*-CAG100-KIN model at the genetic, behavioral and neuropathological levels, we aimed to study the metabolic state of the brain *in vivo* by quantifying the established biomarkers in patient studies[130] and other spinocerebellar ataxia models[131,132]. Nuclear magnetic resonance (NMR) imaging has been extensively utilized to measure abundant brain metabolites, such as glutamate, N-acetylaspartate (NAA), choline and creatine, in a myriad of maladies. NAA is the second most abundant metabolite in the CNS, after glutamate, and gives the largest peak in spectrograms. The N-terminal acetylation of aspartate amino acid yields NAA, which occurs mainly in neurons. Therefore, its deficiency has been established as a reliable biomarker of neuronal loss of malfunction in various neurological disorders without a complete understanding of the underlying molecular mechanism. Still, the main purpose of NAA production has been determined as stocking transportable acetyl-CoA units for energy storage, myelination and utilization in post-translational acetylation of proteins[133–135]. It has been proposed that acetyl-CoA stored in the form of NAA in the CNS is the equivalent of triglycerides constituting the stored energy in the adipose tissue[134,136]. Likewise, glutamate is also an important energy unit fundamentally associated with the core metabolic pathways, such as the TCA cycle, next to its function as an excitatory neurotransmitter[137]. NMR spectroscopy revealed a significant reduction in NAA and glutamate levels in *Atxn2*-CAG100-KIN cerebellum at the terminal stage of disease as expected, and decreased choline levels with a trend towards significance. All three metabolites also showed prominent reductions in cerebrum, which failed to reach statistical significance due to high variation among WT samples. All together, the data once again confirmed the authenticity of this model in possessing yet another aspect of the disease, and pointed out to a drastic energy deficiency in the brain. Glutamate and NAA, and many of the

other important intermediates for a proper nervous function, such as acetate, oxaloacetate and α-ketoglutarate, are all intertwined in an intricate biochemical network and can be converted into one another[138]. Previous findings revealed dysregulations in α-ketoglutarate metabolism, TCA cycle, fatty acid beta-oxidation and branched-chain amino acid degradation pathways caused by ATXN2 loss in different model organisms[94,109], strengthening the possibility of a direct ATXN2 involvement in the disruption of brain metabolic balance.

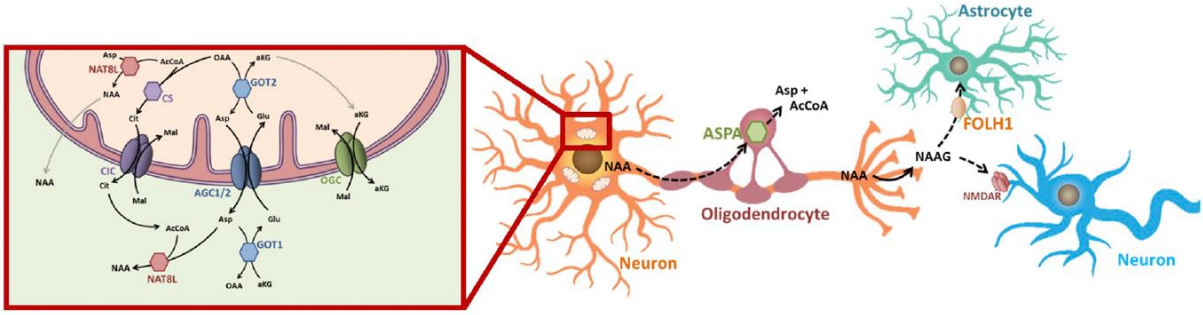

Figure 5: Schematic representation of NAA metabolism[126]. It is produced by NAT8L in neurons, then transported and broken down in oligodendrocytes by ASPA. Its modified version NAAG is alternatively used in synaptic modulation controlled by astrocytic FOLH1 enzyme.

Neuronal N-acetylation of aspartate to produce NAA is performed by N-acetyl-transferase-8-like (NAT8L) enzyme, following which NAA is either transported into oligodendrocytes to be utilized in myelination or further modified into NAAG (N-acetylaspartylglutamate) metabolite and exported into the synaptic cleft for excitatory modulation[139] (**Figure 5**). Its breakdown into aspartate and acetyl-CoA is catalyzed by the oligodendroglial enzyme Aspartoacetylase (ASPA). In the synapse, NAAG is recognized and internalized by the astrocytic receptor Folate Hydrolase 1 (FOLH1/GCPII)[140]. Examining the expression levels of these key enzymes at pre-onset, symptomatic and terminal phases showed progressive dysregulation for all factors in *Atxn2*-CAG100-KIN cerebellum. However, *Folh1* upregulation only started in the terminal stage, *Aspa* downregulation was first evident in the symptomatic phase, and only *Nat8l* expression was found significantly altered at the pre-onset stage progressively decreasing throughout the disease course. NAT8L and ASPA findings were also validated at the protein level, suggesting a chronological chain of events starting with neuronal NAT8L dysfunction, NAA production deficit, oligodendroglial ASPA downregulation due to lack of need, and finally astrocytic FOLH1 upregulation to suppress terminal stage glutamatergic excitotoxicity. Investigation of

additional enzymes involved in aspartate, glutamate, oxaloacetate, a-ketoglutarate, citrate and malate interconversion, and mitochondria-cytosol shuttling only showed minor dysregulations in these pathways, suggesting that the problem lies specifically with NAT8L and NAA production. Hence, the significant deficit in NAA production, and NAA levels *per se*, possibly indicate a prominent myelin loss in *Atxn2*-CAG100-KIN mice, which could explain the strong weight reduction of the brain discussed earlier. In agreement with this notion, SCA2 patients with large ATXN2 expansions displayed myelination defects with widespread leukoencephalopathy in imaging studies[141].

Aside from the loss of myelin fat in the brain, ATXN2-Q100-dependent decrease in NAT8L function could also shed light on the progressive loss of peripheral fat stores due to the regulatory function of NAT8L in white and brown adipose tissue[135,142]. In order to test if *Nat8l* mRNA levels are affected by ATXN2-Q100 pathology also during adipogenesis, WT and *Atxn2*-CAG100-KIN MEFs were subjected to an adipogenic differentiation protocol[143]. While *Nat8l* expression increased significantly in WT cells upon adipogenic stimulus in agreement with its vast importance for this process, *Atxn2*-CAG100-KIN cells failed to enhance *Nat8l* levels under the same conditions. Furthermore, *Nat8l* expression was found significantly decreased in the adipose tissue of *Atxn2*-CAG100-KIN mice, and strikingly also in blood samples from *Atxn2*-CAG100-KIN mice and SCA2 patients. Taken together, the data suggest a direct impact of ATXN2-Q100 pathology on *Nat8l* transcript abundance in various tissues. Continuous *Nat8l* decrease observed in the nervous tissue in parallel to disease progression, and its widespread expression throughout the body demonstrates its value as a potential biomarker to measure the level of ATXN2 toxicity in easily accessible patient materials, such as blood. This notion, and the relevance of *Nat8l* dysregulation in other ATXN2-associated neurodegenerative disorders, such as ALS and Parkinsonism, will have to be examined in future studies.

In conclusion, a much needed authentic model of ATXN2 expansion with strong resemblance to SCA2 patients in terms of lifespan, motor dysfunction, neuropathology and neurometabolism has finally been generated. This model holds the great advantage of dissecting the earliest aspects in disease pathogenesis and measuring the longitudinal effects of ATXN2 toxicity throughout the organism. The first molecular analyses revealed a general energy shortage in the brain with a pronounced early-onset deficit in NAA production, which explained the progressive loss of lipid mass in the nervous tissue and in the body. These findings could pave the way for the establishment of peripheral prognostic biomarkers to assess the disease status and the effect of therapeutic interventions in the future.

5.3. Spinocerebellar lipid profile of SCA2 in mice and men

The involvement of ATXN2 in metabolism has become more intriguing since the first authentic model of the disease revealed energetic dysfunction preceeding the aggregation pathology and neurological signs. Besides the established effect of ATXN2 loss on various metabolic pathways, the earliest markers of expanded ATXN2 pathology also being associated with nutrient and especially lipid metabolism urged us to study the underlying mechanism in further detail. Comparing the lipid profiles of SCA2 patient *post mortem* cerebellar tissue with that of *Atxn2*-CAG100-KIN mouse cerebellum and spinal cord revealed common dysregulations in important lipid groups such as ceramides and sphingomyelins. Investigation of the associated pathways involved in synthesis or breakdown of these lipids in mouse tissues highlighted “hot spots” of molecular disruptions possibly causing such outcomes[144].

First, the cerebellar lipid profiling of a female European SCA2 patient (ATXN2 repeats: 22/52; death at 26 years) was performed with thin layer chromatography in comparison to two age- and sex-matched controls (death at 21 years due to primary lung fibrosis; death at 23 years due to colitis ulcerosa). Strong reductions in sulfatides (down to 17%), galactosylceramides (to 25%), cholesterol (to 40%) and long chain sphingomyelins (that consist of 22- or 24-carbon long fatty acid chains; to 44%) displayed a massive loss in the oligodendrocyte compartment, as all these lipid species are known to be enriched in myelin sheath[145,146]. Short chain sphingomyelins (with C18 fatty acids), representative of the neuron enriched grey matter, did not show a difference in abundance. Among gangliosides, significant reductions were observed in GM1a (to 63%) and GD1b (to 61%) levels. GM1a reduction especially represents and interesting finding, as it can be both neuronal and oligodendroglial, normally localizes to paranodes between myelin blocks on the axon and its abundance normally increases with age in mouse brain due to increased myelin mass and neuron-myelin contact[145–147]. The significant decrease in free fatty acid levels (to 77%) indicates an overall reduction in lipidogenic capacity of the SCA2 cerebellum starting from the most basic metabolites, in line with our previous findings in *Atxn2*-CAG100-KIN cerebellum. Yet, the lack of a dysregulation in short chain sphingomyelins and some ganglioside species (GD1a, GT1b) suggests that the neuronal compartment is capable of compensation in terms of general structural lipids. However, the myelin lipid composition or neuron-myelin interaction sites seem to be affected the most from ATXN2 pathology in agreement with the demyelination observations in SCA2 patients[23,25,148].

Due to the scarcity of patient samples fit for molecular analyses, and the inevitable variations in genetic background, environmental factors throughout life, sample collection and storage, we proceeded our analyses in *Atxn2*-CAG100-KIN mouse. A large number of metabolites were measured by quantitative mass spectrometry in cerebellum and spinal cord tissues at the terminal disease stage of ~14 months. Consistent with the patient data, both *Atxn2*-CAG100-KIN cerebellum and spinal cord tissues showed reduced abundance of ceramide species independent of fatty acid chain length. Sphingosine is another precursor of ceramide, and phosphorylated sphingosine levels were also found downregulated in *Atxn2*-CAG100-KIN cerebellum. Interestingly, sphingomyelin species showed a differential dysregulation depending on the fatty acid chain length as observed in SCA2 cerebellum. Several neuron-associated short chain sphingomyelin species (with C12-22) were found significantly increased in *Atxn2*-CAG100-KIN mouse cerebellum, whereas myelin-associated long chain sphingomyelin species (with C24-26) showed a collective decrease, in agreement with previous findings in ALS patients[149,150], once again reflecting a stronger impact of the ATXN2 pathology on lipid metabolism in the myelin compartment. The consistent accumulation of shorther chain sphingomyelins in parallel to a collective decrease in long chain species could stem from an enzymatic deficit during the elongation step of fatty acid synthesis or in any of the consecutive pathways of the ceramide-sphingomyelin metabolism.

Ceramides play a central role in the vastly elaborate lipid turnover network and can be acquired via direct *de novo* biosynthesis or through breakdown of the more complex sphingomyelins[145]. The *de novo* synthesis exclusively takes place in the ER, starting with the Serine Palmitoyltransferase enzyme complex (SPT) utilizing a palmitoyl-CoA and L-Serine to produce 3-keto-sphinganine, which is reduced to dihydrosphingosine. Afterwards, Ceramide Synthase (CERS) attaches fatty acid chains onto the sphingosine backbones, generating dihydroceramides which are passively transformed into ceramide. After their synthesis, ceramides are transported to the plasma membrane via Golgi apparatus. They can be further utilized to synthesize sphingomyelins by Sphingomyelin Synthase (SMS) to be incorporated into the membrane lipid bilayers. Inversely, membrane-associated sphingomyelins can be broken down to yield ceramides by Sphingomyelinases (SMase) in various subcellular compartments such as the plasma membrane, trans-Golgi network, lysosomes and mitochondria. Consecutively in all these organelles, and also in the ER, ceramides can be further broken down to dihydrosphingosine and fatty acid subunits by Ceramidases (ACER or ASAH) for metabolic turnover upon need. Various isoforms of SMase and ACER/ASAH enzymes that function under distinct pH conditions exist in different organelles[151]. A schematic representation of the examined pathway components with their respective subcellular site of action is depicted in **Figure 6**.

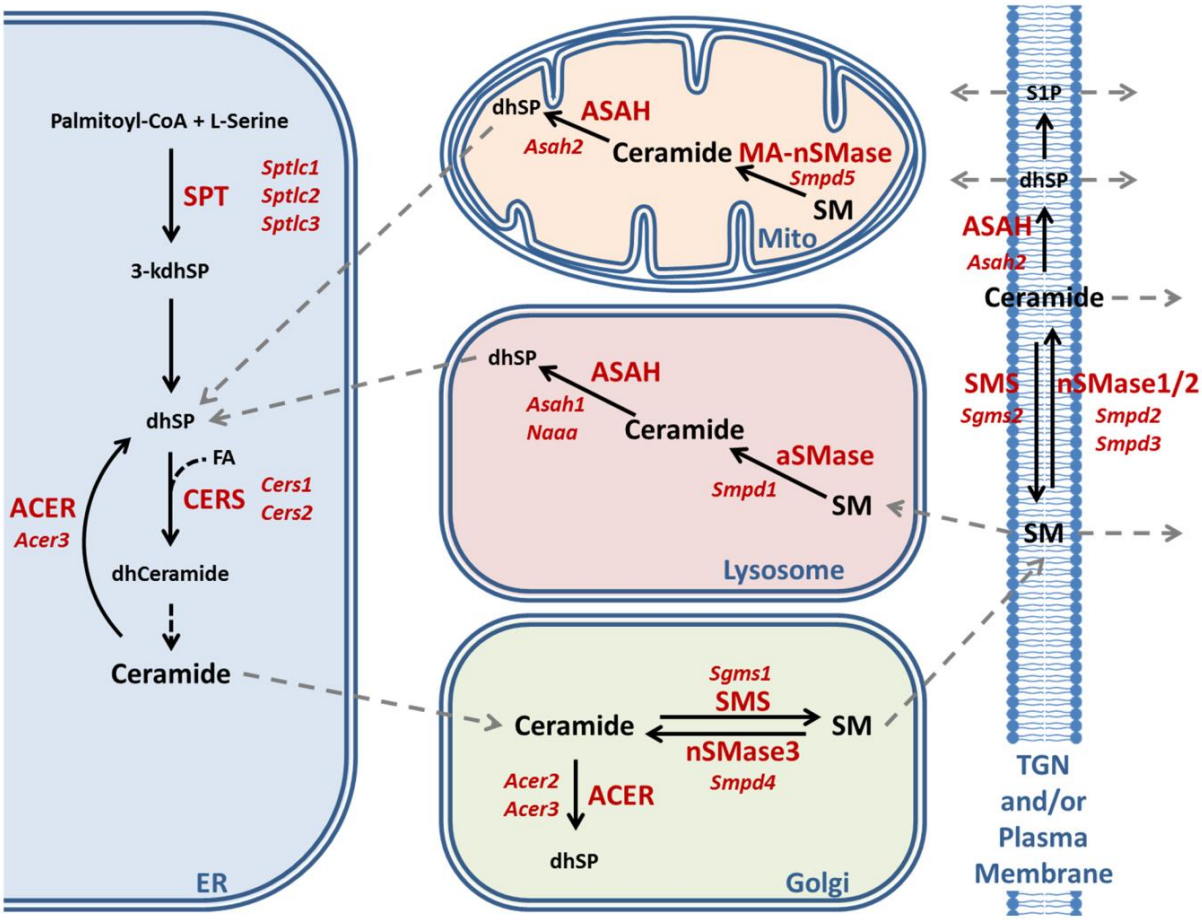

Figure 6: Schematic representation of ceramide-sphingomyelin metabolism[144]. The *de novo* ceramide synthesis and ceramide-sphingomyelin interconversion pathways are shown in distinct subcellular organelles with respective enzyme isoforms.

In order to pinpoint the molecular mechanisms underlying this differential regulation of ceramide and sphingomyelin species, we studied the enzymes involved in *de novo* ceramide synthesis and consecutive pathways. Expression analyses were performed in the cerebellum and spinal cord tissues from *Atxn2*-CAG100-KIN mice, together with *Atxn2*-KO animals to distinguish the ATXN2 loss dependent effects from expansion driven toxicity. To begin with, *de novo* ceramide synthesis was found diminished in *Atxn2*-CAG100-KIN tissues. Most remarkably, neuronal and mature-oligodendroglial CERS isoforms (*Cers1* and *Cers2*, respectively) showed consistent dysregulations in cerebellum and spinal cord at the transcript level. *Cers1* was found downregulated, whereas *Cers2* showed a significant upregulation in both tissues. CERS1 synthesizes neuronal short chain (C18) ceramides, and has been found impotant for proper Purkinje cell function[152]. CERS2 is dominantly expressed in myelinating mature oligodendrocytes, and synthesizes long chain (C24-26)

ceramides[153–156]. Further investigation of their protein levels revealed significant downregulations of both in *Atxn2*-CAG100-KIN cerebellum, suggesting that ceramide synthesis is globally restricted irrespective of the cell types, which is further supported by the reduced abundance of all ceramide species in the metabolome data. While neuronal CERS1 showed a consistent decrease at both transcript and protein levels, the mature oligodendrocytes in *Atxn2*-CAG100-KIN cerebellum seemingly try to compensate the CERS2 protein deficit by upregulating its transcript. The lack of these dysregulations in *Atxn2*-KO cerebellum indicates that ATXN2 aggregation pathology is the underlying cause of ceramide synthesis and myelination defects rather than its loss of function.

At the later steps of *de novo* ceramide biosynthesis, fatty acid chains of various lengths are fused with a sphingosine backbone to generate dihydro-ceramides[157]. As a direct contributor to ceramide synthesis, Elongase isoforms (ELOVL) producing different fatty acid chains were also investigated in *Atxn2*-CAG100-KIN tissues. Common dysregulations in cerebellum and spinal cord were the downregulations of oligodendroglial *Elovl1*, neuronal *Elovl4*, astrocytic *Elovl5* and ubiquitously expressed *Elovl6* transcripts, indicating an overall reduction in the fatty acid elongation capacity. These findings are especially noteworthy in light of the previous documentations of ELOVL1 mutations causing demyelination[158,159], ELOVL6 deficiency leading to obesity[160], and ELOVL4 and ELOVL5 mutations being associated with autosomal dominant ataxia subtypes SCA34 and SCA38[161–163]. Moreover, availability of free fatty acids and consequently higher mTORC1 activity leads to increased expression of *Elovl* isoforms[164–166]. This notion agrees well with our findings here showing decreased abundance of free fatty acids in SCA2 cerebellum as a signal of energetic deficit, which would lead to inactivation of the mTORC1 complex and therefore a reduction in *Elovl* expression in various cell types.

After their *de novo* production in the ER, ceramides are further translocated and utilized for sphingomyelin synthesis in Golgi apparatus and plasma membrane by specific SMS isoforms (*Sgms1* and *Sgms2*, respectively). While the Golgi-associated *Sgms1* showed a reduction in both cerebellum and spinal cord of *Atxn2*-CAG100-KIN mouse, plasma membrane-associated *Sgms2* showed a decrease only in cerebellum. Reduced levels of both isoforms could be caused by a lack of need due to reduced ceramide production and transport from the ER. Although this notion of inefficient ceramide production consecutively leading to reduced sphingomyelin synthesis fits well with the decrease in oligodendrocyte-specific long chain sphingomyelins, it fails to explain how neuronal short chain sphingomyelins have an increased abundance. Alternative to their biosynthesis, breakdown of sphingomyelins could be underlying this phenomenon. Indeed, investigation of various

Sphingomyelinase (SMase) isoforms involved in sphingomyelin breakdown revealed significant downregulation of the lysosomal acid-Sphingomyelinase (aSMase) at the protein level, indicating its reduced capacity to metabolize certain sphingomyelin species. This also constitutes an interesting finding given the fact that aSMase mutations are involved in Niemann-Pick disease type A presenting with a severe neurodegenerative course in the first years of life[167]. Normal levels of Sphingomyelinase isoforms in *Atxn2*-KO tissues ensure the expansion-driven nature of the observed dysregulations in *Atxn2*-CAG100-KIN mice.

Finally, detailed investigation of ceramide breakdown into sphingosine and fatty acids in distinct subcellular compartments revealed a selective effect on neutral-Ceramidase (nCDase, encoded by *Asah2* transcript) in both tissues analyzed. Loss of nCDase activity under energetic stress was previously shown to result in sphingosine-1-phosphate deficiency[168], in line with our metabolome data and expression analysis results here. *Asah2* levels in *Atxn2*-KO cerebellum was found subtly reduced, whereas no change was observed in the spinal cord, collectively rendering its ATXN2-loss dependent dysregulation unlikely.

Overall, dysregulation of the entire ceramide-sphingomyelin metabolism intermediates and many of the enzymes mentioned here has been observed in several other neurodegenerative disorders such as AD, HD, PD, and lipid storage disorders[169], highlighting their importance for an optimal nervous system function. Although several of the neuronal and astrocytic enzyme isoforms were also found altered in *Atxn2*-CAG100-KIN mouse spino-cerebellar tisue, a more prominent dysregulation of the myelin compartment was observed with severe reductions in numerous structural lipids and associated enzyme levels. Given the high demand for lipid species in expanding and maintaining the multi-layered myelin sheath, these findings are understandable. Yet, they still point out to a previously overlooked aspect of ATXN2 pathology equally important in disease: cell-autonomous affection of the non-neuronal cells. Therefore, our findings encourage questioning of the currently established definition of neurodegeneration with selective neuronal death, while in reality multiple cell types seem to response simultaneously.

6. CONCLUSION

From witnessing the discovery of DNA structure, to finding the first disease-causing mutation, enlightening numerous disease mechanisms, and already applying the developed therapeutics in clinic, the last 50 years have seen a great boost in biomedical field. In an ever-growing pool of scientific data and therapeutic hypotheses, one point remains crucial to consider; the potential side effects. Especially in mutation-driven disorders like SCA2, or well-defined sporadic pathomechanisms like TDP-43 aggregation in majority of the ALS cases, it is not only important to understand the pathogenicity of the causative protein, but also to dissect its native function, which pathways it is involved in, what other body parts are affected from disease, and all the potential outcomes of an intervention. Due to its high therapeutic promise, immediate utilization of *ATXN2* ASOs in SCA2 and ALS patients presents itself as an attractive opportunity, before which our understanding of ATXN2 impact on non-neuronal cells and throughout the body has to be completed first.

Of the two main aspects of ATXN2 function, namely RNA-binding SG component vs. regulator of nutrient metabolism, SG dynamics and aggregation has naturally drawn more attention, from which the therapeutic basis of suppressed ATXN2 expression was predicted to stem. However, considering the sharp contrast between aggregation toxicity driven overall atrophy due to energetic deficit vs. ATXN2 loss driven overall metabolic excess with lipid and glycogen accumulation, it seems equally, if not more, likely that the neuroprotection could stem from restoring the metabolic balance. This notion is further backed by the findings that hypercaloric feeding extends survival in ALS mouse models[170], individuals with high body-mass-index have reduced risk for ALS[171], and hypercaloric diet in ALS patients after disease manifestation also increases survival especially in fast-progressing cases[172].

Hence, the understudied metabolic face of ATXN2 toxicity was investigated in the context of this thesis work in peripheral tissues and all cell types of the CNS. The link between ATXN2 and mitochondrial dynamics, through modulation of the mitophagy factor PINK1 levels, was documented for the first time as a result of studying SCA2 patient blood transcriptome and further validations in *Atxn2*-KO mouse tissues. Next, the first authentic SCA2 mouse model (*Atxn2*-CAG100-KIN), with endogenous global expression of the mutant protein throughout the body, was generated and characterized. The initial studies on this model were focused on metabolic effects in the nervous system, first measuring the most abundant brain metabolites in the living mice, and then analyzing a plethora of other metabolites and especially lipid species in distinct regions of the CNS, such as cerebellum and spinal cord. These findings combined, *Atxn2*-CAG100-KIN mouse presented a strong reduction in the abundance of NAA, ceramides and certain sphingomyelin species, all of

which are very important intermediates in myelination and maintenance of the myelin sheath. Detailed investigation of the enzymes involved in NAA production, fatty acid elongation, *de novo* ceramide biosynthesis and ceramide/sphingomyelin interconversion revealed NAA production (from acetyl-CoA and aspartate) as the earliest dysregulation, and fatty acid elongation (linkage of additional acetyl-CoA units to the growing chain) as the most collectively disturbed pathway.

Given that fatty acids of various lengths are the pre-requisite for synthesizing more complex membrane lipids during myelination, and acetyl-CoA is a pre-requisite of both fatty acid elongation and NAA production, all our findings could be traced back to the deficiency of the most simple metabolic unit, connecting not only several arms of the lipid metabolism, but also amino acid degradation, glycolysis and TCA cycle. In the meantime, we have accumulated more data showing decreased levels of cholesterol biosynthesis intermediates in *Atxn2*-CAG100-KIN spinal cord[173], which could similarly arise from an acetyl-CoA deficiency. Additional data also highlighted a cell-autonomous impact of ATXN2 expansion in *Atxn2*-CAG100-KIN oligodendrocytes via altered alternative splicing of the important structural myelin proteins (manuscript in preparation).

The newly generated *Atxn2*-CAG100-KIN mouse undoubtedly provides a unique opportunity to study ATXN2 pathology as a whole in many cell types and tissues. Building on the currently ongoing projects investigating ATXN2 function in oligodendrocytes or peripheral tissues, such as liver and muscle, future studies should address more detailed questions like (i) to which major nutrient groups ATXN2 is responsive and changes localization accordingly, (ii) which factors are dysregulated in the metabolism of these specific nutrients in the absence or toxicity of ATXN2, and (iii) what is the molecular nature of ATXN2 impact on these factors, for instance it could be via direct protein-protein interaction or by binding to their transcript and regulating translational dynamics. Further investigation of the initial findings presented in this thesis, identification of the primary causal dysregulations with in-depth molecular analyses, and their validation in patient material will not only provide the much needed insights regarding the potential side-effects of targeting ATXN2 with ASOs, but could also pave the way for the identification of novel and more “affordable” therapeutic strategies by means of financial and physical burden of these injections.

7. LIST OF FIGURES

Figure 1: Graphical visualization of the pathology in different SCA types 17
Figure 2: Widespread nervous system atrophy in SCA2 18
Figure 3: Protein structure of ATXN2 and its orthologs throughout evolution 23
Figure 4: Schematic representation of ATXN2-associated mechanisms 26
Figure 5: Schematic representation of NAA metabolism 35
Figure 6: Schematic representation of ceramide-sphingomyelin metabolism 39

8. LIST OF ABBREVIATIONS

A2BP1	Ataxin-2 Binding Protein
ACER	Ceramidase
AD	Alzheimer's disease
ADCA	Autosomal dominant cerebellar ataxia
ALDH2	Aldehyde Dehydrogenase 2
ALS	Amyotrophic lateral sclerosis
AO	Age of onset
ASAH	Acylsphingosine Amidohydrolase
ASO	Anti-sense oligonucleotide
ASPA	Aspartoacetylase
ATXN1	Ataxin-1
ATXN2	Ataxin-2
BCAA	Branched chain amino acid
BRCA1	Breast Cancer Type 1 Susceptibility Protein
C	Carbon
C9orf72	Chromosome 9 Open Reading Frame 72
Ca^{2+}	Calcium
CAA	Cytosine-Adenine-Adenine
CACNA1A	Calcium Voltage-Gated Channel Subunit Alpha1 A
CAG	Cytosine-Adenine-Guanine
CDase	Ceramidase
CERS	Ceramide Synthase
Chr.	Chromosome
CNS	Central nervous system
CoA	Coenzyme A
CpG	Cytosine-Guanine
C-terminal	Carboxy terminal
DNA	Deoxyribonucleic acid
EGFR	Epidermal growth factor receptor
ELOVL	Elongation Of Very Long Chain Fatty Acids Protein
ER	Endoplasmic Reticulum
FOLH1	Folate Hydrolase 1
FUS	Fused in sarcoma
GABA	Gamma aminobutyric acid
GCPII	Glutamate Carboxypeptidase 2
GL	Granular cell layer
Grb2	Growth Factor Receptor Bound Protein 2
HD	Huntington's disease
hnRNPA2/B1	Heterogeneous Nuclear Ribonucleoprotein A2/B1
HTT	Huntingtin
kb	kilobase
kDa	kilo Dalton
KEGG	Kyoto Encyclopedia of Genes and Genomes

KIN	Knock-in
KO	Knock-out
Lsm	Like-Sm
LsmAD	Lsm-associated domain
MEF	Murine embryonal fibroblast
ML	Molecular layer
mRNA	messenger RNA
mTORC1	Mechanistic/Mammalian Target of Rapamycin Complex 1
NAA	N-acetylaspartate
NAAG	N-acetylaspartylglutamate
NAT8L	N-Acetyltransferase 8 Like
NMR	Nuclear magnetic resonance
N-terminal	Amino terminal
PABP	Poly(A)-binding protein
PAM2	PABP-interacting motif
PARKIN	Parkinson Protein 2
PD	Parkinson's disease
PI3K	Phosphatidylinositol-4,5-bisphosphate 3-Kinase
PINK1	PTEN-induced kinase 1
PIP2	Phosphatidylinositol-4,5-bisphosphate
PIP3	Phosphatidylinositol-3,4,5-trisphosphate
PKB	Protein kinase B, Akt
PL	Purkinje cell layer
polyQ	poly-Glutamine
PRD	Proline rich domain
PSP	Progressive supranuclear palsy
PTEN	Phosphatase And Tensin Homolog
Q	Glutamine
QKI	Quaking
RAI1	Retinoic Acid Induced 1
RBFOX1	RNA Binding Fox-1 Homolog 1
RBP	RNA-binding protein
RNA	Ribonucleic acid
RNA-seq	RNA-sequencing
SCA1/2/3/34/38	Spinocerebellar ataxia type 1/2/3/34/38
SG	Stress granule
SH3	SRC Homology 3 Domain
SMase	Sphingomyelinase
SMS	Sphingomyelin synthase
SPT	Serine palmitoyltransferase
Src	Protooncogene SRC, Rous Sarcoma
TAS2R38	Taste 2 Receptor Member 38
TCA	Tricarboxylic acid
TDP-43	TAR DNA Binding Protein-43
TIA1	T-Cell-Restricted Intracellular Antigen-1
WT	Wild type

9. REFERENCES

1. Kim, U. K. *et al.* Positional cloning of the human quantitative trait locus underlying taste sensitivity to phenylthiocarbamide. *Science (New York, N.Y.)* **299**; 10.1126/science.1080190 (2003).

2. Edenberg, H. J. & D, P. The Genetics of Alcohol Metabolism.

3. Miki, Y. *et al.* A strong candidate for the breast and ovarian cancer susceptibility gene BRCA1. *Science* **266,** 66–71; 10.1126/science.7545954 (1994).

4. Gusella, J. F. *et al.* A polymorphic DNA marker genetically linked to Huntington's disease. *Nature* **306,** 234–238; 10.1038/306234a0 (1983).

5. MacDonald, M. E. *et al.* Gametic but not somatic instability of CAG repeat length in Huntington's disease. *Journal of Medical Genetics* **30,** 982–986; 10.1136/jmg.30.12.982 (1993).

6. La Spada, A. R., Wilson, E. M., Lubahn, D. B., Harding, A. E. & Fischbeck, K. H. Androgen receptor gene mutations in X-linked spinal and bulbar muscular atrophy. *Nature* **352,** 77–79; 10.1038/352077a0 (1991).

7. Orr, H. T. *et al.* Expansion of an unstable trinucleotide CAG repeat in spinocerebellar ataxia type 1. *Nat Genet* **4,** 221–226; 10.1038/ng0793-221 (1993).

8. WADIA, N. H. & SWAMI, R. K. A NEW FORM OF HEREDO-FAMILIAL SPINOCEREBELLAR DEGENERATION WITH SLOW EYE MOVEMENTS (NINE FAMILIES). *Brain* **94,** 359–374; 10.1093/brain/94.2.359 (1971).

9. Gispert, S. *et al.* Chromosomal assignment of the second locus for autosomal dominant cerebellar ataxia (SCA2) to chromosome 12q23-24.1. *Nat Genet* **4,** 295–299; 10.1038/ng0793-295 (1993).

10. Imbert, G. *et al.* Cloning of the gene for spinocerebellar ataxia 2 reveals a locus with high sensitivity to expanded CAG/glutamine repeats. *Nat Genet* **14,** 285–291; 10.1038/ng1196-285 (1996).

11. Pulst, S. M. *et al.* Moderate expansion of a normally biallelic trinucleotide repeat in spinocerebellar ataxia type 2. *Nat Genet* **14,** 269–276; 10.1038/ng1196-269 (1996).

12. Sanpei, K. *et al.* Identification of the spinocerebellar ataxia type 2 gene using a direct identification of repeat expansion and cloning technique, DIRECT. *Nat Genet* **14,** 277–284; 10.1038/ng1196-277 (1996).

13. Ramachandra, N. B. & Kusuma, L. An understanding of spinocerebellar ataxia. *The Indian journal of medical research* **141,** 148–150; 10.4103/0971-5916.155537 (2015).

14. Mirkin, S. M. Expandable DNA repeats and human disease. *Nature* **447,** 932–940; 10.1038/nature05977 (2007).

15. Bird, T. D. *GeneReviews®. Hereditary Ataxia Overview* (Seattle (WA), 1993).

16. Ruano, L., Melo, C., Silva, M. C. & Coutinho, P. The global epidemiology of hereditary ataxia and spastic paraplegia: a systematic review of prevalence studies. *Neuroepidemiology* **42,** 174–183; 10.1159/000358801 (2014).

17. Cellini, E. *et al.* Clinical and genetic analysis of hereditary and sporadic ataxia in central Italy. *Brain Research Bulletin* **56,** 363–366; 10.1016/S0361-9230(01)00650-5 (2001).

18. Lopes-Cendes, I. *et al.* Frequency of the different mutations causing spinocerebellar ataxia (SCA1, SCA2, MJD/SCA3 and DRPLA) in a large group of Brazilian patients. *Arquivos de neuro-psiquiatria* **55,** 519–529; 10.1590/s0004-282x1997000400001 (1997).

19. Matsumura, R., Futamura, N., Ando, N. & Ueno, S. Frequency of spinocerebellar ataxia mutations in the Kinki district of Japan. *Acta neurologica Scandinavica* **107,** 38–41; 10.1034/j.1600-0404.2003.01347.x (2003).

20. Pujana, M. A. *et al.* Spinocerebellar ataxias in Spanish patients: genetic analysis of familial and sporadic cases. The Ataxia Study Group. *Human genetics* **104,** 516–522; 10.1007/s004390050997 (1999).

21. Hamzeiy, H. *et al.* Elevated Global DNA Methylation Is Not Exclusive to Amyotrophic Lateral Sclerosis and Is Also Observed in Spinocerebellar Ataxia Types 1 and 2. *Neuro-degenerative diseases* **18,** 38–48; 10.1159/000486201 (2018).

22. Lastres-Becker, I., Rüb, U. & Auburger, G. Spinocerebellar ataxia 2 (SCA2). *Cerebellum (London, England)* **7,** 115–124; 10.1007/s12311-008-0019-y (2008).

23. Rüb, U. *et al.* Clinical features, neurogenetics and neuropathology of the polyglutamine spinocerebellar ataxias type 1, 2, 3, 6 and 7. *Progress in neurobiology* **104,** 38–66; 10.1016/j.pneurobio.2013.01.001 (2013).

24. Seidel, K. *et al.* Brain pathology of spinocerebellar ataxias. *Acta neuropathologica* **124,** 1–21; 10.1007/s00401-012-1000-x (2012).

25. Scherzed, W. *et al.* Pathoanatomy of cerebellar degeneration in spinocerebellar ataxia type 2 (SCA2) and type 3 (SCA3). *Cerebellum (London, England)* **11,** 749–760; 10.1007/s12311-011-0340-8 (2012).

26. Chakor, R. T. & Bharote, H. Inherited ataxia with slow saccades. *Journal of postgraduate medicine* **58,** 318–325; 10.4103/0022-3859.105471 (2012).

27. Ağan, K., et al. Spinocerebellar Ataxia Type 2 in a Turkish Family. *Marmara Medical Journal* **19,** 135–138 (2006).

28. https://en.wikipedia.org/wiki/File:MRI_of_human_head_(sagittal_view).jpg.

29. Apps, R. & Garwicz, M. Anatomical and physiological foundations of cerebellar information processing. *Nature reviews. Neuroscience* **6,** 297–311; 10.1038/nrn1646 (2005).

30. Hoxha, E., Tempia, F., Lippiello, P. & Miniaci, M. C. Modulation, Plasticity and Pathophysiology of the Parallel Fiber-Purkinje Cell Synapse. *Frontiers in synaptic neuroscience* **8,** 35; 10.3389/fnsyn.2016.00035 (2016).

31. Albus, J. S. A theory of cerebellar function. *Mathematical Biosciences* **10,** 25–61; 10.1016/0025-5564(71)90051-4 (1971).

32. Sahba, S., Nechiporuk, A., Figueroa, K. P., Nechiporuk, T. & Pulst, S. M. Genomic structure of the human gene for spinocerebellar ataxia type 2 (SCA2) on chromosome 12q24.1. *Genomics* **47,** 359–364; 10.1006/geno.1997.5131 (1998).

33. Costanzi-Porrini, S. *et al.* An interrupted 34-CAG repeat SCA-2 allele in patients with sporadic spinocerebellar ataxia. *Neurology* **54,** 491–493; 10.1212/wnl.54.2.491 (2000).

34. Choudhry, S., Mukerji, M., Srivastava, A. K., Jain, S. & Brahmachari, S. K. CAG repeat instability at SCA2 locus: anchoring CAA interruptions and linked single nucleotide polymorphisms. *Human molecular genetics* **10,** 2437–2446; 10.1093/hmg/10.21.2437 (2001).

35. Charles, P. *et al.* Are interrupted SCA2 CAG repeat expansions responsible for parkinsonism? *Neurology* **69,** 1970–1975; 10.1212/01.wnl.0000269323.21969.db (2007).

36. Babovic-Vuksanovic, D., Snow, K., Patterson, M. C. & Michels, V. V. Spinocerebellar ataxia type 2 (SCA 2) in an infant with extreme CAG repeat expansion. *American journal of medical genetics* **79,** 383–387 (1998).

37. Mao, R. *et al.* Childhood-onset ataxia: testing for large CAG-repeats in SCA2 and SCA7. *American journal of medical genetics* **110,** 338–345; 10.1002/ajmg.10467 (2002).

38. Elden, A. C. *et al.* Ataxin-2 intermediate-length polyglutamine expansions are associated with increased risk for ALS. *Nature* **466,** 1069–1075; 10.1038/nature09320 (2010).

39. Almaguer-Mederos, L. E. *et al.* Estimation of the age at onset in spinocerebellar ataxia type 2 Cuban patients by survival analysis. *Clinical genetics* **78,** 169–174; 10.1111/j.1399-0004.2009.01358.x (2010).

40. Cancel, G. *et al.* Molecular and clinical correlations in spinocerebellar ataxia 2: a study of 32 families. *Human molecular genetics* **6,** 709–715; 10.1093/hmg/6.5.709 (1997).

41. Geschwind, D. H., Perlman, S., Figueroa, C. P., Treiman, L. J. & Pulst, S. M. The prevalence and wide clinical spectrum of the spinocerebellar ataxia type 2 trinucleotide repeat in patients with autosomal dominant cerebellar ataxia. *American Journal of Human Genetics* **60,** 842–850 (1997).

42. Riess, O. *et al.* SCA2 trinucleotide expansion in German SCA patients. *Neurogenetics* **1,** 59–64; 10.1007/s100480050009 (1997).

43. Ragothaman, M. & Muthane, U. Homozygous SCA 2 mutations changes phenotype and hastens progression. *Movement disorders : official journal of the Movement Disorder Society* **23,** 770–771; 10.1002/mds.21950 (2008).

44. Spadafora, P. *et al.* Gene dosage influences the age at onset of SCA2 in a family from southern Italy. *Clinical genetics* **72,** 381–383; 10.1111/j.1399-0004.2007.00868.x (2007).

45. Hayes, S. *et al.* CAG repeat length in RAI1 is associated with age at onset variability in spinocerebellar ataxia type 2 (SCA2). *Human molecular genetics* **9,** 1753–1758; 10.1093/hmg/9.12.1753 (2000).

46. Pulst, S.-M. *et al.* Spinocerebellar ataxia type 2: polyQ repeat variation in the CACNA1A calcium channel modifies age of onset. *Brain : a journal of neurology* **128,** 2297–2303; 10.1093/brain/awh586 (2005).

47. Aguiar, J. *et al.* Identification of the physiological promoter for spinocerebellar ataxia 2 gene reveals a CpG island for promoter activity situated into the exon 1 of this gene and provides data about the origin of the nonmethylated state of these types of islands. *Biochemical and biophysical research communications* **254,** 315–318; 10.1006/bbrc.1998.9929 (1999).

48. Laffita-Mesa, J. M. *et al.* Epigenetics DNA methylation in the core ataxin-2 gene promoter: novel physiological and pathological implications. *Human genetics* **131,** 625–638; 10.1007/s00439-011-1101-y (2012).

49. Bauer, P. O., Zumrova, A., Matoska, V., Mitsui, K. & Goetz, P. Can ataxin-2 be down-regulated by allele-specific de novo DNA methylation in SCA2 patients? *Medical hypotheses* **63,** 1018–1023; 10.1016/j.mehy.2004.03.046 (2004).

50. Lim, J. *et al.* A protein-protein interaction network for human inherited ataxias and disorders of Purkinje cell degeneration. *Cell* **125,** 801–814; 10.1016/j.cell.2006.03.032 (2006).

51. Al-Ramahi, I. *et al.* dAtaxin-2 mediates expanded Ataxin-1-induced neurodegeneration in a Drosophila model of SCA1. *PLoS genetics* **3,** e234; 10.1371/journal.pgen.0030234 (2007).

52. Lessing, D. & Bonini, N. M. Polyglutamine genes interact to modulate the severity and progression of neurodegeneration in Drosophila. *PLoS biology* **6,** e29; 10.1371/journal.pbio.0060029 (2008).

53. Lee, T. *et al.* Ataxin-2 intermediate-length polyglutamine expansions in European ALS patients. *Human molecular genetics* **20,** 1697–1700; 10.1093/hmg/ddr045 (2011).

54. Liu, X. *et al.* ATXN2 CAG repeat expansions increase the risk for Chinese patients with amyotrophic lateral sclerosis. *Neurobiology of aging* **34,** 2236.e5-8; 10.1016/j.neurobiolaging.2013.04.009 (2013).

55. Yu, Z. *et al.* PolyQ repeat expansions in ATXN2 associated with ALS are CAA interrupted repeats. *PloS one* **6,** e17951; 10.1371/journal.pone.0017951 (2011).

56. Borghero, G. *et al.* ATXN2 is a modifier of phenotype in ALS patients of Sardinian ancestry. *Neurobiology of aging* **36,** 2906.e1-5; 10.1016/j.neurobiolaging.2015.06.013 (2015).

57. Gispert, S. *et al.* The modulation of Amyotrophic Lateral Sclerosis risk by ataxin-2 intermediate polyglutamine expansions is a specific effect. *Neurobiology of disease* **45,** 356–361; 10.1016/j.nbd.2011.08.021 (2012).

58. Lahut, S. *et al.* ATXN2 and its neighbouring gene SH2B3 are associated with increased ALS risk in the Turkish population. *PloS one* **7,** e42956; 10.1371/journal.pone.0042956 (2012).

59. van Blitterswijk, M. *et al.* Ataxin-2 as potential disease modifier in C9ORF72 expansion carriers. *Neurobiology of aging* **35,** 2421.e13-7; 10.1016/j.neurobiolaging.2014.04.016 (2014).

60. van Damme, P. *et al.* Expanded ATXN2 CAG repeat size in ALS identifies genetic overlap between ALS and SCA2. *Neurology* **76,** 2066–2072; 10.1212/WNL.0b013e31821f445b (2011).

61. Furtado, S. *et al.* SCA-2 presenting as parkinsonism in an Alberta family: clinical, genetic, and PET findings. *Neurology* **59,** 1625–1627; 10.1212/01.wnl.0000035625.19871.dc (2002).

62. Payami, H. *et al.* SCA2 may present as levodopa-responsive parkinsonism. *Movement disorders : official journal of the Movement Disorder Society* **18,** 425–429; 10.1002/mds.10375 (2003).

63. Nielsen, T. T. *et al.* ATXN2 with intermediate-length CAG/CAA repeats does not seem to be a risk factor in hereditary spastic paraplegia. *Journal of the neurological sciences* **321,** 100–102; 10.1016/j.jns.2012.07.036 (2012).

64. Ross, O. A. *et al.* Ataxin-2 repeat-length variation and neurodegeneration. *Human molecular genetics* **20,** 3207–3212; 10.1093/hmg/ddr227 (2011).

65. Rottnek, M. *et al.* Schizophrenia in a patient with spinocerebellar ataxia 2: coincidence of two disorders or a neurodegenerative disease presenting with psychosis? *The American journal of psychiatry* **165,** 964–967; 10.1176/appi.ajp.2008.08020285 (2008).

66. Zhang, F. *et al.* Association analysis of a functional variant in ATXN2 with schizophrenia. *Neuroscience letters* **562,** 24–27; 10.1016/j.neulet.2013.12.001 (2014).

67. Becker, L. A. *et al.* Therapeutic reduction of ataxin-2 extends lifespan and reduces pathology in TDP-43 mice. *Nature* **544,** 367–371; 10.1038/nature22038 (2017).

68. Scoles, D. R. *et al.* Antisense oligonucleotide therapy for spinocerebellar ataxia type 2. Nature, 544(7650), 362-366. *Nature* **544**; 10.1038/nature22044 (2017).

69. Nechiporuk, T. *et al.* The mouse SCA2 gene: cDNA sequence, alternative splicing and protein expression. *Human molecular genetics* **7,** 1301–1309; 10.1093/hmg/7.8.1301 (1998).

70. Huynh, D. P., Figueroa, K., Hoang, N. & Pulst, S. M. Nuclear localization or inclusion body formation of ataxin-2 are not necessary for SCA2 pathogenesis in mouse or human. *Nat Genet* **26,** 44–50; 10.1038/79162 (2000).

71. Ostrowski, L. A., Hall, A. C. & Mekhail, K. Ataxin-2: From RNA Control to Human Health and Disease. *Genes* **8**; 10.3390/genes8060157 (2017).

72. Auburger, G., Sen, N.-E., Meierhofer, D., Başak, A.-N. & Gitler, A. D. Efficient Prevention of Neurodegenerative Diseases by Depletion of Starvation Response Factor Ataxin-2. *Trends in neurosciences* **40,** 507–516; 10.1016/j.tins.2017.06.004 (2017).

73. He, W. & Parker, R. Functions of Lsm proteins in mRNA degradation and splicing. *Current Opinion in Cell Biology* **12,** 346–350; 10.1016/S0955-0674(00)00098-3 (2000).

74. Albrecht, M., Golatta, M., Wüllner, U. & Lengauer, T. Structural and functional analysis of ataxin-2 and ataxin-3. *European journal of biochemistry* **271,** 3155–3170; 10.1111/j.1432-1033.2004.04245.x (2004).

75. Huynh, D. P., Yang, H.-T., Vakharia, H., Nguyen, D. & Pulst, S. M. Expansion of the polyQ repeat in ataxin-2 alters its Golgi localization, disrupts the Golgi complex and causes cell death. *Human molecular genetics* **12,** 1485–1496; 10.1093/hmg/ddg175 (2003).

76. Yokoshi, M. *et al.* Direct binding of Ataxin-2 to distinct elements in 3' UTRs promotes mRNA stability and protein expression. *Molecular cell* **55,** 186–198; 10.1016/j.molcel.2014.05.022 (2014).

77. Conn, S. J. *et al.* The RNA binding protein quaking regulates formation of circRNAs. *Cell* **160,** 1125–1134; 10.1016/j.cell.2015.02.014 (2015).

78. Ciosk, R., DePalma, M. & Priess, J. R. ATX-2, the C. elegans ortholog of ataxin 2, functions in translational regulation in the germline. *Development (Cambridge, England)* **131,** 4831–4841; 10.1242/dev.01352 (2004).

79. Shibata, H., Huynh, D. P. & Pulst, S. M. A novel protein with RNA-binding motifs interacts with ataxin-2. *Human molecular genetics* **9,** 1303–1313; 10.1093/hmg/9.9.1303 (2000).

80. Hamada, N. *et al.* Role of the cytoplasmic isoform of RBFOX1/A2BP1 in establishing the architecture of the developing cerebral cortex. *Molecular autism* **6,** 56; 10.1186/s13229-015-0049-5 (2015).

81. Li, M.-L. *et al.* Evolution and transition of expression trajectory during human brain development. *BMC evolutionary biology* **20,** 72; 10.1186/s12862-020-01633-4 (2020).

82. Li, J. *et al.* An alternative splicing switch in FLNB promotes the mesenchymal cell state in human breast cancer. *eLife* **7**; 10.7554/eLife.37184 (2018).

83. McCann, C. *et al.* The Ataxin-2 protein is required for microRNA function and synapse-specific long-term olfactory habituation. *Proceedings of the National Academy of Sciences of the United States of America* **108,** E655-62; 10.1073/pnas.1107198108 (2011).

84. Ralser, M. *et al.* An integrative approach to gain insights into the cellular function of human ataxin-2. *Journal of molecular biology* **346,** 203–214; 10.1016/j.jmb.2004.11.024 (2005).

85. Satterfield, T. F. & Pallanck, L. J. Ataxin-2 and its Drosophila homolog, ATX2, physically assemble with polyribosomes. *Human molecular genetics* **15,** 2523–2532; 10.1093/hmg/ddl173 (2006).

86. Mangus, D. A. *et al.* Positive and negative regulation of poly(A) nuclease. *Molecular and cellular biology* **24,** 5521–5533; 10.1128/MCB.24.12.5521-5533.2004 (2004).

87. Lastres-Becker, I. *et al.* Mammalian ataxin-2 modulates translation control at the pre-initiation complex via PI3K/mTOR and is induced by starvation. *Biochimica et biophysica acta* **1862,** 1558–1569; 10.1016/j.bbadis.2016.05.017 (2016).

88. Arsović, A. *et al.* Mouse Ataxin-2 Expansion Downregulates CamKII and Other Calcium Signaling Factors, Impairing Granule-Purkinje Neuron Synaptic Strength. *International journal of molecular sciences* **21**; 10.3390/ijms21186673 (2020).

89. Takahara, T. & Maeda, T. Transient sequestration of TORC1 into stress granules during heat stress. *Molecular cell* **47,** 242–252; 10.1016/j.molcel.2012.05.019 (2012).

90. DeMille, D. *et al.* PAS kinase is activated by direct SNF1-dependent phosphorylation and mediates inhibition of TORC1 through the phosphorylation and activation of Pbp1. *Molecular biology of the cell* **26,** 569–582; 10.1091/mbc.E14-06-1088 (2015).

91. Nonhoff, U. *et al.* Ataxin-2 interacts with the DEAD/H-box RNA helicase DDX6 and interferes with P-bodies and stress granules. *Molecular biology of the cell* **18,** 1385–1396; 10.1091/mbc.e06-12-1120 (2007).

92. Yang, Y.-S. *et al.* Yeast Ataxin-2 Forms an Intracellular Condensate Required for the Inhibition of TORC1 Signaling during Respiratory Growth. *Cell* **177,** 697-710.e17; 10.1016/j.cell.2019.02.043 (2019).

93. Kato, M. *et al.* Redox State Controls Phase Separation of the Yeast Ataxin-2 Protein via Reversible Oxidation of Its Methionine-Rich Low-Complexity Domain. *Cell* **177,** 711-721.e8; 10.1016/j.cell.2019.02.044 (2019).

94. Seidel, G. *et al.* Quantitative Global Proteomics of Yeast PBP1 Deletion Mutants and Their Stress Responses Identifies Glucose Metabolism, Mitochondrial, and Stress Granule Changes. *Journal of proteome research* **16,** 504–515; 10.1021/acs.jproteome.6b00647 (2017).

95. Farg, M. A. *et al.* Ataxin-2 interacts with FUS and intermediate-length polyglutamine expansions enhance FUS-related pathology in amyotrophic lateral sclerosis. *Human molecular genetics* **22,** 717–728; 10.1093/hmg/dds479 (2013).

96. Figley, M. D., Bieri, G., Kolaitis, R.-M., Taylor, J. P. & Gitler, A. D. Profilin 1 associates with stress granules and ALS-linked mutations alter stress granule dynamics. *The Journal of neuroscience : the official journal of the Society for Neuroscience* **34,** 8083–8097; 10.1523/JNEUROSCI.0543-14.2014 (2014).

97. Mackenzie, I. R. *et al.* TIA1 Mutations in Amyotrophic Lateral Sclerosis and Frontotemporal Dementia Promote Phase Separation and Alter Stress Granule Dynamics. *Neuron* **95,** 808-816.e9; 10.1016/j.neuron.2017.07.025 (2017).

98. Hart, M. P. & Gitler, A. D. ALS-associated ataxin 2 polyQ expansions enhance stress-induced caspase 3 activation and increase TDP-43 pathological modifications. *The Journal of neuroscience : the official journal of the Society for Neuroscience* **32,** 9133–9142; 10.1523/JNEUROSCI.0996-12.2012 (2012).

99. Damrath, E. *et al.* ATXN2-CAG42 sequesters PABPC1 into insolubility and induces FBXW8 in cerebellum of old ataxic knock-in mice. *PLoS genetics* **8,** e1002920; 10.1371/journal.pgen.1002920 (2012).

100. Liu, J. *et al.* Deranged calcium signaling and neurodegeneration in spinocerebellar ataxia type 2. *The Journal of neuroscience : the official journal of the Society for Neuroscience* **29,** 9148–9162; 10.1523/JNEUROSCI.0660-09.2009 (2009).

101. Hansen, S. T., Meera, P., Otis, T. S. & Pulst, S. M. Changes in Purkinje cell firing and gene expression precede behavioral pathology in a mouse model of SCA2. *Human molecular genetics* **22,** 271–283; 10.1093/hmg/dds427 (2013).

102. Dell'Orco, J. M., Pulst, S. M. & Shakkottai, V. G. Potassium channel dysfunction underlies Purkinje neuron spiking abnormalities in spinocerebellar ataxia type 2. *Human molecular genetics* **26,** 3935–3945; 10.1093/hmg/ddx281 (2017).

103. Pflieger, L. T. *et al.* Gene co-expression network analysis for identifying modules and functionally enriched pathways in SCA2. *Human molecular genetics* **26,** 3069–3080; 10.1093/hmg/ddx191 (2017).

104. Meera, P., Pulst, S. & Otis, T. A positive feedback loop linking enhanced mGluR function and basal calcium in spinocerebellar ataxia type 2. *eLife* **6**; 10.7554/eLife.26377 (2017).

105. van de Loo, S., Eich, F., Nonis, D., Auburger, G. & Nowock, J. Ataxin-2 associates with rough endoplasmic reticulum. *Experimental neurology* **215,** 110–118; 10.1016/j.expneurol.2008.09.020 (2009).

106. Nonis, D. *et al.* Ataxin-2 associates with the endocytosis complex and affects EGF receptor trafficking. *Cellular signalling* **20,** 1725–1739; 10.1016/j.cellsig.2008.05.018 (2008).

107. Drost, J. *et al.* Ataxin-2 modulates the levels of Grb2 and SRC but not ras signaling. *Journal of molecular neuroscience : MN* **51,** 68–81; 10.1007/s12031-012-9949-4 (2013).

108. Lastres-Becker, I. *et al.* Insulin receptor and lipid metabolism pathology in ataxin-2 knock-out mice. *Human molecular genetics* **17,** 1465–1481; 10.1093/hmg/ddn035 (2008).

109. Meierhofer, D., Halbach, M., Şen, N. E., Gispert, S. & Auburger, G. Ataxin-2 (Atxn2)-Knock-Out Mice Show Branched Chain Amino Acids and Fatty Acids Pathway Alterations. *Molecular & cellular proteomics : MCP* **15,** 1728–1739; 10.1074/mcp.M115.056770 (2016).

110. Newgard, C. B. *et al.* A branched-chain amino acid-related metabolic signature that differentiates obese and lean humans and contributes to insulin resistance. *Cell metabolism* **9,** 311–326; 10.1016/j.cmet.2009.02.002 (2009).

111. Sen, N. E. *et al.* Search for SCA2 blood RNA biomarkers highlights Ataxin-2 as strong modifier of the mitochondrial factor PINK1 levels. *Neurobiology of disease* **96,** 115–126; 10.1016/j.nbd.2016.09.002 (2016).

112. Johri, A. & Beal, M. F. Mitochondrial dysfunction in neurodegenerative diseases. *The Journal of pharmacology and experimental therapeutics* **342,** 619–630; 10.1124/jpet.112.192138 (2012).

113. Klinkenberg, M. *et al.* Restriction of trophic factors and nutrients induces PARKIN expression. *Neurogenetics* **13,** 9–21; 10.1007/s10048-011-0303-8 (2012).

114. Jin, S. M. & Youle, R. J. PINK1- and Parkin-mediated mitophagy at a glance. *Journal of cell science* **125,** 795–799; 10.1242/jcs.093849 (2012).

115. Bonifati, V. Autosomal recessive parkinsonism. *Parkinsonism & Related Disorders* **18,** S4-S6; 10.1016/S1353-8020(11)70004-9 (2012).

116. Valente, E. M. *et al.* Hereditary early-onset Parkinson's disease caused by mutations in PINK1. *Science (New York, N.Y.)* **304,** 1158–1160; 10.1126/science.1096284 (2004).

117. Matsuda, S., Nakanishi, A., Minami, A., Wada, Y. & Kitagishi, Y. Functions and characteristics of PINK1 and Parkin in cancer. *Frontiers in bioscience (Landmark edition)* **20,** 491–501; 10.2741/4321 (2015).

118. O'Flanagan, C. H. & O'Neill, C. PINK1 signalling in cancer biology. *Biochimica et biophysica acta* **1846,** 590–598; 10.1016/j.bbcan.2014.10.006 (2014).

119. McCoy, M. K., Kaganovich, A., Rudenko, I. N., Ding, J. & Cookson, M. R. Hexokinase activity is required for recruitment of parkin to depolarized mitochondria. *Human molecular genetics* **23,** 145–156; 10.1093/hmg/ddt407 (2014).

120. Mei, Y. *et al.* FOXO3a-dependent regulation of Pink1 (Park6) mediates survival signaling in response to cytokine deprivation. *Proceedings of the National Academy of Sciences of the United States of America* **106,** 5153–5158; 10.1073/pnas.0901104106 (2009).

121. Nan Yao *et al.* Inhibition of PINK1/Parkin-dependent mitophagy sensitizes multidrug-resistant cancer cells to B5G1, a new betulinic acid analog. *Cell Death Dis* **10,** 1–16; 10.1038/s41419-019-1470-z.

122. Wiedemeyer, R., Westermann, F., Wittke, I., Nowock, J. & Schwab, M. Ataxin-2 promotes apoptosis of human neuroblastoma cells. *Oncogene* **22,** 401–411; 10.1038/sj.onc.1206150 (2003).

123. Dansithong, W. *et al.* Ataxin-2 regulates RGS8 translation in a new BAC-SCA2 transgenic mouse model. *PLoS genetics* **11,** e1005182; 10.1371/journal.pgen.1005182 (2015).

124. Halbach, M. V. *et al.* Both ubiquitin ligases FBXW8 and PARK2 are sequestrated into insolubility by ATXN2 PolyQ expansions, but only FBXW8 expression is dysregulated. *PloS one* **10,** e0121089; 10.1371/journal.pone.0121089 (2015).

125. Halbach, M. V. *et al.* Atxn2 Knockout and CAG42-Knock-in Cerebellum Shows Similarly Dysregulated Expression in Calcium Homeostasis Pathway. *Cerebellum (London, England)* **16,** 68–81; 10.1007/s12311-016-0762-4 (2017).

126. Sen, N.-E. *et al.* Generation of an Atxn2-CAG100 knock-in mouse reveals N-acetylaspartate production deficit due to early Nat8l dysregulation. *Neurobiology of disease* **132,** 104559; 10.1016/j.nbd.2019.104559 (2019).

127. Abdel-Aleem, A. & Zaki, M. S. Spinocerebellar ataxia type 2 (SCA2) in an Egyptian family presenting with polyphagia and marked CAG expansion in infancy. *Journal of neurology* **255,** 413–419; 10.1007/s00415-008-0690-4 (2008).

128. Helmlinger, D. *et al.* Disease progression despite early loss of polyglutamine protein expression in SCA7 mouse model. *The Journal of neuroscience : the official journal of the Society for Neuroscience* **24,** 1881–1887; 10.1523/JNEUROSCI.4407-03.2004 (2004).

129. Koch, P. *et al.* Excitation-induced ataxin-3 aggregation in neurons from patients with Machado-Joseph disease. *Nature* **480,** 543–546; 10.1038/nature10671 (2011).

130. Wang, P.-S. *et al.* Association between proton magnetic resonance spectroscopy measurements and CAG repeat number in patients with spinocerebellar ataxias 2, 3, or 6. *PloS one* **7,** e47479; 10.1371/journal.pone.0047479 (2012).

131. Oz, G. *et al.* In vivo monitoring of recovery from neurodegeneration in conditional transgenic SCA1 mice. *Experimental neurology* **232,** 290–298; 10.1016/j.expneurol.2011.09.021 (2011).

132. Öz, G. *et al.* Assessing recovery from neurodegeneration in spinocerebellar ataxia 1: Comparison of in vivo magnetic resonance spectroscopy with motor testing, gene expression and histology. *Neurobiology of disease* **74,** 158–166; 10.1016/j.nbd.2014.11.011 (2015).

133. Francis, J. S. *et al.* N-acetylaspartate supports the energetic demands of developmental myelination via oligodendroglial aspartoacylase. *Neurobiology of disease* **96,** 323–334; 10.1016/j.nbd.2016.10.001 (2016).

134. Mehta, V. & Namboodiri, M.A.A. N-Acetylaspartate as an acetyl source in the nervous system. *Molecular Brain Research* **31,** 151–157; 10.1016/0169-328X(95)00044-S (1995).

135. Prokesch, A. *et al.* N-acetylaspartate catabolism determines cytosolic acetyl-CoA levels and histone acetylation in brown adipocytes. *Scientific reports* **6,** 23723; 10.1038/srep23723 (2016).

136. Ariyannur, P. S. *et al.* Methamphetamine-induced neuronal protein NAT8L is the NAA biosynthetic enzyme: implications for specialized acetyl coenzyme A metabolism in the CNS. *Brain Research* **1335,** 1–13; 10.1016/j.brainres.2010.04.008 (2010).

137. Tiwari, V., Ambadipudi, S. & Patel, A. B. Glutamatergic and GABAergic TCA cycle and neurotransmitter cycling fluxes in different regions of mouse brain. *Journal of cerebral blood flow and metabolism : official journal of the International Society of Cerebral Blood Flow and Metabolism* **33,** 1523–1531; 10.1038/jcbfm.2013.114 (2013).

138. Bröer, S. & Palacín, M. The role of amino acid transporters in inherited and acquired diseases. *The Biochemical journal* **436,** 193–211; 10.1042/BJ20101912 (2011).

139. Castellano, G., Dias, C. S., Foerster, B., Li, L. M. & Covolan, R. J. NAA and NAAG variation in neuronal activation during visual stimulation. *Brazilian journal of medical and biological research = Revista brasileira de pesquisas medicas e biologicas* **45**; 10.1590/s0100-879x2012007500128 (2012).

140. Luthi-Carter, R., Barczak, A. K., Speno, H. & Coyle, J. T. Hydrolysis of the neuropeptide N-acetylaspartylglutamate (NAAG) by cloned human glutamate carboxypeptidase II. *Brain Research* **795,** 341–348; 10.1016/S0006-8993(98)00244-3 (1998).

141. Paciorkowski, A. R. *et al.* Massive expansion of SCA2 with autonomic dysfunction, retinitis pigmentosa, and infantile spasms. *Neurology* **77,** 1055–1060; 10.1212/WNL.0b013e31822e5627 (2011).

142. Huber, K. *et al.* N-acetylaspartate pathway is nutrient responsive and coordinates lipid and energy metabolism in brown adipocytes. *Biochimica et biophysica acta. Molecular cell research* **1866,** 337–348; 10.1016/j.bbamcr.2018.08.017 (2019).

143. Zhang, H. H. *et al.* Insulin stimulates adipogenesis through the Akt-TSC2-mTORC1 pathway. *PloS one* **4,** e6189; 10.1371/journal.pone.0006189 (2009).

144. Sen, N.-E. *et al.* In Human and Mouse Spino-Cerebellar Tissue, Ataxin-2 Expansion Affects Ceramide-Sphingomyelin Metabolism. *International journal of molecular sciences* **20**; 10.3390/ijms20235854 (2019).

145. Olsen, A. S. B. & Færgeman, N. J. Sphingolipids: membrane microdomains in brain development, function and neurological diseases. *Open biology* **7**; 10.1098/rsob.170069 (2017).

146. Posse de Chaves, E. & Sipione, S. Sphingolipids and gangliosides of the nervous system in membrane function and dysfunction. *FEBS letters* **584,** 1748–1759; 10.1016/j.febslet.2009.12.010 (2010).

147. Hallett, P. J. *et al.* Glycosphingolipid levels and glucocerebrosidase activity are altered in normal aging of the mouse brain. *Neurobiology of aging* **67,** 189–200; 10.1016/j.neurobiolaging.2018.02.028 (2018).

148. Hoche, F. *et al.* Involvement of the auditory brainstem system in spinocerebellar ataxia type 2 (SCA2), type 3 (SCA3) and type 7 (SCA7). *Neuropathology and applied neurobiology* **34,** 479–491; 10.1111/j.1365-2990.2007.00933.x (2008).

149. Blasco, H. *et al.* Lipidomics Reveals Cerebrospinal-Fluid Signatures of ALS. *Scientific reports* **7,** 17652; 10.1038/s41598-017-17389-9 (2017).

150. Blasco, H. *et al.* A pharmaco-metabolomics approach in a clinical trial of ALS: Identification of predictive markers of progression. *PloS one* **13,** e0198116; 10.1371/journal.pone.0198116 (2018).

151. Hussain, M. M., Jin, W. & Jiang, X.-C. Mechanisms involved in cellular ceramide homeostasis. *Nutrition & metabolism* **9,** 71; 10.1186/1743-7075-9-71 (2012).

152. Zhao, L. *et al.* A deficiency of ceramide biosynthesis causes cerebellar purkinje cell neurodegeneration and lipofuscin accumulation. *PLoS genetics* **7,** e1002063; 10.1371/journal.pgen.1002063 (2011).

153. Becker, I., Wang-Eckhardt, L., Yaghootfam, A., Gieselmann, V. & Eckhardt, M. Differential expression of (dihydro)ceramide synthases in mouse brain: oligodendrocyte-specific expression of CerS2/Lass2. *Histochemistry and cell biology* **129,** 233–241; 10.1007/s00418-007-0344-0 (2008).

154. Imgrund, S. *et al.* Adult ceramide synthase 2 (CERS2)-deficient mice exhibit myelin sheath defects, cerebellar degeneration, and hepatocarcinomas. *The Journal of biological chemistry* **284,** 33549–33560; 10.1074/jbc.M109.031971 (2009).

155. Laviad, E. L. *et al.* Characterization of ceramide synthase 2: tissue distribution, substrate specificity, and inhibition by sphingosine 1-phosphate. *The Journal of biological chemistry* **283,** 5677–5684; 10.1074/jbc.M707386200 (2008).

156. Couttas, T. A. *et al.* Loss of ceramide synthase 2 activity, necessary for myelin biosynthesis, precedes tau pathology in the cortical pathogenesis of Alzheimer's disease. *Neurobiology of aging* **43,** 89–100; 10.1016/j.neurobiolaging.2016.03.027 (2016).

157. Kihara, A. Very long-chain fatty acids: elongation, physiology and related disorders. *Journal of biochemistry* **152,** 387–395; 10.1093/jb/mvs105 (2012).

158. Mueller, N. *et al.* De novo mutation in ELOVL1 causes ichthyosis, acanthosis nigricans, hypomyelination, spastic paraplegia, high frequency deafness and optic atrophy. *Journal of Medical Genetics* **56,** 164–175; 10.1136/jmedgenet-2018-105711 (2019).

159. Kutkowska-Kaźmierczak, A. *et al.* Dominant ELOVL1 mutation causes neurological disorder with ichthyotic keratoderma, spasticity, hypomyelination and dysmorphic features. *Journal of Medical Genetics* **55,** 408–414; 10.1136/jmedgenet-2017-105172 (2018).

160. Shimano, H. Novel qualitative aspects of tissue fatty acids related to metabolic regulation: lessons from Elovl6 knockout. *Progress in lipid research* **51,** 267–271; 10.1016/j.plipres.2011.12.004 (2012).

161. Deák, F., Anderson, R. E., Fessler, J. L. & Sherry, D. M. Novel Cellular Functions of Very Long Chain-Fatty Acids: Insight From ELOVL4 Mutations. *Frontiers in cellular neuroscience* **13,** 428; 10.3389/fncel.2019.00428 (2019).

162. Hoxha, E. *et al.* Motor Deficits and Cerebellar Atrophy in Elovl5 Knock Out Mice. *Frontiers in cellular neuroscience* **11,** 343; 10.3389/fncel.2017.00343 (2017).

163. Di Gregorio, E. *et al.* ELOVL5 mutations cause spinocerebellar ataxia 38. *American Journal of Human Genetics* **95,** 209–217; 10.1016/j.ajhg.2014.07.001 (2014).

164. Wang, W. *et al.* Inhibition of Mammalian Target of Rapamycin Complex 1 (mTORC1) Downregulates ELOVL1 Gene Expression and Fatty Acid Synthesis in Goat Fetal Fibroblasts. *International journal of molecular sciences* **16,** 16440–16453; 10.3390/ijms160716440 (2015).

165. Guo, Z. *et al.* Rapamycin Inhibits Expression of Elongation of Very-long-chain Fatty Acids 1 and Synthesis of Docosahexaenoic Acid in Bovine Mammary Epithelial Cells. *Asian-Australasian journal of animal sciences* **29,** 1646–1652; 10.5713/ajas.15.0660 (2016).

166. Garay-Lugo, N. *et al.* n-3 Fatty acids modulate the mRNA expression of the Nlrp3 inflammasome and Mtor in the liver of rats fed with high-fat or high-fat/fructose diets. *Immunopharmacology and immunotoxicology* **38,** 353–363; 10.1080/08923973.2016.1208221 (2016).

167. Schuchman, E. H. & Desnick, R. J. Types A and B Niemann-Pick disease. *Molecular genetics and metabolism* **120,** 27–33; 10.1016/j.ymgme.2016.12.008 (2017).

168. Sundaram, K. *et al.* Loss of neutral ceramidase protects cells from nutrient- and energy -deprivation-induced cell death. *The Biochemical journal* **473,** 743–755; 10.1042/BJ20150586 (2016).

169. Marco Piccinini *et al.* Deregulated Sphingolipid Metabolism and Membrane Organization in Neurodegenerative Disorders. *Mol Neurobiol* **41,** 314–340; 10.1007/s12035-009-8096-6 (2010).

170. Coughlan, K. S., Halang, L., Woods, I. & Prehn, J. H. M. A high-fat jelly diet restores bioenergetic balance and extends lifespan in the presence of motor dysfunction and lumbar spinal cord motor neuron loss in TDP-43A315T mutant C57BL6/J mice. *Disease models & mechanisms* **9,** 1029–1037; 10.1242/dmm.024786 (2016).

171. Nakken, O., Meyer, H. E., Stigum, H. & Holmøy, T. High BMI is associated with low ALS risk: A population-based study. *Neurology* **93,** e424-e432; 10.1212/WNL.0000000000007861 (2019).

172. Ludolph, A. C. *et al.* Effect of High-Caloric Nutrition on Survival in Amyotrophic Lateral Sclerosis. *Annals of neurology* **87,** 206–216; 10.1002/ana.25661 (2020).

173. Canet-Pons, J. *et al. Atxn2 -CAG100-KnockIn mouse spinal cord shows progressive TDP43 pathology associated with cholesterol biosynthesis suppression* (2019).

10. APPENDIX

I. Publication #1

Declaration of author contributions

Title: PINK1 and Ataxin-2 as modifiers of growth (Review)
Status: Published
Journal: *Oncotarget*, 2017, doi: 10.18632/oncotarget.16636
Authors: Nesli-Ece Sen (NES), Suzana Gispert (SG), Georg Auburger (GA)

Author contributions:

(1) Concept and design
Doctoral candidate (NES): **40%**
Co-author SG: **20%**
Co-author GA: **40%**

(2) Conducting tests and experiments
Doctoral candidate (NES): **n/a**
Co-author SG: **n/a**
Co-author GA: **n/a**

(3) Literature collection
Doctoral candidate (NES): **40%** (Literature search)
Co-author SG: **20%** (Literature knowledge)
Co-author GA: **40%** (Literature knowledge and search)

(4) Analysis and interpretation of data
Doctoral candidate (NES): **35%** (Analysis of primary reference paper)
Co-author SG: **20%** (Interpretation of data and literature)
Co-author GA: **45%** (Interpretation of data and literature)

(5) Drafting of manuscript
Doctoral candidate (NES): **35%**
Co-author SG: **20%**
Co-author GA: **45%**

Editorial

PINK1 and Ataxin-2 as modifiers of growth

Nesli E. Sen, Suzana Gispert and Georg Auburger

A recent report showed PINK1 transcript levels to be up- or down-regulated by the gain or loss of Ataxin-2 function, respectively, in human blood, in a human neural cell line and in mouse tissues [1]. These observations may have profound implications for the regulation of cell growth and may be medically exploited for the treatment of cancer and neural atrophy.

PINK1 is a mitochondrial serine threonine kinase that activates ubiquitin and the ubiquitin ligase PARKIN, triggering the autophagic elimination of dysfunctional mitochondria and of invading bacteria. PINK1 and PARKIN have an established important role for cancer, as regulators of the Warburg effect, and through their tumor suppressor action [2]. Famously, the HeLa tumor cell line with its exceptional growth carries a deletion of the PARKIN gene. Similarly, the Ataxin-2 transcriptional upregulation and its recombinant overexpression were shown to contribute to the spontaneous regression of childhood neuroblastoma tumors and to apoptosis induction in neuroblastoma cells [3].

The gain-of-function of Ataxin-2 via an expansion of its polyglutamine domain also drives neural cells into apoptosis, triggering the neurodegenerative multi-system-atrophy known as SCA2 (Spinocerebellar Ataxia type 2) and contributing to the motor neuron degenerations known as ALS and FTD (Amyotrophic Lateral Sclerosis and Frontotemporal Dementia, respectively). Conversely, the loss of Ataxin-2 triggers obesity and insulin resistance, predisposing to diabetes mellitus and hypertension [4, 5]. Importantly, a highly visible article has just demonstrated that this reduction in Ataxin-2 abundance can be exploited therapeutically to postpone the appearance of motor neuron degeneration in a TDP-43 driven mouse model of ALS, reducing its pathology, and extending its lifespan [Becker-LA et al., Nature 2017; just accepted]. Another such article has confirmed that the antisense-oligonucleotide-driven knockdown of Ataxin-2 will prevent SCA2 [Scoles-DR et al., Nature 2017; just accepted].

In the current knowledge on the hierarchy of disease proteins responsible for the neurodegenerative process in Parkinson's disease, the recent observations [1] would now place Ataxin-2 upstream of PINK1, which is known to regulate PARKIN, and the transcriptional levels of LRRK2 are dependent on PARKIN.

Experiments in human, mouse, worms and yeast over the past 2 years have elucidated also the position of Ataxin-2 within the established cell growth pathways. They confirmed that Pbp1 as the yeast orthologue of Ataxin-2 is being controlled by AMP-kinase phosphorylation signals. Human Ataxin-2 is transcriptionally induced during starvation, and the

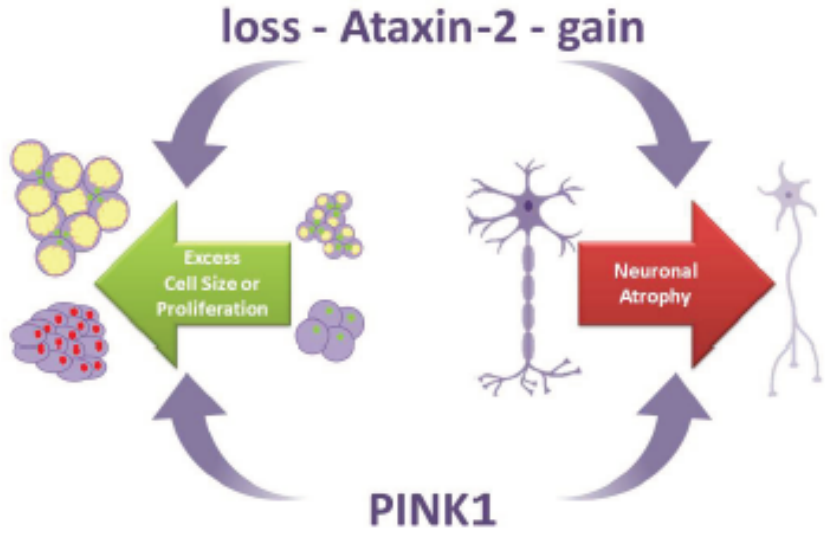

Figure 1: : Two sides of each coin. Neuronal atrophy and tumor regression are triggered by a gain of Ataxin-2 function, while Ataxin-2 deficiency is responsible for obesity and neuroprotection. PINK1 is also responsible for neurodegeneration when its function is deficient, while a gain of PINK1 function acts as tumor suppressor.

Ataxin-2 protein relocalizes to stress granules in periods of glucose deprivation or oxidative stress [6, 7]. Downstream effects of Ataxin-2 include the repression of mTOR-dependent phosphorylation signals, but also the enhancement of PINK1-dependent phosphorylation signals [1, 6-8]. Via Ataxin-2 occurs also a regulation of the cell size, of the availability of lipid and glycogen stores as alternative fuels in times of high bioenergetic demands, and of ribosomal translation during stress periods [6, 8]. These latter global effects of Ataxin-2 are canonical functions of the mTORC1 signaling complex.

Given that the transcript levels of Ataxin-2, PINK1 and PARKIN change several fold during the transition from a nutrient excess to a starvation in amino acids, lipids and glucose [1, 6], their analysis in the blood samples or tumor tissues of patients will also provide a simple read-out that reflects trophic state versus stress responses.

Thus, Ataxin-2 represents a new target to modulate cell growth either in the direction of nutrient excess, neuroprotection, obesity, diabetes and cancer, or conversely into the direction of tumor regression, neural atrophy and apoptosis. The identification of the specific phosphorylation sites that are governing Ataxin-2 function and those phosphorylation events that depend on Ataxin-2 will be a key prerequisite to design specific drugs for the preventive treatment of a wide array of diseases.

Georg Auburger: Department of Neurology, Goethe University Medical School, Frankfurt am Main, Germany

Correspondence to: *Georg Auburger,* ***email*** *auburger@em.uni-frankfurt.de*

Keywords: tumor suppressor, neuroblastoma regression, obesity, motor neuron disease

Received: *March 09, 2017*

Published: *March 28, 2017*

REFERENCES

1. Sen NE, et al. Neurobiol Dis. 2016; 96:115-126.
2. O'Flanagan CH, et al. Biochim Biophys Acta. 2014; 1846:590-598.
3. Wiedemeyer R, et al. Oncogene. 2003; 22:401-411.
4. Auburger G, et al. World J Diabetes. 2014; 5:316-327.
5. Lastres-Becker I, et al. Hum Mol Genet. 2008; 17:1465-1481.
6. Lastres-Becker I, et al. Biochim Biophys Acta. 2016; 1862:1558-1569.
7. DeMille D, et al. Mol Biol Cell. 2015; 26:569-582.
8. Bar DZ, et al. Proc Natl Acad Sci U S A. 2016; 113:E4620-4629.

II. Publication #2

Declaration of author contributions

Title: Generation of an *Atxn2*-CAG100 knock-in mouse reveals N-acetylaspartate production deficit due to early *Nat8l* dysregulation
Status: Published
Journal: *Neurobiol Dis.,* 2019, doi: 10.1016/j.nbd.2019.104559
Authors: Nesli-Ece Sen (NES)*, Julia Canet-Pons (JCP)*, Melanie Vanessa Halbach (MVH)*, Aleksandar Arsovic (AA), Ulrich Pilatus (UP), Whoon-Hyung Chae (WHC), Zeynep-Ece Kaya (ZEK), Kay Seidel (KS), Ewa Rollman (ER), Michel Mittelbronn (MM), David Meierhofer (DM), Chris I. De Zeeuw (CIDZ), Laurens Bosman (LB), Suzana Gispert (SG), Georg Auburger (GA)

Author contributions:

(1) Concept and design
Doctoral candidate (NES): **30%**
Co-author JCP: **20%**
Co-author MVH: **10%**
Co-author SG: **10%**
Co-author GA: **30%**

(2) Conducting tests and experiments
Doctoral candidate (NES): **30%** (Mouse work, tissue collection, expression analyses, biochemical characterization, cell culture experiments, immunostaining)
Co-author JCP: **20%** (Mouse work, tissue collection, behavioral tests, immunostaining)
Co-author MVH: **15%** (Mouse genetics, tissue collection, behavioral tests)
Co-author AA: **15%** (Tissue collection, expression analyses, cell culture experiments)
Co-author WHC: **5%** (NMR spectroscopy)
Co-author SG: **15%** (Mouse genetics, tissue collection, behavioral tests)

(3) Compilation of data sets and figures
Doctoral candidate (NES): **30%** (Behavioral tests, biochemical characterization, expression analyses, NMR spectroscopy, immunostaining)
Co-author JCP: **20%** (Behavioral tests, immunostaining)
Co-author MVH: **20%** (Behavioral tests, immunostaining)
Co-author AA: **10%** (Expression analyses)
Co-author UP: **10%** (NMR spectroscopy)
Co-author SG: **10%** (Mouse genetics, behavioral tests)

(4) Analysis and interpretation of data
Doctoral candidate (NES): **30%** (Biochemical characterization, expression analyses, NMR spectroscopy, immunostaining)
Co-author JCP: **15%** (Behavioral tests, immunostaining)
Co-author MVH: **15%** (Behavioral tests, immunostaining)
Co-author AA: **5%** (Expression analyses)
Co-author UP: **5%** (NMR spectroscopy)
Co-author SG: **10%** (Mouse genetics, behavioral tests)
Co-author GA: **20%** (Interpretation of all data)

(5) Drafting of manuscript
Doctoral candidate (NES): **60%**
Co-author GA: **40%**

Neurobiology of Disease 132 (2019) 104559

Contents lists available at ScienceDirect

Neurobiology of Disease

journal homepage: www.elsevier.com/locate/ynbdi

Generation of an *Atxn2*-CAG100 knock-in mouse reveals *N*-acetylaspartate production deficit due to early *Nat8l* dysregulation

Nesli-Ece Sen[a,1], Júlia Canet-Pons[a,1], Melanie V. Halbach[a,1], Aleksandar Arsovic[a], Ulrich Pilatus[b], Woon-Hyung Chae[c], Zeynep-Ece Kaya[a,d], Kay Seidel[e], Ewa Rollmann[a], Michel Mittelbronn[f,g,h,i,j], David Meierhofer[k], Chris I. De Zeeuw[l,m], Laurens W.J. Bosman[m], Suzana Gispert[a], Georg Auburger[a,*]

[a] Experimental Neurology, Goethe University Medical School, 60590 Frankfurt am Main, Germany
[b] Institute of Neuroradiology, Goethe University Medical School, 60590 Frankfurt am Main, Germany
[c] Georg-Speyer-Haus, Institute for Tumor Biology and Experimental Therapy, 60596 Frankfurt am Main, Germany
[d] Department of Neurology, Cerrahpasa School of Medicine, Istanbul University, 34098 Istanbul, Turkey
[e] Department of Anatomy II, Institute of Clinical Neuroanatomy, Goethe University, 60590 Frankfurt am Main, Germany
[f] Neurological Institute (Edinger Institute), Goethe University, 60590 Frankfurt am Main, Germany
[g] Luxembourg Centre of Neuropathology (LCNP), Luxembourg
[h] Department of Pathology, Laboratoire National de Santé (LNS), Dudelange, Luxembourg
[i] Luxembourg Centre for Systems Biomedicine (LCSB), University of Luxembourg, Esch-sur-Alzette, Luxembourg
[j] Department of Oncology, NORLUX Neuro-Oncology Laboratory, Luxembourg Institute of Health (LIH), Luxembourg
[k] Max Planck Institute for Molecular Genetics, 14195 Berlin, Germany
[l] Netherlands Institute for Neuroscience, Royal Academy of Arts and Sciences, 1105 BA Amsterdam, the Netherlands
[m] Department of Neuroscience, Erasmus Medical Center, 3000 CA Rotterdam, the Netherlands

ARTICLE INFO

Keywords:
N-acetylaspartate
Molecular biomarkers of disease
Polyglutamine expansion
Stress granules
Mitochondrial bioenergetics
RNA processing

ABSTRACT

Spinocerebellar ataxia type 2 (SCA2) is an autosomal dominant neurodegenerative disorder caused by CAG-expansion mutations in the *ATXN2* gene, mainly affecting motor neurons in the spinal cord and Purkinje neurons in the cerebellum. While the large expansions were shown to cause SCA2, the intermediate length expansions lead to increased risk for several atrophic processes including amyotrophic lateral sclerosis and Parkinson variants, e.g. progressive supranuclear palsy. Intense efforts to pioneer a neuroprotective therapy for SCA2 require longitudinal monitoring of patients and identification of crucial molecular pathways. The ataxin-2 (ATXN2) protein is mainly involved in RNA translation control and regulation of nutrient metabolism during stress periods. The preferential mRNA targets of ATXN2 are yet to be determined. In order to understand the molecular disease mechanism throughout different prognostic stages, we generated an *Atxn2*-CAG100-knock-in (KIN) mouse model of SCA2 with intact murine ATXN2 expression regulation. Its characterization revealed somatic mosaicism of the expansion, with shortened lifespan, a progressive spatio-temporal pattern of pathology with subsequent phenotypes, and anomalies of brain metabolites such as *N*-acetylaspartate (NAA), all of which mirror faithfully the findings in SCA2 patients. Novel molecular analyses from stages before the onset of motor deficits revealed a strong selective effect of ATXN2 on *Nat8l* mRNA which encodes the enzyme responsible for NAA synthesis. This metabolite is a prominent energy store of the brain and a well-established marker for neuronal health. Overall, we present a novel authentic rodent model of SCA2, where in vivo magnetic resonance imaging was feasible to monitor progression and where the definition of earliest transcriptional abnormalities was possible. We believe that this model will not only reveal crucial insights regarding the pathomechanism of SCA2 and other ATXN2-associated disorders, but will also aid in developing gene-targeted therapies and disease prevention.

* Corresponding author.
E-mail address: auburger@em.uni-frankfurt.de (G. Auburger).
[1] Joint first authors.

https://doi.org/10.1016/j.nbd.2019.104559
Received 29 May 2019; Received in revised form 16 July 2019; Accepted 30 July 2019
Available online 31 July 2019

1. Introduction

Spinocerebellar ataxia type 2 (SCA2) is an autosomal dominantly inherited neurodegenerative disorder mainly affecting Purkinje cells in the cerebellum and motor neurons in the spinal cord (Auburger et al., 2017). Patients suffer from uncoordinated movement, gait ataxia, dysarthria, and intention tremor. Before the development of ataxia, already a slowing of ocular saccade movements and an increase of muscle cramps appear. In the nervous system, the typical multi-system atrophy progresses over 25 years (Antenora et al., 2018), until patients die from respiratory failure due to motor neuron loss (Lastres-Becker et al., 2008b). In peripheral tissues, atrophy of muscle mass and body fat are prominent at the late immobility stage (Velazquez-Perez et al., 2017b), but it is noteworthy that subcutaneous fat tissue loss appears in craniocervical distribution already at presymptomatic stages. Monitoring the disease progression and assessing therapeutic benefits is aided by the identification of biomarkers that are easily quantified in living patients. A prominent metabolite in brain that is generated by neuronal mitochondria and used in oligodendroglia for myelinogenesis, *N*-acetylaspartate (NAA), can be detected by magnetic resonance imaging (MRI) spectroscopy. It shows reduced levels in SCA2, and in various other progressive neurodegenerative disorders as well as in brain injury (Guerrini et al., 2004). The extent of NAA decrease was found highly correlated with the progression of SCA2 (Cahill Jr. and Veech, 2003; Wang et al., 2012).

Dynamic CAG-repeat expansion mutations in *ATXN2* gene have been identified as the monogenic cause of SCA2. While healthy individuals have 22 repeat units in the first exon of *ATXN2*, encoding a domain with 22 glutamine (Glu, Q) amino acids, SCA2 patients have > 33 repeat units in this region (Auburger et al., 1990; Orozco Diaz et al., 1990; Pulst et al., 1996). Larger repeat expansions lead to earlier disease onset, faster progression, more widespread pathology and earlier death (Almaguer-Mederos et al., 2013; Almaguer-Mederos et al., 2010; Rub et al., 2013; Tuin et al., 2006; Velazquez-Perez et al., 2009; Velazquez-Perez et al., 2004). For instance, patients with 92 and 116 repeat units had clinical manifestation within the first year of life and showed multi-system atrophy of cerebellum, brainstem and cerebrum (Di Fabio et al., 2012; Vinther-Jensen et al., 2013). Aside from the repeat size, the structure of the repeat region also differs between patients and healthy individuals; the normal *ATXN2* allele contains 22 repeats with CAA interruptions in the form of $(CAG)_8CAA(CAG)_4CAA(CAG)_8$. Interestingly, most SCA2 patients lack both CAA units and have pure CAG-repeats instead. As CAA and CAG both code for glutamine, the protein structure remains the same, however instability of a pure CAG-repeat region at DNA level is significantly higher and leads to even larger expansions in the following generations. Intermediate-length expansions of 26–30 repeats with CAA interruptions have been shown to increase the risk of developing motor neuron diseases like ALS (Amyotrophic Lateral Sclerosis) or FTLD (Fronto-Temporal Lobar Dementia) (Elden et al., 2010; Gispert et al., 2012; Lee et al., 2011). Also, a specific haplotype of single nucleotide polymorphisms in *ATXN2* is associated with higher risk of ALS (Lahut et al., 2012). In addition, pathogenic *ATXN2* expansions with CAA interruptions were reported to underlie dopaminergic midbrain neuron atrophy in families with Parkinson's disease (PD) (Gispert et al., 2012; Park et al., 2015).

Ataxin-2 (ATXN2) is an evolutionarily conserved protein in the eukaryotes, associated with mRNA translational regulation and stress response. Under normal conditions, ATXN2 is located in the cytosol, partly associated with the ribosomal machinery at the endoplasmic reticulum (ER), where it modulates protein synthesis (Fittschen et al., 2015; Fleischer et al., 2006; van de Loo et al., 2009). Upon cell damage or bioenergetic deficits, its transcription is enhanced and ATXN2 relocalizes to stress granules (SGs) where mRNAs are stalled to undergo quality control until protein synthesis is resumed after stress (Heck et al., 2014; Kedersha et al., 2013; Lastres-Becker et al., 2016; Nonhoff et al., 2007). Interaction of ATXN2 with mRNAs occur either directly via its N-terminal Lsm and LsmAD domains, or indirectly through interaction with Poly(A) Binding Protein (PABP) via its C-terminal PAM2 motif. ATXN2 also contains several proline-rich motifs interspersed throughout the protein that modulate trophic receptor endocytosis and growth pathways (Auburger et al., 2017; Drost et al., 2013; Lastres-Becker et al., 2008a; Nonis et al., 2008; Lastres-Becker, 2019). It is unclear if ATXN2 binds to many or few RNAs, but its impact on neuronal habituation via specific microRNA interaction and on the circadian rhythm via *Per* mRNA interaction have been reported (Pfeffer et al., 2017; Sudhakaran et al., 2014). Through interaction with specific proteins like TDP-43 and ITPR1, ATXN2 also acts as modulator of RNA splicing and neural excitability (Elden et al., 2010; Liu et al., 2009).

In contrast to the atrophic phenotype in SCA2 patients, loss of ATXN2 in mouse triggers obesity, dyslipidemia, insulin resistance and hepatic accumulation of lipid droplets and glycogen (Lastres-Becker et al., 2008a). *ATXN2* locus polymorphisms in humans were also found associated with obesity, hypertension, diabetes mellitus type 1 and cardiac infarction (Auburger et al., 2014). Strong effects of ATXN2 orthologues on mitochondrial precursor proteins and metabolic enzymes were documented in numerous studies and organisms, further strengthening the modulatory effect of ATXN2 on nutrient metabolism and cellular energetics throughout evolution (Meierhofer, 2016; Seidel et al., 2017; Sen et al., 2016; Sen et al., 2017; Wang and Chen, 2015). Intriguingly, ATXN2 deficiency not only rescues the lethality of yeast PABP deletion (Mangus et al., 1998), but also shows therapeutic promise in flies and mice by mitigating the neurodegenerative process of spinocerebellar ataxias and ALS models (Al-Ramahi et al., 2007; Becker, 2017; Elden et al., 2010; Scoles, 2017).

Currently, there is no curative treatment for SCA2 (Freund et al., 2007). Although several *in vivo* and *in vitro* models for SCA2 were developed, an authentic mouse model mimicking all aspects of the disease was still lacking. Previous animal models largely focused on the overexpression of expanded ATXN2 in Purkinje neurons, so they are unsuitable to study extra-cerebellar deficits or the contribution of other cell types in the central nervous system. Analysis of these mouse mutants showed that ATXN2 protein aggregates accumulate in cytosol rather than the nucleus (Huynh et al., 2000). Purkinje cell-specific Q58- and Q127-ATXN2 expansions alter neuronal excitability (Dell'Orco et al., 2017; Hansen et al., 2013; Liu et al., 2009; Pflieger et al., 2017). Another model with the overexpression of a human Q72-ATXN2 BAC clone containing the physiological promoter and the intact exon-intron structure showed dysregulation of the G-protein signaling factor RGS8 in cerebellum (Dansithong et al., 2015). We recently published the first knock-in (KIN) mouse where normally expressed CAG42-expansion triggers ATXN2 to sequestrate PABP into insolubility in vulnerable brain regions (Damrath et al., 2012). Induction of the ubiquitination enzyme FBXW8 was observed as an effort to degrade Q42-expanded ATXN2 (Halbach et al., 2015). In addition, partial loss-of-function effects were observed to dysregulate calcium homeostasis factors similarly as in *Atxn2*-KO mouse (Halbach, 2017). Unfortunately, the neurological phenotypes appear only after two years in *Atxn2*-CAG42-KIN mice due to slow progression of the disease, making them unsuitable for studying advanced stages of SCA2 within the lifespan of a mouse.

Here, we present a new mouse model of ATXN2 pathology, named *Atxn2*-CAG100-KIN, created by the knock-in of 100 CAG trinucleotide repeat units into the murine *Atxn2* gene with intact murine promoter and exon-intron structure in order to preserve its native expression regulation. Extensive analyses on genetic instability, histology, behavior and in vivo measurements correlate with all aspects of the disease signature observed in patients; they also support the authenticity and value of this model in understanding the molecular mechanisms and in monitoring the disease progression *in vivo* via magnetic resonance spectroscopy. Our initial investigation into the molecular pathogenesis in mouse points to a progressive dysregulation of NAA synthesis in cerebellum, with a strong deficiency of NAA production enzyme *Nat8l*,

which starts from pre-symptomatic stages. Further mechanistic studies proved the direct effect of expanded ATXN2 on diminished *Nat8l* transcript levels also in adipogenic cells. This effect was replicated also in blood of *Atxn2*-CAG100-KIN mice and SCA2 patients, so human *NAT8L* levels show promise as peripheral biomarker.

In this initial study, we have focused on the neuronal aspects of pathology, trying to identify the earliest events that may play an important role in the manifestation and progression of the disease. However, this new model of ATXN2 pathology also allows understanding the involvement of non-neuronal cells in the nervous system, e.g. in view of the role of NAA as a neuron-generated metabolite that is needed for myelination. Our new model also permits the analysis of affected peripheral tissues that have been ignored so far, hopefully leading to the identification of prognostic biomarkers and novel therapies effective at the organism level.

2. Results

2.1. Generation of the Atxn2-CAG100 knock in mouse line and genetic instability

In order to study the progression of neurodegeneration in an authentic rodent model for SCA2, we created the novel *Atxn2*-CAG100 knock-in (KIN) mouse line. For this purpose, a $(CAG)_{100}$ repeat with neighboring sequences was synthesized and inserted into the murine *Atxn2* exon 1 at position Q156 with flanking loxP sites, employing the homologous recombination strategy shown in Fig. 1A and using previously described targeting vectors (Damrath et al., 2012; Lastres-Becker et al., 2008a). Embryonal stem (ES) cell lines with successful knock-in underwent Flp-mediated excision of the neomycin resistance cassette, and verification of the expansion length in heterozygous (CAG1/100) or homozygous (CAG100/100) animals was performed by PCR with Neo-flanking or repeat-flanking primers (Fig. 1B, C, Supplementary Table S1) and Sanger sequencing, resulting in a single homozygous *Atxn2*-CAG100-KIN mouse line.

Genotyping with repeat-flanking primers and with DNA-fragment-length-analysis on polyacrylamide gels initially suggested stability of the expansion size, as previously observed in the *Atxn2*-CAG42-KIN mice (Damrath et al., 2012). In patients, repeat expansions often increase over generations and show a mosaic pattern in the somatic cells (Cancel et al., 1997). To our knowledge, this instability and mosaicism has not been observed in previously generated mouse models of SCA2, while it is a known feature of mice with polyglutamine expansion that model Huntington's disease (Mangiarini et al., 1997). Although genotyping had initially suggested repeat stability in our *Atxn2*-CAG100-KIN mice, periodic testing in successive generations of this colony revealed the occurrence of further expansions and somatic mosaicism (Fig. 1D). The first three panels in Fig. 1D show 3 heterozygous animals from different generations over a period of 4 years, and reveal an increase of the repeat length in time. The calculated PCR product length for the WT allele is 90 bp, whereas the CAG100 allele generates a product of 387 bp. The first mouse has an average expanded allele size of 396.81 bp, with mosaicism ranging from 380 bp to 420 bp. The second mouse shows an exceptional mosaicism range from 405 bp to 476 bp, representing a CAG tract of 128 repeats. The third mouse shows less somatic mosaicism and the average expanded allele length is 470 bp. The bottom panel shows a homozygous KIN animal with no visible WT allele signal at 90 bp, but two expanded alleles with average peaks at 416.65 bp and 475.64 bp. Overall, these findings closely mirror the repeat instability observed in SCA2 patients. To preserve the initial expansion size of the *Atxn2*-CAG100-KIN mouse line, sperm cryopreservation from early generations was carried out. While we keep referring to the animals as *Atxn2*-CAG100-KIN, the CAG-repeat of the animals used was varying within the range shown in Fig. 1D.

2.2. Offspring contains fewer female mutants than expected

It has been shown previously that in the absence of ATXN2, mouse breeding produces less homozygous mutant and less female pups than expected (Kiehl et al., 2006; Lastres-Becker et al., 2008a). Also in invertebrates, gender-related reproductive anomalies have been reported, including female sterility in *D. melanogaster* with ATXN2 mutations and abnormal masculinization of the germline in *C. elegans* with ATX-2 deficiency (Ciosk et al., 2004; Satterfield et al., 2002). For these reasons, gender and genotypes were documented among offspring of 25 CAG1/100 breeder pairs. The litters contained significantly less homozygous mutants than expected (24% less CAG100/100 than WT pups; $p = .009$; χ^2 test with $\chi^2 = 9.384$ and $df = 2$) and less females than expected (12% reduction; $p = .098$; χ^2 test with $\chi^2 = 2.731$ and $df = 2$) (Supplementary Table S2). All data suggest that altered ATXN2 functions may impair embryonal development, with some gender-dependence. Thus, the findings constitute evidence for a partial loss-of-function of CAG100 allele in peripheral tissues, and for the high conservation of ATXN2 function during phylogenesis.

2.3. Initial weight excess reverts over time

Phenotypic and behavioral features of heterozygous and homozygous KIN animals were monitored until the end of lifespan. *Atxn2*-CAG100-KIN mice showed progressive motor deficits with hind limb clasping, reduced strength and ataxia (Supplementary Video S1). Homozygous *Atxn2*-CAG100-KIN animals displayed severe motor deficits around 14 months, which prompted the veterinarians to sacrifice the animals to prevent suffering. Therefore, the maximum lifespan is considered to be 14 months for homozygous animals. Even before the terminal stage of disease, homozygous *Atxn2*-CAG100-KIN animals showed an increased rate of death without known reasons ($p < .001$; $\chi^2 = 65.366$; $df = 2$; Kaplan-Meier survival analysis with Tarone-Ware test; Fig. 2A).

Although all mutants eventually developed a loss of weight compared to WT littermates, female homozygous *Atxn2*-CAG100-KIN animals initially displayed excess weight gain between 5 and 20 weeks. As the disease progressed, they not only lost this extra weight, but went further on towards an atrophic state. Female heterozygotes also showed reduced body mass in later disease stages, but without the initial weight gain ($p < .001$; $F = 70.524$ with 23 degrees of freedom; two-way ANOVA; Fig. 2B). In male mutants, we did not observe the initial weight excess, but they also showed a progressive weight loss relative to WT animals ($p < .001$; $F = 121.651$ with 23 degrees of freedom; two-way ANOVA; Fig. 2C). In male mutants, weight loss became significant already at the age of 10 weeks in heterozygous mice and at 20 weeks in homozygous mice. Even though the homozygous males started to lose weight later than their heterozygous littermates, their weight reduction developed faster and stronger (Fig. 2C). The temporal dynamics of body weight across lifespan might reflect an initial partial loss-of-function phenotype due to the reduced levels and insolubility of expanded ATXN2, followed by the progressive accumulation in cytosolic aggregates with consequent gain-of-function phenotypes.

Eventually, all the mutant mice displayed weight loss, but the time course depended on the dosage of expanded ATXN2 allele and on gender. This is in good agreement with previous reports stating that homozygous SCA2 patients also have earlier disease onset and a particularly severe disease course (Hoche et al., 2011; Ragothaman et al., 2004). Therefore, in order to investigate the maximal pathology and to avoid gender-specific bias, we focused on homozygous animals without gender separation in further neuropathological and expression analyses.

2.4. Initial hyperactivity disappears with ageing; progressive motor deficits are compatible with spinocerebellar ataxia

To determine whether the *Atxn2*-CAG100-KIN mice displayed motor deficits compatible with symptoms observed in SCA2 patients, we

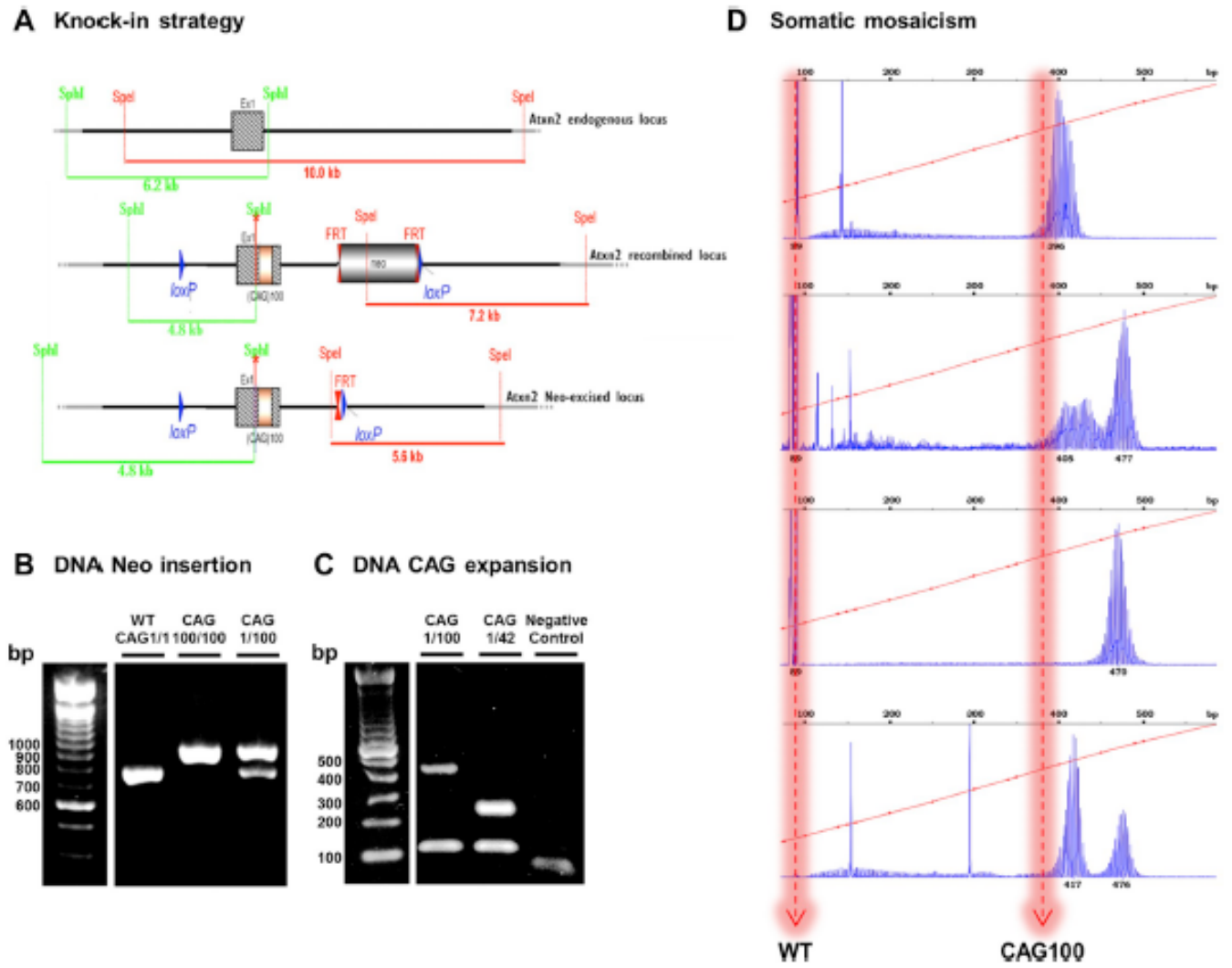

Fig. 1. Generation of *Atxn2*-CAG100 expansion and CAG repeat instability over generations. (A) Schematic diagram of the knock in strategy at exon 1 (Ex1) of the murine *Atxn2* gene on chromosome 5. Names of the restriction enzymes (*SphI*, *SpeI*), expected restriction fragment sizes in kilobases (kB) and position of loxP/FRT target sites of recombinases are marked, which were relevant in the homologous recombination screening and subsequent excision of the Neo-selection cassette. (B) Agarose gel electrophoresis results of genotyping PCR with primers flanking the Neo-excised locus (size of PCR product for CAG1 = 793 bp, CAG100 = 948 bp) and (C) primers flanking the CAG site (size of PCR product for CAG1 = 90 bp, CAG100 = 387 bp, CAG42 = 213 bp). As negative control, water instead of template DNA produced a lower-size band that represents PCR primers. (D) Fragment length analysis of the CAG repeat in three heterozygous (top three panels) and one homozygous knock-in (lower panel) mice. Predicted PCR fragment length of wild type allele is 90 bp, predicted PCR fragment length of CAG100 allele is 387 bp. While the WT allele gives a sharp peak at 90 bp level, all expanded alleles show a hedgehog-like pattern that reflects somatic mosaicism.

conducted a series of behavioral tests in older mice. Paw print analyses were performed to assess free movements in a narrow dark tunnel where the mice walk from one end to the other. Paw prints of *Atxn2*-CAG100-KIN mice at 12 months showed irregular steps and uncoordinated movement (Fig. 2D). To evaluate the particularly vulnerable motor neurons, grip strength analyses were done with *Atxn2*-CAG100-KIN animals from the age of 3 months onward, which revealed a significant decrease in the maximal forelimb efforts over time ($p < .001$; $F = 10.219$ with 7 degrees of freedom; ANOVA). Around the age of 11 months, the forelimb grip strength of *Atxn2*-CAG100-KIN mice became significantly less, while it remained intact in WT littermates ($p < .001$; $F = 9.964$ with 15 degrees of freedom; two-way ANOVA; Fig. 2E). Tests of the motor coordination ability and tenacity to stay on a rotating rod upon slow acceleration showed a significant and stable deficit in *Atxn2*-CAG100-KIN mice from the age of 20 weeks to 12 months, which progressed rapidly at 14 months. Heterozygous *Atxn2*-CAG100-KIN animals appeared normal on the rotarod ($p < .001$; $F = 13.871$ with 14 degrees of freedom; two-way ANOVA with Tukey's post-hoc tests: WT vs. CAG100/100: $p < .001$; WT vs. CAG1/100: $p = .978$; Fig. 2F). Open field tests were conducted to assess spontaneous activity and various motor impairments. Homozygous *Atxn2*-CAG100-KIN animals showed an initial hyperactivity period around the age of 10 weeks in terms of movement time, total distance travelled and horizontal movements (Fig. 2G), as previously described also in *Atxn2*-KO mice (Lastres-Becker et al., 2008a). However, reductions were observed in *Atxn2*-CAG100-KIN animals for all vertical behavior parameters starting from early ages, and worsening progressively (Fig. 2G). These severe deficits in vertical movement indicate problems in balancing upright for explorative or food-seeking purposes, and mirror the gait ataxia in SCA2 patients.

2.5. Deleterious effects of the CAG100 expansion on the transcription and translation of *Atxn2*

The expanded size of *Atxn2* mRNA was confirmed by saturation reverse transcriptase (RT)-PCR in cerebellum of heterozygous (CAG1/

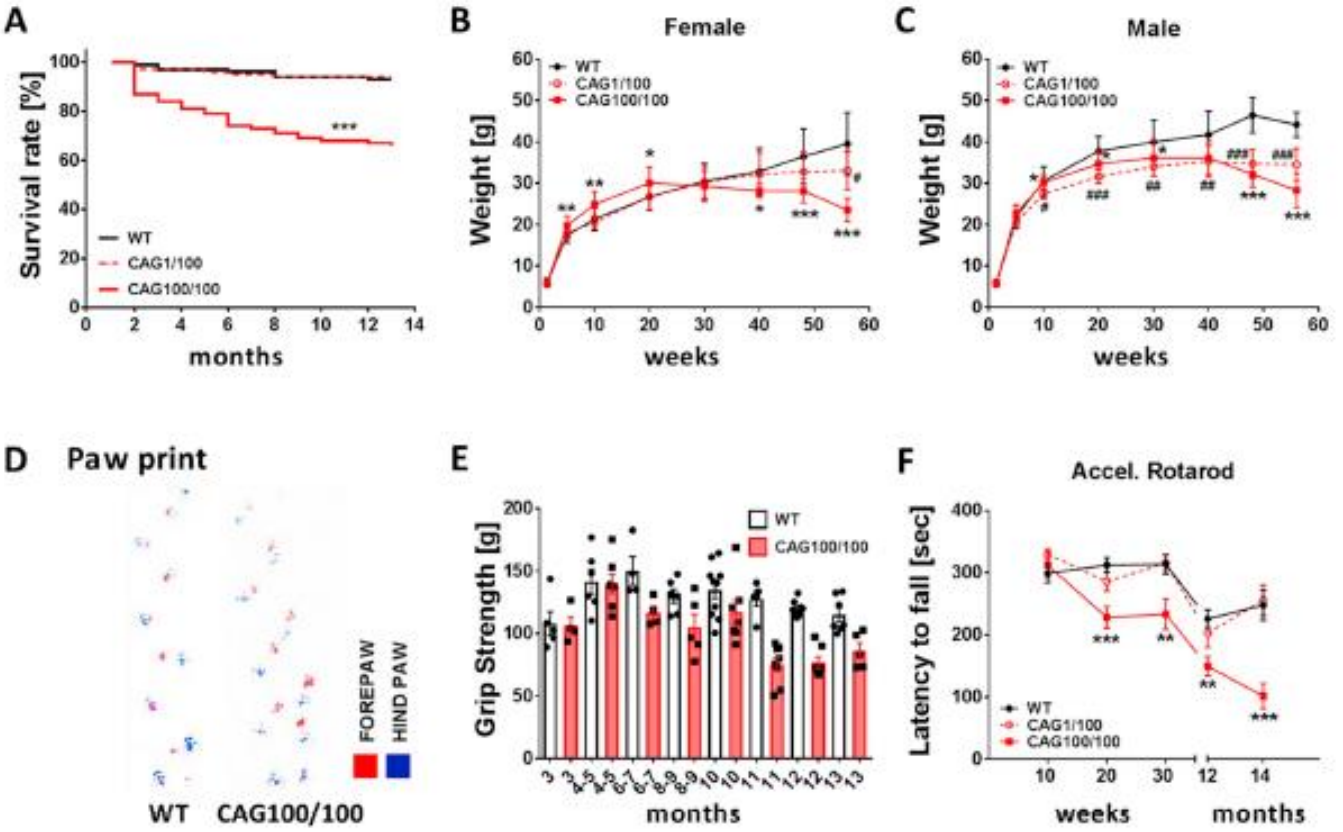

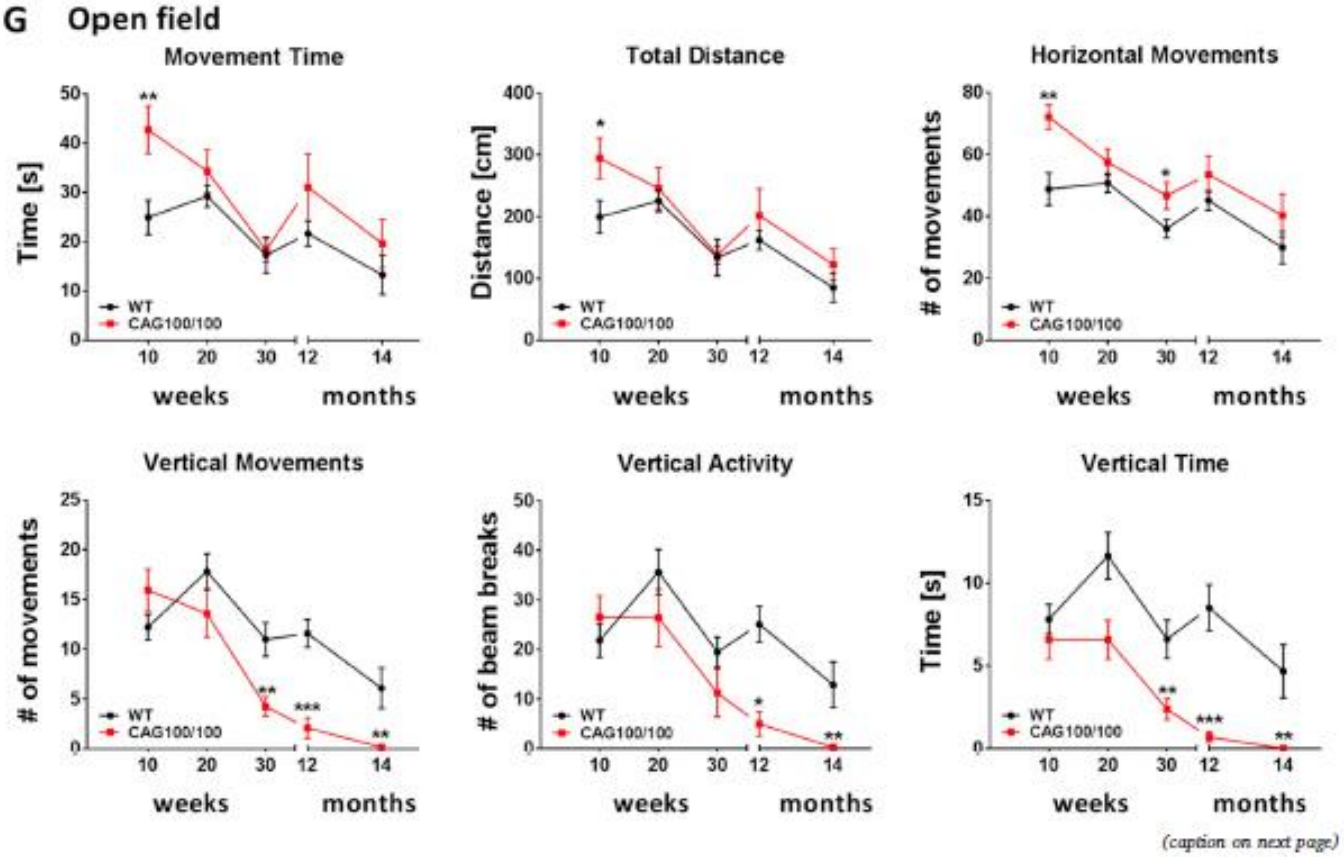

(caption on next page)

Fig. 2. Lifespan, weight and motor phenotypes of *Atxn2*-CAG100-KIN mice across ages. (A) The reduction of the ageing cohort through animals found dead at different ages is shown across the lifespan, before all animals were sacrificed for ethical reasons (100% corresponds to 106 CAG100/100, 235 CAG1/100 and 167 WT animals born initially). (B) Body weight of female and (C) male animals was studied in groups of 4–19 mice per genotype and age. Data is represented as means ± s.d. (D) Paw prints were recorded in 13 WT and 9 CAG100/100 animals at the age of 12 months. (E) Grip strength was assessed in 4–10 animals at the ages indicated. (F) The latency to fall from a rotarod slowly accelerating from 4 to 40 rpm reflected a very early motor deficit among CAG100/100 homozygotes ($n = 22$ animals per genotype for younger age groups, $n = 8$ animals for old ages). (G) Open field analyses of the spontaneous movement activity of mice during a 5 min observation period in an odor-neutral arena recorded in automated manner via infra-red beam breaks for various parameters of locomotion ($n = 8$–23 animals per age and genotype). (For interpretation of the references to colour in this figure legend, the reader is referred to the web version of this article.)

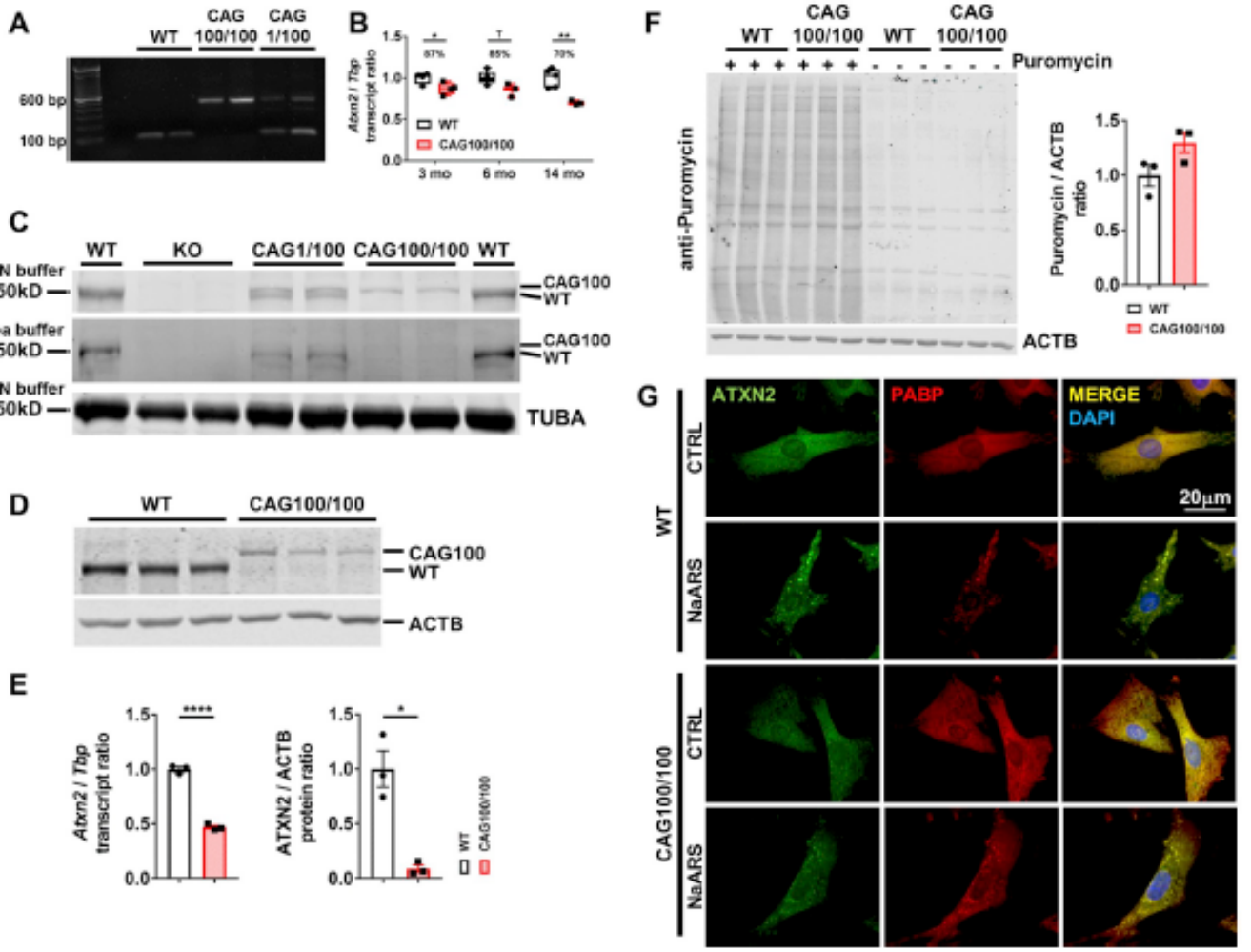

Fig. 3. CAG100 allele shows major protein insolubility, despite mild transcript changes in cerebellum. (A) Analysis of cerebellar cDNA by RT-PCR with primers flanking the CAG site demonstrated the presence of expansion in *Atxn2* mRNA from heterozygous (CAG1/100) and homozygous (CAG100/100) knock-in animals. (B) Expression analysis of *Atxn2* transcript in CAG100/100 cerebellar cDNA showed mild reduction that progressed with age. Statistical analyses were done by unpaired *t*-test with Welch's correction. Box-whiskers plot shows individual values with median and min to max confidence interval. (C) Detection of ATXN2 protein in WT, *Atxn2*-knock out (KO), heterozygous and homozygous *Atxn2*-CAG100-KIN mice cerebellum protein lysates isolated with low-detergent (PN) and high-detergent (Urea) buffers at the age of 14 months. The CAG100 allele in both heterozygous and homozygous knock in animals shows reduced protein abundance compared to the wild type CAG1 allele in PN buffer lysates. A fraction of the WT allele is visible in the Urea buffer lysate of WT and CAG1/100 animals. A faint signal is detected for the expanded CAG100 allele in heterozygous animals, no signal is detected in homozygous animals. (D) ATXN2 immunoblot of 3 different primary murine embryonal fibroblast (MEF) clones from WT and *Atxn2*-CAG100-KIN animals show significantly reduced abundance of CAG100 allele. (E) *Atxn2* mRNA levels measured in 3 different *Atxn2*-CAG100-KIN MEF clones showed a reduction to 47% ($p < .0001$) compared to their WT pairs. Quantification of ATXN2 protein levels (blot shown in panel A) showed a reduction to 9% ($p = .0283$) in RIPA lysate. No protein was detected in high-detergent containing SDS lysate (data not shown). Statistical analyses were done by Ratio paired *t*-test. Bar graphs show individual values together with mean ± s.e.m. (F) Puromycin incorporation analysis in 3 different WT and *Atxn2*-CAG100-KIN MEF clones showed no significant difference in global translation rate. Statistical analysis was done by Ratio paired *t*-test. Bar graph shows individual values together with mean ± s.e.m. (G) Immunocytochemical detection of ATXN2 localization in WT and *Atxn2*-CAG100-KIN MEFs under normal (CTRL) and sodium arsenite (NaARS, 0.5 mM, 45 min) induced oxidative stress conditions. Both WT and expanded ATXN2 localize to stress granules under stress. ACTB: beta-actin, TUBA: alpha-tubulin.

100) and homozygous (CAG100/100) knock-in mice (Fig. 3A). The expression level of the expanded *Atxn2* mRNA was measured at 3 months, 6 months and 14 months, which are the important time points in the lifespan of *Atxn2*-CAG100-KIN colony according to phenotypic and behavioral assessments presented in Fig. 2. Expanded *Atxn2* mRNA showed a significant, yet small reduction to 87%

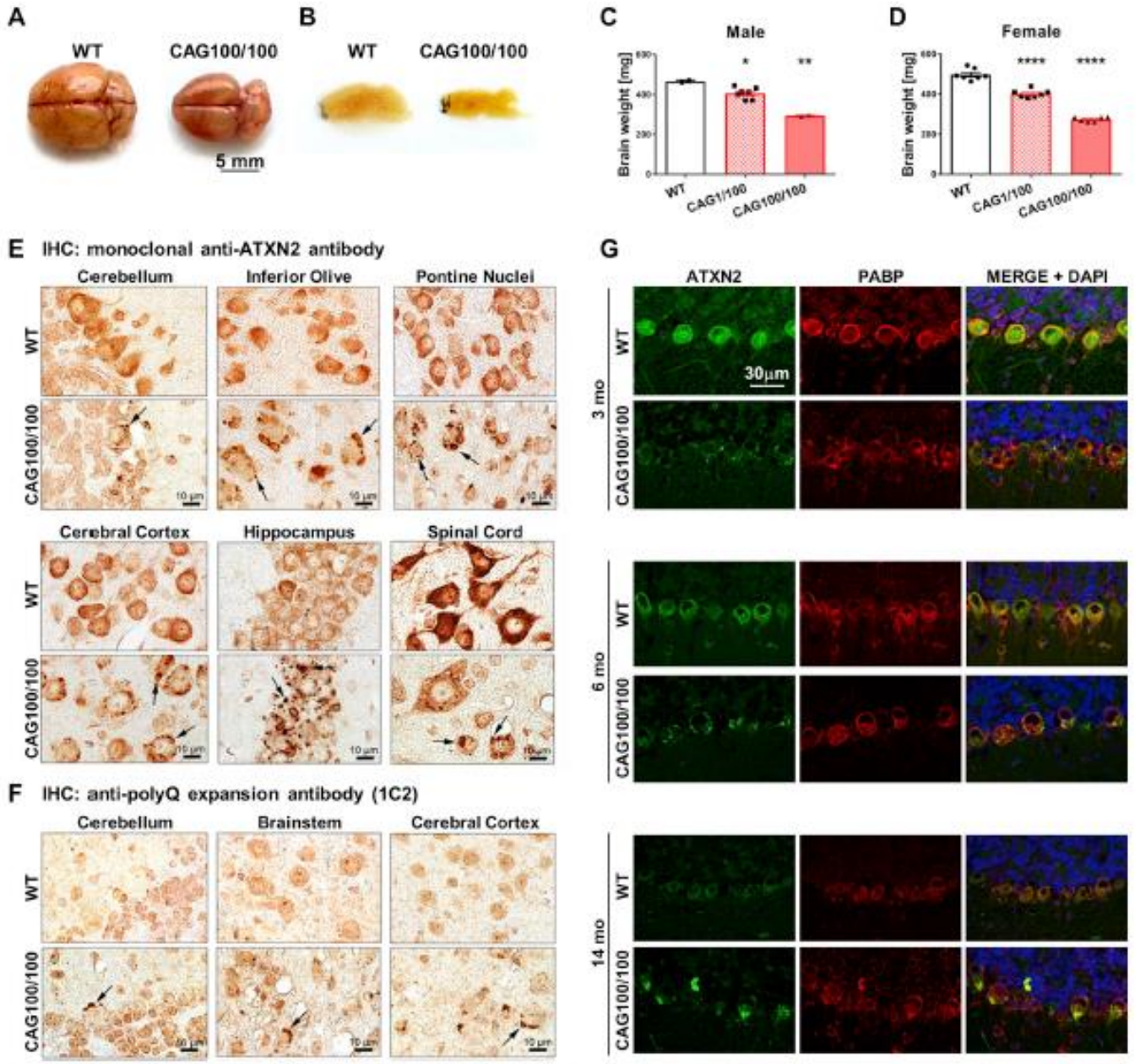

Fig. 4. Brain pathology of *Atxn2*-CAG100-KIN mice at the age of 14 months. (A) Representative brain photos are shown after sacrifice (seen from above) and (B) after dehydration and embedding in paraffin (as sagittal section). Statistical evaluation of brain weight for WT, heterozygous (CAG1/100), and homozygous (CAG100/100) animals was assessed separately for male (C) and female (D) animals (for males, reduction to 0.81% vs. 0.55%, $p = .03$ vs. 0.001; for females, reduction to 0.87% vs. 0.63%, $p < .00001$ vs. $< .00001$; tested by ANOVA with multiple testing correction after Bonferroni). Bar graphs show individual values together with mean ± s.e.m. (E) Immunohistochemical (IHC) visualization of puncta or large aggregates across various brain regions using paraffin-embedded sections stained with ATXN2 and (F) monoclonal polyQ expansion antibody 1C2 using DAB detection. (G) Immunofluorescent staining of ATXN2 and PABP in cerebellum of WT and *Atxn2*-CAG100-KIN mice across ages.

($p = .0418$) at 3 months, decreased to 85% ($p = .0669$) at 6 months, and decreased further to 70% ($p = .0029$) at 14 months, which is the terminal stage of the disease (Fig. 3B).

Next, we studied the abundance and solubility of the expanded ATXN2 protein in cerebellum of heterozygous (CAG1/100) and homozygous (CAG100/100) knock-in animals at 14 months (Fig. 3C). Expanded ATXN2-CAG100 protein was visible in the soluble fraction obtained by low-detergent PN buffer in both heterozygous and homozygous knock-in animals. However, the ATXN2-CAG100 allele abundance in both genotypes was reduced compared to the WT allele. The insoluble or membrane-bound protein fraction obtained by high-detergent Urea buffer showed a portion of the normal ATXN2 allele in WT and heterozygous (CAG1/100) animals. Although a small fraction of expanded CAG100 allele was visible in the Urea fraction in heterozygous animals, no ATXN2-CAG100 signal was detected in the Urea fraction of homozygous animals (Fig. 3C). This loss of the urea-soluble ATXN2-CAG100 is probably due to the ongoing aggregation process. It is well established that expanded ATXN2 protein tends to form intracellular aggregates that sequestrate known interactor proteins such as Poly(A)-Binding Protein (PABP), as shown in previously generated mouse models and SCA2 patients (Damrath et al., 2012). In the previously generated *Atxn2*-CAG42-KIN mice, which showed only mild

neurological signs at the end of normal mouse lifespan, the expanded ATXN2 protein in the aggregates could be solubilized and observed in immunoblots with both RIPA and SDS/Urea buffers (Damrath et al., 2012), whereas the ATXN2-CAG100 could not be solubilized by Urea. This ATXN2-CAG100 deficiency (Fig. 3C) might be partially explained also by inefficient translation of the expanded *Atxn2* mRNA, given that this expansion in the DNA also seems to decrease the *Atxn2* transcript production or stability (Fig. 3B).

In order to study the protein dynamics of ATXN2-CAG100, different clones of primary murine embryonal fibroblast (MEF) lines were generated from WT and homozygous *Atxn2*-CAG100-KIN animals. Under normal culture conditions, the expanded ATXN2 protein was detectable only in RIPA lysate of both WT and *Atxn2*-CAG100-KIN cells (Fig. 3D). No ATXN2 protein was detected in SDS lysate (data not shown). Quantification of the expanded *Atxn2* transcript in these cells revealed a reduction to 47% (Fig. 3E, $p \leq .0001$), and quantification of the protein signal presented in Fig. 3D revealed a drastic reduction to 9% ($p = .0283$). To rule out the possibility that *Atxn2*-CAG100-KIN affect PABP-dependent mRNA translation at the global level, puromycin-incorporation assays were carried out with three different MEF clones. They observed no significant difference in overall translation rate between normal and mutant cells (KIN 130%, $p = .2280$) (Fig. 3F). Immunocytochemical analysis of MEF under normal culture conditions showed a diffuse cytosolic distribution of ATXN2 in both WT and *Atxn2*-CAG100-KIN cells (Fig. 3G). PABP also showed diffuse cytosolic localization as expected. As established for WT cells, also in *Atxn2*-CAG100-KIN cells both ATXN2 and PABP localized to cytoplasmic ribonucleoprotein particles known as stress granules (SG), when oxidative stress occurred upon sodium-arsenite (NaARS) treatment. Thus, in peripheral cells the expanded ATXN2 protein was severely reduced in abundance, but had the correct subcellular localization and its stress-response capabilities remained intact.

Overall, these observations indicate that the CAG100 expansion reduces the total protein levels of soluble ATXN2. Thus, loss-of-function effects will be prominent in peripheral cells, where the aggregation of the expanded disease protein does not occur, which is excitation-induced and restricted to postmitotic cells such as neurons (Koch et al., 2011).

2.6. Progressive brain atrophy and neuronal aggregation throughout the central nervous system

At the terminal stage of the disease, analysis of the *Atxn2*-CAG100-KIN brain revealed atrophy and weight loss for both sexes in homozygous mice, and to a lesser extent also in heterozygous mice despite the lack of neurological disease signs at that age (Fig. 4A–D). Immunohistochemical analysis of ATXN2 protein with a monoclonal antibody in WT and *Atxn2*-CAG100-KIN brains revealed high signals in many neuron populations, particularly in specific brainstem nuclei (inferior olive and pons), cerebellum, ventral forebrain areas, cerebral cortex and hippocampus, showing good agreement with publically available in-situ hybridization data of wild type mice at the Allen Brain Atlas (Supplementary Fig. S1). Upon further examination by light microscopy, cytosolic aggregates of ATXN2-CAG100 were observed in the typical regions affected by neurodegeneration in SCA2 (Estrada et al., 1999; Giuffrida et al., 1999), such as cerebellar Purkinje neurons, inferior olivary neurons and pontine nuclei neurons (Fig. 4E upper rows). Aggregates were also detectable in cerebral cortical and hippocampal neurons and in spinal cord motor neurons, where they were particularly large (Fig. 4E lower rows). In all these regions, the cytosolic aggregates were confirmed to contain expanded ATXN2 protein upon immunostaining with the monoclonal anti-polyQ antibody 1C2 (Fig. 4F). Further investigation of the cerebellar Purkinje neurons via electron microscopy also confirmed the presence of cytosolic protein aggregates (black arrowheads in Supplementary. Fig. S2). As cerebellar dysfunction and neuropathology are considered the most prominent and common aspects of dominant ataxias, we focused on cerebellar ATXN2 pathology and its progression throughout lifespan in *Atxn2*-CAG100-KIN mice. Immunofluorescent detection of ATXN2, together with its known interactor PABP, was performed in 3-, 6- and 14-month-old mice cerebella (Fig. 4G). ATXN2 was found highly expressed in Purkinje cells, and showed a diffuse distribution in WT samples across all ages. ATXN2-CAG100, on the other hand, was found accumulated in numerous smaller aggregates starting from the pre-symptomatic age of 3 months. Insolubility of the mutant ATXN2 protein and size of the aggregates increased progressively with age; showing multiple larger puncta at 6 months and a very large unified aggregate towards the axon hillock at 14 months. PABP signal in WT samples was also found highly expressed in Purkinje cell soma throughout lifespan. Although the small aggregates in *Atxn2*-CAG100-KIN cerebellum at 3 months did not seem to sequester PABP into insolubility, larger ATXN2-CAG100 aggregates starting from 6 months also showed PABP immunoreactivity, which was severely worsened at 14 months (Fig. 4G).

Double immunofluorescence was able to show the co-localization of ATXN2-positive cytosolic aggregates with ubiquitin signals (Supplementary Fig. S3A) and p62 signals (Supplementary Fig. S3B) in cerebellum, brainstem and spinal cord, suggesting that they undergo the classical elimination via autophago-lysosomal pathways (Lee et al., 2015). Again, particularly large protein aggregates could be observed in spinal cord motor neurons (Supplementary Fig. S3, lowest row), in good agreement with the preferential vulnerability of motor neurons in pre-symptomatic stages of human SCA2 (Velazquez-Perez et al., 2014). Thus, the neuropathological pattern in *Atxn2*-CAG100-KIN mouse closely mirrors the selective vulnerability of specific neuron populations known from human SCA2.

2.7. Significant reductions of N-acetylaspartate and glutamate levels in Atxn2-CAG100-KIN cerebellum in vivo

After establishing that *Atxn2*-CAG100-KIN mice bear the genetic, behavioral and neuropathological hallmarks of SCA2, we used magnetic resonance imaging to study the mice *in vivo* and employed spectroscopy to assess whether molecular changes occur similar to patients. Data of the right cerebral hemisphere and middle part of the cerebellum were collected from age- and sex- matched WT and *Atxn2*-CAG100-KIN animals between the ages 12 and 14 months. Fig. 5A shows representative images for voxel positioning and the spectra obtained. Quantification of the main peaks showed a general decrease in total *N*-acetylaspartate (tNAA = NAA and NAAG), glutamate (Glu) and choline (Cho) levels when normalized to myoinositol (MI) in both cerebellum and cerebrum, while creatine (Cre) remained unchanged (Fig. 5A). Pairwise statistical analyses revealed that only tNAA (57%, $p = .0241$) and Glu (77%, $p = .0192$) reductions in cerebellum reached significance, whereas other metabolites suffered from high variation among controls. A decrease in NAA levels has been observed before in the context of many neurodegenerative disorders, and is considered to be a biomarker of neuronal dysfunction or death (Ariyannur et al., 2010). Large cohort studies with autosomal dominant cerebellar ataxia and multiple system atrophy (MSA) patients demonstrated a reduction in tNAA levels in most of subtypes of spinocerebellar ataxia, however tNAA deficit has the highest correlation with SCA2 pathology and progression among all disease types investigated (Cahill Jr. and Veech, 2003; Wang et al., 2012).

Overall, the spectroscopic and histological analyses of *Atxn2*-CAG100-KIN mouse brain showing the spatio-temporal neuropathology pattern known from SCA2 patients, together with the previously shown features of somatic mosaicism, fertility changes and progressive motor dysfunction, collectively prove the authenticity and value of this newly generated mouse model of Ataxin-2 pathology.

2.8. Important factors of NAA metabolism are altered in Atxn2-CAG100-KIN mouse cerebellum

Taking advantage of our new SCA2 mouse model to study earliest

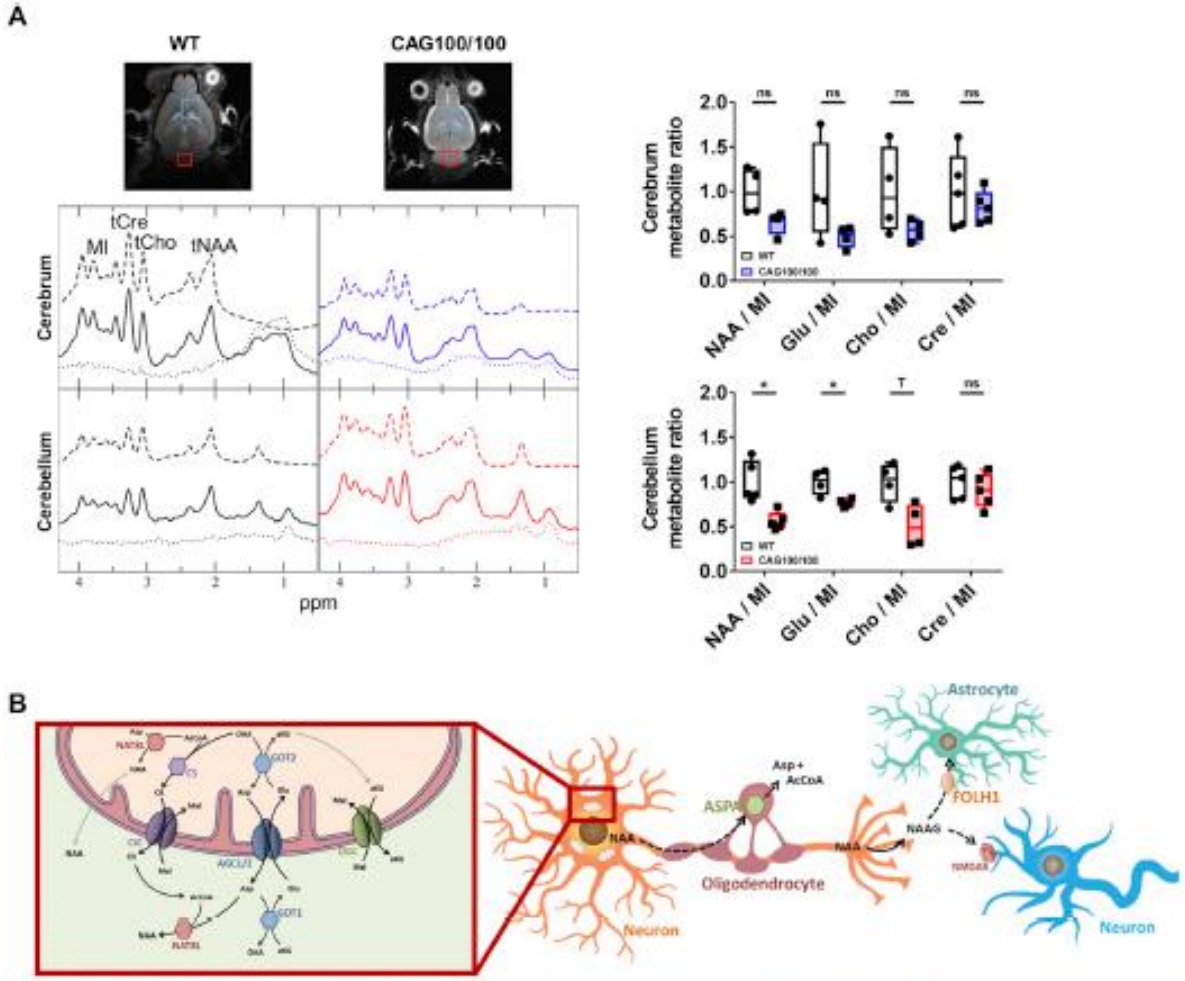

Fig. 5. Altered *N*-acetylaspartate (NAA) and glutamate (Glu) levels in *Atxn2*-CAG100-KIN mouse cerebellum. (A) Magnetic resonance spectroscopy of WT and *Atxn2*-CAG100-KIN mice showed significantly reduced NAA and glutamate levels in cerebellum (in red), but not in cerebrum (in blue) when normalized to myoinositol (MI) levels. Representative images show the approximate regions from where the data was acquired in cerebrum (blue boxes) and cerebellum (red boxes). Representative spectrograms are shown for both cerebellar and cerebral measurements in WT and CAG100/100 animals (dashed lines: fitted data, solid lines: original spectrum data, dotted lines: residuum). Statistical analyses were done by Ratio paired t-test. Box-whiskers plot shows individual values with median and min to max confidence interval. Cerebellum: NAA: 57%, $p = .0241$; Glu: 77%, $p = .0192$; Cho: 48%, $p = .0616$; Cre: 90%, $p = .5217$. Cerebrum: NAA: 67%, $p = .1578$; Glu: 54%, $p = .1889$; Cho: 61%, $p = .2392$; Cre: 87%, $p = .6136$. (B) Schematic illustration of NAA metabolism within neurons and among different cell types in the nervous system. AcCoA: acetyl-coA, AGC1/2: Mitochondrial Aspartate Glutamate Carrier 1/2, aKG: alpha-ketoglutarate, Asp: aspartate, ASPA: Aspartoacetylase, CIC: Citrate Transport Protein, Cit: citrate, CS: Citrate Synthase, FOLH1: Folate Hydrolase 1, Glu: glutamate, GOT1: Glutamic-Oxaloacetic Transaminase 1, GOT2: Glutamic-Oxaloacetic Transaminase 2, Mal: malate, NAA: *N*-acetylaspartate, NAAG: *N*-acetylaspartylglutamate, NAT8L: N-Acetyltransferase 8 Like, NMDAR: *N*-methyl-D-aspartate receptor, OAA: oxaloacetate, OGC: Mitochondrial 2-Oxoglutarate/Malate Carrier Protein. (For interpretation of the references to colour in this figure legend, the reader is referred to the web version of this article.)

stages of pathology, we asked what enzymatic changes underlie the altered NAA metabolism, and how early the molecular dysregulations occur. Fig. 5B depicts the major aspects of NAA production, intercellular transport and utilization. NAA is synthesized via N-terminal acetylation of aspartate by the enzyme N-Acetyltransferase-8-Like (NAT8L) in neurons (Ariyannur et al., 2010). Although some studies suggested that NAT8L is localized in the cytoplasmic/ER compartment, increasing numbers of studies provided evidence that NAT8L is a mitochondrial/microsomal protein (Ariyannur et al., 2008; Ariyannur et al., 2010; Kedersha and Anderson, 2007; Lu et al., 2004; Wang et al., 2012). Following its synthesis and export into neuronal cytoplasm, NAA is transported into the oligodendrocytes where it is broken down by the enzyme Aspartoacetylase (ASPA) into aspartate and acetate residues. Acetate is further processed into acetyl-CoA and utilized in the production of fatty acids for myelination (Jaeken et al., 1984). A portion of NAA can be converted into *N*-acetylaspartylglutamate (NAAG) at the axon termini and secreted into synaptic cleft as a modulator of glutamatergic excitation. Excess NAAG in the synapse is taken up by the astrocytes through the transporter protein Folate Hydrolase 1 (FOLH1) to prevent excitotoxicity, converted back into NAA and excreted from the CNS to the blood stream (Besse et al., 2015).

We studied the transcript and protein levels of three enzymes that conduct important steps in NAA turnover; NAT8L, ASPA and FOLH1. In order to delineate the causality chain of expression alterations, we examined these enzymes at pre-symptomatic, early symptomatic and terminal stages of the disease in *Atxn2*-CAG100-KIN mouse cerebellum (Fig. 6A). At the transcript level, *Nat8l* showed a significant reduction in all ages studied; starting with a reduction to 76% ($p = .0080$) at 3 months, progressing to 67% ($p = .0018$) at 6 months and further down to 46% ($p = .0003$) in 14-month-old animals. In comparison, *Aspa* mRNA only showed a significant reduction to 72% ($p = .0425$) at the early symptomatic stage of 6 months, and was progressively diminished to 50% ($p = .0020$) in 14-month-old animals. Transcript levels of the NAAG uptake protein *Folh1* only became significantly

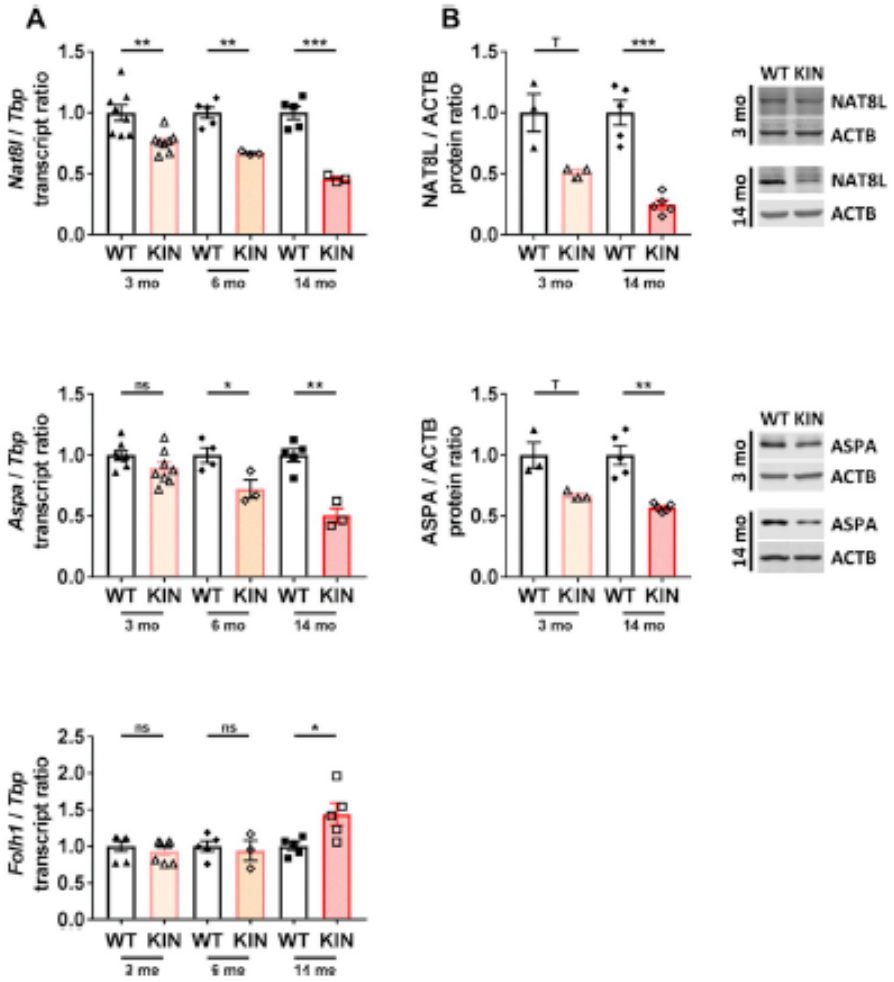

Fig. 6. Transcript and protein levels of NAA metabolism enzymes in cerebellum across ages. (A) Transcript and (B) protein levels of key components in NAA synthesis (NAT8L), NAA breakdown (ASPA) and NAAG transport into astrocytes for excretion (FOLH1) were measured in *Atxn2*-CAG100-KIN mouse cerebellum with WT controls at indicated ages. Statistical analyses were done by unpaired t-test with Welch's correction. Bar graphs show individual values together with mean ± s.e.m. ACTB: beta-actin, mo: months old, T: trend towards significance ($.05 < p < .10$).

affected at the terminal stage of the disease with an increase to 140% ($p = .0425$) at 14 months (Fig. 6A). At the protein level, NAT8L showed a similar expression profile to that of its transcript at respective ages; a decrease to 51% ($p = .0847$) at 3 months and stronger dysregulation down to 25% ($p = .0009$) in 14-month-old animals (Fig. 6B). Protein levels of ASPA at the pre-symptomatic stage of 3 months showed a reduction to 67% ($p = .0838$), and was progressively decreased to 57% ($p = .0047$) at the terminal stage of the disease (Fig. 6B). Protein levels of FOLH1 could not be assessed due to the lack of a reliable antibody for immunoblotting.

All in all, the expression data suggest that the first dysregulation of the NAA metabolism occurs in the synthesis of NAA by NAT8L in neurons starting from pre-symptomatic stage. This is followed by a reduction in oligodendrocytic ASPA levels at early symptomatic stage, which may be an adaptive mechanism to reduced NAA production and supplementation into glia. Finally, the transcript levels of FOLH1 being induced only at the terminal stage of disease indicates that the excitotoxicity burden in the synapses increases during disease progression.

2.9. Dysregulation of NAA production is not due to mislocalization or altered turnover of associated metabolites

After establishing that early in the disease course the generation of NAA is affected, we focused on enzymes that regulate the mitochondrial/cytoplasmic shuttling and availability of the relevant metabolites for this pathway within the neurons. As depicted in Fig. 5B, there are three types of metabolite shuttle proteins for the transport of metabolites across mitochondrial membranes. AGC1 (encoded by *Slc25a12* gene) and AGC2 (*Slc25a13*) are responsible for aspartate-glutamate transport, CIC (*Slc25a1*) is responsible for citrate-malate transport and OGC (*Slc25a11*) is responsible for malate-α-ketoglutarate transport. Inside the mitochondrial matrix, glutamate and oxaloacetate can be metabolized by Glutamic-Oxaloacetic Transaminase 2 (GOT2) into aspartate and α-ketoglutarate. The inverse reaction of aspartate and α-ketoglutarate forming glutamate and oxaloacetate is catalyzed by Glutamic-Oxaloacetic Transaminase 1 (GOT1) in the cytoplasm. Oxaloacetate, together with acetyl-CoA, can also be metabolized to citrate by Citrate Synthase (CS) in mitochondria (Fig. 5B).

Measurement of the metabolite transporters showed only minor downregulations in 14-month-old *Atxn2*-CAG100-KIN mouse cerebellum (Supplementary Fig. 4A); *Slc25a12* (93%, $p = .5114$), *Slc25a13* (84%, $p = .0719$), *Slc25a1* (80%, $p = .0026$) and *Slc25a11* (90%, $p = .0576$). Measurement of enzymes involved in metabolic processes also showed only minor downregulations in 14-month-old *Atxn2*-CAG100-KIN mouse cerebellum (Supplementary Fig. 4A); *Got1* (82%, $p = .0019$), *Got2* (89%, $p = .1022$), *Cs* (81%, $p = .0057$). Among these enzymes, AGC1 and GOT2 were also studied at the protein level in 14-month-old *Atxn2*-CAG100-KIN mouse cerebellum, as they are directly

involved in aspartate metabolism. No significant change was observed for both enzymes in RIPA soluble lysate (Supplementary Fig. 4B; AGC1: 86%, $p = .3352$, GOT2: 120%, $p = .0543$). Since both AGC1 and GOT2 are mitochondrial membrane-bound or -encapsulated proteins, SDS lysates were also tested to eliminate the possibility of mitochondria not being fully solubilized by RIPA buffer. Again, no significant difference were seen in both proteins (Supplementary Fig. 4B; AGC1: 94%, $p = .4093$, GOT2: 76%, $p = .0547$). This set of results suggests that the NAA production deficit is due to altered NAT8L levels in *Atxn2*-CAG100-KIN mouse, but not due to unavailability, mislocalization or deranged metabolism of aspartate or any associated metabolite.

2.10. ATXN2 modulates Nat8l expresston tn adipogenic fate and peripheral blood

While most studies focus on the role of NAT8L in the central nervous system for NAA production and myelination, this enzyme is also known to be an important regulator of adipogenic fate in the peripheral tissues (Huber et al., 2019; Kedersha and Anderson, 2007; Prokesch et al., 2016). In order to mechanistically show the direct effect of mutant ATXN2 on the transcriptional dysregulation of *Nat8l*, we treated WT and *Atxn2*-CAG100-KIN MEFs with an adipogenic differentiation regimen for 7 days as depicted in Fig. 7A. Expression profiling confirmed the successful induction of adipogenesis, as indicated by the massive upregulation of *Adipoq* (WT 100% to 3000%; KIN 180% to 3400%) as a marker of adipogenesis (Fig. 7B). Under the same conditions, *Atxn2* transcript showed a significant 1.4-fold induction in both WT and *Atxn2*-CAG100-KIN cells (WT 100% to 140%; KIN 60% to 88%), a finding which provides evidence that the transcriptional regulation of the knock-in allele is intact. As observed before, the expression levels of expanded *Atxn2* in *Atxn2*-CAG100-KIN cells were significantly lower than that of WT in both normal and adipogenic conditions (Fig. 7B). *Nat8l* transcript was not significantly different in *Atxn2*-CAG100-KIN cells under normal conditions. Upon adipogenesis in WT cells, *Nat8l* levels showed a big upregulation from 100% to 550%, proving once again the validity of adipogenic differentiation protocol and also the importance of *Nat8l* in this process. However, the transcriptional induction of *Nat8l* was completely repressed in *Atxn2*-CAG100-KIN cells upon adipogenic differentiation (Fig. 7B; KIN 98% to 150%), confirming a direct effect of ATXN2 expansion on the transcriptional regulation of *Nat8l* in cells outside the nervous system.

Finally, in order to test the effect of mutant ATXN2 on *Nat8l* in easily accessible peripheral tissues, and to establish an initial study for the molecular disease biomarkers, we analyzed abdominal adipose tissue from 3-month-old *Atxn2*-CAG100-KIN mice and blood samples from 14-month-old *Atxn2*-CAG100-KIN mice, as well as late symptomatic/terminal stage SCA2 patients. *Atxn2* transcript was significantly reduced in the adipose tissue to 64% ($p = .0456$), and *Nat8l* transcript was also significantly diminished to 58% ($p = .0110$; Fig. 7C). *Atxn2* transcript in blood samples of *Atxn2*-CAG100-KIN mice showed a significant decrease to 45% ($p = .0003$; Fig. 7D), similar to the previously shown expression deficit in *Atxn2*-CAG100-KIN MEFs. A dramatic decrease of *Nat8l* to 50% ($p = .0016$) was detected in *Atxn2*-CAG100-KIN mouse blood samples (Fig. 7D), further strengthening the direct effect of ATXN2 on *Nat8l* mRNA levels. Expression of *ATXN2* transcript in peripheral blood samples of four SCA2 patients and healthy controls showed higher variation compared to blood samples from *Atxn2*-CAG100-KIN mice (Fig. 7E). While two patients (#1 and #3) showed a decrease in *ATXN2* expression compared to their respective age- and sex-matched healthy controls, one patient (#4) showed no change, and one patient (#2) interestingly showed an increase in *ATXN2* expression. Measurement of *NAT8L* levels in SCA2 patient blood samples also revealed high variation among individuals of the same group; however, the comparison of *NAT8L* levels in each patient with the respective control consistently showed a decrease (44% on average) (Fig. 7E). Statistical analysis of the patient data with Ratio paired *t*-test revealed this consistent decrease in *NAT8L* levels to be significant (44%, $p = .0318$), but showed no significance for *ATXN2* expression changes (91%, $p = .5218$).

In conclusion, the magnetic resonance spectroscopy data from *Atxn2*-CAG100-KIN mouse cerebellum at 14 months and the expression analyses at different stages of the disease point to a NAA production deficit caused by dysregulated *Nat8l* expression, which starts very early at pre-symptomatic stages. Analyses in mouse primary fibroblasts under adipogenic treatment and in abdominal adipose tissue from mice, as well as blood samples from mice and patients corroborate this direct effect of expanded ATXN2 on *Nat8l* transcript reduction. Thus, *Nat8l* expression in blood is a candidate biomarker when assessing preventive treatments in SCA2.

3. Discussion

We generated a genetic mouse model of ATXN2 pathology, which faithfully reflects the spatial distribution of affected neural pathways with the preferential vulnerability of motor neurons, brainstem and cerebellar neurons resulting in chronically progressive locomotor deficits. The neurodegenerative process affects the nervous system with cytosolic inclusion bodies of ATXN2 in the characteristic pattern of olivo-ponto-cerebellar atrophy (OPCA), as was carefully documented in patients (Auburger, 2012; Estrada et al., 1999; Gierga et al., 2005; Hoche et al., 2011; Rub et al., 2006; Rub et al., 2004; Rub et al., 2005a; Rub et al., 2003a; Rub et al., 2005b; Rub et al., 2003b; Rub et al., 2007). The aggregates are particularly large in spinal motor neurons in our mouse model, and indeed it was recently shown in SCA2 mutation carriers that motor neuron degeneration appears even before the onset of cerebellar ataxia, accompanied by muscle cramps, impaired conduction velocity due to axon demyelination and the loss of subcutaneous fat tissue (Velazquez-Perez et al., 2001; Velazquez-Perez et al., 2014; Velazquez-Perez et al., 2016; Velazquez-Perez et al., 2017a). In good agreement with the early vulnerability of motor neurons and cerebellar circuits, the locomotor behavior data reflect a reduced performance on the accelerating rotarod from the age of 5 months, together with a steady decrease of peripheral grip strength from the age of 6–7 months onward, and balance problems during vertical movements in the open field from the age of 7 months. As the first knock-in model of SCA2 with shortened survival and endogenous regulation of ATXN2 expression and distribution, it will enable us to address the question to what degree loss-of-function effects e.g. in blood or fibroblasts exist in addition to the toxic gain-of-function effects that dominate in neural tissues. In this knock-in model it will also be possible to test substances that repress the transcription activity of the expanded *Atxn2* gene promoter. These issues cannot be answered in previously available transgenic overexpression models of SCA2.

Our initial observations regarding the gain- versus loss-of-function issue came from the phenotypic analyses of the mice throughout lifespan. Weight measurements showed an initial increase in female homozygous *Atxn2*-CAG100-KIN mice at pre-symptomatic stage, which progressively deteriorated and turned into a systemic tissue atrophy when locomotor deficits appeared. Considering that the most prominent phenotypic feature of *Atxn2*-KO mice is lipid accumulation and obesity, we suspected that this initial weight excess might be due to a partial loss-of-function effect caused by the mutant protein not being fully functional. Moreover, reduced number of female mutants and motor hyperactivity of the *Atxn2*-CAG100-KIN mice in early life also correlates well with the same phenotypes observed in *Atxn2*-KO animals reported previously (Lastres-Becker et al., 2008a). Interestingly, the change in body weight showing an initial increase followed by progressive decrease was not only observed in our mouse model, but also in SCA2 families upon careful longitudinal assessment (Abdel-Aleem and Zaki, 2008). Our further histological and biochemical studies showed the progressive aggregation of mutant ATXN2 protein in nervous tissue, and a strongly reduced abundance in peripheral tissues

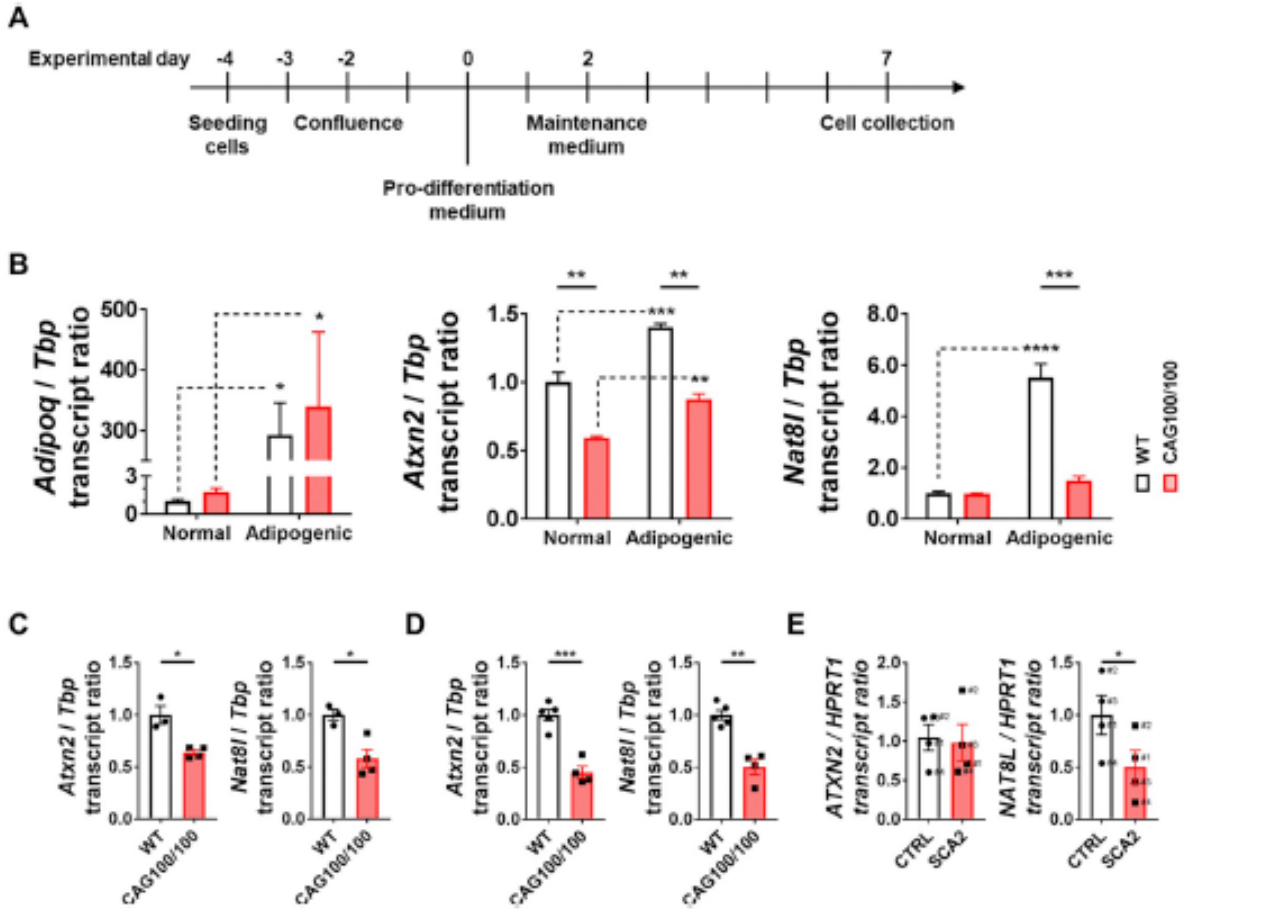

Fig. 7. *Nat8l* levels are modulated by mutant ATXN2 in adipogenic differentiation and blood. (A) Experimental timeline of MEF adipogenic differentiation protocol. (B) Expression analyses of *Adipoq* (Adiponectin, as a marker of adipogenesis), *Atxn2* and *Nat8l* in normal and adipogenic *Atxn2*-CAG100-KIN cells. Statistical analyses were done by Two-way ANOVA with Sidak's multiple test correction. Bar graphs show individual values together with mean ± s.e.m. (C) Expression analyses of *Atxn2* and *Nat8l* in *Atxn2*-CAG100-KIN white adipose tissue at the age of 3 months. Statistical analyses were done by unpaired t-test with Welch's correction. Bar graphs show individual values together with mean ± s.e.m. (D) Expression analyses of *Atxn2* and *Nat8l* in *Atxn2*-CAG100-KIN peripheral blood at the age of 14 months. Statistical analyses were done by unpaired t-test with Welch's correction. Bar graphs show individual values together with mean ± s.e.m. (E) Expression analyses of *ATXN2* and *NAT8L* in peripheral blood samples of SCA2 patients compared to age- and sex-matched healthy controls. Statistical analyses were done by Ratio paired t-test. Bar graphs show individual values together with mean ± s.e.m.

without aggregation. Similar findings of neurodegeneration with reduced levels and insolubility of polyQ expanded disease proteins were also reported for SCA7 (Helmlinger et al., 2004). For polyQ expanded Ataxin-3 it was shown that expression and solubility was normal in induced pluripotent stem cells, fibroblasts or glia cells, but changed to an insoluble aggregated state upon neuronal differentiation and exposure to excitatory stimuli such as glutamate (Koch et al., 2011). These previous observations explain our findings that ATXN2-CAG100 is quite soluble in fibroblasts, although severely decreased in abundance, while it appears to go into immediate insolubility and aggregation in neural tissue since pre-manifest stages.

After the initial weight excess, the progressive loss of body and also brain weight is compatible with the insidious increase of expanded ATXN2 toxicity due to aggregate formation. ATXN2 is expressed in pancreas and affects the islet beta-cells in their trophic state and insulin secretion (Lastres-Becker et al., 2008a), so we assume that aggregated ATXN2 toxicity affects these postmitotic cells via the known effects of ATXN2 on mTORC1 signaling and nutrient metabolism in general (Bar, 2016; DeMille et al., 2015; Lastres-Becker et al., 2016; Meierhofer, 2016; Seidel et al., 2017; Takahara and Maeda, 2012; Yang et al., 2019), thus triggering a depletion of body fat stores. Similarly, the observed strong weight reduction of the brain in *Atxn2*-CAG100-KIN mice might be explained largely by the loss of myelin fat. Very large *ATXN2* expansions in SCA2 patients clearly trigger myelination defects, since these patients develop widespread leukoencephalopathy observed upon brain imaging (Pacłorkowski et al., 2011). The fact that expanded ATXN2 reduces *Nat8l* levels obviously may contribute to a decrease in myelin and brain weight. Moreover, the same pathomechanism might be partly responsible for the progressive atrophy of peripheral fat stores, as NAT8L has been reported as an important regulator of adipogenesis in white and brown adipose tissue (Huber et al., 2019; Kedersha and Anderson, 2007; Prokesch et al., 2016).

Aside from the pathological pattern and locomotor deficits, *Atxn2*-CAG100-KIN mice also reflect the metabolite profile documented in SCA2 patients previously in terms of decreased NAA, glutamate and choline levels (Cahill Jr. and Veech, 2003; Wang et al., 2012). This is similar to mouse models of other spinocerebellar ataxia types, such as SCA1 (Emery, 2005; Oz et al., 2015; Oz et al., 2011), where NAA levels were studied in parallel to histology to define the progression of neurodegeneration. NAA is the second most abundant metabolite in the brain after glutamate, and is predominantly synthesized in neurons via N-terminal acetylation of aspartate amino acid. Due to its high abundance and appearance as the largest peak in spectrograms, NAA deficiency has been widely used as a biomarker of neuronal loss or dysfunction in a number of neuropathological conditions, although it has never been clarified what is the underlying molecular mechanism of

this deficit (Cao et al., 2013b). It is well-established that the main purpose of NAA synthesis in the nervous system is to stock acetyl-CoA units in a transportable form for energy storage and acetylation reactions, which control gene expression and protein function. The only resident energy stores in the brain are small amounts of glycogen in astrocytes, so it is reasonable that the nervous system developed ways to ensure the interconversion of critical precursors for energy metabolism, such as glutamate and NAA that can easily be converted into α-ketoglutarate, acetate and oxaloacetate. It has been proposed that acetyl-CoA stored in the form of NAA in the CNS is the equivalent of triglycerides constituting the stored energy in the adipose tissue (Ariyannur et al., 2010). Indeed, our previous investigations on the physiological function of ATXN2 showed that yeast α-ketoglutarate dehydrogenase levels were affected by the loss of ATXN2. Also, fatty acid beta-oxidation and branched-chain amino acid degradation pathways within mitochondria were found severely affected by ATXN2 deficiency in mouse (Meierhofer, 2016; Seidel et al., 2017). Our current findings also point out to a mitochondrial enzyme, NAT8L, to be altered more than other NAA turnover enzymes, since earliest stages in the disease course and to a greater extent.

NAT8L was identified as the highly specialized *N*-acetyltransferase carrying out the synthesis of NAA. It is also involved in ATP-dependent axon growth and the inhibition of methamphetamine action by inducing dopamine uptake in nucleus accumbens (Della Nave et al., 2004; Faught, 2011). A single case carrying a 19 bp deletion mutation in *NAT8L* has been reported to have no detectable NAA peak in the NMR spectrogram, and to present with mild hypomyelination (Wang et al., 2012). This contrasts with Canavan disease (CD) where deleterious *ASPA* mutations lead to NAA accumulation in the brain, triggering severe progressive leukodystrophy and paralysis in infants and children (Jaeken et al., 1984). It was proposed that *NAT8L* dysfunction leads to a later and milder disease course compared to *ASPA* deficiency simply due to the availability of aspartate and acetate metabolites. On the one hand in CD, neurons utilize their aspartate and acetyl-CoA stores to synthesize NAA and transport it into oligodendrocytes. However, due to the lack of ASPA function, NAA cannot be broken down, myelination cannot occur and excess NAA is excreted from the CNS. This puts both oligodendrocytes and neurons into an energy deficit given that the main source of energy is constantly being pumped out to the blood. In *NAT8L* deficiency, on the other hand, aspartate and acetate molecules are not trapped in an un-degradable form, but rather NAA production simply does not occur. Both the neurons and oligodendrocytes can survive for a limited time utilizing other forms of energy stores, therefore myelination can take place, although at a decreased level (Ariyannur et al., 2010). This hypothesis correlates well with our findings that cerebellar NAA and *Nat8l* levels are significantly downregulated starting from pre-manifest stage, and decreasing with age. The deficit in *Aspa* levels later during disease progression may be a response to reduced *Nat8l* and NAA production, rather than being causative in disease manifestation.

In our spectroscopic data collection and analysis methodology, NAA and its downstream metabolite NAAG are visualized together within the same peak, and therefore are quantified together. NAAG is synthesized via the ATP-dependent condensation of NAA and glutamate. High levels of NAAG Synthase (NAAGS) and NAAG have been found in central nervous system, particularly spinal cord and brainstem, and in testis. In cerebellum, the highest expression of NAAGS occurs in Bergmann glia in the Purkinje cell layer. After its synthesis in neurons, NAAG is released from the synaptic terminals to act as a modulator of glutamatergic synapses, and excess NAAG is taken up and degraded by FOLH1 enzyme synthesized by astrocytes (Besse et al., 2015). It is known that ASPA deficiency leads to the accumulation of NAA and also NAAG in the CNS, however it is unknown how NAAG levels change in NAT8L deficiency, or in the context of many disorders with which NAA decrease was found to be associated. Quantification of the spectroscopic data acquired from *Atxn2*-CAG100-KIN cerebrum and cerebellum shows a consistent decrease in both tNAA and glutamate levels. The concentration of NAA in CNS is over 25 times higher than NAAG (Moffett and Namboodiri, 1995), and the detected tNAA peak is most probably dominated by NAA over NAAG. Nevertheless, it is reasonable to assume that NAAG levels must also be diminished in the mutant mice as the two building blocks, NAA and glutamate, were found significantly reduced.

In order to delineate the cause of NAA deficiency in *Atxn2*-CAG100-KIN mice, we have analyzed several important steps in NAA turnover at the molecular level and came to the conclusion that NAT8L is the earliest and strongest dysregulation. Then, we went on to analyze additional factors important in aspartate and acetyl-CoA turnover, hypothesizing that reduced availability of these metabolites in correct subcellular organelles might underlie the NAT8L reduction in response to impaired substrate levels. Among these factors, AGC1 (*Slc25a12*) was of special interest since it is the dominant cytoplasm/mitochondria aspartate transporter in brain, and its malfunction has been shown to cause global cerebral hypomyelination, severe hypotonia and seizures in infants (Broer and Palacin, 2011). AGC1 deficient mice also showed hypomyelination due to severely reduced aspartate levels and NAA synthesis, as also demonstrated in vitro (Broer and Palacin, 2011; Cao et al., 2013a). However, none of the factors including AGC1 showed a major dysregulation even at the terminal stage of the disease in *Atxn2*-CAG100-KIN mouse cerebellum, further strengthening our impression that NAT8L stands out as the main affected factor responsible for NAA deficiency in our mutant.

Both NAA and NAT8L have been widely studied in the context of nervous system metabolism and myelination. However, an additional role of NAT8L in regulating lipid metabolism outside the brain, namely in adipocytes, has been established rather recently. NAT8L expression was shown to be relatively high in white and brown adipose tissues and adipogenic cell lines, where it facilitates the balance between nutrient metabolism and lipolysis/lipogenesis (Huber et al., 2019; Kedersha and Anderson, 2007). In addition, acetyl-CoA released by the breakdown of NAA was shown to regulate histone acetylation, thus modulating the transcriptional profile of adipocytes by an epigenetic mechanism (Prokesch et al., 2016). Considering this vast importance of NAT8L in adipogenesis, we subjected primary MEF cells from WT and *Atxn2*-CAG100-KIN animals to an adipogenic differentiation regimen to test the effect of mutant ATXN2 on the transcriptional regulation of *Nat8l* in vitro. The induction of *Nat8l* in WT cells upon adipogenic differentiation was observed in line with the previous reports. Strikingly, this transcriptional induction was completely lost in *Atxn2*-CAG100-KIN cells under the same treatment. Likewise, a reduction of *Nat8l* transcript was observed in adipose tissue at the pre-symptomatic stage of 3 months in mutant mice. Additional analyses conducted with mutant mouse and SCA2 patient blood samples revealed a similar genotype effect at transcript level. The high variation of *ATXN2* and *NAT8L* transcript levels in human samples will be limiting for their use as molecular biomarkers of disease, but of course any out-bred population with a wide variability in nutrient intake and diverse environmental factors will always have a quite broad range of mRNA responses to stimuli and stress. In addition, the SCA2 patients analyzed in the framework of this study had smaller expansion sizes, but more advanced disease duration than our in-bred *Atxn2*-CAG100-KIN mice with minimum genetic, environmental or pathological differences. The applicability of these findings and the value of *NAT8L* as a disease marker remain to be validated in large SCA2 cohorts and in the context of other ATXN2-related disorders such as ALS or Parkinsonism syndromes.

Why is the *Nat8l* mRNA dysregulation observed early in peripheral adipose tissues of our mouse mutant, while the NAA deficits occur only later in cumulative manner in the nervous system? It is known from SCA2 patients that NAA reduction upon brain imaging and the ensuing demyelination indeed are late progression markers, while the loss of subcutaneous fat is a presymptomatic feature (Diallo et al., 2017; Medrano-Montero et al., 2018; Scherzed et al., 2012; Wang et al., 2012). When peripheral fat and protein stores are depleted by

malnutrition or atrophic disease, the overall brain is relatively spared from the general weight loss and logarithmically correlated to body weight, while myelin loss is linearly correlated to body size (Royland et al., 1992). Malnutrition is initially compensated by a rise in metabolic rates of liver/kidney glycogen to maintain energy supply to the brain via increased glycogenic activity, until the necessary protection of muscle mass triggers a switch to ketogenic breakdown of triglycerides stored in the adipose tissues (Emery, 2005). Ketone bodies help individuals with high body-mass-index to survive 3–4-fold longer starvation periods (Cahill Jr. and Veech, 2003). A higher body-mass-index lowers the risk to die from motor neuron diseases like ALS (Nakken, 2019). The relative sparing of brain neurons and the generation of NAA in the neuronal mitochondria may explain why the central nervous system shows later disease manifestation in SCA2 than the subcutaneous fat stores. If this delay can be exploited to replete body stores of fat via hypercaloric diets, then it may become possible to postpone or mitigate the neurodegeneration, as already shown for ALS (Wills et al., 2014).

In conclusion, an authentic mouse model of SCA2 has been generated that mirrors numerous aspects of disease pathology, motor deficit and metabolic alterations without the potential off-target effects of an over-expression or transgenic strategy. It offers unique opportunities to accurately elucidate molecular mechanisms in a tissue- and cell-specific manner. Moreover, it represents an excellent tool for the development of molecular biomarkers in the assessment of disease progression or the effect of therapeutic manipulations. Overall, the molecular findings presented here provide insights into very early disease stages, where future curative therapies have to be applied and assessed.

4. Materials and methods

4.1. Generation of *Atxn2-CAG100* knock-in mice

For the generation of *Atxn2*-CAG100 knock-in (KIN) mice we modified the previously described pKO-*Sca2*-vector (Lastres-Becker et al., 2008a). The existing targeting construct had additional restriction sites inserted to permit the Southern blot analysis of Flp-mediated excision events, then the exon 1 region was modified between the unique restriction sites Eco47III and *Sgr*AI with the insertion of a CAG100 repeat (custom-made by GeneArt, Regensburg) at position Q156 and with the G > A creation of an additional *Sph*I restriction site 422 basepairs (bp) upstream the CAG repeat without alteration of the amino acid sequence, naming the modified vector NOW1-HR. The instability of large CAG repeats in bacteria was restrained by using the recombination-deficient SURE strain (Stratagene, now Agilent, Santa Clara) of *E. coli* bacteria and cultured at 30 °C for several hours on LB medium plates. Sequence verification of individual clones and *Sac*II digestion to control expansion length were performed before electroporating Kpn1 linearized vector into *Mus musculus* 129Sv/Pas strain embryonal stem (ES) cells to allow for homologous recombination at the endogenous *Atxn2* locus. The integration was confirmed in 6 ES cell clones as described previously (Damrath et al., 2012), employing the strategy depicted in Fig. 1A and the primers detailed in Table S1. Flp mediated excision was used to remove the neomycin resistance cassette. One correctly targeted ES cell line with verified expansion length of CAG100 was injected into *Mus musculus* C57BL/6 strain blastocysts. This work was outsourced to Genoway (Lyon, France).

4.2. Animals

All animals were housed at the Central Animal Facility (ZFE) of the Goethe University Medical School, Frankfurt am Main, at mfd Diagnostics GmbH in Wendelsheim, Germany, FELASA-certified facility. They were kept in individually ventilated cages at a 12 h-light/12 h-dark cycle under routine health monitoring and fed *ad libitum*. All procedures were in accordance with the German Animal Welfare Act, the Council Directive of 24th November 1986 (86/609/EWG) with Annex II and the ETS123 (European Convention for the Protection of Vertebrate Animals). Mice were backcrossed from a mixed 129Sv/Pas × C57BL/6 strain for at least 8 generations into the C57BL/6 strain. Heterozygous mating was employed. Among offspring littermates, the homozygous *Atxn2*-CAG100-KIN and WT animals of the same sex were selected and aged in neighboring cages for subsequent case-control comparisons in neuropathology and expression studies. Sperm cryopreservation was carried out at Genoway (Lyon, France) and the mice will in due course be made available through the EMMA mouse repository, where the *Atxn2*-CAG42-KIN line is already available, see https://www.infrafrontier.eu/search.

4.3. Genotyping of *Atxn2-CAG100-KIN* mice

DNA was isolated from ear punches and the genotyping PCR was performed. TaKaRa LA Taq-Polymerase (Takara Bio Inc., Japan) was used to amplify the neomycin cassette excised locus with the primer pair NOW1-K2 5′-TGAGTTGACTCCACAGGGAGGTGAGC-3′ and NOW1-H2 5′-CCATCTCGCCAGCCCGTAAGATTC-3′ flanking this site. The conditions were: initial denaturation at 94 °C for 3′, followed by 30 cycles of denaturation at 94 °C for 15″, annealing at 68 °C for 4′, elongation at 68 °C for 4′, and a final elongation step at 68 °C for 9′. The wild-type (WT) allele is predicted to yield an amplification product of 793 bp and the CAG100 allele of 948 bp. For amplification of the CAG repeat, the primers Sca2Ex1_Fwd5 5′-CCCCGCCCGGCGTGCGAGCCGG TGTAT-3′ and Sca2Ex1_Rev2 5′-CGGGCTTGCGGCCAGTGG-3′ were used. CAG100 allele has a predicted length of 387 bp, while WT allele has 90 bp. Initial denaturation at 98 °C for 3′, followed by 39 cycles of denaturation at 98 °C for 40″, annealing at 60 °C for 40″, elongation at 72 °C for 1′ and a final elongation step at 72 °C for 7′ was used. For exact sizing by fragment length analysis, these PCR products were purified with the QIAquick PCR Purification Kit. Samples were processed in 96 well plates on an Applied Biosystems 3730 DNA analyzer (StarSEQ GmbH, Mainz), sizing the peaks in comparison to a Genescan 500 LIZ standard and analyzing the electropherogram with the Peak Scanner 2.0 software as previously reported (Gispert et al., 2012).

4.4. Body weight and behavioral observations

Offspring with WT or CAG1/100 and CAG100/100 genotype of similar ages and identical sex were used as case-control pairs for phenotypic comparisons. Sudden death of animals was documented together with the relevant age information. Mice were weighed before behavioral testing. In contrast to all other measurements, male and female animals were separated for weight analyses due to strong gender-specific weight differences. Brain weight was measured after cervical dislocation, dissection and removal of the olfactory bulb, employing an analytical balance. If not otherwise stated, male and female animals were used for phenotype studies without separation. Grip strength was assessed by measuring the peak force of the fore limbs in 10 trials per mouse on an electronic grip strength meter (TSE, Bad Homburg). Paw prints were evaluated by painting the forepaws with a non-toxic red ink, the hind limbs of mice with blue. The mice were placed at one end of a dark tunnel, so that their walk to the other end will leave paw prints on the white paper that covers the floor (tunnel 6 cm high × 9 cm wide × 40 cm long). Footprint movement patterns were analyzed as described previously (Damrath et al., 2012). Assessment on an accelerating rotarod apparatus (model 7650 Robert & Jones, Ugo Basile, Comerio) and in an open field arena (Versamax, Omnitech, Columbus, Ohio) were performed as previously described (Damrath et al., 2012). During the acceleration of the rotarod from 4 to 40 rpm, every mouse had four consecutive 6 min trials interrupted by at least 10 min of break without previous training. The latency to fall was recorded for each trial; the mean value of the four trails was calculated and used for statistical analysis. Video recording occurred at ages from

10 to 14 months. For the beam test, the animals had to walk across a surface with length of ~1 m and a diameter of 18 mm. For the clasping test mice were suspended by their tails for about 1 min. Behavioral analyses were always conducted at the same daytime to avoid variances caused by circadian rhythm.

4.5. Generation of murine embryonal fibroblasts, cell culture and treatments

Primary murine embryonal fibroblast (MEF) cultures were generated from wild type (WT) and homozygous *Atxn2*-CAG100-KIN embryos around E15–18 as described earlier (Lastres-Becker et al., 2016). Culture preparation medium consisted of high glucose DMEM (Gibco), 15% BS (PAA Cell Culture Company), 1 × L-glutamine (Gibco) and 2 × Penicillin-Streptomycin (Gibco). Medium was changed daily for the first three days. Once confluent, the cells were transferred into a T25 flask and were cultured in growth medium (high glucose DMEM, 15% BS, 1 × L-glutamine, 1 × Penicillin-Streptomycin).

For RNA and protein isolation, WT and *Atxn2*-CAG100-KIN MEF cultures were grown to confluency, and cell pellets were obtained by scraping and centrifugation. For immunocytochemistry, cells were trypsinized and counted. 5×10^4 cells were seeded on 12 mm cover slips. 24 h after seeding, cells were washed with PBS and the medium was replaced with either normal growth medium or growth medium supplemented with 0.5 mM sodium arsenite (NaARS, Sigma) for 45 min. Then, the medium was aspirated and cells were washed with PBS before fixation for immunocytochemistry (see below). For puromycin incorporation analysis, 50×10^5 cells were seeded on 6-well plates the day before experiment. Puromycin (Santa Cruz) at the final concentration of 5 μM was added to the culture medium for 20 min, after which cells were washed with PBS, scraped and centrifuged to obtain the cell pellet.

4.6. Adipogenic differentiation of MEFs

Adipogenic differentiation of WT and *Atxn2*-CAG100-KIN MEFs was performed as reported (Zhang et al., 2009), and as depicted in Fig. 7A. Briefly, 5×10^5 cells were seeded in 6-well plates and grown in normal MEF culture medium described above, 1–2 days later confluency was achieved. Two days post-confluency, culture medium was replaced with pro-differentiation medium [normal culture medium supplemented with 830 nM insulin (Sigma), 1 μM dexamethasone (Cayman Chemicals), 0.5 mM 3-isobutyl-1-methylxanthine (IBMX, Cayman Chemicals), and 5 μM troglitazone (Cayman Chemicals)]. Two days later pro-differentiation medium was replaced with maintenance medium [normal culture medium supplemented with 830 nM insulin]. Maintenance medium was replaced every two days until harvest on Day 7. Control cells without adipogenic differentiation were seeded in parallel and were collected on Day 0 for expression analyses.

4.7. Nuclear and cytoplasmic fractionation of cerebellum

After cervical dislocation, whole brain was removed and cerebellum was dissected. Half of fresh cerebellum was homogenized in Hypotonic Nuclear Extraction (HNE) Buffer [100 mM NaCl, 50 mM Tris-HCl pH 7.4, 10 mM $MgCl_2$, 1% Triton-X, 40 U/ml RNaseOUT (Invitrogen)], with a motor pestle. After rotation at 4 °C for 10 min, and centrifugation at 1000 × *g* for 10 min at 4 °C, supernatant was collected into a new tube as "cytoplasmic" fraction and was frozen. The pellet was washed 2 × in cold HNE buffer and centrifuged, the final pellet consisting of the "nuclear" fraction was frozen until further processing.

4.8. RNA isolation and expression analysis

Whole brain was removed after cervical dislocation; cerebellum and two hemispheres were dissected into separate tubes and immediately frozen in liquid nitrogen. Abdominal adipose tissue was collected and frozen in liquid nitrogen. RNA extraction from cerebellum, adipose tissue and cultured cells was performed with TRIzol Reagent (Sigma Aldrich) according to user manual. Collection of blood samples from SCA2 patients and age- and sex-matched controls after overnight fasting, and processing of the blood samples has been described previously (Sen et al., 2016). RNA isolation from total blood with PAXgene Blood RNA Kit (Qiagen) was performed according to manufacturer's instructions. Total blood samples from mice was collected via cardiac withdrawal into EDTA tubes and frozen until processed. RNA isolation from mouse blood samples was performed with TRI Reagent BD (Sigma Aldrich) according to manufacturer's instructions.

Synthesis of cDNA from 1 μg of total RNA template was performed by the SuperScript IV VILO kit (ThermoFisher) according to manufacturer's instructions. The expanded *Atxn2* transcript was amplified from cerebellar cDNA with RT-PCR using primers flanking the CAG site and was assessed in a 2% agarose gel. To assess the gene expression changes, quantitative real-time PCR analyses were performed with StepOnePlus Real-Time PCR System (Applied Biosystems) equipment. cDNA from 25 ng total RNA was used for each PCR reaction with 1 μl TaqMan® Assay, 10 μl FastStart Universal Probe Master 2 × (Rox) Mix and ddH_2O up to 20 μl of total volume. The mouse specific TaqMan® Assays utilized for this study are: *Aspa* (Mm00480867_m1), *Atxn2* (Mm01199894_m1), *Cs* (Mm00466043_m1), *Folh1* (Mm00489655_m1), *Got1* (Mm01195792_g1), *Got2* (Mm00494703_m1), *Nat8l* (Mm01217217_m1), *Slc25a1* (Mm00467666_m1), *Slc25a11* (Mm00455209_m1), *Slc25a12* (Mm00552464_m1), *Slc25a13* (Mm00489442_m1) and *Tbp* (Mm00446973_m1). The human specific TaqMan® Assays utilized for this study are: *ATXN2* (Hs00268077_m1), *NAT8L* (Hs00402258_m1) and *HPRT1* (Hs99999909-m1). The PCR conditions were 50 °C for 2 min, 95 °C for 10 min, followed by 40 cycles of 95 °C for 15 s and 60 °C for 1 min. U2 snRNA (*Rnu2*) and *Actb* levels were analyzed with SYBR Green primers (U2-Forward: 5'-CTCGGCCTTTTGGCTAAGAT-3', U2-Reverse: 5'-CGTTCCTGGAGGTACTGCAA-3', *Actb*-Forward: 5'-GGAAATCGTGCG TGACATCAAAG-3', *Actb*-Reverse: 5'-CATACCCAAGAAGGAAGGC TGG-3') in a reaction of cDNA from 25 ng total RNA, 5 pmole/μl primers, 10 μl qPCR Mastermix Plus for SYBR Green I (Eurogentec) and ddH_2O up to 20 μl of total volume. The PCR conditions were 95 °C for 10 min, followed by 40 cycles of 95 °C for 15 s and 60 °C for 1 min and a melt curve stage of 95 °C for 15 s, 60 °C for 1 min and 95 °C for 15 s. Gene expression data was analyzed using $2^{-\Delta\Delta Ct}$ method (Livak and Schmittgen, 2001) with *Tbp*, *Actb* and *HPRT1* as housekeeping genes.

4.9. Protein extraction and western blots

Cerebellar tissue was homogenized with a motor pestle in 5-10 × weight/volume amount of either PN buffer [PBS, 1% NP-40, 150 mM NaCl] or RIPA buffer [50 mM Tris-HCl (pH 8.0), 150 mM NaCl, 2 mM EDTA, 1% Igepal CA-630 (Sigma), 0.5% sodium deoxycholate, 0.1% SDS and Complete Protease Inhibitor Cocktail (Roche)]. Following centrifugation, the PN buffer pellets were dissolved in Urea buffer [8 M Urea, 10 mM tris(2-carboxyethyl)phosphine hydrochloride (TCEP, Carl Roth), 40 mM 2-chloroacetamide (2-CAA, Sigma Aldrich), 100 mM Tris-HCl and Complete Protease Inhibitor Cocktail (Roche)] in order to obtain insoluble proteins. Cell pellets from MEF cultures were homogenized in RIPA buffer. Protein concentration was determined with a Spectrophotometer (Eppendorf) using 5 × Bradford Reagent (Roti-Quant, Carl Roth). 20 μg of total proteins were mixed with 2 × loading buffer [250 mM Tris-HCl pH 7.4, 20% Glycerol, 4% SDS, 10% 2-Mercaptoethanol, 0.005% Bromophenol blue], incubated at 90 °C for 2 min, separated on polyacrylamide gels and were transferred to Nitrocellulose membranes (GE Healthcare). The membranes were blocked in 5% BSA/TBS-T, and incubated overnight at 4 °C with primary antibodies against ASPA (Thermo Fischer, PA5–29180), ACTB (Sigma #A5441, 1:10000), ATXN2 (Proteintech #21776–1-AP), GOT2 (Acris #AM06383SU-N, 1:500), NAT8L (Abbexa, abx431860), PABP (Abcam ab21060), Puromycin (Merck Millipore, MABE343), SLC25A12

(AGC1) (abcam, ab200201), TUBA (abcam, ab-15246). Fluorescently labeled secondary goat anti-mouse (IRDye 800CW, Li-Cor, 1:10,000) and goat anti-rabbit (IRDye 680RD, Li-Cor, 1:10000) antibodies were incubated for 1 h at room temperature. Membranes were visualized using Li-Cor Odyssey Classic instrument. The image analysis to quantify signal intensities was performed using ImageStudio software.

4.10. Perfusion

Mice were anesthetized with an overdose of Ketaset (300 mg/kg) and Domitor (3 mg/kg) by an intraperitoneal injection. To assess the anesthetic depth, the withdrawal reflex was monitored. Intracardial perfusion was done with phosphate buffer saline (PBS) followed by 4% paraformaldehyde (PFA) in 0.1 M PBS. For paraffin embedded sections, the tissue was post-fixed overnight in 4% PFA at 4 °C, dehydrated and incubated in paraplast for 24 h at 56 °C. All tissues were cut and mounted in 7 μm-thick slices using a microtome. For cryosections, the tissue was also post-fixed overnight in 4% PFA at 4 °C, immersed in 30% sucrose until it sank, cut with a cryostat in 30 μm-thick slices and kept in cryoprotection solution (30% ethylene glycol, 25% glycerin, 0.01% sodium azide in 0.1 M PBS) at −20 °C until used.

4.11. Histology and immunostaining

For immunocytochemistry, 5×10^4 cells from WT and *Atxn2*-CAG100-KIN MEF cultures were seeded on 12 mm cover slips. Next day, the cells were washed and stressed with 0.5 mM NaARS supplemented in the DMEM growth medium for 45 min at 37 °C. Control cells were washed and supplemented with only DMEM growth medium for 45 min. Cells were washed once before fixation with 4% paraformaldehyde/PBS at room temperature (RT) for 20 min, then were permeabilized with 0.1% Triton-X-100/PBS for 20 min at RT. Blocking was done with 3% BSA/PBS solution for 1 h at RT. Primary antibody incubation with PABP (Abcam ab21060, 1:100) and ATXN2 (BD Biosciences #611378, 1:100) antibodies was performed in 3% BSA/PBS for 1 h at RT. Secondary antibody incubation with goat anti-rabbit-Alexa Fluor 546 (Molecular Probes, 1:1000), goat anti-mouse-Alexa Fluor 488 (Molecular Probes, 1:1000) antibodies and DAPI was performed in 3% BSA/PBS for 1 h at RT in dark. The coverslips were mounted on glass slides with fluorescent mounting medium (Thermo Fisher) and dried overnight. Cell imaging was performed using Zeiss Axiovert 200 M inverted microscope using a 100 × objective, and ImageJ software was used to merge images.

For immunohistochemistry, paraffin embedded sections were rehydrated in a descending alcohol series. Bull's Eye Decloaker (1:20) was used for antigen retrieval and the sections were incubated with the following primary antibodies overnight: anti-1C2 (Millipore #MAB1574, 1:800), anti-ATXN2 (BD Bioscience #611378, 1:50), anti-p62 (Santa Cruz #sc25575, 1:50) and anti-Ubiquitin (UBQ, Dako #ZO458, 1:100). For DAB stainings, Vector NovaRED Peroxidase kit was used after blocking the endogenous peroxidase with 100% methanol, 30% H_2O_2 in Tris/HCl pH 7.6 (1:1:18) for 30 min. For fluorescent stainings, goat anti-rabbit-Alexa Fluor 546 (Molecular Probes, 1:1000), goat anti-mouse-Alexa Fluor 488 (Molecular Probes, 1:1000) antibodies and DAPI was used for 1 h at RT in dark. The Leica 090–135-001 microscope was utilized for single immunohistochemical stainings at magnitude 60×. Double immunofluorescence stainings with anti-ATXN2 (BD Bioscience #611378, 1:50) and PABP (Abcam ab21060, 1:250) was performed on free-floating cryosections. Secondary antibodies goat anti-mouse Alexa Fluor 488 (Molecular Probes, 1:1000), goat anit-rabbit Alexa Fluor 568 (Molecular Probes, 1:1000) and DAPI were incubated. Imaging was done with the confocal microscope Nikon eclipse TE2000-E at 40× magnification.

4.12. 1H-MR spectroscopy and data analysis

MR spectroscopy was performed using a 7 Tesla Small Animal MR Scanner (PharmaScan, Bruker, Ettlingen, Germany) with a volume coil as transmitter and a head surface coil for signal reception. Data were acquired with the Paravision 6.0.1 software. For MR scans, mice were anesthetized with isoflurane (2%) and stabilized in the prone position with a tooth holder. Body temperature was maintained at 36–37 °C with a built-in animal waterbed (Bruker, Ettlingen, Germany). Respiration rate was monitored and kept constant at 80–100 breaths per minute continuously throughout the measurement. For identifying the target areas on T2-weighted images, a localized T2-multislice Turbo rapid acquisition with relaxation enhancement was acquired (T2 TurboRARE; TE/TR = 33 ms/2500 ms, FOV = 20 × 20 mm, 11 slices, 0.5 mm slice thickness, acquisition matrix = 256 × 256, flip angle 90°). Single voxel spectroscopy (SVS) was performed using the point resolved spectroscopy sequence (PRESS) with an echo time (TE) of 16.5 ms, a repetition time (TR) of 2500 ms, spectral width of 3301.6 Hz and 2048 points data size. One voxel of 3 mm × 3 mm × 3 mm was placed in the cerebrum as indicated in Fig. 5A and 64 acquisitions were averaged in approximately 3 min. Another voxel of 2 mm × 2 mm × 2 mm was placed in the cerebellum and 256 acquisitions were averaged in approximately 12 min. The target selection was based on T2-weighted MRI data from the imaging protocol. The volume of interest (VOI) was selected to contain only brain tissue without interference of the skull. For each measurement, homogeneity after shimming, measured as the full width at half maximum (FWHM) of the water peak was below 25 Hz. MR spectroscopic data was processed using the java-based MR user interface spectroscopic analysis package (jMRUI version 5.2) employing AQSES (Automated Quantification of Short Time Echo MRS), a time domain quantification method with which the residual water component could be filtered during the post-processing. Additionally, Cramer Rao lower bounds (CRLBs) of the metabolites of interest could be obtained from the quantification procedure. The following metabolites were included in the analysis: alanine (Ala), aspartate (Asp), ascorbate/vitamin C (Asc), glycerophosphocholine (GPC), phosphocholine (PCho), creatine (Cr), phosphocreatine (PCr), glucose (Glc), glutamine (Gln), glutamate (Glu), glutathione (GSH), glycine (Gly), myo-inositol (myo-Ins), lactate (Lac), *N*-acetylaspartate (NAA), *N*-acetylaspartylglutamate (NAAG), phosphoethanolamine (PE), scyllo-inositol (scyllo-Ins) and taurine (Tau). The respective basis data sets were generated by quantum-mechanical simulation using NMR-SCOPE-B, which is provided in the jMRUI package. Chemical shifts and scalar coupling constants were obtained from the literature (Govindaraju et al., 2000). Based on literature, the following terms were defined to determine aggregated values for metabolites that are difficult to separate from each other: tCho = GPC + PCho, tCr = PCr + Cr, tNAA = NAA + NAAG.

4.13. Electron microscopy

The tissue samples were fixed overnight using 2.5% glutaraldehyde buffered in cacodylate. The embedding procedure comprised fixation in 1% osmium tetroxide, dehydration in a graded ethanol series intermingled by an incubation step with uranyl acetate (between the 50% and 90% ethanol step) and finally rinsing in propylene oxide. The specimens were then embedded in epoxy resins that polymerized for 16 h at 60 °C. After embedding, first semi-thin sections (0.5 μm) were cut using an ultramicrotome (Leica Ultracut UCT, Deerfield, IL, USA) with a diamond knife. Sections were stained with Toluidine blue, placed on glass slides and examined by light microscopy to select appropriate areas for ultrathin preparation. Ultrathin sections (50–70 nm) were cut again using an ultramicrotome. Sections were mounted on copper grids and contrasted with uranyl acetate for 2–3 h at 42 °C and lead citrate for 20 min at RT. These samples were imaged and digital pictures were taken with a FEI Tecnai G2 Spirit Biotwin TEM (Hillsboro, OR) at an operating voltage of 120 kV.

4.14. Statistical analyses

Unless specified otherwise, all statistical tests were performed as unpaired Student's *t*-test with Welch's correction using GraphPad Prism software version 4.03 (2005) after establishing that each population was normally distributed (one-sided Kolmogorov-Smirnov test). Figures display mean values and standard error of the mean (s.e.m.). Values $p < .05$ were considered significant and marked with asterisks $^{*}p < .05$, $^{**}p < .01$, $^{***}p < .001$, $^{****}p < .0001$.

Supplementary data to this article can be found online at https://doi.org/10.1016/j.nbd.2019.104559.

Acknowledgements

The authors wish to thank Gabriele Köpf for technical assistance, and the staff at the Zentrale Forschungs-Einrichtung at Frankfurt University Medical School for their assistance with animal assessments.

Competing interests

No competing interests declared.

Funding

This work was supported by the Deutsche Forschungs-Gemeinschaft [AU 96/11-1, 113], the European Research Council Starting Grant [ERC-Stg, 680235] (MSc), the Netherlands Organization for Scientific Research (NWO-ALW; CIDZ), the Dutch Organization for Medical Sciences (ZonMW; CIDZ), Life Sciences (CIDZ), and ERC-adv and ERC-POC (CIDZ), and the Max Planck Society. Michel Mittelbronn would like to thank the Luxembourg National Research Fund (FNR) for the support [FNR PEARL P16/BM/11192868 grant].

References

Abdel-Aleem, A., Zaki, M.S., 2008. Spinocerebellar ataxia type 2 (SCA2) in an Egyptian family presenting with polyphagia and marked CAG expansion in infancy. J. Neurol. 255, 413–419.
Almaguer-Mederos, L.E., et al., 2010. Estimation of the age at onset in spinocerebellar ataxia type 2 Cuban patients by survival analysis. Clin. Genet. 78, 169–174.
Almaguer-Mederos, L.E., et al., 2013. Estimation of survival in spinocerebellar ataxia type 2 Cuban patients. Clin. Genet. 83, 293–294.
Al-Ramahi, I., et al., 2007. dAtaxin-2 mediates expanded Ataxin-1-induced neurodegeneration in a *Drosophila* model of SCA1. PLoS Genet. 3, e234.
Antenora, A., et al., 2018. Predictors of survival in spinocerebellar ataxia type 2 population from southern Italy. Neurol. Sci. 39, 1857–1860.
Ariyannur, P.S., et al., 2008. N-acetylaspartate synthesis in the brain: mitochondria vs. microsomes. Brain Res. 1227, 34–41.
Ariyannur, P.S., et al., 2010. Methamphetamine-induced neuronal protein NAT8L is the NAA biosynthetic enzyme: implications for specialized acetyl coenzyme A metabolism in the CNS. Brain Res. 1335, 1–13.
Auburger, G.W., 2012. Spinocerebellar ataxia type 2. Handb. Clin. Neurol. 103, 423–436.
Auburger, G., et al., 1990. Autosomal dominant ataxia: genetic evidence for locus heterogeneity from a Cuban founder-effect population. Am. J. Hum. Genet. 46, 1163–1177.
Auburger, G., et al., 2014. 12q24 locus association with type 1 diabetes: SH2B3 or ATXN2? World J. Diabetes 5, 316–327.
Auburger, G., et al., 2017. Efficient prevention of neurodegenerative diseases by depletion of starvation response factor Ataxin-2. Trends Neurosci. 40, 507–516.
Bar, D.Z., et al., 2016. Cell size and fat content of dietary-restricted *Caenorhabditis elegans* are regulated by ATX-2, an mTOR repressor. Proc. Natl. Acad. Sci. U. S. A. 113, E4620–E6429.
Becker, L.A., et al., 2017. Therapeutic reduction of ataxin 2 extends lifespan and reduces pathology in TDP-43 mice. Nature 544, 367–371.
Besse, A., et al., 2015. The GABA transaminase, ABAT, is essential for mitochondrial nucleoside metabolism. Cell Metab. 21, 417–427.
Broer, S., Palacin, M., 2011. The role of amino acid transporters in inherited and acquired diseases. Biochem. J. 436, 193–211.
Cahill Jr., G.F., Veech, R.L., 2003. Ketoacids? Good medicine? Trans. Am. Clin. Climatol. Assoc. 114, 149–161 (discussion 162-3).
Cancel, G., et al., 1997. Molecular and clinical correlations in spinocerebellar ataxia 2: a study of 32 families. Hum. Mol. Genet. 6, 709–715.
Cao, J., et al., 2013a. GABA transaminases from Saccharomyces cerevisiae and *Arabidopsis thaliana* complement function in cytosol and mitochondria. Yeast 30, 279–289.
Cao, J., et al., 2013b. GABA shunt mediates thermotolerance in *Saccharomyces cerevisiae* by reducing reactive oxygen production. Yeast 30, 129–144.
Closk, R., et al., 2004. ATX-2, the C. elegans ortholog of ataxin 2, functions in translational regulation in the germline. Development 131, 4831–4841.
Damrath, E., et al., 2012. ATXN2-CAG42 sequesters PABPC1 into insolubility and induces FBXW8 in cerebellum of old ataxic knock-in mice. PLoS Genet. 8, e1002920.
Dansithong, W., et al., 2015. Ataxin-2 regulates RGS8 translation in a new BAC-SCA2 transgenic mouse model. PLoS Genet. 11, e1005182.
Della Nave, R., et al., 2004. ADC mapping of neurodegeneration in the brainstem and cerebellum of patients with progressive ataxias. NeuroImage 22, 698–705.
Dell'Orco, J.M., et al., 2017. Potassium channel dysfunction underlies Purkinje neuron spiking abnormalities in spinocerebellar ataxia type 2. Hum. Mol. Genet. 26, 3935–3945.
DeMille, D., et al., 2015. PAS kinase is activated by direct SNF1-dependent phosphorylation and mediates inhibition of TORC1 through the phosphorylation and activation of Pbp1. Mol. Biol. Cell 26, 569–582.
Di Fabio, R., et al., 2012. Infantile childhood onset of spinocerebellar ataxia type 2. Cerebellum 11, 526–530.
Diallo, A., et al., 2017. Body mass index decline is related to spinocerebellar Ataxia disease progression. Mov. Disord. Clin. Pract. 4, 689–697.
Drost, J., et al., 2013. Ataxin-2 modulates the levels of Grb2 and SRC but not ras signaling. J. Mol. Neurosci. 51, 68–81.
Elden, A.C., et al., 2010. Ataxin-2 intermediate-length polyglutamine expansions are associated with increased risk for ALS. Nature 466, 1069–1075.
Emery, P.W., 2005. Metabolic changes in malnutrition. Eye 19, 1029–1034.
Estrada, R., et al., 1999. Spinocerebellar ataxia 2 (SCA2): morphometric analyses in 11 autopsies. Acta Neuropathol. 97, 306–310.
Faught, E., 2011. Vigabatrin therapy for refractory complex partial seizures: review of clinical trial experience in the United States. Acta Neurol. Scand. 29–35 Supplementum.
Fittschen, M., et al., 2015. Genetic ablation of ataxin-2 increases several global translation factors in their transcript abundance but decreases translation rate. Neurogenetics 16, 181–192.
Fleischer, T.C., et al., 2006. Systematic identification and functional screens of uncharacterized proteins associated with eukaryotic ribosomal complexes. Genes Dev. 20, 1294–1307.
Freund, H.J., et al., 2007. Subthalamic-thalamic DBS in a case with spinocerebellar ataxia type 2 and severe tremor-a unusual clinical benefit. Mov. Disord. 22, 732–735.
Gierga, K., et al., 2005. Involvement of the cranial nerves and their nuclei in spinocerebellar ataxia type 2 (SCA2). Acta Neuropathol. 109, 617–631.
Gispert, S., et al., 2012. The modulation of amyotrophic lateral sclerosis risk by ataxin-2 intermediate polyglutamine expansions is a specific effect. Neurobiol. Dis. 45, 356–361.
Giuffrida, S., et al., 1999. Supratentorial atrophy in spinocerebellar ataxia type 2: MRI study of 20 patients. J. Neurol. 246, 383–388.
Govindaraju, V., et al., 2000. Proton NMR chemical shifts and coupling constants for brain metabolites. NMR Biomed. 13, 129–153.
Guerrini, L., et al., 2004. Brainstem neurodegeneration correlates with clinical dysfunction in SCA1 but not in SCA2. A quantitative volumetric, diffusion and proton spectroscopy MR study. Brain J. Neurol. 127, 1785–1795.
Halbach, M.V., et al., 2015. Both ubiquitin ligases FBXW8 and PARK2 are sequestrated into insolubility by ATXN2 PolyQ expansions, but only FBXW8 expression is dysregulated. PLoS One 10, e0121089.
Halbach, M.V., et al., 2017. Atxn2 knockout and CAG42-knock-in cerebellum shows similarly dysregulated expression in calcium homeostasis pathway. Cerebellum 16, 68–81.
Hansen, S.T., et al., 2013. Changes in Purkinje cell firing and gene expression precede behavioral pathology in a mouse model of SCA2. Hum. Mol. Genet. 22, 271–283.
Heck, M.V., et al., 2014. Dysregulated expression of lipid storage and membrane dynamics factors in Tia1 knockout mouse nervous tissue. Neurogenetics 15, 135–144.
Helmlinger, D., et al., 2004. Disease progression despite early loss of polyglutamine protein expression in SCA7 mouse model. J. Neurosci. 24, 1881–1887.
Hoche, F., et al., 2011. Spinocerebellar ataxia type 2 (SCA2): identification of early brain degeneration in one monozygous twin in the initial disease stage. Cerebellum 10, 245–253.
Huber, K., et al., 2019. N-acetylaspartate pathway is nutrient responsive and coordinates lipid and energy metabolism in brown adipocytes. Biochim. Biophys. Acta, Mol. Cell Res. 1866, 337–348.
Huynh, D.P., et al., 2000. Nuclear localization or inclusion body formation of ataxin-2 are not necessary for SCA2 pathogenesis in mouse or human. Nat. Genet. 26, 44–50.
Jaeken, J., et al., 1984. Gamma-aminobutyric acid-transaminase deficiency: a newly recognized inborn error of neurotransmitter metabolism. Neuropediatrics 15, 165–169.
Kedersha, N., Anderson, P., 2007. Mammalian stress granules and processing bodies. Methods Enzymol. 431, 61–81.
Kedersha, N., et al., 2013. Stress granules and cell signaling: more than just a passing phase? Trends Biochem. Sci. 38, 494–506.
Kiehl, T.R., et al., 2006. Generation and characterization of Sca2 (ataxin-2) knockout mice. Biochem. Biophys. Res. Commun. 339, 17–24.
Koch, P., et al., 2011. Excitation-induced ataxin-3 aggregation in neurons from patients with Machado-Joseph disease. Nature 480, 543–546.
Lahut, S., et al., 2012. ATXN2 and its neighbouring gene SH2B3 are associated with increased ALS risk in the Turkish population. PLoS One 7, e42956.
Lastres-Becker, I., et al., 2008a. Insulin receptor and lipid metabolism pathology in ataxin-2 knock-out mice. Hum. Mol. Genet. 17, 1465–1481.
Lastres-Becker, I., et al., 2008b. Spinocerebellar ataxia 2 (SCA2). Cerebellum 7, 115–124.
Lastres-Becker, I., et al., 2016. Mammalian ataxin-2 modulates translation control at the pre-initiation complex via PI3K/mTOR and is induced by starvation. Biochim.

Biophys. Acta 1862, 1558–1569.
Lastres-Becker, I., et al., 2019. New alternative splicing variants of the *ATXN2* transcript. Neurological Research and Practice 1, 22.
Lee, T., et al., 2011. Ataxin-2 intermediate-length polyglutamine expansions in European ALS patients. Hum. Mol. Genet. 20, 1697–1700.
Lee, J.K., et al., 2015. Role of autophagy in the pathogenesis of amyotrophic lateral sclerosis. Biochim. Biophys. Acta 1852, 2517–2524.
Liu, J., et al., 2009. Deranged calcium signaling and neurodegeneration in spinocerebellar ataxia type 2. J. Neurosci. 29, 9148–9162.
Livak, K.J., Schmittgen, T.D., 2001. Analysis of relative gene expression data using real-time quantitative PCR and the 2(−Delta Delta C(T)) Method. Methods 25, 402–408.
Lu, Z.H., et al., 2004. N-Acetylaspartate synthase is bimodally expressed in microsomes and mitochondria of brain. Brain Res. Mol. Brain Res. 122, 71–78.
Mangiarini, L., et al., 1997. Instability of highly expanded CAG repeats in mice transgenic for the Huntington's disease mutation. Nat. Genet. 15, 197–200.
Mangus, D.A., et al., 1998. Pbp1p, a factor interacting with *Saccharomyces cerevisiae* poly (A)-binding protein, regulates polyadenylation. Mol. Cell. Biol. 18, 7383–7396.
Medrano-Montero, J., et al., 2018. Early cranial nerve dysfunction is correlated to altered facial morphology in spinocerebellar ataxia type 2. Investig. Discapacidad 7, 53–66.
Meierhofer, D., et al., 2016. Ataxin-2 (Atxn2)-knock-out mice show branched chain amino acids and fatty acids pathway alterations. Mol. Cell. Proteomics 15, 1728–1739.
Moffett, J.R., Namboodiri, M.A., 1995. Differential distribution of N-acetylaspartylglutamate and N-acetylaspartate immunoreactivities in rat forebrain. J. Neurocytol. 24, 409–433.
Nakken, O., et al., 2019. High BMI is associated with low ALS risk: a population-based study. Neurology 93, e424–e432.
Nonhoff, U., et al., 2007. Ataxin-2 interacts with the DEAD/H-box RNA helicase DDX6 and interferes with P-bodies and stress granules. Mol. Biol. Cell 18, 1385–1396.
Nonis, D., et al., 2008. Ataxin-2 associates with the endocytosis complex and affects EGF receptor trafficking. Cell. Signal. 20, 1725–1739.
Orozco Diaz, G., et al., 1990. Autosomal dominant cerebellar ataxia: clinical analysis of 263 patients from a homogeneous population in Holguin, Cuba. Neurology 40, 1369–1375.
Oz, G., et al., 2011. In vivo monitoring of recovery from neurodegeneration in conditional transgenic SCA1 mice. Exp. Neurol. 232, 290–298.
Oz, G., et al., 2015. Assessing recovery from neurodegeneration in spinocerebellar ataxia 1: comparison of in vivo magnetic resonance spectroscopy with motor testing, gene expression and histology. Neurobiol. Dis. 74, 158–166.
Paciorkowski, A.R., et al., 2011. Massive expansion of SCA2 with autonomic dysfunction, retinitis pigmentosa, and infantile spasms. Neurology 77, 1055–1060.
Park, H., et al., 2015. Parkinsonism in spinocerebellar ataxia. Biomed. Res. Int. 2015 125273.
Pfeffer, M., et al., 2017. Impact of Ataxin-2 knock out on circadian locomotor behavior and PER immunoreaction in the SCN of mice. Chronobiol. Int. 34, 129–137.
Pflieger, L.T., et al., 2017. Gene co-expression network analysis for identifying modules and functionally enriched pathways in SCA2. Hum. Mol. Genet. 26, 3069–3080.
Prokesch, A., et al., 2016. N-acetylaspartate catabolism determines cytosolic acetyl-CoA levels and histone acetylation in brown adipocytes. Sci. Rep. 6, 23723.
Pulst, S.M., et al., 1996. Moderate expansion of a normally biallelic trinucleotide repeat in spinocerebellar ataxia type 2. Nat. Genet. 14, 269–276.
Ragothaman, M., et al., 2004. Complex phenotypes in an Indian family with homozygous SCA2 mutations. Ann. Neurol. 55, 130–133.
Royland, J., et al., 1992. How much undernourishment is required to retard brain myelin development. Neurochem. Int. 21, 269–274.
Rub, U., et al., 2003a. Thalamic involvement in a spinocerebellar ataxia type 2 (SCA2) and a spinocerebellar ataxia type 3 (SCA3) patient, and its clinical relevance. Brain J. Neurol. 126, 2257–2272.
Rub, U., et al., 2003b. Anatomically based guidelines for systematic investigation of the central somatosensory system and their application to a spinocerebellar ataxia type 2 (SCA2) patient. Neuropathol. Appl. Neurobiol. 29, 418–433.
Rub, U., et al., 2004. Damage to the reticulotegmental nucleus of the pons in spinocerebellar ataxia type 1, 2, and 3. Neurology 63, 1258–1263.
Rub, U., et al., 2005a. Extended pathoanatomical studies point to a consistent affection of the thalamus in spinocerebellar ataxia type 2. Neuropathol. Appl. Neurobiol. 31, 127–140.
Rub, U., et al., 2005b. Spinocerebellar ataxias types 2 and 3: degeneration of the precerebellar nuclei isolates the three phylogenetically defined regions of the cerebellum. J. Neural Transm. 112, 1523–1545.
Rub, U., et al., 2006. Degeneration of ingestion-related brainstem nuclei in spinocerebellar ataxia type 2, 3, 6 and 7. Neuropathol. Appl. Neurobiol. 32, 635–649.
Rub, U., et al., 2007. Consistent affection of the central somatosensory system in spinocerebellar ataxia type 2 and type 3 and its significance for clinical symptoms and rehabilitative therapy. Brain Res. Rev. 53, 235–249.
Rub, U., et al., 2013. Clinical features, neurogenetics and neuropathology of the polyglutamine spinocerebellar ataxias type 1, 2, 3, 6 and 7. Prog. Neurobiol. 104, 38–66.
Satterfield, T.F., et al., 2002. A Drosophila homolog of the polyglutamine disease gene SCA2 is a dosage-sensitive regulator of actin filament formation. Genetics 162, 1687–1702.
Scherzed, W., et al., 2012. Pathoanatomy of cerebellar degeneration in spinocerebellar ataxia type 2 (SCA2) and type 3 (SCA3). Cerebellum 11, 749–760.
Scoles, D.R., 2017. Antisense oligonucleotide therapy for spinocerebellar ataxia type 2. Nature 544, 362–366.
Seidel, G., et al., 2017. Quantitative global proteomics of yeast PBP1 deletion mutants and their stress responses identifies glucose metabolism, mitochondrial, and stress granule changes. J. Proteome Res. 16, 504–515.
Sen, N.E., et al., 2016. Search for SCA2 blood RNA biomarkers highlights Ataxin-2 as strong modifier of the mitochondrial factor PINK1 levels. Neurobiol. Dis. 96, 115–126.
Sen, N.E., et al., 2017. PINK1 and Ataxin-2 as modifiers of growth. Oncotarget 8, 32382–32383.
Sudhakaran, I.P., et al., 2014. FMRP and Ataxin-2 function together in long-term olfactory habituation and neuronal translational control. Proc. Natl. Acad. Sci. U. S. A. 111, E99–E108.
Takahara, T., Maeda, T., 2012. Transient sequestration of TORC1 into stress granules during heat stress. Mol. Cell 47, 242–252.
Tuin, I., et al., 2006. Stages of sleep pathology in spinocerebellar ataxia type 2 (SCA2). Neurology 67, 1966–1972.
van de Loo, S., et al., 2009. Ataxin-2 associates with rough endoplasmic reticulum. Exp. Neurol. 215, 110–118.
Velazquez-Perez, L., et al., 2001. Hereditary ataxias in Cuba. Historical, epidemiological, clinical, electrophysiological and quantitative neurological features. Rev. Neurol. 32, 71–76.
Velazquez-Perez, L., et al., 2004. Saccade velocity is controlled by polyglutamine size in spinocerebellar ataxia 2. Ann. Neurol. 56, 444–447.
Velazquez-Perez, L., et al., 2009. Saccade velocity is reduced in presymptomatic spinocerebellar ataxia type 2. Clin. Neurophysiol. 120, 632–635.
Velazquez-Perez, L., et al., 2014. Progression of early features of spinocerebellar ataxia type 2 in individuals at risk: a longitudinal study. Lancet Neurol. 13, 482–489.
Velazquez-Perez, L., et al., 2016. Abnormal corticospinal tract function and motor cortex excitability in non-ataxic SCA2 mutation carriers: a TMS study. Clin. Neurophysiol. 127, 2713–2719.
Velazquez-Perez, L., et al., 2017a. Early corticospinal tract damage in prodromal SCA2 revealed by EEG-EMG and EMG-EMG coherence. Clin. Neurophysiol. 128, 2493–2502.
Velazquez-Perez, L.C., et al., 2017b. Spinocerebellar Ataxia type 2: Clinicogenetic aspects, mechanistic insights, and management approaches. Front. Neurol. 8, 472.
Vinther-Jensen, T., et al., 2013. Germ-line CAG repeat instability causes extreme CAG repeat expansion with infantile-onset spinocerebellar ataxia type 2. Eur. J. Hum. Genet. 21, 626–629.
Wang, X., Chen, X.J., 2015. A cytosolic network suppressing mitochondria-mediated proteostatic stress and cell death. Nature 524, 481–484.
Wang, P.S., et al., 2012. Association between proton magnetic resonance spectroscopy measurements and CAG repeat number in patients with spinocerebellar ataxias 2, 3, or 6. PLoS One 7, e47479.
Wills, A.M., et al., 2014. Hypercaloric enteral nutrition in patients with amyotrophic lateral sclerosis: a randomised, double-blind, placebo-controlled phase 2 trial. Lancet 383, 2065–2072.
Yang, Y.S., et al., 2019. Yeast Ataxin-2 forms an intracellular condensate required for the inhibition of TORC1 signaling during respiratory growth. Cell 177 697–710 e17.
Zhang, H.H., et al., 2009. Insulin stimulates adipogenesis through the Akt-TSC2-mTORC1 pathway. PLoS One 4, e6189.

III. Publication #3

Declaration of author contributions

Title: In Human and Mouse Spino-Cerebellar Tissue, Ataxin-2 Expansion Affects Ceramide-Sphingomyelin Metabolism
Status: Published
Journal: *Int J Mol Sci.,* 2019, doi: 10.3390/ijms20235854

Authors: Nesli-Ece Sen (NES), Aleksandar Arsovic (AA), David Meierhofer (DM), Susanne Brodesser (SB), Carola Oberschmidt (CO), Julia Canet-Pons (JCP), Zeynep-Ece Kaya (ZEK), Melanie Vanessa Halbach (MVH), Suzana Gispert (SG), Konrad Sandhoff (KS), Georg Auburger (GA)

Author contributions:

(1) Concept and design
Doctoral candidate (NES): **40%**
Co-author DM: **20%**
Co-author GA: **40%**

(2) Conducting tests and experiments
Doctoral candidate (NES): **50%** (Tissue collection, expression analyses)
Co-author AA: **30%** (Tissue collection, expression analyses)
Co-author DM: **10%** (Mass spectrometry metabolomics)
Co-author SB: **5%** (Thin layer chromatography)
Co-author CO: **5%** (Thin layer chromatography)

(3) Compilation of data sets and figures
Doctoral candidate (NES): **60%** (TLC data, metabolome data, expression analyses)
Co-author AA: **15%** (Expression analyses)
Co-author DM: **15%** (Mass spectrometry metabolomics)
Co-author SB: **5%** (Thin layer chromatography)
Co-author CO: **5%** (Thin layer chromatography)

(4) Analysis and interpretation of data
Doctoral candidate (NES): **30%** (TLC data, metabolome data, expression analyses)
Co-author DM: **15%** (Mass spectrometry metabolomics)
Co-author SB: **5%** (Thin layer chromatography)
Co-author CO: **5%** (Thin layer chromatography)
Co-author KS: **20%** (Interpretation of all data)
Co-author GA: **25%** (Interpretation of all data)

(5) Drafting of manuscript
Doctoral candidate (NES): **50%**
Co-author KS: **10%**
Co-author GA: **40%**

International Journal of
Molecular Sciences

MDPI

Article

In Human and Mouse Spino-Cerebellar Tissue, Ataxin-2 Expansion Affects Ceramide-Sphingomyelin Metabolism

Nesli-Ece Sen [1,2], Aleksandar Arsovic [1], David Meierhofer [3], Susanne Brodesser [4], Carola Oberschmidt [1], Júlia Canet-Pons [1], Zeynep-Ece Kaya [1,5], Melanie-Vanessa Halbach [1], Suzana Gispert [1], Konrad Sandhoff [4,*] and Georg Auburger [1,*]

1 Experimental Neurology, Building 89, Goethe University Medical Faculty, Theodor Stern Kai 7, 60590 Frankfurt am Main, Germany; nesliecesen@gmail.com (N.-E.S.); arsovicalexandar@gmail.com (A.A.); carolaoberschmidt@gmx.net (C.O.); jcanetpons@gmail.com (J.C.-P.); zeynepcekaya@hotmail.com (Z.-E.K.); melanie.halbach@gmx.de (M.-V.H.); Gispert-Sanchez@em.uni-frankfurt.de (S.G.)
2 Faculty of Biosciences, Goethe-University, 60438 Frankfurt am Main, Germany
3 Max Planck Institute for Molecular Genetics, Ihnestrasse 63-73, 14195 Berlin, Germany; Meierhof@molgen.mpg.de
4 Membrane Biology and Lipid Biochemistry Unit, Life and Medical Sciences Institute, University of Bonn, 53121 Bonn, Germany; susanne.brodesser@uk-koeln.de
5 Cerrahpasa School of Medicine, Istanbul University, 34098 Istanbul, Turkey
* Correspondence: sandhoff@uni-bonn.de (K.S.); auburger@em.uni-frankfurt.de (G.A.); Tel.: +49-228-73-5346 (K.S.); +49-69-6301-7428 (G.A.)

Received: 4 November 2019; Accepted: 20 November 2019; Published: 21 November 2019

Abstract: Ataxin-2 (human gene symbol *ATXN2*) acts during stress responses, modulating mRNA translation and nutrient metabolism. Ataxin-2 knockout mice exhibit progressive obesity, dyslipidemia, and insulin resistance. Conversely, the progressive ATXN2 gain of function due to the fact of polyglutamine (polyQ) expansions leads to a dominantly inherited neurodegenerative process named spinocerebellar ataxia type 2 (SCA2) with early adipose tissue loss and late muscle atrophy. We tried to understand lipid dysregulation in a SCA2 patient brain and in an authentic mouse model. Thin layer chromatography of a patient cerebellum was compared to the lipid metabolome of *Atxn2*-CAG100-Knockin (KIN) mouse spinocerebellar tissue. The human pathology caused deficits of sulfatide, galactosylceramide, cholesterol, C22/24-sphingomyelin, and gangliosides GM1a/GD1b despite quite normal levels of C18-sphingomyelin. Cerebellum and spinal cord from the KIN mouse showed a consistent decrease of various ceramides with a significant elevation of sphingosine in the more severely affected spinal cord. Deficiency of C24/26-sphingomyelins contrasted with excess C18/20-sphingomyelin. Spinocerebellar expression profiling revealed consistent reductions of CERS protein isoforms, *Sptlc2* and *Smpd3*, but upregulation of *Cers2* mRNA, as prominent anomalies in the ceramide–sphingosine metabolism. Reduction of *Asah2* mRNA correlated to deficient S1P levels. In addition, downregulations for the elongase *Elovl1*, *Elovl4*, *Elovl5* mRNAs and ELOVL4 protein explain the deficit of very long-chain sphingomyelin. Reduced ASMase protein levels correlated to the accumulation of long-chain sphingomyelin. Overall, a deficit of myelin lipids was prominent in SCA2 nervous tissue at prefinal stage and not compensated by transcriptional adaptation of several metabolic enzymes. Myelination is controlled by mTORC1 signals; thus, our human and murine observations are in agreement with the known role of ATXN2 yeast, nematode, and mouse orthologs as mTORC1 inhibitors and autophagy promoters.

Keywords: olivo-ponto-cerebellar atrophy (OPCA); amyotrophic lateral sclerosis (ALS); leukodystrophy; ceramide synthase (CERS2/CERS1); serine palmitoyltransferase 2 (*Sptlc2*); neutral sphingomyelinase (*Smpd3*); neutral ceramidase (*Asah2*); fatty acid elongase (*Elovl1/4/5*); SCA34; SCA38; acid sphingomyelinase (ASMase; *Smpd1*)

1. Introduction

Spinocerebellar ataxia type 2 (SCA2) is an autosomal, dominantly inherited, multi-system neurodegenerative movement disorder [1–6] which was originally separated from other ataxias because of the early conspicuous slowing of eye tracking jumps [7–11]. It is caused by unstable expansion mutations of a $(CAG)_8$-CAA-$(CAG)_4$-CAA-$(CAG)_{8or9}$ repetitive structure that encodes a polyglutamine (polyQ) domain in ataxin-2 (gene symbol *ATXN2*) [12–15]. Expansions beyond 34 repeat units (34Q) cause the monogenic disorder SCA2 at old age with slow progression; larger expansions or higher expression dosage trigger earlier manifestation age, more widespread pathology, and stronger decrease in lifespan [12,16–20]. Shorter expansions of intermediate size between 27Q and 32Q increase the risk to be affected by motor neuron degeneration in amyotrophic lateral sclerosis (ALS) and fronto-temporal lobar dementia (FTLD) [21–23]. In addition, they elevate the risk of suffering from Parkinson's disease variants such as progressive supranuclear palsy (PSP) [24–26]. The formation of aggregates of the microtubule-associated protein tau (MAPT) is similar to the neurodegenerative disorders ALS, FTLD, and PSP [27].

While the rarity of SCA2 initially restricted interest, massive attention was aroused when research in flies and in yeast showed that the prevention of several neurodegenerative disorders can be achieved by genetic knockout (KO) or mRNA depletion of ataxin-2 orthologs [28–30]. Furthermore, genetic variants of ataxin-2 contribute to the lifespan of centenarians [31,32]. Recently, it was also confirmed in mice that injections of antisense-oligonucleotides against ataxin-2 into the cerebrospinal fluid (CSF) of SCA2 and ALS mouse models were able to prevent the neurodegenerative process, with an extension of lifespan up to >10 fold in some animals [33,34]. Thus, clinical trials on the benefits of ataxin-2 depletion in patients with SCA2 and ALS are imminent. Interestingly, both the subcellular localization and the transcriptional expression of ataxin-2 are modulated by nutrient deprivation and other stressors [35,36], providing additional therapeutic options to minimize the biosynthesis of expanded *ATXN2*.

What critical functions does ataxin-2 serve to have such a dramatic impact either in beneficial or deleterious manners? Its phylogenetically conserved protein domains include Lsm (Like Sm) and LsmAD (Lsm-associated domain) RNA-binding domains towards the *N*-terminus [15] and towards the C-terminus, a PAM2 motif (PABP-interacting motif 2) that associates with poly(A)-binding protein, a crucial regulator of mRNA stability [37]. Thus, *ATXN2* interacts with mRNAs both in a direct and indirect manner [38]. An alternatively spliced exon of the ataxin-2 mRNA encodes a proline-rich domain [39] which is responsible for the direct influence of *ATXN2* on the growth factor receptor (tyrosine kinase) endocytosis machinery, via direct interactions with the SH3 domain of several internalization factors [40,41]. The subcellular localization of *ATXN2* protein is cytosolic, mainly at the rough endoplasmic reticulum mRNA translation apparatus [42,43]. During stress periods, however, ataxin-2 relocalizes to cytosolic stress granules [44] where the quality control of mRNAs occurs and where triage decisions are made about mRNA degradation in P-bodies [45]. The minor presence of ataxin-2 at the plasma membrane and its functional impact are not yet well studied. The polyQ domain, which has a pathogenic role in human, is not conserved in mice [46].

The genetic deletion of ataxin-2 orthologs rescues the lethality of poly(A)-binding-protein-KO in yeast [47], triggers phenotypes of large cell size and fat accumulation in nematodes [48], produces female sterility in flies [49], and results in obesity, insulin resistance, hyperlipidemia, and infertility in mice [50]. Conversely, the knockin (KIN) of a large CAG100 expansion into the mouse *Atxn2* gene leads to progressive weight loss and brain atrophy, movement deficits, as well as reduced production

of the abundant brain metabolite *N*-acetyl-aspartate (NAA) in neuronal mitochondria that is trafficked to oligodendroglia to support axon myelination [51]. The first phenotype deficits become apparent around 10 weeks of age; the KIN lifespan is limited to 14 months [51]. The expansion impairs the transcription and translation of ataxin-2 and leads to a partial loss of function initially in most body cells; however, expanded *ATXN2* protein becomes insoluble and aggregated in postmitotic neurons under the influence of calcium-triggered excitation [51–54], driving the relentless atrophy of the nervous system.

The main sites of pathology that underlie characteristic SCA2 motor deficits are the cerebellar Purkinje cells and spinal cord motor neurons [55,56]. The earliest symptoms comprise uncoordinated gait, difficulties in balancing gait and posture, impaired speech (dysarthria), intention tremor, impaired motor learning, and the typical slowing of saccadic eye jumps [57,58]. Very early sensory neuropathy is complicated over time by motor neuropathy leading to areflexia as well as autonomic deficits [59–63]. Later, during disease progression, unbalanced postures of joints (dystonia), muscle cramps followed by tissue wasting (amyotrophy), and difficulties in swallowing (dysphagia) appear [64]. The final stages involve cardiac, gastrointestinal, and respiratory failure [65]. The first signs of the disease usually start in the 3rd to 4th decade of life and progressively increase in severity, across a disease course of usually 10–20 years [66]. In contrast to the main neurodegenerative diseases, the thalamus and hypothalamus are also affected in SCA2 with consequences for sleep and circadian rhythms [67–70]. Patients also suffer from peripheral tissue anomalies, such as atrophy of the peripheral fat stores, which starts at pre-symptomatic stages in cervico-cranial distribution and becomes massive and global at pre-terminal age [64]. Loss of CNS fat is a likely feature during the massive brain atrophy, and brain-imaging monitoring of SCA2 progression is focused not only on volumetry [71] but also on the gradually reduced levels of NAA metabolite as the most abundant building block of myelin [51,72].

Traditional notions about neurodegenerative disorders assumed that only specific neuron populations are affected. Over the past years, research on blood cells and skin fibroblasts confirmed that subclinical alterations are also detectable in other cell types [73–75]. The relevance of sphingolipid anomalies for many neurodegenerative processes was recently reviewed [76]. Particularly, the discovery of ELOVL4 mutations as the cause of deficits in very long-chain fatty acids that lead to spinocerebellar ataxia type 34 [77] called our attention to the fact that general membrane lipid homeostasis problems that will affect any cell population may show the earliest manifestations with a phenotype similar to SCA2. To elucidate pathology in more molecular detail, we used the rare opportunity of a SCA2 patient who volunteered for cerebellar autopsy to define the SCA2 brain lipid profile in humans. As validation and for a dissection of underlying expression changes, our recently generated *Atxn2*-CAG100-KIN mouse as the most authentic animal model of SCA2 was employed. Overall, this first effort to define the lipid pathology in SCA2 demonstrated novel anomalies of sphingolipids and identified the associated expression adaptations of lipid metabolism enzymes.

2. Results

2.1. SCA2 Cerebellum: Lipid Profile

The cerebellar tissue of a Central European SCA2 patient (female, age at death—26 years, *ATXN2* CAG-repeat genotype 52/22) who was characterized in various neuropathological studies [52,55,56,78–88] versus two age/sex-matched controls obtained from BrainNet-Europe (death at 21 years from primary lung fibrosis; death at 23 years from colitis ulcerosa) underwent lipid extraction, thin layer chromatography, and densitometric quantification of the stained bands. Two technical replicates of patient tissue were analyzed to control variation across the cerebellar diameter.

There was a strong reduction of those lipids that are typical for the myelin sheaths around axons, namely, a decrease of sulfatide to 17% and of galactosylceramide to 25%. Also, a substantial reduction of sphingomyelins containing a 22 or 24 carbon fatty acid chain to 44%, which are enriched together with galactosylceramide in myelin [89–91], contrasted with unchanged levels of sphingomyelins containing

an 18 carbon fatty acid chain (99%), which are prominent in the grey matter. Moreover, cholesterol, as the main lipid in myelin, was diminished to 40%, whereas free fatty acids were decreased only to 77%. Among gangliosides, which are enriched in neuronal membranes, reductions were observed for GM1a (63%) and GD1b (61%). GM1a also occurs in myelin sheets and is elevated in contrast to GD1b during the ageing process in mouse brain tissue [92]; thus, the GM1a reduction in the SCA2 patient cerebellum may be particularly noteworthy. GM1a is enriched in lipid rafts at paranodes and plays an important role for the localization of myelin-associated proteins [93,94] (Figure 1).

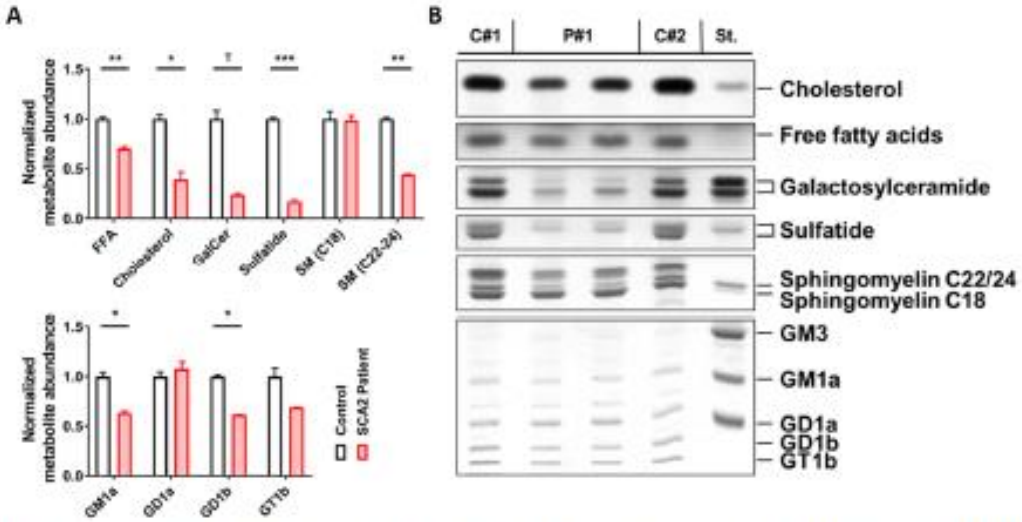

Figure 1. Cerebellar lipid profiles of one spinocerebellar ataxia type 2 (SCA2) patient. Technical duplicates (P#1 and P#2) were studied versus two age/sex-matched controls (C#1 and C#2) which were used to normalize all values. (**A**) Significant decreases in the abundance of free fatty acids, cholesterol, sulfatide, and very long-chain sphingomyelin (C22-24 SM) were observed in SCA2, and galactosylceramide (GalCer) appeared strongly reduced; for gangliosides, significant deficits in GM1a and GD1b were also observed. (**B**) Thin layer chromatography images of the lipid species analyzed in the adjacent bar graphs. Student's *t*-tests were used with Welch's correction; ^{T} $p < 0.1$, * $p < 0.05$, ** $p < 0.01$, *** $p < 0.001$.

All findings were compatible with the severe demyelination which was observed histologically in this SCA2 patient [55,82,83] and which is particularly prominent when *ATXN2* polyQ expansions are large [95]. In this context, it is important to note that the mutant disease protein ataxin-2 is not only expressed in neurons but also in oligodendrocytes and astrocytes as recently shown by RNAseq in different brain cell types (https://www.brainrnaseq.org/). It is also relevant to know that SCA2 has an identical pattern of neurodegeneration as multiple system atrophy (MSA) [56,96] where progressive aggregation of alpha-synuclein oligomers in oligodendrocytes acts as a causal trigger of pathogenesis and usually leads to either cerebellar or Parkinsonian manifestation [97] just like SCA2 [98]. Therefore, we considered the observed alterations as credible and asked further which lipid anomalies occurred at earlier ages and what enzymatic changes occurred in parallel. In view of the facts that (i) the postmortem interval before autopsy may distort protein and RNA expression profiles in the patient brain, (ii) a high number of samples are desirable, and (iii) prefinal disease stages would provide insights into maximal molecular dysregulation, we decided to explore the authentic mouse model of SCA2 at the end of its lifespan.

2.2. *Atxn2-CAG100-Knockin Mouse Tissues: Global Metabolome Profiles*

Cerebellar and spinal cord tissues from the SCA2 mouse model (six homozygous mutants at age 13–15 months just before death due to the fact of nervous system atrophy [51] versus six wildtype sex-matched littermates) were studied by quantitative label-free mass spectrometry in an unbiased metabolomics approach (see Supplementary Materials Table S1A,B for a list of compounds with individual data). The findings were quality controlled with Pearson correlations, principal component analyses, statistical analyses with adjustment for multiple testing, and volcano plots.

Consistently, the nervous tissue in cerebellum and in spinal cord showed lower amounts of free ceramide species. Specifically, in *Atxn2*-CAG100-KIN cerebellum (Figure 2) but also in the spinal cord (Figure S1), volcano plot analysis revealed all free ceramide species to have lower abundance regardless of chain length. In contrast, there was elevated abundance of sphingomyelins containing 12–22 carbon chain fatty acids (>30% increase) which were enriched in brain grey matter. Sphingomyelin species d18:1/22:1, d18:0/20:2, d18:0/22:3, and d18:1/20:0 showed a clearly significant upregulation in cerebellum upon volcano plot statistics, heat map analysis, and the visualization of variance. Interestingly, four sphingomyelin species containing 24–26 carbon fatty acid chains, which were enriched in brain white matter, showed consistent reduction to more than 30% in *Atxn2*-CAG100-KIN cerebellum (Figure 2A–C). These findings suggest that long-chain sphingomyelins accumulate in neurons, but the enzymatic elongation to the very long-chain sphingomyelin species required for myelination is impaired. Cerebellar levels of the angiogenesis and neurotrophin modulator sphingosine-1-phosphate (S1P) [99,100] were found significantly decreased to 44% upon Student's *t*-test analysis, while volcano plot statistics showed a similar decrease without significance (Figure 2C). In the more severely affected spinal cord, S1P levels were at 81% without significance, while sphingosine was found accumulated to >230% with high significance upon volcano plot statistics (Figure S1).

The reductions of ceramides and very long-chain sphingomyelin compounds in our SCA2 mouse model reflected the myelin deficits known from SCA2 patient cerebellum. It is known that deficiencies of C22–24 chain sphingolipids correlate with myelin deficits and contribute to the appearance of gliosis and encephalopathy [101]. As a completely novel and important insight, the mouse data revealed significant accumulations of sphingosines. This elevation is known to occur in cell culture upon serum deprivation [102] and might simply be due to the increased breakdown of glycosphingolipids in lysosomes as a byproduct of the neurodegenerative process [103]. Similar increases of sphingosine with parallel decreases of myelin markers were observed in the inflammatory demyelination process of multiple sclerosis patients; in this autoimmune process, it was shown that the conversion of ceramides to sphingosine can be toxic for oligodendrocytes [104]. Also, in patients with metabolic disorder, the accumulation of a specific sphingosine can trigger gliosis and leukodystrophy via TLR2-mediated activation of innate immunity [105]. Thus, the excess sphingosine observed in the SCA2 mouse spinal cord may be a simple byproduct of brain tissue destruction or alternatively contribute to enhanced demyelination. The degeneration of the long and strongly myelinated spinocerebellar and pyramidal tracts as well as the dorsal columns is an early and prominent feature of SCA2 patients [59–62,78,79,83,106]. It remained unclear whether this excess sphingosine is a pathological feature that is being compensated by homeostatic adaptations or if it is a purposeful result of cellular efforts. Therefore, we attempted to elucidate the underlying enzymatic changes by analyzing the crucial enzymes of ceramide–sphingomyelin metabolism depicted in Figure 3.

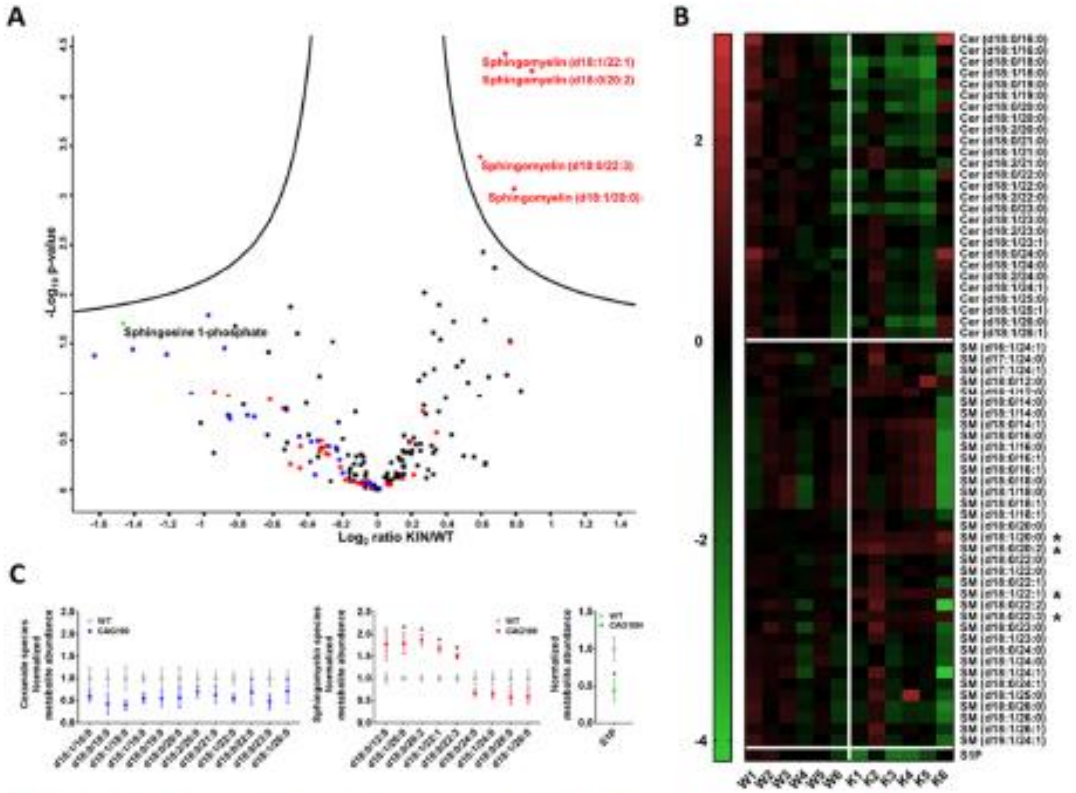

Figure 2. Targeted metabolome analysis of >12 month old *Atxn2*-CAG100-KIN cerebellum. (**A**) Volcano plot of differentially regulated metabolites ordered by log2 fold change on the *x*-axis versus significance (−log10 *p*-value) on the *y*-axis using a false discovery rate of 0.05 and an S0 of 0.1. Metabolites above the "volcano" lines were considered significantly regulated using the Perseus software (v1.6.6.0). Ceramides are depicted in blue, sphingomyelins in red, sphingosine 1-phosphate in green, and all others in black. (**B**) Heat map of all the ceramide and sphingomyelin species sorted by carbon chain length, which were measured in the targeted metabolome analysis, showing the metabolite abundances for individual mice. Image was generated with GraphPad Prism (v.7) software using normalized intensity values. Metabolites showing significant dysregulation in the volcano plot were marked with asterisks. A general consistent tendency to decreased levels in knockin (KIN) cerebellum was detected for all ceramide species as well as the very long-chain sphingomyelin species as visualized by green field color. (**C**) Normalized abundances of all ceramide and sphingomyelin species and sphingosine-1-phosphate that showed >30% up- or downregulations in the metabolome data. Graphs were generated with GraphPad Prism (v.7) software using normalized fold-change values. Unpaired Student's *t*-test showed significant increases for four sphingomyelin species with long-chain fatty acids (up to d18:0/22:3), consistent with the volcano plot. Sphingomyelins with very long-chains were found consistently decreased, and all ceramide species were found decreased irrespective of chain length. The decrease in sphingosine-1-phosphate abundance was also found significant upon unpaired student's t-test in contrast to volcano plot statistics.

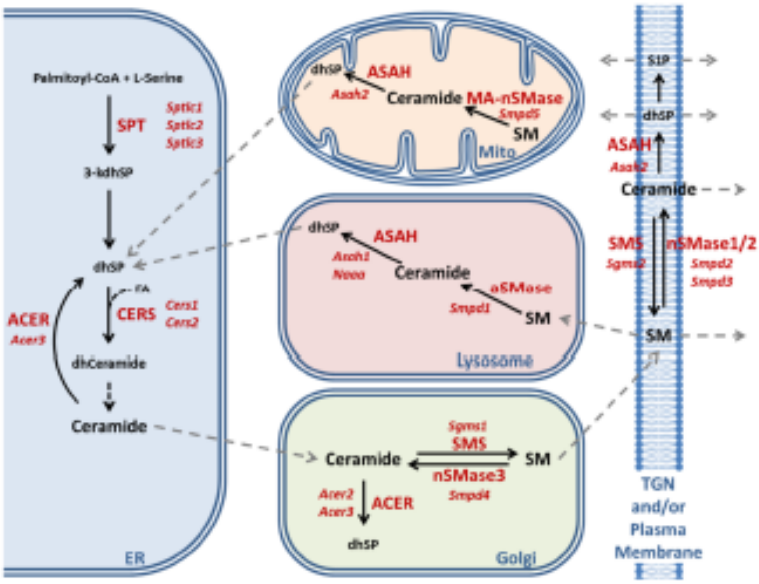

Figure 3. Schematic representation of ceramide–sphingomyelin metabolism modified after References [107,108]. The abbreviations together with information about differential cell type expression, subcellular localizations, and substrate preference for various enzyme isoforms are listed at the end of the article.

2.3. Enzymatic Production of Ceramide in Atxn2-CAG100-KIN Mouse Nervous System

The studies of *Atxn2*-CAG100-KIN mouse spinocerebellar tissues were performed in comparison to *Atxn2*-KO tissues to assess whether observed anomalies are due to the partial loss of function of the aggregating insoluble ataxin-2 protein or mediated by a gain-of-function effect that is specific to polyQ neurotoxicity. Mechanistic insights about the enzymatic regulations may also permit to distinguish between pathogenic events and compensatory efforts within the diverse brain cells. To assess the roles of diverse enzyme isoforms for different cell types and subcellular compartments, public database knowledge from the PubMed, GeneCards, BrainRNAseq, and Allen mouse brain in situ hybridization websites was integrated.

There are two main pathways of ceramide production: de novo biosynthesis and sphingomyelin breakdown. Degradation products of sphingomyelin and ceramide can also be recovered in the form of sphingosine and incorporated in de novo synthesis in a mechanism known as salvage pathway. All pathways are tightly controlled by different sets of enzymes or enzyme complexes in distinct subcellular compartments (Figure 3). *De novo* synthesis occurs exclusively in the ER, starting with the condensation of one palmitoyl-CoA with one L-serine molecule catalyzed by the ternary serine palmitoyltransferase (SPT) enzyme complex to produce 3-keto-sphinganine that is reduced to dihydrosphingosine (dhSP). The transcripts for *Sptlc1* and either *Sptlc2* or *Sptlc3* encode the catalytic core subunits of the SPT complex. Then, ceramide synthases (CERS) catalyze the addition of fatty acid subunits onto the sphingosine backbone, leading to the production of dihydroceramide which is slowly converted into ceramide. Expression analysis of de novo ceramide synthesis pathway components revealed a consistent minor downregulation of *Sptlc2* in both cerebellum and spinal cord (cerebellum: 95%, $p = 0.1962$; spinal cord: 83%, $p = 0.0044$) (Figure 4A). Interestingly, *Sptlc3* showed a bigger downregulation in spinal cord (58%, $p = 0.0342$), but its levels were increased in cerebellum without significance (186%, $p = 0.2262$). Mutations in the *SPTLC2* and *SPTLC1* genes were recently shown to trigger HSAN1 (hereditary sensory and autonomic neuropathy 1) due to the deficient sphingolipid synthesis and precursor metabolite accumulation [109,110]. The CERS enzyme isoforms showed consistent dysregulations in cerebellum and spinal cord with significant downregulations of the *Cers1* transcripts (cerebellum: 78%, $p = 0.0147$; spinal cord: 72%, $p = 0.0116$) and significant upregulations of *Cers2* transcripts (cerebellum: 126%,

$p = 0.0098$; spinal cord: 128%, $p = 0.0143$) (Figure 4A). It is interesting to note that *Cers2* is mainly expressed in myelinating oligodendrocytes and responsible for the production of very long-chain C26 ceramides [111]; thus, its dysfunction leads to myoclonic epilepsy due to the myelin instability from C24–26 deficiency [112]; in comparison, *Cers1* metabolizes C18 ceramides; its mutation also leads to myoclonic epilepsy [113], but *Cers1* is also critical for cerebellar Purkinje neurons [114]. Further investigation of these isoforms at the protein level with quantitative immunoblots in the cerebellar tissue of 14 month old *Atxn2*-CAG100-KIN mice revealed both CERS1 and CERS2 abundance to be diminished with significance (CERS1 77%, $p = 0.0021$; CERS2 72%, $p = 0.0002$) (Figure 4C). Therefore, both the white and grey matter of the central nervous system seems to have deficient ceramide synthesis due to the low levels of relevant proteins. While the CERS1 deficiency in neurons, astroglia, and oligodendrocyte precursors could be initiated by lower transcript levels of *Cers1*, the mature oligodendrocytes show an effort towards compensating the pathological CERS2 deficit and increasing very long-chain ceramide production as building blocks for myelin as evidenced by the upregulation of *Cers2* transcript. Neither the downregulation of *Sptlc2* nor the *Cers1*/*Cers2* mRNA dysregulations were observed in the *Atxn2*-KO tissue; thus, these polyQ-expansion triggered effects play a role only in the progressive pathogenesis of SCA2.

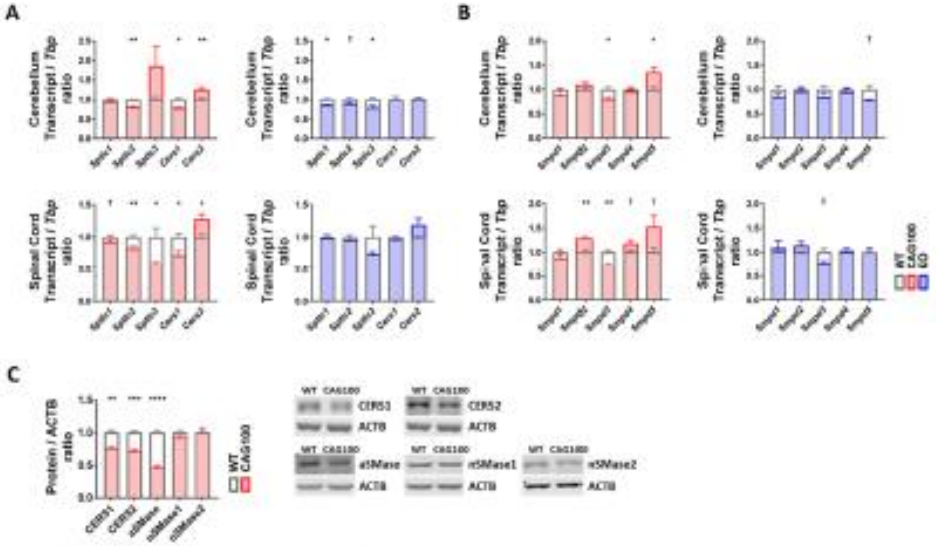

Figure 4. Transcript and protein levels of the enzymes involved in ceramide production were studied in the cerebellum and spinal cord of *Atxn2*-CAG100-KIN and *Atxn2*-KO mice. (**A**) Expression levels of the de novo ceramide synthesis pathway components. (**B**) Expression levels of different sphingomyelinase isoforms catalyzing the breakdown of sphingomyelin species into ceramide. (**C**) Protein levels of the de novo ceramide synthesis (CERS1, CERS2) and sphingomyelin breakdown (aSMase, nSMase1, nSMase2) pathway components in >12 month old *Atxn2*-CAG100-KIN cerebellum tissue. Student's *t*-test was used with Welch's correction; ^{T} $p < 0.1$, * $p < 0.05$, ** $p < 0.01$, *** $p < 0.001$, **** $p < 0.0001$.

The breakdown of sphingomyelin into ceramide is more complex: five different sphingomyelinase (SMase) isoforms are employed in different subcellular compartments. Because of their dependence on the physiological pH of the respective organelle, they are named acid or neutral sphingomyelinases (aSMase, nSMase). Analysis of all five isoforms encoded by *Smpd1–5* transcripts in *Atxn2*-CAG100-KIN cerebellum and spinal cord showed minor but consistent dysregulations in both tissues (Figure 4B). Of note, *Smpd1* mRNA coding for aSMase in lysosomes showed no dysregulation at the transcript level (cerebellum: 88%, $p = 0.3347$; spinal cord: 89%, $p = 0.2494$). The levels of *Smpd2* coding for nSMase1, which is responsible for stress-activated generation of ceramide [115] in the plasma membranes mainly of lymphocytes, were found significantly upregulated in spinal cord (129%, $p = 0.0033$). The *Smpd3* transcript coding for nSMase2, which generates stress-induced ceramide in the plasma

membrane and Golgi apparatus mainly of neurons [116], was found significantly downregulated in both tissues (cerebellum: 81%, $p = 0.0176$; spinal cord: 73%, $p = 0.0043$). Given that nSMase2 inactivation triggers neurotoxicity with TDP-43 aggregation via impaired exosome formation, and TDP-43 pathology is a characteristic hallmark of motor neuron degeneration in SCA2, this dysregulation appears to be a pathogenic event [28,33,117]. In addition, nSMase2 deficiency triggers tauopathy, and ataxin-2 deficiency has a specific rescue effect not only for TDP-43 neurotoxicity but also in general on tauopathies [29,118], so the chronic transcriptional downregulation of *Smpd3* might be a contributor to the SCA2-specific process of neurodegeneration. The transcript *Smpd4* coding for nSMase3 in the ER and the Golgi apparatus was found unchanged, while *Smpd5* coding for mitochondrial nSMase (MA-nSMase) was found upregulated in both tissues, reaching significance in cerebellum (cerebellum: 135%, $p = 0.0454$; spinal cord: 153%, $p = 0.0940$). This increase may be relevant for the generation of ceramides that trigger apoptosis via the mitochondrial pathway [108,119,120]. Further investigation of aSMase, nSMase1, and nSMase2 protein levels in cerebellum interestingly revealed a strong decrease in aSMase (47%, $p < 0.0001$) and no change for nSMase1 (93%, $p = 0.1997$) or nSMase2 (99%, $p = 0.9933$) levels, contrasting with the transcript data perhaps because of the limited sensitivity of Western blots for <2 fold changes or due to the inadequate antibody quality (Figure 4C). Mutations of aSMase trigger the neuronopathic NPA variant of Niemann–Pick disease [121]. The decrease in aSMase levels could act to maintain high sphingomyelin levels and might contribute to the low ceramide levels observed in the metabolome data. In *Atxn2*-KO tissues, none of the sphingomyelinase isoforms showed a significant change (Figure 4B), indicating that the dysregulations observed in KIN tissues are specific to the polyQ expansion driven ataxin-2 aggregation and may contribute to the progressive pathogenesis of SCA2.

2.4. Utilization of Ceramide in *Atxn2*-CAG100-KIN Mouse Tissues

Addressing the breakdown of ceramides to sphingosine by acid ceramidase in lysosomes (aCDase, encoded by *Asah1*), neutral ceramidase in the plasma membrane and mitochondria (nCDase, encoded by *Asah2*), acid ceramidase-like protein mainly in macrophages (encoded by *Naaa*), and alkaline ceramidases (encoded by *Acer2* for the Golgi apparatus and by *Acer3* for the ER/Golgi compartment), a significant change in consistency in both brain tissues was documented only for the *Asah2* reduction (cerebellum: 58%, $p = 0.0049$; spinal cord: 64%, $p = 0.0041$) (Figure 5A). These findings indicate that the elevated levels of sphingosine in the spinal cord accumulate without transcriptional adaptations of the relevant enzymes, e.g., an induction of the specific lysosomal enzyme.

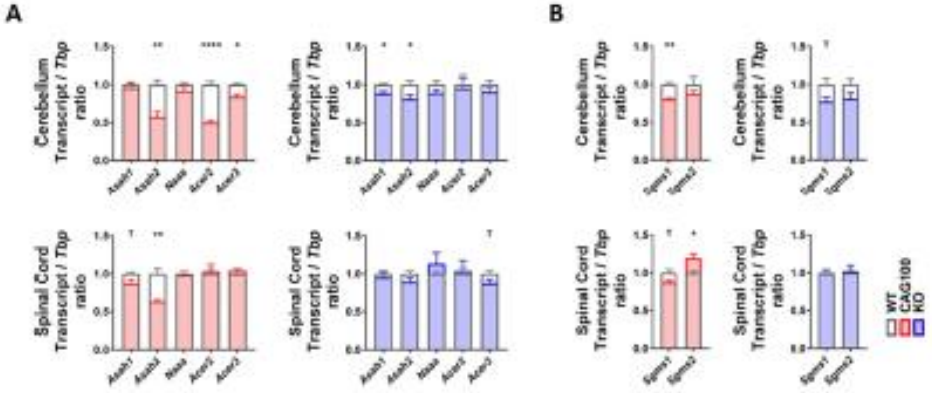

Figure 5. Transcript levels of the enzymes utilizing ceramide were studied in the cerebellum and spinal cord of *Atxn2*-CAG100-KIN and *Atxn2*-KO mice. (**A**) Expression levels of ceramidase isoforms involved in ceramide breakdown into sphingosine/sphinganine. (**B**) Expression levels of sphingomyelin synthase isoforms catalyzing the synthesis of sphingomyelin species utilizing ceramide. Student's *t*-test was used with Welch's correction; ^{T} $p < 0.1$, * $p < 0.05$, ** $p < 0.01$, **** $p < 0.0001$.

The observed *Asah2* mRNA reduction would serve to maintain ceramide and minimize the production of sphingosine [122], so it does not explain the sphingosine accumulation. A deficiency of nCDase protects from ER stress and from nutrient-deprivation-induced necroptosis via autophagy, while decreasing the formation of S1P at the plasma membrane [123–125]; thus, this enzyme downregulation is in good agreement with the low S1P levels observed in the KIN cerebellum and may play a compensatory role.

2.5. Production of Very Long-Chain Fatty Acids by Elongases in Atxn2-CAG100-KIN Nervous Tissues

To assess the elongation of long-chain to very long-chain sphingolipids that are needed, for example, for mature myelin, the expression profile of the relevant diverse long-chain fatty acyl elongase isoforms in the ER [126] was documented. With consistency for the cerebellum and spinal cord in the Atxn2-CAG100-KIN, there were significant reductions of mRNA levels for oligodendroglial *Elovl1* (cerebellum: 59%, $p = 0.0013$; spinal cord: 79%, $p = 0.0089$), neuronal *Elovl4* (cerebellum: 78%, $p = 0.0005$; spinal cord: 65%, $p = 0.0012$), astrocytic *Elovl5* (cerebellum: 61%, $p = 0.0022$; spinal cord: 72%, $p = 0.0231$), and the ubiquitous C12-16 PUFA-targeting *Elovl6* (cerebellum: 71%, $p = 0.0145$; spinal cord: 77%, $p = 0.0493$) (Figure 6A). For *Elovl2* and *Elovl7*, a significant downregulation was observed only in the cerebellum (*Elovl2*: 67%, $p = 0.0149$; *Elovl7*: 72%, $p = 0.0307$). Deactivating mutations in *Elovl1* trigger hypomyelination [127,128], while deficiency of *Elovl6* leads to general obesity in mice [129]. Neuronal ELOVL4 and astrocytic ELOVL5, where inactivating mutations are known to result in ataxia variants named SCA34 and SCA38 [77,130,131], were investigated further regarding protein abundance and exhibited significantly diminished levels for ELOVL4 (46%, $p = 0.0002$), while the antibody for ELOVL5 did not generate specific bands (Figure 6B). In contrast, in the *Atxn2*-KO tissue the dysregulations with nominal significance in Student's *t*-tests showed no consistency between the cerebellum and spinal cord. Thus, the consistent and strong elongase decreases in KIN tissue are specific effects of the polyQ-expansion-driven ataxin-2 aggregation and may contribute to the progressive pathogenesis of SCA2.

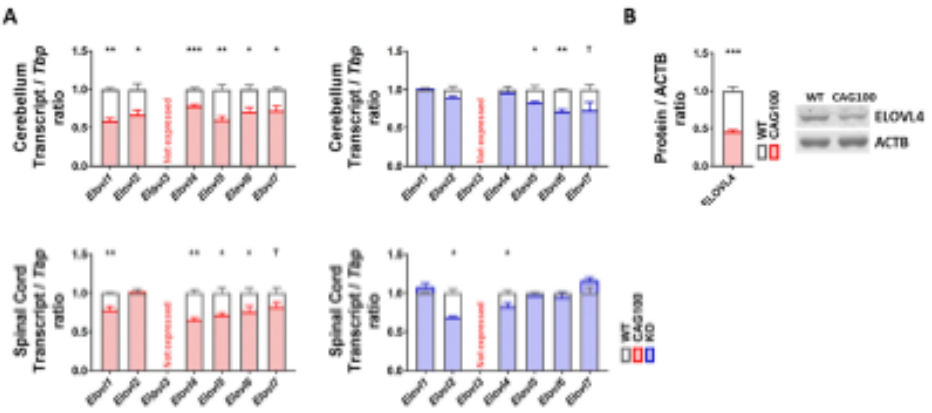

Figure 6. Strong and consistent downregulations were observed for elongase enzymes in the cerebellum and spinal cord of *Atxn2*-CAG100-KIN and *Atxn2*-KO mice which would affect synthesis of very long-chain fatty acids. (**A**) Transcript expression levels for different elongase isoforms. (**B**) Protein levels of ELOVL4 were documented in >12 month old *Atxn2*-CAG100-KIN cerebellum tissue. Student's *t*-tests were used with Welch's correction; $^{T}\ p < 0.1$, $^{*}\ p < 0.05$, $^{**}\ p < 0.01$, $^{***}\ p < 0.001$.

3. Discussion

The lipid profiling efforts in a SCA2 patient cerebellum and in spinocerebellar tissues from an authentic SCA2 mouse model showed deficits for very long-chain C24 sphingomyelin as the main consistent finding in both organisms. A reduction of very long-chain sphingomyelin was also observed in the CSF and blood of ALS patients, and this deficit correlated with lowest survival [132,133].

Sphingomyelin of C24 length interacts with cholesterol in lipid bilayers as important stabilizing elements for the plasma membrane, particularly in myelinating glia cells [134,135]. Although our study is limited to the analysis of one patient cerebellum and six mutant versus six WT mice, the results gain credibility in light of our previous report on sphingolipid anomalies also in the *Atxn2*-KO brain [50] and in view of our findings submitted in parallel on the suppression of cholesterol biosynthesis in the nervous tissue of our new *Atxn2*-CAG100-KIN mouse [136]. Contrary to the scenario in SCA2, C24 sphingomyelin accumulates with cholesterol in adrenoleukodystrophy [137] throughout the white matter, also leading to a demyelinating process. The enzyme ELOVL1 is the major fatty acid elongase in the endoplasmic reticulum that is responsible for the production of C24 sphingolipids [126], and, indeed, *Elovl1* mRNA shows a strong almost two-fold reduction in the KIN cerebellum. This deficit of very long-chain sphingomyelin species was accompanied by multiple other anomalies including early steps of fatty acid biosynthesis (like the CERS1 deficit) in diverse subcellular compartments and various brain cell types, indicating a general rather than highly specific disturbance of lipid metabolism. The excess C18-SM observed in old KIN cerebellum is known to have a specific regulatory impact on the retrograde vesicle flow in Golgi cisterns [138]. The excess sphingosine observed in old KIN spinal cord was previously implicated in demyelination, while it also has potent inhibitory effects on PKC-phosphorylation, an established risk factor for ataxia and ALS [104,139–142]. Overall, the findings extend our previous report that already the synthesis of the metabolite NAA from acetyl-CoA and aspartate by neuronal mitochondria, which is delivered to oligodendrocytes and crucial for myelin production, is impaired in the *Atxn2*-CAG100-KIN mouse as well as in SCA2 patients [51].

It is interesting to ask by what mechanisms the converse depletion of ataxin-2 can be neuroprotective both in SCA2 mouse models and in mouse models of motor neuron degeneration with an ALS phenotype by TDP-43 neurotoxicity [28,33,34]. Cerebellar cholesterol in the *Atxn2*-KO mouse was found unchanged, although blood cholesterol was elevated. Overall sphingomyelin species were diminished with elevations of ceramide species, sulfatide, and GM1/GD1 gangliosides in contrast to the SCA2 profile. Altogether, the *Atxn2*-KO mice showed obesity and hepatosteatosis [50] in contrast to the progressive loss of weight and fat stores in the *Atxn2*-CAG100-KIN mice [51]. Despite the overall contrast in fat availability, the significant and consistent enzymatic regulations documented above were specific for the KIN mice and were not mirrored in KO tissue.

Considering in detail whether specific enzymatic changes are rather compensatory efforts or probably pathogenic and whether they represent SCA2-typical pathology, a complex picture emerges with alternative interpretation possibilities. The prominent downregulation of most fatty acid elongases at the endoplasmic reticulum in both cerebellar and spinal tissue, particularly of *Elovl1*/*Elovl4*/*Elovl5*, seems clearly deleterious for all brain cell types, and this general effect seems quite specific for SCA2. In the case of *Asah2* deficiency, its protective role against ER stress and nutrient-deprivation-induced necroptosis via autophagy was already mentioned, and a similar downregulation was also observed for Alzheimer's disease [143]. Regarding ceramide synthases, the reduction of CERS2 protein may be connected to the S1P decrease, since CERS2 activity is regulated by this lipid signaling pathway via two sphingosine-1-phosphate receptor-like residues on CERS2 that operate independently [144,145]. The CERS2 inactivity appears pathogenic in view of the cellular effort to upregulate *Cers2* transcripts; it would reduce the levels of very long-chain ceramides in mature oligodendroglia. But, in Figure 2, the C26 ceramides are relatively normal, so this anomaly might be well compensated. Decreased CERS2 protein levels were also reported for the hypomyelination pathology in Niemann–Pick type C disease [146], and, interestingly, they were observed to precede tau pathology at a preclinical stage of Alzheimer's disease [111]. The reduction of CERS1 protein in the *Atxn2*-CAG100-KIN mouse was accompanied by a decrease of *Cers1* mRNA and correlated with the mild deficiency of many ceramide species. Inactivity of CERS1 protein leads to preferential degeneration of cerebellar Purkinje neurons, and *Cers1* mRNA downregulation was reported in tauopathies [147], so a pathogenic role of CERS1 deficiency in SCA2 is likely. Similarly, a deficiency of *Smpd3* encoding nSMase2, as detected in the KIN nervous tissue, was reported to cause TDP-43 neurotoxicity and tauopathy, while ataxin-2 depletion

protects against TDP-43 aggregation and tauopathies. Thus, this dysregulation appears to be another pathogenic event with SCA2-typical features. It appears most promising as a molecular biomarker for neuroprotective treatments in SCA2 and ALS [28,29,33,117,118]. In comparison, the subtle deficiency of *Sptlc2* mRNA in the KIN mouse is associated with the peripheral neuropathy in HSAN1, and the marked deficit of aSMase protein in the KIN mouse is associated with the neuronopathic NPC disorder, so both events in SCA2 may contribute to pathogenesis, but they mediate two relatively unspecific clinical aspects.

It is very difficult to judge the deleterious or protective impact of the decreased aSMase abundance, also because it is an unspecific phospholipase C that cleaves a multitude of phospholipids. Of course it might have an unbalancing toxic effect on cholesterol dynamics and, subsequently, on glycolipid turnover [148], but it might also reflect a compensatory event to limit the breakdown of important sphingomyelin to toxic ceramide species that contributes to neurodegeneration in Wilson's disease [149] as an unspecific maintenance effort for membranes. Acid sphingomyelinase deficiency was found protective also for high-fat-diet triggered ER stress and limits autophagic flux but it increases p62 and may enhance protein aggregation processes [150]. Importantly, aSMase activity is regulated by many additional mechanisms beyond its expression and abundance. Indeed, it is possible that the reduced abundance of aSMase protein represents only a homeostatic response to maintain normal function, since a deficit of cholesterol and sphingomyelin species can increase aSMase activity [151]. The activity of aSMase is regulated more than 10 fold by interaction with sphingolipid activator proteins (SAPs) in intralysosomal luminal vesicles (ILVs) which is modulated by the concentration of membrane lipids and their degradation compounds such as various sphingoid bases as well as drugs [152–154].

Which of these molecular dysregulations might represent a primary event under direct influence of ATXN2 polyQ expansion which other dysregulations might constitute secondary consequences? All ELOVL isoforms act in the endoplasmic reticulum where most of the *ATXN2* protein has its physiological localization and plays an important role for ER dynamics [43,155]. Similarly, CERS1 and CERS2 have an ER/Golgi distribution as well as the protein encoded by *Sptlc2*. In contrast, *Asah2* and *Smpd3* encode factors that are associated with the plasma membrane where *ATXN2* interacts with the receptor tyrosine kinase endocytosis machinery [40,41,156]. While all these events occur at sites of *ATXN2* presence, the deficit of aSMase in lysosomes is most likely secondary. With respect to the brain cell types that are affected by each factor, the dysregulations of *Elovl1* expression and CERS2 abundance are crucial for myelinating cells; *Elovl6*, CERS1, *Asah2*, and *Sptlc2* are quite ubiquitous; *Elovl4* and *Smpd3* are mainly neuronal; *Elovl5* is mainly astrocytic. Thus, most pathological enzyme adaptations and lipid anomalies coincide in mature oligodendrocytes, while the affection of neuronal molecules is more limited. Given that ataxin-2 expression occurs not only in neurons but also in glia cells during stress periods like nutrient deprivation, the demyelination is not necessarily a downstream indirect consequence of axonal degeneration but may represent a cell-autonomous early pathology.

It is known that lipid synthesis and myelin formation is under the control of mTORC1 signaling [157–159]. It is particularly noteworthy here that *Elovl1* expression is downregulated upon inhibition of mTORC1, and the medium-chain fatty acid availability acts via mTORC1 signaling to trigger *Elovl5* and *Elovl6* expression [160–163]. Given that ataxin-2 orthologs in yeast, nematodes, and mice were shown to play a conserved role as inhibitors of mTORC1 signaling and growth [36,48,164–166], the broad repression of *Elovl1/4/5/6* in cerebellum and spinal cord as well as the repression of *Elovl2/7* in cerebellum may be a very sensitive and specific reflection of this ancient control of *ATXN2* over lipid metabolism. In view of reports that the sphingosine-kinase-1 dependent generation of S1P during nutrient starvation inhibits mTORC1 signals and induces autophagy to protect cells from apoptotic cell death [167], the S1P deficit in the KIN cerebellum might be seen to counteract the excessive mTORC1 repression by *ATXN2* aggregates in a compensatory effort. Acting in the same pathway, the deficiency of *Smpd3* encoding nSMase2 acts via reduced microdomain ceramide to promote hyaluronan synthesis and secretion, enhancing mTOR phosphorylation [168]. Thus, both events at the plasma membrane might play a protective role. It is still controversial by what direct or indirect mechanism ataxin-2

restricts mTORC1 phosphorylation and growth. Firstly, an influence on lysosomal-associated RHEB; secondly, a sequestration of mTORC1 complex subunits in stress granules; thirdly, indirect effects via lipid internalization and via mitochondrial lipid-breakdown under control of ataxin-2 may all contribute to this regulation of cell size and lipid stores [48,75,169–173]. However, *ATXN2* can directly associate with RNAs to modulate their quality control and degradation, so it is also conceivable that the reduced levels of most *Elovl1-7* mRNAs, the *Smpd3*, *Sptlc2*, and *Asah2* mRNA are due to their selective direct sequestration into insoluble *ATXN2* aggregates, stress granules or P-bodies.

As a clinical anecdote, we observed a SCA2 patient with long polyQ expansion to have an unusually long survival with the habit of eating a quarter or a half pound of butter per day. It is conceivable that this diet rescued some of the deficits in cholesterol and very long-chain fatty acids, firstly via an increased supply of precursor metabolites and secondly via enhanced expression of mTORC1-dependent enzymes. Thus, our novel knowledge about metabolic deficiencies in SCA2 may pave the way to identify specific nutrient supplements that alleviate disease progression.

It is important to emphasize that elevated sphingosine and low S1P are also known to modulate inflammation and apoptosis. High sphingosine levels have long been known to accompany the inflammatory myelin destruction in multiple sclerosis patients [174]. Increased angiogenesis, vascular permeability, and inflammation can be among the consequences of deficient extracellular S1P [175,176]. Such neuroinflammatory mechanisms were recently shown to be crucial for the progression of neurodegenerative processes as in Parkinson's disease to the stage of cell death [177,178]. The increase of pro-apoptotic sphingosine effects and the decrease of anti-apoptotic S1P effects [179–181] in our SCA2 mouse model may both contribute to pathogenesis. The corresponding downregulations of CERS1/CERS2 protein and of *Asah2* mRNA levels would then also be interpreted as drivers of pathology. Thus, it is fortunate that a synthetic sphingosine analog with pro-survival activity is available with FDA approval under the name FTY720 (fingolimod) which was observed to restrict the inflammatory demyelination of axons [182,183] and might modify the disease progression also in SCA2.

4. Materials and Methods

4.1. Lipid Extraction from Human Post-Mortem Tissue and Thin Layer Chromatography

For the quantification of diverse lipids, cerebellar tissue from one German SCA2 patient in technical duplicates (female, age at onset 6 years, age at death 26 years, *ATXN2* CAG expansion size 52, clinical description and neuropathology already reported [78]) and two sex/age-matched control individuals (BrainNet-Europe in Munich, a female who died at age 21 due to the presence of primary pulmonary fibrosis and a female who died at age 23 due to the presence of colitis ulcerosa). The analysis of human brain autopsies was reviewed by the ethics committee of the Goethe University Medical Faculty with approval code 258/18 (27 November 2018). Samples of 500 mg wet weight were dissected and processed by a previously published protocol [50]. In brief, sample homogenization was done after addition of chloroform, methanol, and water. The lipid extraction occurred over 24 h at 37 °C. After separation of insoluble tissue rests by filtration, the samples were divided and processed separately as described subsequently. Given that phospholipids would migrate together with gangliosides during thin layer chromatography (TLC), they were exposed to mild alkaline hydrolysis and the saponified extracts were desalted by reversed phase 18 chromatography. The other half of the samples remained untreated for the analysis of free fatty acids, since fatty acids that are released from phospholipids during alkaline hydrolysis would distort the content of endogenous fatty acids. All samples were then processed by anion exchange chromatography with diethyl-aminoethyl (DEAE)-sepharose to separate anionic (free fatty acids, sulfatide, gangliosides) versus neutral lipids (cholesterol, galactosylceramide, sphingomyelin, phosphatidylethanolamine, phosphatidylcholine). After another desalting of samples, the lipids were separated by TLC in different solvent systems. After staining of TLC plates in a phosphoric acid/cupric sulfate reagent, the quantification of lipids was performed by densitometry of the visualized bands.

4.2. Animals and Genotyping

All animals were housed at the Central Animal Facility (ZFE) of the Goethe University Medical School in Frankfurt am Main, Germany, placed in individually ventilated cages at a 12 h light/12 h dark cycle, monitored for health routinely with sentinels, and fed ad libitum. Upon manifestation of movement deficits, mutant animals were separated from competing WT controls and provided with a gel diet on the cage floor. All procedures were performed in accordance with the German Animal Welfare Act, the Council Directive of 24 November 1986 (86/609/EWG) with Annex II and the ETS123 (European Convention for the Protection of Vertebrate Animals). The animal experiments were revised by the Regierungspräsidium Darmstadt with approval code V54-19c20/15-FK/1083). Housing and genotyping of both *Atxn2*-CAG100-Knockin (KIN) and *Atxn2*-Knockout (KO) mice were done as previously reported [50,51].

4.3. Targeted Metabolome Analysis with Mass Spectrometry

Approximately 25–40 mg frozen tissue of six *Atxn2*-CAG100-KIN cerebella and six healthy WT cerebella from male mice at ages between 13 and 15 months were used for metabolite profiling. Metabolite extraction and tandem LC-MS measurements were done as previously reported by us [184]. In brief, methyl-tert-butyl ester (MTBE), methanol, ammonium acetate, and water were used for metabolite extraction. The subsequent separation was performed on an LC instrument (1290 series UHPLC; Agilent, Santa Clara, CA, USA) online coupled to a triple quadrupole hybrid ion trap mass spectrometer, QTrap 6500 (Sciex, Foster City, CA, USA), as reported previously [185]. Normalization was done according to used amounts of tissues and subsequently by internal standards, namely, by sphingomyelin (d18:1/12:0) and C12 ceramide (d18:1/12:0) for the lipids (Avanti Polar Lipids, Alabaster, AL, USA), while isotope labeled amino acids were used for other metabolites according to Reference [185]. Analyses were not focused on cholesterol biosynthesis and the steroidogenic pathway metabolites for technical reasons, and these quantifications will be the subject of a separate manuscript. The mass spectrometry data were deposited to the PeptideAtlas repository. At https://db.systemsbiology.net/sbeams/cgi/PeptideAtlas/PASS_View?identifier=PASS01475, all original LC-MS generated QTrap wiff-files as well as MuliQuant-processed peak integration q.session files can be downloaded.

The metabolite identification was based on three levels: (i) the correct retention time, (ii) up to three MRMs, (iii) and a matching MRM ion ratio of tuned pure metabolites as a reference [185]. Relative quantification was performed using MultiQuant software v.2.1.1 (Sciex, Foster City, CA, USA). The integration settings were a peak splitting factor of two and a Gaussian smoothing of two. All peaks were reviewed manually. Only the average peak area of the first transition was used for calculations. Normalization was conducted according to thte used amounts of tissues and subsequently by internal standards.

4.4. Mouse RNA Isolation and Expression Analyses

Following cervical dislocation, whole brain was isolated and cerebellum and spinal cord samples were isolated into separate tubes and immediately frozen in liquid nitrogen. The number of mice analyzed for each tissue is as follows: cerebellum 5 WT versus 3 KIN, 4 WT versus 4 KO; spinal cord 5 WT versus 5 KIN, 4 WT versus 4 KO. The RNA extraction from all sample types was performed with TRIzol Reagent (Sigma–Aldrich, St. Louis, MO, USA) according to the user's manual. One miligram of total RNA was used as a template for cDNA synthesis utilizing SuperScript IV VILO kit (Thermo Scientific, Schwerte, Germany) according to the manufacturer's instructions. Gene expression levels were determined via quantitative real-time PCR using StepOnePlus Real-Time PCR System (Applied Biosystems, Thermo Scientific, Schwerte, Germany). The cDNA from 25 ng total RNA was used for each PCR reaction with 1 µL TaqMan® Assay, 10 µL FastStart Universal Probe Master 2× (Rox) Mix (Roche, Basel, Switzerland), and ddH_2O up to 20 µL of total volume. The TaqMan® Assays utilized for

this study were: *Acer2* (Mm00519876_m1), *Acer3* (Mm00502940_m1), *Asah1* (Mm00480021_m1), *Asah2* (Mm00479659_m1), *Cers1* (Mm03024093_mH), *Cers2* (Mm00504086_m1), *Elovl1* (Mm01188316_g1), *Elovl2* (Mm00517086_ m1), *Elovl3* (Mm00468164_m1), *Elovl4* (Mm00521704_m1), *Elovl5* (Mm00506717_ m1), *Elovl6* (Mm00851223_s1), *Elovl7* (Mm00512434_m1), *Naaa* (Mm01341699_m1), *Sgms1* (Mm00522643_ m1), *Sgms2* (Mm00512327_m1), *Smpd1* (Mm00488318_m1), *Smpd2* (Mm00486247_m1), *Smpd3* (Mm00491359_ m1), *Smpd4* (Mm00547173_m1), *Smpd5* (Mm01205829_g1), *Sptlc1* (Mm00447343_m1), *Sptlc2* (Mm00448871_m1), *Sptlc3* (Mm01278138_m1), and *Tbp* (Mm00446973_m1). The PCR conditions were 50 °C for 2 min and 95 °C for 10 min, followed by 40 cycles of 95 °C for 15 s and 60 °C for 1 min. Gene expression data were analyzed using a 2−ΔΔCt method [186] with *Tbp* as the housekeeping gene.

4.5. Protein Extraction and Quantitative Immunoblots

Frozen cerebellar tissue from 5 WT versus 5 KIN animals were homogenized in 5–10× *w/v* amount of RIPA buffer (50 mM Tris-HCl (pH 8.0), 150 mM NaCl, 2 mM EDTA, 1% Igepal CA-630 (Sigma–Aldrich, St. Louis, MO, USA), 0.5% sodium deoxycholate, 0.1% SDS and Complete Protease Inhibitor Cocktail (Roche, Basel, Switzerland)) with a motor pestle. Twenty miligrams of total protein was mixed with 2× loading buffer (250 mM Tris-HCl pH 7.4, 20% glycerol, 4% SDS, 10% 2-mercaptoethanol, 0.005% bromophenol blue) and incubated at 90 °C for 2 min. Loading samples were separated on polyacrylamide gels and were transferred to Nitrocellulose membranes (Protran, GE Healthcare, Chicago, IL, USA). The membranes were blocked in 5% BSA/TBS-T and incubated overnight at 4 °C with primary antibodies. Primary antibodies utilized in this study were: ACTB (Sigma–Aldrich, St. Louis, MO, USA, #A5441, 1:10,000), aSMase (ASM) (Santa Cruz Biotechnology, Dallas, TX, USA, sc-9817), CERS1 (MyBioSource, San Diego, CA, USA, MBS2523738), CERS2 (Bethyl Laboratories, Montgomery, TX, USA, A303-193A), ELOVL4 (Proteintech, Rosemont, IL, USA, 55023-1-AP), nSMase1 (Abcam, Cambridge, UK, ab131330), and nSMase2 (Abcam, Cambridge, UK, ab199399). Fluorescent-labeled secondary goat anti-mouse (IRDye 800CW, Licor Biosciences, Lincoln, NE, USA) and goat anti-rabbit (IRDye 680RD, Licor Biosciences, Lincoln, NE, USA) antibodies were incubated for 1 h at room temperature. Membranes were visualized using Li-Cor Odyssey Classic instrument, and image analysis was performed using ImageStudio software (LI-COR, Lincoln, NE, USA).

4.6. Statistical Analyses

All statistical tests for expression analyses were performed using unpaired Student's *t*-tests with Welch's correction on GraphPad Prism software version 7 after establishing that each population was normally distributed (one-sided Kolmogorov–Smirnov test). Graphs display mean values with standard error of the mean (SEM). Values $p < 0.05$ were considered significant and marked with asterisks: $p < 0.05$ *, $p < 0.01$ **, $p < 0.001$ ***, $p < 0.0001$ ****.

5. Conclusions

Overall, the traditional concept of SCA2, as a primary neurodegenerative disorder with axonal atrophy followed by a secondary demyelination, may have to be revised in favor of a multi-system nervous atrophy that affects large neurons in the cerebellum and spinal cord preferentially but extends its pathology to all neurons, oligodendrocytes, and other glia cells eventually due to the broad disturbance of lipid homeostasis. The pronounced myelin instability may be explained via the influence of *ATXN2* expression in mature oligodendrocytes on mTORC1 suppression and autophagy. Clearly, the lipid profile of SCA2 brain tissue shows consistent and strong deficits of very long-chain sphingomyelins and the relevant ELOVL enzymes that are crucial for myelin versus comparatively mild neuronal anomalies.

Supplementary Materials: Supplementary materials can be found at http://www.mdpi.com/1422-0067/20/23/5854/s1.

Author Contributions: Conceptualization, K.S. and G.A.; methodology, N.-E.S., D.M., S.B. and S.G.; software, D.M.; validation, N.-E.S., A.A., C.O., J.C.-P., Z.-E.K. and S.G.; formal analysis, S.B.; investigation, N.-E.S., A.A., D.M., S.B., C.O., J.C.-P., Z.-E.K., M.-V.H., S.G.; resources, M.-V.H.; data curation, D.M.; writing—original draft preparation, N.-E.S., S.B. and G.A.; writing—review and editing, N.-E.S., D.M., K.S., G.A.; visualization, N.-E.S., D.M. and S.B.; supervision, D.M., S.G., K.S. and G.A.; project administration, G.A.; funding acquisition, K.S. and G.A.

Funding: This research was funded by the Deutsche Forschungsgemeinschaft, grant numbers AU96/11-1 and AU96/11-3. In addition, it was supported by the Max Planck Society.

Acknowledgments: We are grateful for the technical assistance of Gabriele Köpf in Frankfurt and of Beata Lukaszewsa-McGreal in Berlin.

Conflicts of Interest: The authors declare no conflict of interest. The funders had no role in the design of the study; in the collection, analyses, or interpretation of data; in the writing of the manuscript, or in the decision to publish the results.

Abbreviations

°C	degree Celsius
ΔΔCt	Delta-Delta-Count-Threshold
3-kdhSP	3-Keto-dihydro-sphingosine
aCDase	acid Ceramidase, encoded by *Asah1*
ACER	alkaline Ceramidase
Acer2	alkaline Ceramidase 2 (Golgi Ceramidase)
Acer3	alkaline Ceramidase 3 (ER and Golgi Ceramidase)
ACTB	Actin-B
ALS	Amyotrophic Lateral Sclerosis, spinal motor neuron atrophy at adult age, tauopathy
ASAH	*N*-Acylsphingosine Amidohydrolase (acid or neutral Ceramidase)
Asah1	*N*-Acylsphingosine Amidohydrolase 1 (lysosomal acid Ceramidase)
Asah2	*N*-Acylsphingosine Amidohydrolase 2 (plasma membrane/mitoch. neutral Ceramidase)
ASMase	acid Sphingomyelinase
ATXN2	Ataxin-2
BSA	Bovine serum albumin
C22 chain	Chain with a length comprising 22 carbons
CAG	Cytosine-adenine-guanine
cDNA	Complementary deoxyribo-nucleic acid
Cer	Ceramide
Cers1	Ceramide Synthase 1 (primary in brain, C18 ceramide, ER of neurons, astrocytes and OPC)
Cers2	Ceramide Synthase 2 (very long-chain ceramides, mainly in ER of mature oligodendroglia)
CoA	Coenzyme-A
CSF	Cerebrospinal fluid
d18:0	Di-hydroxy sphingoid base, 18 carbon chain length, 0 double bonds
DEAE	Diethyl-aminoethyl
dhSP	Dihydro-sphingosine
EDTA	Ethylene-Diamine-Tetra-Acetic acid
Elovl1	Elongation of very long-chain fatty acids protein 1 (oligodendrocyte, C22–26 SFA)
Elovl2	Elongation of very long-chain fatty acids protein 2 (astrocyte, C20–22 PUFA)
Elovl3	Elongation of very long-chain fatty acids protein 3 (eye, cholesterol/odd-chain elongase)
Elovl4	Elongation of very long-chain fatty acids protein 4 (neurons, C24–26 SFA)
Elovl5	Elongation of very long-chain fatty acids protein 5 (astrocyte, C18 PUFA)
Elovl6	Elongation of very long-chain fatty acids protein 6 (ubiquitous, C12–16 PUFA)
Elovl7	Elongation of very long-chain fatty acids protein 7 (oligodendrocyte, C16–20 SFA+PUFA)
ER	Endoplasmic reticulum
FA	Fatty acid
FDA	Federal Drug Administration
FTLD	Fronto-temporal lobar degeneration/dementia, cortical motor neuron atrophy, tauopathy
GalCer	Galactosyl-ceramide
GD1b	Ganglioside 1b with Di-NANA binding

GM1a	Ganglioside 1a with Mono-NANA binding
GT1b	Ganglioside 1b with Tri-NANA binding
h	Hour
HCl	Hydrochloric acid
HSAN1	Hereditary sensory and autonomic neuropathy type 1
ILVs	Intralysosomal luminal vesicles
K1	KIN sample 1
KIN	Knockin (of CAG100 mutation into *Atxn2* gene, in this case)
KO	Knockout (of *Atxn2* gene, in this case)
LC-MS	Liquid chromatography mass spectrometry
MA-nSMase	Mitochondria-associated neutral sphingomyelinase
MAPT	Microtubule-associated protein tau
µL	Microliter
µg	Microgram
mg	Milli-gram
min	Minute
Mito	Mitochondria
mRNA	Messenger RNA
MSA	Multi-system atrophy
MTBE	Methyl-tert-butyl ester
mTORC1	Mechanistic target of rapamycin complex 1, a kinase responsible for cell growth signals
Naaa	*N*-Acylethanolamine acid amidase (acid ceramidase-like protein, mainly in macrophages)
NaCl	Sodiumchloride
NANA	*N*-acetyl-neuraminic acid
nCDase	Neutral Ceramidase, encoded by *Asah2*
ng	Nanogram
NPA	Niemann–Pick type A, caused by mutations in the aSMase *Smpd1*, neurovisceral picture
NPB	Niemann–Pick type B, caused by mutations in the aSMase *Smpd1*, visceral picture
NPC	Niemann–Pick type C, caused by *Npc1*/*Npc2* mutations, neuronopathic picture
NSMase	Neutral Sphingomyelinase
nSMase1	Neutral Sphingomyelinase 1 (encoded by *Smpd2*)
OPC	Ooligodendrocyte precursor cell
OPCA	Olivo-ponto-cerebellar atrophy
PCR	Polymerase chain reaction
PKC	Protein kinase C
polyQ	polyGlutamine
PSP	Progressive supranuclear palsy (Parkinson plus), dopaminergic neuron atrophy, tauopathy
PUFA	Poly-unsaturated fatty acid
RHEB	Ras homolog enriched in brain, mTORC1-binding protein
RIPA	Radio-immuno precipitation assay
RNA	Ribonucleic acid
s	Second
S1P	Sphingosine-1-phosphate
SAPs	sphingolipid activator proteins
SCA2	Spino-cerebellar ataxia type 2, caused by polyQ expansions in ataxin-2
SCA34	Spino-cerebellar ataxia type 34, caused by inactivity of ELOVL4
SCA38	Spino-cerebellar ataxia type 38, caused by inactivity of ELOVL5
SDS	Sodium-dodecyl-sulfate
s.e.m.	Standard error of the mean
SFA	Saturated fatty acid
Sgms1	Sphingomyelin synthase 1 (Golgi location)
Sgms2	Sphingomyelin synthase 2 (plasma membrane location)
Smpd1	Sphingomyelin phosphodiesterase 1 (acid lysosomal SMase)
Smpd2	Sphingomyelin phosphodiesterase 2 (neutral plasma membrane SMase, immune cells)
Smpd3	Sphingomyelin phosphodiesterase 3 (neutral Golgi+ plasma membrane SMase, brain stress)
Smpd4	Sphingomyelin phosphodiesterase 4 (neutral ER/Golgi membrane SMase)

Smpd5	Sphingomyelin phosphodiesterase 5 (ER and mitochondria-associated neutral SMase)
SM	Sphingomyelin
SMase	Sphingomyelinase
SMS	Sphingomyelin synthase
SPT	Serine palmitoyltransferase
Sptlc1	Serine palmitoyltransferase long-chain base subunit 1
Sptlc2	Serine palmitoyltransferase long-chain base subunit 2 (for C18 substrates, in ER)
Sptlc3	Serine palmitoyltransferase long-chain base subunit 3 (for C12-16 substrates)
Suppl.	Supplementary
Tbp	TATA-binding protein
TBS-T	Tris-buffered saline with Tween20
TGN	Trans-Golgi network
TLC	Thin layer chromatography
TLR2	Toll-like receptor 2
W1	WT sample 1
WT	Wild-type

References

1. Hernandez, A.; Magarino, C.; Gispert, S.; Santos, N.; Lunkes, A.; Orozco, G.; Heredero, L.; Beckmann, J.; Auburger, G.G. Genetic mapping of the spinocerebellar ataxia 2 (SCA2) locus on chromosome 12q23-q24.1. *Genomics* **1995**, *25*, 433–435. [CrossRef]
2. Belal, S.; Cancel, G.; Stevanin, G.; Hentati, F.; Khati, C.; Ben Hamida, C.; Auburger, G.; Agid, Y.; Ben Hamida, M.; Brice, A. Clinical and genetic analysis of a Tunisian family with autosomal dominant cerebellar ataxia type 1 linked to the SCA2 locus. *Neurology* **1994**, *44*, 1423–1426. [CrossRef] [PubMed]
3. Auburger, G.; Diaz, G.O.; Capote, R.F.; Sanchez, S.G.; Perez, M.P.; del Cueto, M.E.; Meneses, M.G.; Farrall, M.; Williamson, R.; Chamberlain, S.; et al. Autosomal dominant ataxia: Genetic evidence for locus heterogeneity from a Cuban founder-effect population. *Am. J. Hum. Genet.* **1990**, *46*, 1163–1177. [PubMed]
4. Orozco Diaz, G.; Nodarse Fleites, A.; Cordoves Sagaz, R.; Auburger, G. Autosomal dominant cerebellar ataxia: Clinical analysis of 263 patients from a homogeneous population in Holguin, Cuba. *Neurology* **1990**, *40*, 1369–1375. [CrossRef]
5. Gispert, S.; Twells, R.; Orozco, G.; Brice, A.; Weber, J.; Heredero, L.; Scheufler, K.; Riley, B.; Allotey, R.; Nothers, C.; et al. Chromosomal assignment of the second locus for autosomal dominant cerebellar ataxia (SCA2) to chromosome 12q23-24.1. *Nat. Genet.* **1993**, *4*, 295–299. [CrossRef]
6. Gispert, S.; Lunkes, A.; Santos, N.; Orozco, G.; Ha-Hao, D.; Ratzlaff, T.; Aguiar, J.; Torrens, L.; Heredero, L.; Brice, A.; et al. Localization of the candidate gene D-amino acid oxidase outside the refined 1-cM region of spinocerebellar ataxia 2. *Am. J. Hum. Genet.* **1995**, *57*, 972–975.
7. Rodriguez-Labrada, R.; Velazquez-Perez, L.; Auburger, G.; Ziemann, U.; Canales-Ochoa, N.; Medrano-Montero, J.; Vazquez-Mojena, Y.; Gonzalez-Zaldivar, Y. Spinocerebellar ataxia type 2: Measures of saccade changes improve power for clinical trials. *Mov. Disord.* **2016**, *31*, 570–578. [CrossRef]
8. Rodriguez-Labrada, R.; Velazquez-Perez, L.; Seigfried, C.; Canales-Ochoa, N.; Auburger, G.; Medrano-Montero, J.; Sanchez-Cruz, G.; Aguilera-Rodriguez, R.; Laffita-Mesa, J.; Vazquez-Mojena, Y.; et al. Saccadic latency is prolonged in Spinocerebellar Ataxia type 2 and correlates with the frontal-executive dysfunctions. *J. Neurol. Sci.* **2011**, *306*, 103–107. [CrossRef]
9. Velazquez-Perez, L.; Seifried, C.; Abele, M.; Wirjatijasa, F.; Rodriguez-Labrada, R.; Santos-Falcon, N.; Sanchez-Cruz, G.; Almaguer-Mederos, L.; Tejeda, R.; Canales-Ochoa, N.; et al. Saccade velocity is reduced in presymptomatic spinocerebellar ataxia type 2. *Clin. Neurophysiol.* **2009**, *120*, 632–635. [CrossRef]
10. Velazquez-Perez, L.; Seifried, C.; Santos-Falcon, N.; Abele, M.; Ziemann, U.; Almaguer, L.E.; Martinez-Gongora, E.; Sanchez-Cruz, G.; Canales, N.; Perez-Gonzalez, R.; et al. Saccade velocity is controlled by polyglutamine size in spinocerebellar ataxia 2. *Ann. Neurol.* **2004**, *56*, 444–447. [CrossRef]
11. Auburger, G.W. Spinocerebellar ataxia type 2. *Handb. Clin. Neurol.* **2012**, *103*, 423–436. [PubMed]
12. Pulst, S.M.; Nechiporuk, A.; Nechiporuk, T.; Gispert, S.; Chen, X.N.; Lopes-Cendes, I.; Pearlman, S.; Starkman, S.; Orozco-Diaz, G.; Lunkes, A.; et al. Moderate expansion of a normally biallelic trinucleotide repeat in spinocerebellar ataxia type 2. *Nat. Genet.* **1996**, *14*, 269–276. [CrossRef] [PubMed]

13. Sanpei, K.; Takano, H.; Igarashi, S.; Sato, T.; Oyake, M.; Sasaki, H.; Wakisaka, A.; Tashiro, K.; Ishida, Y.; Ikeuchi, T.; et al. Identification of the spinocerebellar ataxia type 2 gene using a direct identification of repeat expansion and cloning technique, DIRECT. *Nat. Genet.* **1996**, *14*, 277–284. [CrossRef] [PubMed]
14. Imbert, G.; Saudou, F.; Yvert, G.; Devys, D.; Trottier, Y.; Garnier, J.M.; Weber, C.; Mandel, J.L.; Cancel, G.; Abbas, N.; et al. Cloning of the gene for spinocerebellar ataxia 2 reveals a locus with high sensitivity to expanded CAG/glutamine repeats. *Nat. Genet.* **1996**, *14*, 285–291. [CrossRef] [PubMed]
15. Auburger, G.; Sen, N.E.; Meierhofer, D.; Basak, A.N.; Gitler, A.D. Efficient Prevention of Neurodegenerative Diseases by Depletion of Starvation Response Factor Ataxin-2. *Trends Neurosci.* **2017**, *40*, 507–516. [CrossRef]
16. Almaguer-Mederos, L.E.; Mesa, J.M.L.; Gonzalez-Zaldivar, Y.; Almaguer-Gotay, D.; Cuello-Almarales, D.; Aguilera-Rodriguez, R.; Falcon, N.S.; Gispert, S.; Auburger, G.; Velazquez-Perez, L. Factors associated with ATXN2 CAG/CAA repeat intergenerational instability in Spinocerebellar ataxia type 2. *Clin. Genet.* **2018**, *94*, 346–350. [CrossRef]
17. Hoche, F.; Baliko, L.; den Dunnen, W.; Steinecker, K.; Bartos, L.; Safrany, E.; Auburger, G.; Deller, T.; Korf, H.W.; Klockgether, T.; et al. Spinocerebellar ataxia type 2 (SCA2): Identification of early brain degeneration in one monozygous twin in the initial disease stage. *Cerebellum* **2011**, *10*, 245–253. [CrossRef]
18. Estrada, R.; Galarraga, J.; Orozco, G.; Nodarse, A.; Auburger, G. Spinocerebellar ataxia 2 (SCA2): Morphometric analyses in 11 autopsies. *Acta Neuropathol.* **1999**, *97*, 306–310. [CrossRef]
19. Schols, L.; Gispert, S.; Vorgerd, M.; Menezes Vieira-Saecker, A.M.; Blanke, P.; Auburger, G.; Amoiridis, G.; Meves, S.; Epplen, J.T.; Przuntek, H.; et al. Spinocerebellar ataxia type 2. Genotype and phenotype in German kindreds. *Arch. Neurol.* **1997**, *54*, 1073–1080. [CrossRef]
20. Riess, O.; Laccone, F.A.; Gispert, S.; Schols, L.; Zuhlke, C.; Vieira-Saecker, A.M.; Herlt, S.; Wessel, K.; Epplen, J.T.; Weber, B.H.; et al. SCA2 trinucleotide expansion in German SCA patients. *Neurogenetics* **1997**, *1*, 59–64. [CrossRef]
21. Lahut, S.; Omur, O.; Uyan, O.; Agim, Z.S.; Ozoguz, A.; Parman, Y.; Deymeer, F.; Oflazer, P.; Koc, F.; Ozcelik, H.; et al. ATXN2 and its neighbouring gene SH2B3 are associated with increased ALS risk in the Turkish population. *PLoS ONE* **2012**, *7*, e42956. [CrossRef] [PubMed]
22. Gispert, S.; Kurz, A.; Waibel, S.; Bauer, P.; Liepelt, I.; Geisen, C.; Gitler, A.D.; Becker, T.; Weber, M.; Berg, D.; et al. The modulation of Amyotrophic Lateral Sclerosis risk by ataxin-2 intermediate polyglutamine expansions is a specific effect. *Neurobiol. Dis.* **2012**, *45*, 356–361. [CrossRef] [PubMed]
23. Rubino, E.; Mancini, C.; Boschi, S.; Ferrero, P.; Ferrone, M.; Bianca, S.; Zucca, M.; Orsi, L.; Pinessi, L.; Govone, F.; et al. ATXN2 intermediate repeat expansions influence the clinical phenotype in frontotemporal dementia. *Neurobiol. Aging* **2019**, *73*, 231. [CrossRef] [PubMed]
24. Schols, L.; Reimold, M.; Seidel, K.; Globas, C.; Brockmann, K.; Hauser, T.K.; Auburger, G.; Burk, K.; den Dunnen, W.; Reischl, G.; et al. No parkinsonism in SCA2 and SCA3 despite severe neurodegeneration of the dopaminergic substantia nigra. *Brain* **2015**, *138*, 3316–3326. [CrossRef]
25. Wang, L.; Aasly, J.O.; Annesi, G.; Bardien, S.; Bozi, M.; Brice, A.; Carr, J.; Chung, S.J.; Clarke, C.; Crosiers, D.; et al. Large-scale assessment of polyglutamine repeat expansions in Parkinson disease. *Neurology* **2015**, *85*, 1283–1292. [CrossRef]
26. Ross, O.A.; Rutherford, N.J.; Baker, M.; Soto-Ortolaza, A.I.; Carrasquillo, M.M.; DeJesus-Hernandez, M.; Adamson, J.; Li, M.; Volkening, K.; Finger, E.; et al. Ataxin-2 repeat-length variation and neurodegeneration. *Hum. Mol. Genet.* **2011**, *20*, 3207–3212. [CrossRef]
27. Taylor, L.M.; McMillan, P.J.; Kraemer, B.C.; Liachko, N.F. Tau tubulin kinases in proteinopathy. *Febs J.* **2019**, *286*, 2434–2446. [CrossRef]
28. Elden, A.C.; Kim, H.J.; Hart, M.P.; Chen-Plotkin, A.S.; Johnson, B.S.; Fang, X.; Armakola, M.; Geser, F.; Greene, R.; Lu, M.M.; et al. Ataxin-2 intermediate-length polyglutamine expansions are associated with increased risk for ALS. *Nature* **2010**, *466*, 1069–1075. [CrossRef]
29. Shulman, J.M.; Feany, M.B. Genetic modifiers of tauopathy in Drosophila. *Genetics* **2003**, *165*, 1233–1242.
30. Al-Ramahi, I.; Perez, A.M.; Lim, J.; Zhang, M.; Sorensen, R.; de Haro, M.; Branco, J.; Pulst, S.M.; Zoghbi, H.Y.; Botas, J. dAtaxin-2 mediates expanded Ataxin-1-induced neurodegeneration in a Drosophila model of SCA1. *PLoS Genet.* **2007**, *3*, e234. [CrossRef]
31. Auburger, G.; Gispert, S.; Lahut, S.; Omur, O.; Damrath, E.; Heck, M.; Basak, N. 12q24 locus association with type 1 diabetes: SH2B3 or ATXN2? *World J. Diabetes* **2014**, *5*, 316–327. [CrossRef] [PubMed]

32. Sebastiani, P.; Solovieff, N.; Puca, A.; Hartley, S.W.; Melista, E.; Andersen, S.; Dworkis, D.A.; Wilk, J.B.; Myers, R.H.; Steinberg, M.H.; et al. Genetic signatures of exceptional longevity in humans. *Science* **2010**, 2010. [CrossRef]
33. Becker, L.A.; Huang, B.; Bieri, G.; Ma, R.; Knowles, D.A.; Jafar-Nejad, P.; Messing, J.; Kim, H.J.; Soriano, A.; Auburger, G.; et al. Therapeutic reduction of ataxin-2 extends lifespan and reduces pathology in TDP-43 mice. *Nature* **2017**, *544*, 367–371. [CrossRef]
34. Scoles, D.R.; Meera, P.; Schneider, M.D.; Paul, S.; Dansithong, W.; Figueroa, K.P.; Hung, G.; Rigo, F.; Bennett, C.F.; Otis, T.S.; et al. Antisense oligonucleotide therapy for spinocerebellar ataxia type 2. *Nature* **2017**, *544*, 362–366. [CrossRef]
35. Aguiar, J.; Santurlidis, S.; Nowok, J.; Alexander, C.; Rudnicki, D.; Gispert, S.; Schulz, W.; Auburger, G. Identification of the physiological promoter for spinocerebellar ataxia 2 gene reveals a CpG island for promoter activity situated into the exon 1 of this gene and provides data about the origin of the nonmethylated state of these types of islands. *Biochem. Biophys. Res. Commun.* **1999**, *254*, 315–318. [CrossRef] [PubMed]
36. Lastres-Becker, I.; Nonis, D.; Eich, F.; Klinkenberg, M.; Gorospe, M.; Kotter, P.; Klein, F.A.; Kedersha, N.; Auburger, G. Mammalian ataxin-2 modulates translation control at the pre-initiation complex via PI3K/mTOR and is induced by starvation. *Biochim. Et Biophys. Acta* **2016**, *1862*, 1558–1569. [CrossRef] [PubMed]
37. Damrath, E.; Heck, M.V.; Gispert, S.; Azizov, M.; Nowock, J.; Seifried, C.; Rub, U.; Walter, M.; Auburger, G. ATXN2-CAG42 sequesters PABPC1 into insolubility and induces FBXW8 in cerebellum of old ataxic knock-in mice. *PLoS Genet.* **2012**, *8*, e1002920. [CrossRef]
38. Yokoshi, M.; Li, Q.; Yamamoto, M.; Okada, H.; Suzuki, Y.; Kawahara, Y. Direct binding of Ataxin-2 to distinct elements in 3' UTRs promotes mRNA stability and protein expression. *Mol. Cell* **2014**, *55*, 186–198. [CrossRef]
39. Lastres-Becker, I.; Nonis, D.; Nowock, J.; Auburger, G. New alternative splicing variants of the ATXN2 transcript. *Neurol. Res. Pract.* **2019**, *1*, 22. [CrossRef]
40. Drost, J.; Nonis, D.; Eich, F.; Leske, O.; Damrath, E.; Brunt, E.R.; Lastres-Becker, I.; Heumann, R.; Nowock, J.; Auburger, G. Ataxin-2 modulates the levels of Grb2 and SRC but not ras signaling. *J. Mol. Neurosci.* **2013**, *51*, 68–81. [CrossRef]
41. Nonis, D.; Schmidt, M.H.H.; van de Loo, S.; Eich, F.; Dikic, I.; Nowock, J.; Auburger, G. Ataxin-2 associates with the endocytosis complex and affects EGF receptor trafficking. *Cell. Signal.* **2008**, *20*, 1725–1739. [CrossRef] [PubMed]
42. Fittschen, M.; Lastres-Becker, I.; Halbach, M.V.; Damrath, E.; Gispert, S.; Azizov, M.; Walter, M.; Muller, S.; Auburger, G. Genetic ablation of ataxin-2 increases several global translation factors in their transcript abundance but decreases translation rate. *Neurogenetics* **2015**, *16*, 181–192. [CrossRef] [PubMed]
43. van de Loo, S.; Eich, F.; Nonis, D.; Auburger, G.; Nowock, J. Ataxin-2 associates with rough endoplasmic reticulum. *Exp. Neurol.* **2009**, *215*, 110–118. [CrossRef] [PubMed]
44. Nonhoff, U.; Ralser, M.; Welzel, F.; Piccini, I.; Balzereit, D.; Yaspo, M.L.; Lehrach, H.; Krobitsch, S. Ataxin-2 interacts with the DEAD/H-box RNA helicase DDX6 and interferes with P-bodies and stress granules. *Mol. Biol. Cell* **2007**, *18*, 1385–1396. [CrossRef] [PubMed]
45. Anderson, P.; Kedersha, N. Stress granules: The Tao of RNA triage. *Trends Biochem. Sci.* **2008**, *33*, 141–150. [CrossRef] [PubMed]
46. Jimenez-Lopez, D.; Guzman, P. Insights into the evolution and domain structure of Ataxin-2 proteins across eukaryotes. *BMC Res. Notes* **2014**, *7*, 453. [CrossRef]
47. Mangus, D.A.; Amrani, N.; Jacobson, A. Pbp1p, a factor interacting with Saccharomyces cerevisiae poly(A)-binding protein, regulates polyadenylation. *Mol. Cell. Biol.* **1998**, *18*, 7383–7396. [CrossRef]
48. Bar, D.Z.; Charar, C.; Dorfman, J.; Yadid, T.; Tafforeau, L.; Lafontaine, D.L.; Gruenbaum, Y. Cell size and fat content of dietary-restricted Caenorhabditis elegans are regulated by ATX-2, an mTOR repressor. *Proc. Natl. Acad. Sci. USA* **2016**, *113*, E4620–E4629. [CrossRef]
49. Satterfield, T.F.; Jackson, S.M.; Pallanck, L.J. A Drosophila homolog of the polyglutamine disease gene SCA2 is a dosage-sensitive regulator of actin filament formation. *Genetics* **2002**, *162*, 1687–1702.
50. Lastres-Becker, I.; Brodesser, S.; Lutjohann, D.; Azizov, M.; Buchmann, J.; Hintermann, E.; Sandhoff, K.; Schurmann, A.; Nowock, J.; Auburger, G. Insulin receptor and lipid metabolism pathology in ataxin-2 knock-out mice. *Hum. Mol. Genet.* **2008**, *17*, 1465–1481. [CrossRef]

51. Sen, N.E.; Canet-Pons, J.; Halbach, M.V.; Arsovic, A.; Pilatus, U.; Chae, W.H.; Kaya, Z.E.; Seidel, K.; Rollmann, E.; Mittelbronn, M.; et al. Generation of an Atxn2-CAG100 knock-in mouse reveals N-acetylaspartate production deficit due to early Nat8l dysregulation. *Neurobiol. Dis.* **2019**, *132*, 104559. [CrossRef] [PubMed]
52. Seidel, K.; Siswanto, S.; Fredrich, M.; Bouzrou, M.; den Dunnen, W.F.A.; Ozerden, I.; Korf, H.W.; Melegh, B.; de Vries, J.J.; Brunt, E.R.; et al. On the distribution of intranuclear and cytoplasmic aggregates in the brainstem of patients with spinocerebellar ataxia type 2 and 3. *Brain Pathol.* **2017**, *27*, 345–355. [CrossRef] [PubMed]
53. Halbach, M.V.; Gispert, S.; Stehning, T.; Damrath, E.; Walter, M.; Auburger, G. Atxn2 Knockout and CAG42-Knock-in Cerebellum Shows Similarly Dysregulated Expression in Calcium Homeostasis Pathway. *Cerebellum* **2017**, *16*, 68–81. [CrossRef] [PubMed]
54. Koch, P.; Breuer, P.; Peitz, M.; Jungverdorben, J.; Kesavan, J.; Poppe, D.; Doerr, J.; Ladewig, J.; Mertens, J.; Tuting, T.; et al. Excitation-induced ataxin-3 aggregation in neurons from patients with Machado-Joseph disease. *Nature* **2011**, *480*, 543–546. [CrossRef]
55. Rub, U.; Schols, L.; Paulson, H.; Auburger, G.; Kermer, P.; Jen, J.C.; Seidel, K.; Korf, H.W.; Deller, T. Clinical features, neurogenetics and neuropathology of the polyglutamine spinocerebellar ataxias type 1, 2, 3, 6 and 7. *Prog. Neurobiol.* **2013**, *104*, 38–66. [CrossRef]
56. Lastres-Becker, I.; Rub, U.; Auburger, G. Spinocerebellar ataxia 2 (SCA2). *Cerebellum* **2008**, *7*, 115–124. [CrossRef]
57. Fernandez-Ruiz, J.; Velasquez-Perez, L.; Diaz, R.; Drucker-Colin, R.; Perez-Gonzalez, R.; Canales, N.; Sanchez-Cruz, G.; Martinez-Gongora, E.; Medrano, Y.; Almaguer-Mederos, L.; et al. Prism adaptation in spinocerebellar ataxia type 2. *Neuropsychologia* **2007**, *45*, 2692–2698. [CrossRef]
58. Freund, H.J.; Barnikol, U.B.; Nolte, D.; Treuer, H.; Auburger, G.; Tass, P.A.; Samii, M.; Sturm, V. Subthalamic-thalamic DBS in a case with spinocerebellar ataxia type 2 and severe tremor-A unusual clinical benefit. *Mov. Disord.* **2007**, *22*, 732–735. [CrossRef]
59. Velazquez-Perez, L.; Rodriguez-Labrada, R.; Torres-Vega, R.; Ortega-Sanchez, R.; Medrano-Montero, J.; Gonzalez-Pina, R.; Vazquez-Mojena, Y.; Auburger, G.; Ziemann, U. Progression of corticospinal tract dysfunction in pre-ataxic spinocerebellar ataxia type 2: A two-years follow-up TMS study. *Clin. Neurophysiol.* **2018**, *129*, 895–900. [CrossRef]
60. Velazquez-Perez, L.; Tunnerhoff, J.; Rodriguez-Labrada, R.; Torres-Vega, R.; Ruiz-Gonzalez, Y.; Belardinelli, P.; Medrano-Montero, J.; Canales-Ochoa, N.; Gonzalez-Zaldivar, Y.; Vazquez-Mojena, Y.; et al. Early corticospinal tract damage in prodromal SCA2 revealed by EEG-EMG and EMG-EMG coherence. *Clin. Neurophysiol.* **2017**, *128*, 2493–2502. [CrossRef]
61. Velazquez-Perez, L.; Tunnerhoff, J.; Rodriguez-Labrada, R.; Torres-Vega, R.; Belardinelli, P.; Medrano-Montero, J.; Pena-Acosta, A.; Canales-Ochoa, N.; Vazquez-Mojena, Y.; Gonzalez-Zaldivar, Y.; et al. Corticomuscular Coherence: A Novel Tool to Assess the Pyramidal Tract Dysfunction in Spinocerebellar Ataxia Type 2. *Cerebellum* **2017**, *16*, 602–606. [CrossRef] [PubMed]
62. Velazquez-Perez, L.; Rodriguez-Labrada, R.; Torres-Vega, R.; Medrano Montero, J.; Vazquez-Mojena, Y.; Auburger, G.; Ziemann, U. Abnormal corticospinal tract function and motor cortex excitability in non-ataxic SCA2 mutation carriers: A TMS study. *Clin. Neurophysiol.* **2016**, *127*, 2713–2719. [CrossRef] [PubMed]
63. Velazquez-Perez, L.; Rodriguez-Labrada, R.; Cruz-Rivas, E.M.; Fernandez-Ruiz, J.; Vaca-Palomares, I.; Lilia-Campins, J.; Cisneros, B.; Pena-Acosta, A.; Vazquez-Mojena, Y.; Diaz, R.; et al. Comprehensive study of early features in spinocerebellar ataxia 2: Delineating the prodromal stage of the disease. *Cerebellum* **2014**, *13*, 568–579. [CrossRef] [PubMed]
64. Medrano Montero, J.; Velasquez-Perez, L.; Rodriguez-Diaz, J.; Canales Ochoa, N.; Pena-Acosta, A.; Almaguer, L.E.; Estupinan-Rodriguez, A.; Auburger, G. Early cranial nerve dysfunction is correlated to altered facial morphology in spinocerebellar ataxia type 2. *Investig. En Discapac.* **2018**, *7*, 53–66.
65. Magana, J.J.; Velazquez-Perez, L.; Cisneros, B. Spinocerebellar ataxia type 2: Clinical presentation, molecular mechanisms, and therapeutic perspectives. *Mol. Neurobiol.* **2013**, *47*, 90–104. [CrossRef]
66. Almaguer-Mederos, L.E.; Falcon, N.S.; Almira, Y.R.; Zaldivar, Y.G.; Almarales, D.C.; Gongora, E.M.; Herrera, M.P.; Batallan, K.E.; Arminan, R.R.; Manresa, M.V.; et al. Estimation of the age at onset in spinocerebellar ataxia type 2 Cuban patients by survival analysis. *Clin. Genet.* **2010**, *78*, 169–174. [CrossRef]

67. Rodriguez-Labrada, R.; Galicia-Polo, L.; Canales-Ochoa, N.; Voss, U.; Tuin, I.; Pena-Acosta, A.; Estupinan-Rodriguez, A.; Medrano-Montero, J.; Vazquez-Mojena, Y.; Gonzalez-Zaldivar, Y.; et al. Sleep spindles and K-complex activities are decreased in spinocerebellar ataxia type 2: Relationship to memory and motor performances. *Sleep Med.* **2019**, *60*, 188–196. [CrossRef]
68. Pfeffer, M.; Gispert, S.; Auburger, G.; Wicht, H.; Korf, H.W. Impact of Ataxin-2 knock out on circadian locomotor behavior and PER immunoreaction in the SCN of mice. *Chronobiol. Int.* **2017**, *34*, 129–137. [CrossRef]
69. Velazquez-Perez, L.; Voss, U.; Rodriguez-Labrada, R.; Auburger, G.; Canales Ochoa, N.; Sanchez Cruz, G.; Galicia Polo, L.; Haro Valencia, R.; Aguilera Rodriguez, R.; Medrano Montero, J.; et al. Sleep disorders in spinocerebellar ataxia type 2 patients. *Neuro-Degener. Dis.* **2011**, *8*, 447–454. [CrossRef]
70. Tuin, I.; Voss, U.; Kang, J.S.; Kessler, K.; Rub, U.; Nolte, D.; Lochmuller, H.; Tinschert, S.; Claus, D.; Krakow, K.; et al. Stages of sleep pathology in spinocerebellar ataxia type 2 (SCA2). *Neurology* **2006**, *67*, 1966–1972. [CrossRef]
71. Reetz, K.; Rodriguez-Labrada, R.; Dogan, I.; Mirzazade, S.; Romanzetti, S.; Schulz, J.B.; Cruz-Rivas, E.M.; Alvarez-Cuesta, J.A.; Aguilera Rodriguez, R.; Gonzalez Zaldivar, Y.; et al. Brain atrophy measures in preclinical and manifest spinocerebellar ataxia type 2. *Ann. Clin. Transl. Neurol.* **2018**, *5*, 128–137. [CrossRef] [PubMed]
72. Wang, P.S.; Chen, H.C.; Wu, H.M.; Lirng, J.F.; Wu, Y.T.; Soong, B.W. Association between proton magnetic resonance spectroscopy measurements and CAG repeat number in patients with spinocerebellar ataxias 2, 3, or 6. *PLoS ONE* **2012**, *7*, e47479. [CrossRef] [PubMed]
73. Auburger, G.; Klinkenberg, M.; Drost, J.; Marcus, K.; Morales-Gordo, B.; Kunz, W.S.; Brandt, U.; Broccoli, V.; Reichmann, H.; Gispert, S.; et al. Primary skin fibroblasts as a model of Parkinson's disease. *Mol. Neurobiol.* **2012**, *46*, 20–27. [CrossRef]
74. Lahut, S.; Gispert, S.; Omur, O.; Depboylu, C.; Seidel, K.; Dominguez-Bautista, J.A.; Brehm, N.; Tireli, H.; Hackmann, K.; Pirkevi, C.; et al. Blood RNA biomarkers in prodromal PARK4 and rapid eye movement sleep behavior disorder show role of complexin 1 loss for risk of Parkinson's disease. *Dis. Models Mech.* **2017**, *10*, 619–631. [CrossRef] [PubMed]
75. Sen, N.E.; Drost, J.; Gispert, S.; Torres-Odio, S.; Damrath, E.; Klinkenberg, M.; Hamzeiy, H.; Akdal, G.; Gulluoglu, H.; Basak, A.N.; et al. Search for SCA2 blood RNA biomarkers highlights Ataxin-2 as strong modifier of the mitochondrial factor PINK1 levels. *Neurobiol. Dis.* **2016**, *96*, 115–126. [CrossRef] [PubMed]
76. Pujol-Lereis, L.M. Alteration of Sphingolipids in Biofluids: Implications for Neurodegenerative Diseases. *Int. J. Mol. Sci.* **2019**, *20*, 3564. [CrossRef] [PubMed]
77. Deak, F.; Anderson, R.E.; Fessler, J.L.; Sherry, D.M. Novel Cellular Functions of Very Long Chain-Fatty Acids: Insight From ELOVL4 Mutations. *Front. Cell. Neurosci.* **2019**, *13*, 428. [CrossRef]
78. Rub, U.; Del Turco, D.; Del Tredici, K.; de Vos, R.A.; Brunt, E.R.; Reifenberger, G.; Seifried, C.; Schultz, C.; Auburger, G.; Braak, H. Thalamic involvement in a spinocerebellar ataxia type 2 (SCA2) and a spinocerebellar ataxia type 3 (SCA3) patient, and its clinical relevance. *Brain* **2003**, *126*, 2257–2272. [CrossRef]
79. Rub, U.; Schultz, C.; Del Tredici, K.; Gierga, K.; Reifenberger, G.; de Vos, R.A.; Seifried, C.; Braak, H.; Auburger, G. Anatomically based guidelines for systematic investigation of the central somatosensory system and their application to a spinocerebellar ataxia type 2 (SCA2) patient. *Neuropathol. Appl. Neurobiol.* **2003**, *29*, 418–433. [CrossRef]
80. Rub, U.; Del Turco, D.; Burk, K.; Diaz, G.O.; Auburger, G.; Mittelbronn, M.; Gierga, K.; Ghebremedhin, E.; Schultz, C.; Schols, L.; et al. Extended pathoanatomical studies point to a consistent affection of the thalamus in spinocerebellar ataxia type 2. *Neuropathol. Appl. Neurobiol.* **2005**, *31*, 127–140. [CrossRef]
81. Rub, U.; Gierga, K.; Brunt, E.R.; de Vos, R.A.; Bauer, M.; Schols, L.; Burk, K.; Auburger, G.; Bohl, J.; Schultz, C.; et al. Spinocerebellar ataxias types 2 and 3: Degeneration of the pre-cerebellar nuclei isolates the three phylogenetically defined regions of the cerebellum. *J. Neural Transm.* **2005**, *112*, 1523–1545. [CrossRef] [PubMed]
82. Gierga, K.; Burk, K.; Bauer, M.; Orozco Diaz, G.; Auburger, G.; Schultz, C.; Vuksic, M.; Schols, L.; de Vos, R.A.; Braak, H.; et al. Involvement of the cranial nerves and their nuclei in spinocerebellar ataxia type 2 (SCA2). *Acta Neuropathol.* **2005**, *109*, 617–631. [CrossRef] [PubMed]

83. Rub, U.; Seidel, K.; Ozerden, I.; Gierga, K.; Brunt, E.R.; Schols, L.; de Vos, R.A.; den Dunnen, W.; Schultz, C.; Auburger, G.; et al. Consistent affection of the central somatosensory system in spinocerebellar ataxia type 2 and type 3 and its significance for clinical symptoms and rehabilitative therapy. *Brain Res. Rev.* **2007**, *53*, 235–249. [CrossRef] [PubMed]
84. Rub, U.; Brunt, E.R.; Petrasch-Parwez, E.; Schols, L.; Theegarten, D.; Auburger, G.; Seidel, K.; Schultz, C.; Gierga, K.; Paulson, H.; et al. Degeneration of ingestion-related brainstem nuclei in spinocerebellar ataxia type 2, 3, 6 and 7. *Neuropathol. Appl. Neurobiol.* **2006**, *32*, 635–649. [CrossRef] [PubMed]
85. Hoche, F.; Seidel, K.; Brunt, E.R.; Auburger, G.; Schols, L.; Burk, K.; de Vos, R.A.; den Dunnen, W.; Bechmann, I.; Egensperger, R.; et al. Involvement of the auditory brainstem system in spinocerebellar ataxia type 2 (SCA2), type 3 (SCA3) and type 7 (SCA7). *Neuropathol. Appl. Neurobiol.* **2008**, *34*, 479–491. [CrossRef] [PubMed]
86. Scherzed, W.; Brunt, E.R.; Heinsen, H.; de Vos, R.A.; Seidel, K.; Burk, K.; Schols, L.; Auburger, G.; Del Turco, D.; Deller, T.; et al. Pathoanatomy of cerebellar degeneration in spinocerebellar ataxia type 2 (SCA2) and type 3 (SCA3). *Cerebellum* **2012**, *11*, 749–760. [CrossRef] [PubMed]
87. Seidel, K.; Siswanto, S.; Brunt, E.R.; den Dunnen, W.; Korf, H.W.; Rub, U. Brain pathology of spinocerebellar ataxias. *Acta Neuropathol.* **2012**, *124*, 1–21. [CrossRef]
88. Rub, U.; Farrag, K.; Seidel, K.; Brunt, E.R.; Heinsen, H.; Burk, K.; Melegh, B.; von Gall, C.; Auburger, G.; Bohl, J.; et al. Involvement of the cholinergic basal forebrain nuclei in spinocerebellar ataxia type 2 (SCA2). *Neuropathol. Appl. Neurobiol.* **2013**, *39*, 634–643. [CrossRef]
89. Olsen, A.S.B.; Faergeman, N.J. Sphingolipids: Membrane microdomains in brain development, function and neurological diseases. *Open Biol.* **2017**, *7*, 170069. [CrossRef]
90. Baumann, N.; Pham-Dinh, D. Biology of oligodendrocyte and myelin in the mammalian central nervous system. *Physiol. Rev.* **2001**, *81*, 871–927. [CrossRef]
91. Imgrund, S.; Hartmann, D.; Farwanah, H.; Eckhardt, M.; Sandhoff, R.; Degen, J.; Gieselmann, V.; Sandhoff, K.; Willecke, K. Adult ceramide synthase 2 (CERS2)-deficient mice exhibit myelin sheath defects, cerebellar degeneration, and hepatocarcinomas. *J. Biol. Chem.* **2009**, *284*, 33549–33560. [CrossRef] [PubMed]
92. Hallett, P.J.; Huebecker, M.; Brekk, O.R.; Moloney, E.B.; Rocha, E.M.; Priestman, D.A.; Platt, F.M.; Isacson, O. Glycosphingolipid levels and glucocerebrosidase activity are altered in normal aging of the mouse brain. *Neurobiol. Aging* **2018**, *67*, 189–200. [CrossRef] [PubMed]
93. Posse de Chaves, E.; Sipione, S. Sphingolipids and gangliosides of the nervous system in membrane function and dysfunction. *FEBS Lett.* **2010**, *584*, 1748–1759. [CrossRef] [PubMed]
94. Yoshihara, T.; Satake, H.; Nishie, T.; Okino, N.; Hatta, T.; Otani, H.; Naruse, C.; Suzuki, H.; Sugihara, K.; Kamimura, E.; et al. Lactosylceramide synthases encoded by B4galt5 and 6 genes are pivotal for neuronal generation and myelin formation in mice. *PLoS Genet.* **2018**, *14*, e1007545. [CrossRef] [PubMed]
95. Paciorkowski, A.R.; Shafrir, Y.; Hrivnak, J.; Patterson, M.C.; Tennison, M.B.; Clark, H.B.; Gomez, C.M. Massive expansion of SCA2 with autonomic dysfunction, retinitis pigmentosa, and infantile spasms. *Neurology* **2011**, *77*, 1055–1060. [CrossRef] [PubMed]
96. Yagishita, S.; Inoue, M. Clinicopathology of spinocerebellar degeneration: Its correlation to the unstable CAG repeat of the affected gene. *Pathol. Int.* **1997**, *47*, 1–15. [CrossRef]
97. Jellinger, K.A. Multiple System Atrophy: An Oligodendroglioneural Synucleinopathy1. *J. Alzheimer's Dis.* **2018**, *62*, 1141–1179. [CrossRef]
98. Park, H.; Kim, H.J.; Jeon, B.S. Parkinsonism in spinocerebellar ataxia. *Biomed Res. Int.* **2015**, *2015*, 125273. [CrossRef]
99. Saini, H.S.; Coelho, R.P.; Goparaju, S.K.; Jolly, P.S.; Maceyka, M.; Spiegel, S.; Sato-Bigbee, C. Novel role of sphingosine kinase 1 as a mediator of neurotrophin-3 action in oligodendrocyte progenitors. *J. Neurochem.* **2005**, *95*, 1298–1310. [CrossRef]
100. Di Pardo, A.; Maglione, V. Sphingolipid Metabolism: A New Therapeutic Opportunity for Brain Degenerative Disorders. *Front. Neurosci.* **2018**, *12*, 249. [CrossRef]
101. Ben-David, O.; Pewzner-Jung, Y.; Brenner, O.; Laviad, E.L.; Kogot-Levin, A.; Weissberg, I.; Biton, I.E.; Pienik, R.; Wang, E.; Kelly, S.; et al. Encephalopathy caused by ablation of very long acyl chain ceramide synthesis may be largely due to reduced galactosylceramide levels. *J. Biol. Chem.* **2011**, *286*, 30022–30033. [CrossRef] [PubMed]

102. Suzuki, E.; Handa, K.; Toledo, M.S.; Hakomori, S. Sphingosine-dependent apoptosis: A unified concept based on multiple mechanisms operating in concert. *Proc. Natl. Acad. Sci. USA* **2004**, *101*, 14788–14793. [CrossRef] [PubMed]
103. Grassi, S.; Chiricozzi, E.; Mauri, L.; Sonnino, S.; Prinetti, A. Sphingolipids and neuronal degeneration in lysosomal storage disorders. *J. Neurochem.* **2019**, *148*, 600–611. [CrossRef] [PubMed]
104. Miller, L.G., Jr.; Young, J.A.; Ray, S.K.; Wang, G.; Purohit, S.; Banik, N.L.; Dasgupta, S. Sphingosine Toxicity in EAE and MS: Evidence for Ceramide Generation via Serine-Palmitoyltransferase Activation. *Neurochem. Res.* **2017**, *42*, 2755–2768. [CrossRef] [PubMed]
105. Snook, E.R.; Fisher-Perkins, J.M.; Sansing, H.A.; Lee, K.M.; Alvarez, X.; MacLean, A.G.; Peterson, K.E.; Lackner, A.A.; Bunnell, B.A. Innate immune activation in the pathogenesis of a murine model of globoid cell leukodystrophy. *Am. J. Pathol.* **2014**, *184*, 382–396. [CrossRef] [PubMed]
106. Velazquez-Perez, L.; Rodriguez-Labrada, R.; Torres-Vega, R.; Montero, J.M.; Vazquez-Mojena, Y.; Auburger, G.; Ziemann, U. Central motor conduction time as prodromal biomarker in spinocerebellar ataxia type 2. *Mov. Disord.* **2016**, *31*, 603–604. [CrossRef]
107. Hussain, M.M.; Jin, W.; Jiang, X.C. Mechanisms involved in cellular ceramide homeostasis. *Nutr. Metab.* **2012**, *9*, 71. [CrossRef]
108. Airola, M.V.; Hannun, Y.A. Sphingolipid metabolism and neutral sphingomyelinases. *Handb. Exp. Pharmacol.* **2013**, *215*, 57–76.
109. Cui, M.; Ying, R.; Jiang, X.; Li, G.; Zhang, X.; Zheng, J.; Tam, K.Y.; Liang, B.; Shi, A.; Gobel, V.; et al. A Model of Hereditary Sensory and Autonomic Neuropathy Type 1 Reveals a Role of Glycosphingolipids in Neuronal Polarity. *J. Neurosci.* **2019**, *39*, 5816–5834. [CrossRef]
110. Rotthier, A.; Auer-Grumbach, M.; Janssens, K.; Baets, J.; Penno, A.; Almeida-Souza, L.; Van Hoof, K.; Jacobs, A.; De Vriendt, E.; Schlotter-Weigel, B.; et al. Mutations in the SPTLC2 subunit of serine palmitoyltransferase cause hereditary sensory and autonomic neuropathy type I. *Am. J. Hum. Genet.* **2010**, *87*, 513–522. [CrossRef]
111. Couttas, T.A.; Kain, N.; Suchowerska, A.K.; Quek, L.E.; Turner, N.; Fath, T.; Garner, B.; Don, A.S. Loss of ceramide synthase 2 activity, necessary for myelin biosynthesis, precedes tau pathology in the cortical pathogenesis of Alzheimer's disease. *Neurobiol. Aging* **2016**, *43*, 89–100. [CrossRef] [PubMed]
112. Mosbech, M.B.; Olsen, A.S.; Neess, D.; Ben-David, O.; Klitten, L.L.; Larsen, J.; Sabers, A.; Vissing, J.; Nielsen, J.E.; Hasholt, L.; et al. Reduced ceramide synthase 2 activity causes progressive myoclonic epilepsy. *Ann. Clin. Transl. Neurol.* **2014**, *1*, 88–98. [CrossRef] [PubMed]
113. Vanni, N.; Fruscione, F.; Ferlazzo, E.; Striano, P.; Robbiano, A.; Traverso, M.; Sander, T.; Falace, A.; Gazzerro, E.; Bramanti, P.; et al. Impairment of ceramide synthesis causes a novel progressive myoclonus epilepsy. *Ann. Neurol.* **2014**, *76*, 206–212. [CrossRef] [PubMed]
114. Mullen, T.D.; Hannun, Y.A.; Obeid, L.M. Ceramide synthases at the centre of sphingolipid metabolism and biology. *Biochem. J.* **2012**, *441*, 789–802. [CrossRef]
115. Yabu, T.; Shiba, H.; Shibasaki, Y.; Nakanishi, T.; Imamura, S.; Touhata, K.; Yamashita, M. Stress-induced ceramide generation and apoptosis via the phosphorylation and activation of nSMase1 by JNK signaling. *Cell Death Differ.* **2015**, *22*, 258–273. [CrossRef]
116. Wheeler, D.; Knapp, E.; Bandaru, V.V.; Wang, Y.; Knorr, D.; Poirier, C.; Mattson, M.P.; Geiger, J.D.; Haughey, N.J. Tumor necrosis factor-alpha-induced neutral sphingomyelinase-2 modulates synaptic plasticity by controlling the membrane insertion of NMDA receptors. *J. Neurochem.* **2009**, *109*, 1237–1249. [CrossRef]
117. Iguchi, Y.; Eid, L.; Parent, M.; Soucy, G.; Bareil, C.; Riku, Y.; Kawai, K.; Takagi, S.; Yoshida, M.; Katsuno, M.; et al. Exosome secretion is a key pathway for clearance of pathological TDP-43. *Brain* **2016**, *139*, 3187–3201. [CrossRef]
118. Stoffel, W.; Jenke, B.; Schmidt-Soltau, I.; Binczek, E.; Brodesser, S.; Hammels, I. SMPD3 deficiency perturbs neuronal proteostasis and causes progressive cognitive impairment. *Cell Death Dis.* **2018**, *9*, 507. [CrossRef]
119. Hernandez-Corbacho, M.J.; Salama, M.F.; Canals, D.; Senkal, C.E.; Obeid, L.M. Sphingolipids in mitochondria. *Biochim. Et Biophys. Acta. Mol. Cell Biol. Lipids* **2017**, *1862*, 56–68. [CrossRef]
120. Lin, G.; Wang, L.; Marcogliese, P.C.; Bellen, H.J. Sphingolipids in the Pathogenesis of Parkinson's Disease and Parkinsonism. *Trends Endocrinol. Metab.* **2019**, *30*, 106–117. [CrossRef]
121. Schuchman, E.H.; Desnick, R.J. Types A and B Niemann-Pick disease. *Mol. Genet. Metab.* **2017**, *120*, 27–33. [CrossRef] [PubMed]

122. Mao, C.; Obeid, L.M. Ceramidases: Regulators of cellular responses mediated by ceramide, sphingosine, and sphingosine-1-phosphate. *Biochim. Et Biophys. Acta* **2008**, *1781*, 424–434. [CrossRef] [PubMed]
123. Tani, M.; Sano, T.; Ito, M.; Igarashi, Y. Mechanisms of sphingosine and sphingosine 1-phosphate generation in human platelets. *J. Lipid Res.* **2005**, *46*, 2458–2467. [CrossRef] [PubMed]
124. Sundaram, K.; Mather, A.R.; Marimuthu, S.; Shah, P.P.; Snider, A.J.; Obeid, L.M.; Hannun, Y.A.; Beverly, L.J.; Siskind, L.J. Loss of neutral ceramidase protects cells from nutrient- and energy -deprivation-induced cell death. *Biochem. J.* **2016**, *473*, 743–755. [CrossRef]
125. Monick, M.M.; Cameron, K.; Powers, L.S.; Butler, N.S.; McCoy, D.; Mallampalli, R.K.; Hunninghake, G.W. Sphingosine kinase mediates activation of extracellular signal-related kinase and Akt by respiratory syncytial virus. *Am. J. Respir. Cell Mol. Biol.* **2004**, *30*, 844–852. [CrossRef]
126. Kihara, A. Very long-chain fatty acids: Elongation, physiology and related disorders. *J. Biochem.* **2012**, *152*, 387–395. [CrossRef]
127. Mueller, N.; Sassa, T.; Morales-Gonzalez, S.; Schneider, J.; Salchow, D.J.; Seelow, D.; Knierim, E.; Stenzel, W.; Kihara, A.; Schuelke, M. De novo mutation in ELOVL1 causes ichthyosis, acanthosis nigricans, hypomyelination, spastic paraplegia, high frequency deafness and optic atrophy. *J. Med. Genet.* **2019**, *56*, 164–175. [CrossRef]
128. Kutkowska-Kazmierczak, A.; Rydzanicz, M.; Chlebowski, A.; Klosowska-Kosicka, K.; Mika, A.; Gruchota, J.; Jurkiewicz, E.; Kowalewski, C.; Pollak, A.; Stradomska, T.J.; et al. Dominant ELOVL1 mutation causes neurological disorder with ichthyotic keratoderma, spasticity, hypomyelination and dysmorphic features. *J. Med. Genet.* **2018**, *55*, 408–414. [CrossRef]
129. Shimano, H. Novel qualitative aspects of tissue fatty acids related to metabolic regulation: Lessons from Elovl6 knockout. *Prog. Lipid Res.* **2012**, *51*, 267–271. [CrossRef]
130. Hoxha, E.; Gabriele, R.M.C.; Balbo, I.; Ravera, E.; Masante, L.; Zambelli, V.; Albergo, C.; Mitro, N.; Caruso, D.; Di Gregorio, E.; et al. Motor Deficits and Cerebellar Atrophy in Elovl5 Knock Out Mice. *Front. Cell. Neurosci.* **2017**, *11*, 343. [CrossRef]
131. Di Gregorio, E.; Borroni, B.; Giorgio, E.; Lacerenza, D.; Ferrero, M.; Lo Buono, N.; Ragusa, N.; Mancini, C.; Gaussen, M.; Calcia, A.; et al. ELOVL5 mutations cause spinocerebellar ataxia 38. *Am. J. Hum. Genet.* **2014**, *95*, 209–217. [CrossRef] [PubMed]
132. Blasco, H.; Veyrat-Durebex, C.; Bocca, C.; Patin, F.; Vourc'h, P.; Kouassi Nzoughet, J.; Lenaers, G.; Andres, C.R.; Simard, G.; Corcia, P.; et al. Lipidomics Reveals Cerebrospinal-Fluid Signatures of ALS. *Sci. Rep.* **2017**, *7*, 17652. [CrossRef] [PubMed]
133. Blasco, H.; Patin, F.; Descat, A.; Garcon, G.; Corcia, P.; Gele, P.; Lenglet, T.; Bede, P.; Meininger, V.; Devos, D.; et al. A pharmaco-metabolomics approach in a clinical trial of ALS: Identification of predictive markers of progression. *PLoS ONE* **2018**, *13*, e0198116. [CrossRef] [PubMed]
134. McIntosh, T.J.; Simon, S.A.; Needham, D.; Huang, C.H. Structure and cohesive properties of sphingomyelin/cholesterol bilayers. *Biochemistry* **1992**, *31*, 2012–2020. [CrossRef]
135. Saher, G.; Brugger, B.; Lappe-Siefke, C.; Mobius, W.; Tozawa, R.; Wehr, M.C.; Wieland, F.; Ishibashi, S.; Nave, K.A. High cholesterol level is essential for myelin membrane growth. *Nat. Neurosci.* **2005**, *8*, 468–475. [CrossRef]
136. Canet-Pons, J.; Sen, N.E.; Arsovic, A.; Almaguer-Mederos, L.E.; Halbach, M.V.; Key, J.; Doering, C.; Kerksiek, A.; Picchiarelli, G.; Cassel, R.; et al. Atxn2-CAG100-KnockIn mouse spinal cord shows progressive TDP-43 pathology associated with cholesterol biosynthesis suppression. *bioRxiv* **2019**. [CrossRef]
137. Brown, F.R., 3rd; Chen, W.W.; Kirschner, D.A.; Frayer, K.L.; Powers, J.M.; Moser, A.B.; Moser, H.W. Myelin membrane from adrenoleukodystrophy brain white matter–biochemical properties. *J. Neurochem.* **1983**, *41*, 341–348. [CrossRef]
138. Contreras, F.X.; Ernst, A.M.; Haberkant, P.; Bjorkholm, P.; Lindahl, E.; Gonen, B.; Tischer, C.; Elofsson, A.; von Heijne, G.; Thiele, C.; et al. Molecular recognition of a single sphingolipid species by a protein's transmembrane domain. *Nature* **2012**, *481*, 525–529. [CrossRef]
139. Hannun, Y.A.; Bell, R.M. Regulation of protein kinase C by sphingosine and lysosphingolipids. *Clin. Chim. Acta* **1989**, *185*, 333–345. [CrossRef]
140. Shimobayashi, E.; Kapfhammer, J.P. Calcium Signaling, PKC Gamma, IP3R1 and CAR8 Link Spinocerebellar Ataxias and Purkinje Cell Dendritic Development. *Curr. Neuropharmacol.* **2018**, *16*, 151–159. [CrossRef]

141. Noh, K.M.; Hwang, J.Y.; Shin, H.C.; Koh, J.Y. A novel neuroprotective mechanism of riluzole: Direct inhibition of protein kinase C. *Neurobiol. Dis.* **2000**, *7*, 375–383. [CrossRef] [PubMed]
142. Krieger, C.; Lanius, R.A.; Pelech, S.L.; Shaw, C.A. Amyotrophic lateral sclerosis: The involvement of intracellular Ca2+ and protein kinase C. *Trends Pharmacol. Sci.* **1996**, *17*, 114–120. [CrossRef]
143. Avramopoulos, D.; Wang, R.; Valle, D.; Fallin, M.D.; Bassett, S.S. A novel gene derived from a segmental duplication shows perturbed expression in Alzheimer's disease. *Neurogenetics* **2007**, *8*, 111–120. [CrossRef] [PubMed]
144. Levy, M.; Futerman, A.H. Mammalian ceramide synthases. *Iubmb Life* **2010**, *62*, 347–356. [CrossRef]
145. Becker, I.; Wang-Eckhardt, L.; Yaghootfam, A.; Gieselmann, V.; Eckhardt, M. Differential expression of (dihydro)ceramide synthases in mouse brain: Oligodendrocyte-specific expression of CerS2/Lass2. *Histochem. Cell Biol.* **2008**, *129*, 233–241. [CrossRef]
146. Yang, F.; Guan, Y.; Feng, X.; Rolfs, A.; Schluter, H.; Luo, J. Proteomics of the corpus callosum to identify novel factors involved in hypomyelinated Niemann-Pick Type C disease mice. *Mol. Brain* **2019**, *12*, 17. [CrossRef]
147. Maphis, N.M.; Jiang, S.; Binder, J.; Wright, C.; Gopalan, B.; Lamb, B.T.; Bhaskar, K. Whole Genome Expression Analysis in a Mouse Model of Tauopathy Identifies MECP2 as a Possible Regulator of Tau Pathology. *Front. Mol. Neurosci.* **2017**, *10*, 69. [CrossRef]
148. Anheuser, S.; Breiden, B.; Sandhoff, K. Ganglioside GM2 catabolism is inhibited by storage compounds of mucopolysaccharidoses and by cationic amphiphilic drugs. *Mol. Genet. Metab.* **2019**. [CrossRef]
149. Lang, P.A.; Schenck, M.; Nicolay, J.P.; Becker, J.U.; Kempe, D.S.; Lupescu, A.; Koka, S.; Eisele, K.; Klarl, B.A.; Rubben, H.; et al. Liver cell death and anemia in Wilson disease involve acid sphingomyelinase and ceramide. *Nat. Med.* **2007**, *13*, 164–170. [CrossRef]
150. Fucho, R.; Martinez, L.; Baulies, A.; Torres, S.; Tarrats, N.; Fernandez, A.; Ribas, V.; Astudillo, A.M.; Balsinde, J.; Garcia-Roves, P.; et al. ASMase regulates autophagy and lysosomal membrane permeabilization and its inhibition prevents early stage non-alcoholic steatohepatitis. *J. Hepatol.* **2014**, *61*, 1126–1134. [CrossRef]
151. Bhuvaneswaran, C.; Venkatesan, S.; Mitropoulos, K.A. Lysosomal accumulation of cholesterol and sphingomyelin: Evidence for inhibition of acid sphingomyelinase. *Eur. J. Cell Biol.* **1985**, *37*, 98–106. [PubMed]
152. Anheuser, S.; Breiden, B.; Sandhoff, K. Membrane lipids and their degradation compounds control GM2 catabolism at intralysosomal luminal vesicles. *J. Lipid Res.* **2019**, *60*, 1099–1111. [CrossRef] [PubMed]
153. Breiden, B.; Sandhoff, K. Emerging mechanisms of drug-induced phospholipidosis. *Biol. Chem.* **2019**. [CrossRef] [PubMed]
154. Breiden, B.; Sandhoff, K. Lysosomal Glycosphingolipid Storage Diseases. *Annu. Rev. Biochem.* **2019**, *88*, 461–485. [CrossRef] [PubMed]
155. Del Castillo, U.; Gnazzo, M.M.; Sorensen Turpin, C.G.; Nguyen, K.C.Q.; Semaya, E.; Lam, Y.; de Cruz, M.A.; Bembenek, J.N.; Hall, D.H.; Riggs, B.; et al. Conserved role for Ataxin-2 in mediating endoplasmic reticulum dynamics. *Traffic* **2019**, *20*, 436–447. [CrossRef]
156. Ralser, M.; Nonhoff, U.; Albrecht, M.; Lengauer, T.; Wanker, E.E.; Lehrach, H.; Krobitsch, S. Ataxin-2 and huntingtin interact with endophilin-A complexes to function in plastin-associated pathways. *Hum. Mol. Genet.* **2005**, *14*, 2893–2909. [CrossRef]
157. Lamming, D.W.; Sabatini, D.M. A Central role for mTOR in lipid homeostasis. *Cell Metab.* **2013**, *18*, 465–469. [CrossRef]
158. Laplante, M.; Sabatini, D.M. Regulation of mTORC1 and its impact on gene expression at a glance. *J. Cell Sci.* **2013**, *126*, 1713–1719. [CrossRef]
159. Figlia, G.; Gerber, D.; Suter, U. Myelination and mTOR. *Glia* **2018**, *66*, 693–707. [CrossRef]
160. Wang, W.; He, Q.; Guo, Z.; Yang, L.; Bao, L.; Bao, W.; Zheng, X.; Wang, Y.; Wang, Z. Inhibition of Mammalian Target of Rapamycin Complex 1 (mTORC1) Downregulates ELOVL1 Gene Expression and Fatty Acid Synthesis in Goat Fetal Fibroblasts. *Int. J. Mol. Sci.* **2015**, *16*, 16440–16453. [CrossRef]
161. Wehbe, Z.; Alatibi, K.; Jellusova, J.; Spiekerkoetter, U.; Tucci, S. The fate of medium-chain fatty acids in very long-chain acylCoA dehydrogenase deficiency (VLCADD): A matter of sex? *Biochim. Et Biophys. Acta. Mol. Cell Biol. Lipids* **2019**, *1864*, 1591–1605. [CrossRef] [PubMed]
162. Guo, Z.; Wang, Y.; Feng, X.; Bao, C.; He, Q.; Bao, L.; Hao, H.; Wang, Z. Rapamycin Inhibits Expression of Elongation of Very-long-chain Fatty Acids 1 and Synthesis of Docosahexaenoic Acid in Bovine Mammary Epithelial Cells. *Asian-Australas. J. Anim. Sci.* **2016**, *29*, 1646–1652. [CrossRef] [PubMed]

163. Garay-Lugo, N.; Dominguez-Lopez, A.; Miliar Garcia, A.; Aguilar Barrera, E.; Gomez Lopez, M.; Gomez Alcala, A.; Martinez Godinez Mde, L.; Lara-Padilla, E. n-3 Fatty acids modulate the mRNA expression of the Nlrp3 inflammasome and Mtor in the liver of rats fed with high-fat or high-fat/fructose diets. *Immunopharmacol. Immunotoxicol.* **2016**, *38*, 353–363. [CrossRef] [PubMed]
164. DeMille, D.; Badal, B.D.; Evans, J.B.; Mathis, A.D.; Anderson, J.F.; Grose, J.H. PAS kinase is activated by direct SNF1-dependent phosphorylation and mediates inhibition of TORC1 through the phosphorylation and activation of Pbp1. *Mol. Biol. Cell* **2015**, *26*, 569–582. [CrossRef]
165. Kato, M.; Yang, Y.S.; Sutter, B.M.; Wang, Y.; McKnight, S.L.; Tu, B.P. Redox State Controls Phase Separation of the Yeast Ataxin-2 Protein via Reversible Oxidation of Its Methionine-Rich Low-Complexity Domain. *Cell* **2019**, *177*, 711–721. [CrossRef] [PubMed]
166. Yang, Y.S.; Kato, M.; Wu, X.; Litsios, A.; Sutter, B.M.; Wang, Y.; Hsu, C.H.; Wood, N.E.; Lemoff, A.; Mirzaei, H.; et al. Yeast Ataxin-2 Forms an Intracellular Condensate Required for the Inhibition of TORC1 Signaling during Respiratory Growth. *Cell* **2019**, *177*, 697–710. [CrossRef]
167. Lavieu, G.; Scarlatti, F.; Sala, G.; Carpentier, S.; Levade, T.; Ghidoni, R.; Botti, J.; Codogno, P. Regulation of autophagy by sphingosine kinase 1 and its role in cell survival during nutrient starvation. *J. Biol. Chem.* **2006**, *281*, 8518–8527. [CrossRef]
168. Qin, J.; Berdyshev, E.; Poirer, C.; Schwartz, N.B.; Dawson, G. Neutral sphingomyelinase 2 deficiency increases hyaluronan synthesis by up-regulation of Hyaluronan synthase 2 through decreased ceramide production and activation of Akt. *J. Biol. Chem.* **2012**, *287*, 13620–13632. [CrossRef]
169. Thedieck, K.; Holzwarth, B.; Prentzell, M.T.; Boehlke, C.; Klasener, K.; Ruf, S.; Sonntag, A.G.; Maerz, L.; Grellscheid, S.N.; Kremmer, E.; et al. Inhibition of mTORC1 by astrin and stress granules prevents apoptosis in cancer cells. *Cell* **2013**, *154*, 859–874. [CrossRef]
170. Meierhofer, D.; Halbach, M.; Sen, N.E.; Gispert, S.; Auburger, G. Ataxin-2 (Atxn2)-Knock-Out Mice Show Branched Chain Amino Acids and Fatty Acids Pathway Alterations. *Mol. Cell. Proteom.* **2016**, *15*, 1728–1739. [CrossRef]
171. Seidel, G.; Meierhofer, D.; Sen, N.E.; Guenther, A.; Krobitsch, S.; Auburger, G. Quantitative Global Proteomics of Yeast PBP1 Deletion Mutants and Their Stress Responses Identifies Glucose Metabolism, Mitochondrial, and Stress Granule Changes. *J. Proteome Res.* **2017**, *16*, 504–515. [CrossRef] [PubMed]
172. Halbach, M.V.; Stehning, T.; Damrath, E.; Jendrach, M.; Sen, N.E.; Basak, A.N.; Auburger, G. Both ubiquitin ligases FBXW8 and PARK2 are sequestrated into insolubility by ATXN2 PolyQ expansions, but only FBXW8 expression is dysregulated. *PLoS ONE* **2015**, *10*, e0121089. [CrossRef] [PubMed]
173. Sen, N.E.; Gispert, S.; Auburger, G. PINK1 and Ataxin-2 as modifiers of growth. *Oncotarget* **2017**, *8*, 32382–32383. [CrossRef] [PubMed]
174. Moscatelli, E.A.; Isaacson, E. Gas liquid chromatographic analysis of sphingosine bases in sphingolipids of human normal and multiple sclerosis cerebral white matter. *Lipids* **1969**, *4*, 550–555. [CrossRef] [PubMed]
175. Obinata, H.; Hla, T. Sphingosine 1-phosphate and inflammation. *Int. Immunol.* **2019**, *31*, 617–625. [CrossRef]
176. Jones, Z.B.; Ren, Y. Sphingolipids in spinal cord injury. *Int. J. Physiol. Pathophysiol. Pharmacol.* **2016**, *8*, 52–69.
177. Torres-Odio, S.; Key, J.; Hoepken, H.H.; Canet-Pons, J.; Valek, L.; Roller, B.; Walter, M.; Morales-Gordo, B.; Meierhofer, D.; Harter, P.N.; et al. Progression of pathology in PINK1-deficient mouse brain from splicing via ubiquitination, ER stress, and mitophagy changes to neuroinflammation. *J. Neuroinflammation* **2017**, *14*, 154. [CrossRef]
178. Sliter, D.A.; Martinez, J.; Hao, L.; Chen, X.; Sun, N.; Fischer, T.D.; Burman, J.L.; Li, Y.; Zhang, Z.; Narendra, D.P.; et al. Parkin and PINK1 mitigate STING-induced inflammation. *Nature* **2018**, *561*, 258–262. [CrossRef]
179. Young, M.M.; Kester, M.; Wang, H.G. Sphingolipids: Regulators of crosstalk between apoptosis and autophagy. *J. Lipid Res.* **2013**, *54*, 5–19. [CrossRef]
180. Molino, S.; Tate, E.; McKillop, W.M.; Medin, J.A. Sphingolipid pathway enzymes modulate cell fate and immune responses. *Immunotherapy* **2017**, *9*, 1185–1198. [CrossRef]
181. Giussani, P.; Tringali, C.; Riboni, L.; Viani, P.; Venerando, B. Sphingolipids: Key regulators of apoptosis and pivotal players in cancer drug resistance. *Int. J. Mol. Sci.* **2014**, *15*, 4356–4392. [CrossRef] [PubMed]
182. Albeituni, S.; Stiban, J. Roles of Ceramides and Other Sphingolipids in Immune Cell Function and Inflammation. *Adv. Exp. Med. Biol.* **2019**, *1161*, 169–191. [PubMed]
183. Tsai, H.C.; Han, M.H. Sphingosine-1-Phosphate (S1P) and S1P Signaling Pathway: Therapeutic Targets in Autoimmunity and Inflammation. *Drugs* **2016**, *76*, 1067–1079. [CrossRef] [PubMed]

184. Kurschner, G.; Zhang, Q.; Clima, R.; Xiao, Y.; Busch, J.F.; Kilic, E.; Jung, K.; Berndt, N.; Bulik, S.; Holzhutter, H.G.; et al. Renal oncocytoma characterized by the defective complex I of the respiratory chain boosts the synthesis of the ROS scavenger glutathione. *Oncotarget* **2017**, *8*, 105882–105904. [CrossRef]
185. Gielisch, I.; Meierhofer, D. Metabolome and proteome profiling of complex I deficiency induced by rotenone. *J. Proteome Res.* **2015**, *14*, 224–235. [CrossRef]
186. Livak, K.J.; Schmittgen, T.D. Analysis of relative gene expression data using real-time quantitative PCR and the 2(-Delta Delta C(T)) Method. *Methods* **2001**, *25*, 402–408. [CrossRef]

IV. Written Declarations

D E C L A R A T I O N

I herewith declare that I have not previously participated in any doctoral examination procedure in a mathematics or natural science discipline.

Frankfurt am Main, _____ , _____

Date Signature

Author's Declaration

I herewith declare that I have produced my doctoral dissertation on the topic of:

"**The Role of Ataxin-2 in Metabolism and Disease**"

independently and using only the tools indicated therein. In particular, all references borrowed from external sources are clearly acknowledged and identified.

I confirm that I have respected the principles of good scientific practice and have not made use of the services of any commercial agency in respect of my doctorate.

Frankfurt am Main, _____ , _____

Date Signature

V. Complete List of Publications of the Candidate

Publications are listed chronologically:

Key J, Sen NE, Arsović A, Krämer S, Hülse R, Khan NN, Meierhofer D, Gispert S, Koepf G, Auburger G. **Systematic Surveys of Iron Homeostasis Mechanisms Reveal Ferritin Superfamily and Nucleotide Surveillance Regulation to be Modified by PINK1 Absence.** *Cells.* 2020 Oct 2;9(10):E2229. doi: 10.3390/cells9102229.

Arsović A, Halbach MV, Canet-Pons J, Esen-Sehir D, Döring C, Freudenberg F, Czechowska N, Seidel K, Baader SL, Gispert S, Sen NE*, Auburger G*. **Mouse Ataxin-2 Expansion Downregulates CamKII and Other Calcium Signaling Factors, Impairing Granule-Purkinje Neuron Synaptic Strength.** *Int J Mol Sci.* 2020 Sep 12;21(18):E6673. doi: 10.3390/ijms21186673.

Tunca C, … , Şen NE, … , Başak AN. **Revisiting the complex architecture of ALS in Turkey: Expanding genotypes, shared phenotypes, molecular networks, and a public variant database.** *Hum Mutat.* 2020 Aug;41(8):e7-e45. doi: 10.1002/humu.24055.

Key J, Harter PN, Sen NE, Gradhand E, Auburger G, Gispert S. **Mid-Gestation lethality of Atxn2l-Ablated Mice.** *Int J Mol Sci.* 2020 Jul 20;21(14):5124. doi: 10.3390/ijms21145124.

Sen NE, Arsovic A, Meierhofer D, Brodesser S, Oberschmidt C, Canet-Pons J, Kaya ZE, Halbach MV, Gispert S, Sandhoff K, Auburger G. **In Human and Mouse Spino-Cerebellar Tissue, Ataxin-2 Expansion Affects Ceramide-Sphingomyelin Metabolism.** *Int J Mol Sci.* 2019 Nov 21;20(23). doi: 10.3390/ijms20235854.

Sen NE*, Canet-Pons J*, Halbach MV*, Arsovic A, Pilatus U, Chae WH, Kaya ZE, Seidel K, Rollmann E, Mittelbronn M, Meierhofer D, De Zeeuw CI, Bosman L, Gispert S, Auburger G. **Generation of an *Atxn2*-CAG100 knock-in mouse reveals N-acetylaspartate production deficit due to early Nat8l dysregulation.** *Neurobiol Dis.* 2019 Dec;132:104559. doi: 10.1016/j.nbd.2019.104559.

Auburger G*, Gispert S, Torres-Odio S, Jendrach M, Brehm N, Canet-Pons J, Key J, Sen NE. **SerThr-PhosphoProteome of Brain from Aged PINK1-KO+A53T-SNCA Mice Reveals pT1928-MAP1B and pS3781-ANK2 Deficits, as Hub between Autophagy and Synapse Changes.** *Int J Mol Sci.* 2019 Jul 4;20(13). doi: 10.3390/ijms20133284.

Hamzeiy H, Savaş D, Tunca C, Şen NE, Gündoğdu Eken A, Şahbaz I, Calini D, Tiloca C, Ticozzi N, Ratti A, Silani V, Başak AN. **Elevated Global DNA Methylation Is Not Exclusive to Amyotrophic Lateral Sclerosis and Is Also Observed in Spinocerebellar Ataxia Types 1 and 2.** *Neurodegener Dis.* 2018;18(1):38-48. doi: 10.1159/000486201.

Auburger G, Sen NE, Meierhofer D, Başak AN, Gitler AD. **Efficient Prevention of Neurodegenerative Diseases by Depletion of Starvation Response Factor Ataxin-2.** *Trends Neurosci.* 2017 Aug;40(8):507-516. doi: 10.1016/j.tins.2017.06.004.

Sen NE, Gispert S, Auburger G. **PINK1 and Ataxin-2 as modifiers of growth.** *Oncotarget.* 2017 May 16;8(20):32382-32383. doi: 10.18632/oncotarget.16636.

Seidel G, Meierhofer D, Sen NE, Guenther A, Krobitsch S, Auburger G. **Quantitative Global Proteomics of Yeast PBP1 Deletion Mutants and Their Stress Responses Identifies Glucose Metabolism, Mitochondrial, and Stress Granule Changes.** *J Proteome Res.* 2017 Feb 3;16(2):504-515. doi: 10.1021/acs.jproteome.6b00647.

Sen NE, Drost J, Gispert S, Torres-Odio S, … , Başak AN, Auburger G. **Search for SCA2 blood RNA biomarkers highlights Ataxin-2 as strong modifier of the mitochondrial factor PINK1 levels.** *Neurobiol Dis.* 2016 Dec;96:115-126. doi: 10.1016/j.nbd.2016.09.002.

Meierhofer D, Halbach M, Şen NE, Gispert S, Auburger G. **Ataxin-2 (Atxn2)-Knock-Out Mice Show Branched Chain Amino Acids and Fatty Acids Pathway Alterations.** *Mol Cell Proteomics.* 2016 May;15(5):1728-39. doi: 10.1074/mcp.M115.056770.

Halbach MV, Stehning T, Damrath E, Jendrach M, Şen NE, Başak AN, Auburger G. **Both ubiquitin ligases FBXW8 and PARK2 are sequestrated into insolubility by ATXN2 PolyQ expansions, but only FBXW8 expression is dysregulated.** *PLoS One.* 2015 Mar 19;10(3):e0121089. doi: 10.1371/journal.pone.0121089.

Özoğuz A, … , Sen NE, … , Landers JE, Brown RH, Başak AN. **The distinct genetic pattern of ALS in Turkey and novel mutations.** *Neurobiol Aging.* 2015 Apr;36(4):1764.e9-1764.e18. doi: 10.1016/j.neurobiolaging.2014.12.032.